UNIVERSITY OF SOUTHAMPTON

FACULTY OF ENGINEERING AND PHYSICAL SCIENCES

PHYSICS AND ASTRONOMY

ON THE SINGULARITIES OF SCATTERING AMPLITUDES: FROM CLUSTER ADJACENCY TO TROPICAL GEOMETRY

by

JACK ALEXANDER FOSTER

ORCID ID: 0000-0003-0289-010X

Thesis for the degree of Doctor of Philosophy

October 2020

University of Southampton

Abstract

Faculty of Engineering and Physical Sciences

Physics and Astronomy

Doctor of Philosophy

**On the Singularities of Scattering Amplitudes:
From Cluster Adjacency to Tropical Geometry**

by Jack Alexander Foster

Planar maximally supersymmetric Yang-Mills theory ($\mathcal{N} = 4$ SYM) is a unique quantum field theory. Its interesting properties include conformal symmetry at the quantum level, expected integrability, and being a prime example of the AdS/CFT correspondence. Witten's twistor string theory [1] reignited an interest in this theory, leading to enormous progress in utilising its special features to uncover new mathematical structures, such as the Grassmannian [2], and to better understand gauge theory in general. One such feature is the hidden dual conformal symmetry in SYM [3, 4] which led to the introduction of momentum twistors [5] as useful variables when describing scattering amplitudes in SYM. It was then shown in [6] that the kinematic space parametrised by these momentum twistors, itself a Grassmannian, comes equipped with a particular mathematical structure called a cluster algebra. It was shown that scattering amplitudes in SYM depend on cluster coordinates and, at least for six and seven-points, the cluster algebra provided all the singularities, or alphabet, for all known amplitudes in SYM. The ultimate hope is that by understanding all the analytic structure of the functions scattering amplitudes consist of, one could simply write down the form of an amplitude without the need for an explicit calculation. The overarching theme of this thesis is to better understand the analytic properties of scattering amplitudes, mainly (but not exclusively) in SYM. Although this thesis has two parts, the main focus is on cluster algebras; extracting the information they contain about amplitudes and exploring their relationship with other areas of mathematics, as well as what those relationships imply for the singularity properties of amplitudes. In the first part, we introduce and develop the notion of cluster adjacency and how it controls the poles and branch cuts an amplitude is allowed to have. We also provide an example of how cluster adjacency can aid in computations in calculating the seven-point, four-loop, NMHV scattering amplitude. The second part expands on the discussion started in [7] linking tropical geometry to scattering amplitudes in the biadjoint ϕ^3 theory. We demonstrate how the connection between tropical Grassmannians and cluster algebras allows for straightforward calculation of amplitudes in this theory. We go on to utilise this connection to generalise the notion of cluster adjacency and conjecture how different helicity configurations (MHV, NMHV, etc.) may each have their own cluster adjacency rules. Finally, tropical geometry allows us to approach certain issues with eight-point scattering in SYM. Namely, the infinite set of cluster coordinates provided by cluster algebra associated with eight-point scattering, as well as generating the algebraic singularities known to appear even at one-loop for N^2MHV amplitudes.

This thesis is based on [8–13] with considerable overlap with these papers.

Contents

List of Figures

List of Tables

UNIVERSITY OF Southampton

Academic Thesis: Declaration Of Authorship

I, Jack Foster

declare that this thesis and the work presented in it are my own and has been generated by me as the result of my own original research.

On the Singularities of Scattering Amplitudes: From Cluster Adjacency to Tropical Geometry

I confirm that:

1. This work was done wholly or mainly while in candidature for a research degree at this University;
2. Where any part of this thesis has previously been submitted for a degree or any other qualification at this University or any other institution, this has been clearly stated;
3. Where I have consulted the published work of others, this is always clearly attributed;
4. Where I have quoted from the work of others, the source is always given. With the exception of such quotations, this thesis is entirely my own work;
5. I have acknowledged all main sources of help;
6. Where the thesis is based on work done by myself jointly with others, I have made clear exactly what was done by others and what I have contributed myself;
7. Either none of this work has been published before submission, or parts of this work have been published as:
    - Cluster Adjacency Properties of Scattering Amplitudes in N=4 Supersymmetric Yang-Mills Theory *Physics Review Letters* 120.16 (2018), p. 161601 (with James Drummond and Omer Gurdogan)
    - Cluster adjacency beyond MHV *JHEP* 03 (2019), p. 086 (with James Drummond and Omer Gurdogan)
    - Cluster adjacency and the four-loop NMHV heptagon *JHEP* 03 (2019) p. 087 (with James Drummond, Omer Gurdogan, and Georgios Papathanasiou)
    - Tropical Grassmannians, cluster algebras and scattering amplitudes *JHEP* 04 (2020) p. 146 (with James Drummond, Omer Gurdogan, and Chrysostomos Kalousios

Signed: Jack Foster

Date: 1/10/2020

Acknowledgements

It is with great pleasure that I express my gratitude to my supervisor James Drummond for his patience, guidance, and close collaboration over the course of my PhD. I have had many exciting and fascinating experiences over these four years for which I will be forever grateful. The success of my PhD would not have been possible without the help of Ömer Gürdoğan, whose constant patience and aid helped me through many points of our research.

I am also grateful for my fellow PhD students, from various generations, at the University of Southampton. With special thanks to Hynek Paul and Elena Perdomo as we started our PhD's together and remained good friends throughout. I would also like to thank Sam Rowley, our friendship and early gym sessions have been of great support to me.

I would also like to extend my gratitude to my Master's project supervisor, Gabrielle Travaglini from Queen Mary University of London, for introducing me to the field of scattering amplitudes, the subject of this thesis. Without him I would not be doing a PhD.

My deepest gratitude goes to my parents, Mark and Karen Foster, my grandmother Jean Gaston-Parry, and the rest of my family, whose love and support throughout my life have helped me get here.

Finally, I would like to thank Chas Brickland for his companionship, attentiveness, and support through these challenging final years of my PhD. He also deserves special thanks for proofreading parts of this thesis.

My research at the University of Southampton is supported by the European Research Council consolidator grant 648630 IQFT.

Introduction

Our current understanding of the fundamental laws of elementary particles comes from a quantum field theory (QFT) called the Standard Model of Particle Physics (SM). This QFT consists of two sectors, *Quantum Chromodynamics* (QCD) and *Electroweak Theory*, which govern the strong and electroweak forces respectively. We test and explore these theories at particle colliders such as the Large Hadron Collider (LHC). Here beams of high energy protons are collided together and detectors surrounding the interaction point record data about the particles produced in the collision. This data is then compared against predictions from the SM from which we can assess the accuracy of our theory.

The object which is calculated from the theory and measured against collider data is called a scattering cross section. Roughly speaking, a scattering cross section is the probability that a specific process will take place in a collision of incoming particles. In order to calculate a cross section we must first calculate a *scattering amplitude*. Scattering amplitudes are formally defined as the overlap between an incoming state of n_i particles and an outgoing state of n_f particles

$$S_{if} \equiv \langle 1, \ldots, n_i | 1, \ldots, n_f \rangle \tag{0.0.1}$$

where S_{if} is an element of the *S-matrix* and $|1, \ldots, n\rangle$ is an n-particle momentum eigenstate. The incoming and outgoing states are free (non-interacting) and the elements of the S-matrix account for finite time.

In general, scattering amplitudes are difficult to calculate and exact computations are often impossible to perform. The textbook-standard method for computing scattering amplitudes begins with the corresponding correlation function of local gauge-invariant operators $\mathcal{O}_i$

$$\langle \mathcal{O}_1(x_1) \cdots \mathcal{O}_n(x_n) \rangle = \int d[\Psi] \mathcal{O}_1(x_1) \cdots \mathcal{O}_n(x_n) e^{-S_{\text{Euc}}[\Psi]}, \tag{0.0.2}$$

where $d[\Psi]$ corresponds to the integration over all possible field configurations of the fundamental fields Ψ, and

$$S_{\text{Euc}} = \int d^4x \mathcal{L}[\Psi(x)] \tag{0.0.3}$$

is the Euclidean action (obtained by Wick rotation $t \to it$). From the correlation functions one employs the Lehmann-Symanzik-Zimmermann (LSZ) reduction prescription [14]; this amounts to Fourier transforming the correlator of fundamental fields to momentum space and requiring the fields to be momentum eigenstates i.e. plane waves. The Feynman rules for the theory in question can now be extracted from its Lagrangian, which for a weakly

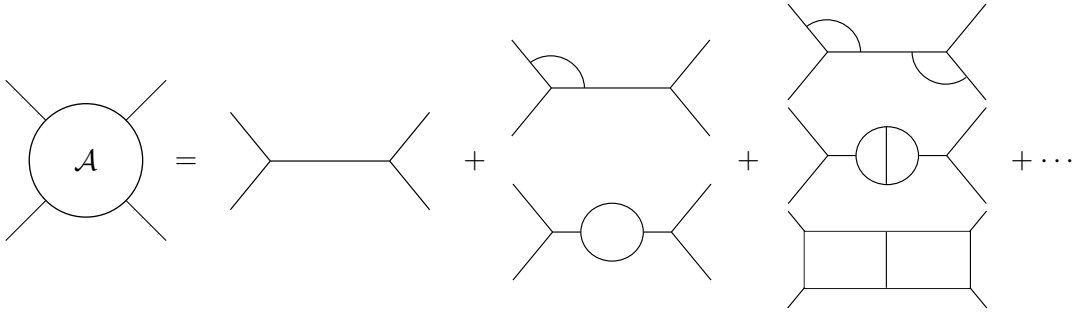

Figure 1: A perturbative expansion in Feynman diagrams where only a few diagrams are shown at each loop order.

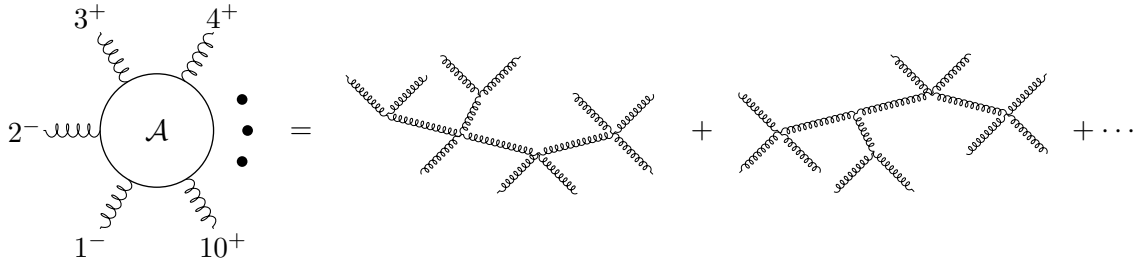

$$+ \text{ 10 million terms } = \frac{\langle 12\rangle^4}{\langle 12\rangle\langle 23\rangle\cdots\langle 10\,1\rangle}$$

Figure 2: A ten-point tree-level gluon amplitude is a sum of over ten million terms which remarkably produces a single term.

coupled theory has the form

$$\mathcal{L} = \mathcal{L}_{\text{free}} + g\mathcal{L}_{\text{int}}, \quad g \ll 1, \tag{0.0.4}$$

where $\mathcal{L}_{\text{free}}$ provides the propagator and $\mathcal{L}_{\text{int}}$ provides the interaction terms. If a theory can be decomposed in the manner of (0.0.4) one can perform a perturbative expansion in terms of Feynman diagrams of increasing loop order, as shown in Figure 1. This is due to expanding the exponential in (0.0.2) resulting in all correlation functions becoming a series in g. The Feynman rules are used to build mathematical expressions corresponding to the diagram in question and for each loop an integral over all possible values of loop momenta has to be performed. These loop integrals constitute a significant bottleneck in efficiently calculating amplitudes.

The Feynman diagram method is straightforward and mechanical, meaning it can readily be set up on a computer and automatically calculate terms of higher and higher order. However, due to the rapidly increasing number of diagrams at each loop order, the computations quickly become insurmountable, even for the simplest of events. Moreover, even the best supercomputers cannot handle the complex collisions taking place at the LHC. In short, relying on Feynman diagrams will be impractical for higher precision experiments.

Beyond computational difficulty, there are other indicators that the Feynman diagram

approach is less than ideal. For instance, Feynman diagrams contain a large amount of redundancy. Individual diagrams may produce physically impossible final states, the probability of these processes occurring only shown to be zero when the diagrams are summed together. Individual diagrams are also gauge-dependent however the final amplitude is not. One of the most popular indicators that Feynman diagrams may not be the best tool is the Parke-Taylor amplitude [15]. Parke and Taylor initially showed that tree-level amplitudes with particular helicity configurations for the external particles vanished, noticing that the first non-vanishing case had a simple closed form. This came from painstaking work, simplifying pages of four-momenta contractions from many diagrams into a remarkable formula, demonstrated in Figure 2.

The analytic behaviour of scattering amplitudes has been a subject of great interest for decades [16]. Recent developments in the theory of amplitudes have led to the application of an array of mathematical ideas to their calculation. The study of poles in tree-level amplitudes led to the BCFW recursion relations [17] as well as unitarity cuts of integrals [18]. Related ideas have been applied to constructing the S-matrix of massive theories directly [19, 20], inspired by recent developments in the numerical bootstrap for conformal field theories [21, 22]. The combination of these ideas has fed into new constructions of loop integrands for many amplitudes [23, 24]. The study of polylogarithmic iterated integrals [25–28] has led to a much greater understanding of loop integrals and motivated a greater push to classify and understand more general functions of elliptic type and beyond [29–34]. These developments have inspired recent advances [35] in the well-studied subject of differential equations for loop integrals [36–39] which have been applied to processes of interest for QCD or gauge theories in general. It is clear that the greater understanding we have of the role of singularities in field theory amplitudes, the greater our ability is to calculate them, and the deeper our understanding of field theory becomes.

In this thesis, we will focus on the study of poles and branch cuts in perturbative amplitudes and the algebraic and geometrical structures which govern their appearance. In this regard, a helpful toy model is the planar limit of $\mathcal{N} = 4$ super Yang-Mills theory where many approaches can be taken to calculate amplitudes. In perturbation theory, an analytic bootstrap programme has been employed for certain amplitudes, allowing the construction of explicit data for many loop orders [40–49]. A different technique, relying on the relation of the planar amplitudes with light-like Wilson loops [50–55], is based on multiple expansions in a near-collinear OPE limit [56–60]. This is much like correlation functions of local operators in conformal field theories. Many of these techniques were developed as a consequence of the gauge/string duality wherein SYM is dual to type IIB string theory on anti-de Sitter space [61]. The interplay of these techniques has revealed surprising structures at the heart of scattering amplitudes.

An important observation about perturbative amplitudes came with the work of [6] and was explored further in e.g. [62] where a link was made between the locations of branch point singularities in scattering amplitudes and cluster algebras related to Grassmannian spaces $\mathrm{Gr}(4, n)$. Cluster algebras were introduced and developed in [63–65] and are an area of intense ongoing research. Their relation to scattering amplitudes was first discussed in

[23] in the context of on-shell diagrams. This connection relates the cluster $\mathcal{A}$-coordinates of the cluster algebra with the symbol letters (potential logarithmic branch cuts) of the scattering amplitude. The cluster algebra connection explains the simple nine-letter alphabet of singularities previously found in six-particle amplitudes [66] and it has been exploited in the context of the analytic bootstrap programme up to high loop orders [40, 42–44, 46, 47, 49]. Moreover, the link to cluster algebras suggests a 42 letter alphabet for seven-particle amplitudes which has successfully been used to bootstrap amplitudes in [10, 45, 48].

In Chapter 2, we will describe and extend the connection between cluster algebras and amplitudes to the interplay of such singularities with each other. Specifically, we notice that the cluster algebras also control the possible sequences of such branch cut singularities; a non-trivial analytic continuation around a given singularity may only be followed by certain others. The set of which singularities are visible on any given Riemann sheet is dictated by the clusters themselves. We refer to this property of amplitudes as 'cluster adjacency'. The adjacency relations we find encompass the Steinmann relations [67, 68] which place constraints on consecutive discontinuities of amplitudes [69]. Such relations can be made manifest on appropriately defined infrared finite quantities, these then become a powerful constraint in the analytic bootstrap programme [47]. An equivalent set of conditions on multiple discontinuities is that of the extended Steinmann relations [70].

We first introduce cluster adjacency in terms of the symbols of loop integrals. In Chapter 3, we will extend the notion of cluster adjacency to tree-level amplitudes, illustrating that not only the amplitude obeys cluster adjacency, but that individual BCFW terms that make up the amplitude are also cluster adjacent. In this, we can associate each term to a subalgebra of the full cluster algebra, thus providing a geometric interpretation for individual BCFW terms through the cluster polytope. We then employ our working understanding of the cluster adjacency of branch points of loops and poles of trees to calculate an amplitude where there is interplay between them - the seven-point, four-loop, NMHV amplitude in SYM. The structure of NMHV loop amplitudes in conjunction with cluster adjacency indicates that their poles and branch points are not independent, and we utilise this to simplify our calculation. Having obtained our four-loop result we then analyse the amplitude in multi-Regge kinematics. The multi-Regge or high-energy limit, originally studied within the analytic S-matrix programme [71] and QCD [72–74], is the arena where realistically occurring scattering configurations meet a beautiful simplification of their dynamical description in terms of effective, two-dimensional degrees of freedom. Particularly for $\mathcal{N} = 4$ SYM theory, this simplicity has allowed for the identification of the space of functions required to describe the amplitude of an arbitrary number of external gluons n at any loop order in the limit [75, 76]. In fact, for $n = 6$, this has even led to the determination of the amplitude at finite coupling [77].

In this limit, amplitudes develop large logarithms in some of the kinematic variables (1.3.51), and so at each loop order they reduce to a polynomial of these logarithms. The highest order of these corresponds to the leading logarithmic approximation (LLA), with an obvious generalisation to the (next-to)^k-leading logarithmic approximation (N^{k}LLA).

The analysis of our four-loop amplitude provides a check of the consistency of our result with the expected structure of the Fourier-Mellin representation described in [76, 78] at LLA and NLLA. It then also provides new predictions at the next two logarithmic orders. The four-loop results are provided in [10], as are the new predictions for the amplitudes in multi-Regge kinematics.

Recently, many connections have been made between the study of tropical geometry and scattering amplitudes in quantum field theory and string theory. One connection is via the study of massless scattering amplitudes via the scattering equations [79–81]. In the simplest setting these equations describe tree-level biadjoint ϕ^3 amplitudes. In this context there is an auxiliary space; the moduli space of n points on a Riemann sphere, which is related to the kinematics of the n-point massless scattering amplitude via the scattering equations. The moduli space is the configuration space of n points in $\mathbb{P}^1$ which is equivalent to the Grassmannian $\mathrm{Gr}(2,n)$ (modulo local rescalings). The biadjoint ϕ^3 amplitude can be computed by evaluating certain Parke-Taylor type factors on solutions of the scattering equations. The final expression obtained after summing all solutions is equal to the traditional Feynman diagram expression.

In [7], a connection of the above picture to the tropical Grassmannian was made. The tropical version of a space is a simplification in which the defining non-linear equations are treated in a piecewise linear fashion. Despite this simplification, the tropical space retains much information from the original. In particular, each ϕ^3 Feynman diagram can be associated to a maximal cone of the tropical Grassmannian $\mathrm{Gr}(2,n)$. This picture is closely related [11] to the kinematic associahredron picture of [82].

Moreover, in [7] a generalisation of the above picture to Grassmannians $\mathrm{Gr}(k,n)$ was given. In the generalised setting of $\mathrm{Gr}(k,n)$, there is no known standard field theory formulation for the amplitudes. However, it was conjectured that the associated generalised amplitude obtained from the scattering equations can again be written as a sum over maximal cones of the tropical Grassmannian.

In Chapter 4, we will review this connection and how triangulating the tropical Grassmannian allows one to compute ϕ^3 amplitudes. We will then demonstrate how a tropical Grassmannian's corresponding cluster algebra provides one particular triangulation in a straightforward way, providing examples for various $\mathrm{Gr}(k,n)$.

In Chapter 5, we continue discussing the connection between the tropical Grassmannian and cluster algebras already partly explored in [83]. We describe a family of tropical fans related to Grassmannian cluster algebras. These fans are related to the kinematic space of massless scattering processes in a number of ways. For each fan associated to the Grassmannian $\mathrm{Gr}(k,n)$, there is a notion of a generalised ϕ^3 amplitude, as well as an associated set of scattering equations which further generalise the $\mathrm{Gr}(k,n)$ scattering equations that have been recently introduced. Here we focus mostly on the cases related to finite Grassmannian cluster algebras and we explain how face variables for the cluster polytopes are simply related to the scattering equations. For the Grassmannians $\mathrm{Gr}(4,n)$ the tropical fans we describe are related to the singularities (or symbol letters) of loop amplitudes in planar SYM. We show how each choice of tropical fan leads to a natural

class of polylogarithms, generalising the notion of cluster adjacency and we describe how the currently known loop data fit into this classification.

In Chapter 6, we argue that connections between cluster algebras and tropical geometry provide a natural language for postulating a finite alphabet for scattering amplitudes beyond six and seven points, where the corresponding Grassmannian cluster algebras are infinite. We also address the appearance of algebraic singularities in the symbol alphabet of scattering amplitudes in the context of planar SYM. Starting from eight-points, as well as polynomials in Plücker coordinates, algebraic roots show up in the symbol of the amplitude. These appear already at one loop due to the presence of four-mass-box type cuts. As well as generating natural, finite sets of letters, the tropical fans we discuss provide letters containing square roots. Remarkably, the minimal fan we consider provides all the square root letters recently discovered in an explicit two-loop eight-point NMHV calculation.

Finally, Chapter 7 contains concluding remarks of the work presented throughout this thesis as well as possible outlooks for future research.

Part I

Cluster Adjacency

Chapter 1

Review

1.1 On-shell methods for scattering amplitudes

In this chapter, we will review various methods and techniques used in the calculation of scattering amplitudes. Some of these will be relevant later in this thesis while others are necessary stepping stones to the central mathematical structures. These will also highlight the hidden simplicities of amplitudes that textbook methods fail to capture.

1.1.1 Colour decomposition

In general, scattering amplitudes in gauge theory are functions of momenta, wavefunctions and colour factors of external states, as well as the coupling constant(s). In order to simplify amplitude calculations, it is useful to separate the colour factors out.

In gauge theory, the colour factors enter through the interaction terms in the Lagrangian via structure constants of the gauge group. The colour factors of the three and four-gluon vertices are given in Figure 1.1 where the t^a are the generators of the fundamental representation of $SU(N)$, f^{abc} are the gauge group structure constants, and $a = 1, \ldots, N^2 - 1$.

In order to absorb factors of 2, we can redefine the t^a and f^{abc}

$$t^a \to \sqrt{2}t^a, \quad f^{abc} \to \sqrt{2}f^{abc}, \tag{1.1.1}$$

which allows us to write the Lie bracket as

$$\left[t^a, t^b\right] = f^{abc}t^c. \tag{1.1.2}$$

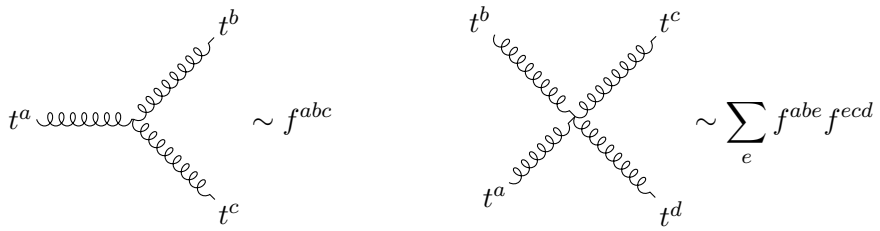

Figure 1.1: Colour structure of the three and four-gluon interaction vertices

We can choose a diagonal basis for the generators such that

$$\mathrm{Tr}(t^a t^b) = \delta^{ab}, \tag{1.1.3}$$

allowing us to write the structure constants in terms of the generators

$$f^{abc} = \mathrm{Tr}(t^a [t^b, t^c]), \tag{1.1.4}$$

rendering the f^{abc} totally anti-symmetric in all indices. Finally we note the identity

$$(t^a)^j_i (t^a)^l_k = \delta^l_i \delta^j_k - \frac{1}{N} \delta^j_i \delta^l_k \tag{1.1.5}$$

which can be used to merge traces. In the large N limit, the $1/N$ term drops out and all amplitudes are proportional to a single trace over the n generators associated to each of the n particles. In this limit all Feynman diagrams can be drawn in a plane hence it is known as the *planar* limit. Amplitudes in the planar limit have the general form

$$\mathcal{A}_n^{planar} = g_{YM}^{n-2} \sum_{\sigma \in S_n/\mathbb{Z}_n} \mathrm{Tr}(t^{a_{\sigma(1)}} t^{a_{\sigma(2)}} \dots t^{a_{\sigma(n)}}) A_n(\sigma(1), \sigma(2), \dots, \sigma(n)) \tag{1.1.6}$$

where g_{YM} is the Yang-Mills coupling constant. The A_n function on the right-hand side is known as a *partial* or *colour-ordered* amplitude which contain all kinematical information. These partial amplitudes are simpler than the full amplitudes as they only receive contributions from a fixed cyclic ordering of the external particles which is what allows us to draw them on a plane. We can think of these planar amplitudes as being drawn on a disk, with marked points on the boundary representing the external states. Non-planar amplitudes can be drawn on surfaces with more than one boundary however we shall not be discussing non-planar amplitudes in this thesis.

1.1.2 Spinor-helicity formalism

For the scattering of massless particles, it is particularly useful to introduce new variables which automatically satisfy the on-shell condition. They also often render the analytic expressions of scattering amplitudes in a much more compact form compared to the standard four-vector notation. We start by contracting the four-vector p_i^μ with the Pauli matrices which gives us a matrix

$$p_{\alpha\dot{\alpha}} = p_\mu \sigma^\mu_{\alpha\dot{\alpha}} = \begin{pmatrix} p_0 + p_3 & p_1 - ip_2 \\ p_1 + ip_2 & p_0 - p_3 \end{pmatrix}, \quad \sigma^\mu_{\alpha\dot{\alpha}} = (\mathbb{1}, \vec{\sigma}). \tag{1.1.7}$$

Here the mass-shell condition can be expressed as the determinant of $p_{i,\alpha\dot{\alpha}}$

$$\det(p_{\alpha\dot{\alpha}}) = p_0^2 - p_1^2 - p_2^2 - p_3^2 = m^2. \tag{1.1.8}$$

As a 2×2 matrix, the rank of $p_{\alpha\dot{\alpha}}$ must be at most 2 and therefore we can write it as

$$p_{\alpha\dot{\alpha}} = \lambda_\alpha \tilde{\lambda}_{\dot{\alpha}} + \mu_\alpha \tilde{\mu}_{\dot{\alpha}}, \tag{1.1.9}$$

where λ, μ and $\tilde{\lambda}, \tilde{\mu}$ are commuting Weyl spinors in the $(0, 1/2)$ and $(1/2, 0)$ representations of the Lorentz group respectively. In the case of massless particles

$$\det(p_{\alpha\dot{\alpha}}) = 0, \tag{1.1.10}$$

hence the light-like four-momenta may be written as

$$p_{i,\alpha\dot{\alpha}} = \lambda_{i\alpha}\tilde{\lambda}_{i\dot{\alpha}}. \tag{1.1.11}$$

The λ_α and $\tilde{\lambda}_{\dot{\alpha}}$ are called *helicity spinors*. For real four-momenta with Lorentzian signature the spinors are related to each other by $(\lambda_{i\alpha})^* = \pm\tilde{\lambda}_{i\dot{\alpha}}$.

A massless four-vector has only three degrees-of-freedom. This is reflected in the spinors through a scaling invariance

$$(\lambda, \tilde{\lambda}) \mapsto (t\lambda, t^{-1}\tilde{\lambda}), \quad t \neq 0, \tag{1.1.12}$$

called the *little group scaling*. Physically, the *little group* is the subset of Lorentz transformations which leave the momentum of an on-shell particle invariant. We can build Lorentz-invariant quantities out of spinors using the $SU(2)$ invariant tensors

$$\epsilon_{\alpha\beta} = \epsilon_{\dot{\alpha}\dot{\beta}} = \begin{pmatrix} 0 & 1 \\ -1 & 0 \end{pmatrix}. \tag{1.1.13}$$

Contracting spinors with the above tensor gives the following spinor products

$$\langle ij\rangle := \langle\lambda_i\lambda_j\rangle = \epsilon_{\alpha\beta}\lambda_i^\alpha\lambda_j^\beta =: -\langle ji\rangle \tag{1.1.14}$$

$$[ij] := [\tilde{\lambda}_i\tilde{\lambda}_j] = \epsilon^{\dot{\alpha}\dot{\beta}}\tilde{\lambda}_{i\dot{\alpha}}\tilde{\lambda}_{j\dot{\beta}} =: -[ji]. \tag{1.1.15}$$

where we also use $\epsilon_{\alpha\beta}$, $\epsilon_{\dot{\alpha}\dot{\beta}}$ as well as their inverses $\epsilon^{\alpha\beta}$, $\epsilon^{\dot{\alpha}\dot{\beta}}$ to raise and lower spinor indices. For massless particles, we may write Mandelstam invariants s_{ij} in terms of these spinor brackets

$$s_{ij} = (p_i + p_j)^2 = 2p_i \cdot p_j = p_i^{\alpha\dot{\alpha}}p_{j\alpha\dot{\alpha}} = \langle ij\rangle[ji]. \tag{1.1.16}$$

It is worth noting that s_{ij} vanishes when either $\lambda_i \propto \lambda_j$ or $\tilde{\lambda}_i \propto \tilde{\lambda}_j$. Physically, this means p_i, p_j are collinear.

Spinors are elements of a two-dimensional vector space so three or more of them must be linearly dependent from which we can derive the *Schouten identity*

$$\langle ij\rangle\langle kl\rangle + \langle ik\rangle\langle lj\rangle + \langle il\rangle\langle jk\rangle = 0, \tag{1.1.17}$$

and similarly for the conjugated spinors. We will see later these angle brackets can also be interpreted as minors of a $2 \times n$ matrix and the Schouten identity is a consequence of the linear dependence of the minors. Finally, we must still impose momentum conservation on these variables

$$\sum_{i=1}^{n} p_i = 0 \quad \rightarrow \quad \sum_{i=1}^{n}\langle ai\rangle[ib] = 0. \tag{1.1.18}$$

Fermion polarisations

For massless fermions, the Dirac equation degenerates into two Weyl equations

$$\not{p}v_\pm(p) = 0, \quad \overline{u}_\pm(p)\not{p} = 0, \tag{1.1.19}$$

where the subscript $\pm$ refers to the helicity of the particle (in the massless case). The conjugates are related to these wavefunctions via $u_\pm = v_\mp$ and $\overline{v}_\pm = \overline{u}_\mp$. The spinors $\lambda, \tilde{\lambda}$

provide a natural basis for solutions of these equations

$$u_+(p) = v_-(p) = \begin{pmatrix} \lambda_\alpha \\ 0 \end{pmatrix}, \quad u_-(p) = v_+(p) = \begin{pmatrix} 0 \\ \tilde{\lambda}^{\dot{\alpha}} \end{pmatrix} \tag{1.1.20}$$

$$\bar{u}_+(p) = \bar{v}_-(p) = \begin{pmatrix} 0 & \tilde{\lambda}_{\dot{\alpha}} \end{pmatrix}, \quad \bar{u}_-(p) = \bar{v}_+(p) = \begin{pmatrix} \lambda^\alpha & 0 \end{pmatrix} \tag{1.1.21}$$

hence the polarisation spinors are simply

$$\epsilon^\alpha_{-1/2} = \lambda^\alpha, \quad \epsilon^{\dot{\alpha}}_{+1/2} = \tilde{\lambda}^{\dot{\alpha}}. \tag{1.1.22}$$

Gauge boson polarisations

For gauge bosons with helicity ± 1, the polarisation vectors must satisfy $p_{\alpha\dot{\alpha}}\epsilon^{\alpha\dot{\alpha}} = 0$. Thus the solutions can be written, up to a gauge transformation, as

$$\epsilon^{\alpha\dot{\alpha}}_{+,i} = c_+ \frac{\tilde{\lambda}_i^{\dot{\alpha}}\mu_i^\alpha}{\langle\lambda_i\mu_i\rangle}, \quad \epsilon^{\alpha\dot{\alpha}}_{-,i} = c_- \frac{\lambda_i^\alpha\tilde{\mu}_i^{\dot{\alpha}}}{[\tilde{\lambda}_i\tilde{\mu}_i]}, \tag{1.1.23}$$

where $\mu, \tilde{\mu}$ are *arbitrary* reference spinors which are linearly independent of $\lambda, \tilde{\lambda}$ and c_+, c_- are non-zero constants. It is worth noting that we can redefine the reference spinors

$$\mu \to \mu + \delta\mu, \quad \tilde{\mu} \to \tilde{\mu} + \delta\tilde{\mu}, \tag{1.1.24}$$

such that the $\epsilon_\pm$ only change by a shift proportional to $p_{\alpha\dot{\alpha}}$. This is equivalent to a gauge transformation which leaves the amplitude invariant hence we may choose $\mu, \tilde{\mu}$ for *every* external particle to simplify calculations.

A typical example of the power of spinor-helicity variables is the amplitude for n gluons where all but two gluons have positive helicity and the others have negative helicity. These are the *Maximally Helicity Violating*, or MHV, amplitudes, which at tree-level are given by the Parke-Taylor factor [15]

$$A_n^{\text{MHV}}(1^+, \ldots, i^-, \ldots, j^-, \ldots, n^+) = \delta^{(4)}\left(\sum_{i=1}^n \lambda_\alpha\tilde{\lambda}_{\dot{\alpha}}\right)\frac{\langle ij\rangle^4}{\langle 12\rangle\langle 23\rangle\cdots\langle n1\rangle}, \tag{1.1.25}$$

where the delta function enforces momentum conservation. The parity-conjugate of (1.1.25), the *anti-MHV* or $\overline{\text{MHV}}$ amplitude, has the same form except with square brackets

$$A_n^{\overline{\text{MHV}}}(1^-, \ldots, i^+, \ldots, j^+, \ldots, n^-) = \delta^{(4)}\left(\sum_{i=1}^n \lambda_\alpha\tilde{\lambda}_{\dot{\alpha}}\right)\frac{[ij]^4}{[12][23]\cdots[n1]}. \tag{1.1.26}$$

For six external gluons the above result is equivalent to the sum of 220 diagrams just at tree-level. This fact is hidden when we express these amplitudes in four-vectors and can only be seen when we introduce spinor-helicity variables.

1.1.3 BCFW

The Britto-Cachazo-Feng-Witten (BCFW) recursion relation [17, 84] is a very powerful on-shell technique for calculating scattering amplitudes using their analytic properties (locations of singularities). It allows us to recursively express a tree-level amplitude in terms of amplitudes with only three particles. First we will explore the special kinematics of

three-particle scattering in a massless theory. It should also be noted that similar recursion relations exist for massive particles [85] and loop amplitudes [86, 87].

The three-point gluon amplitude

For real null momenta, there are no three-point amplitudes as

$$p_1^\mu + p_2^\mu + p_3^\mu = 0 \quad \rightarrow \quad p_1 \cdot p_2 = p_2 \cdot p_3 = p_3 \cdot p_1 = 0, \tag{1.1.27}$$

leaves no invariants amplitudes could depend on. The only solution to the above conditions is that all momenta are collinear, $p_1 \parallel p_2 \parallel p_3$.

The situation is different for complex momenta, $p_i \in \mathbb{C}$. In this case $\lambda_i, \tilde{\lambda}_i$ are independent and $\langle ij\rangle[ji] = 0$ can be solved by either $\langle ij\rangle = 0, \forall\, i,j = 1,2,3$ or $[ij] = 0, \forall\, i,j = 1,2,3$. Hence either $\lambda_1^\alpha \propto \lambda_2^\alpha \propto \lambda_3^\alpha$ (collinear left-handed spinors) or $\tilde{\lambda}_1^\alpha \propto \tilde{\lambda}_2^\alpha \propto \tilde{\lambda}_3^\alpha$ (collinear right-handed spinors) solve the constraints $p_i \cdot p_j = 0$. The two choices correspond to the three-gluon MHV and $\overline{\text{MHV}}$ amplitudes respectively. They are given by

$$A_3^{\text{MHV}}(i^-, j^-) = \frac{\langle ij\rangle^4}{\langle 12\rangle\langle 23\rangle\langle 31\rangle}, \quad A_3^{\overline{\text{MHV}}}(i^+, j^+) = \frac{[ij]^4}{[12][23][31]}. \tag{1.1.28}$$

These results can be argued to be the only functional forms compatible with the helicity assignments of the external particles and the vanishing of $\langle ij\rangle$ and $[ij]$, respectively, up to a free constant which is identified with the coupling constant [88].

The recursion relation

Now that we have the fundamental building blocks with which to build amplitudes, we can now discuss the BCFW recursion relation itself.

We begin by introducing a complex shift to two of the spinors, which preserves the on-shell condition, and see how the amplitude behaves. You can shift any two legs but for simplicity we shall shift the spinors of two neighbouring legs, 1 and n.

$$\begin{aligned} \lambda_1 &\rightarrow \hat{\lambda}_1(z) = \lambda_1 - z\lambda_n, \\ \tilde{\lambda}_n &\rightarrow \hat{\tilde{\lambda}}_n(z) = \tilde{\lambda}_n + z\tilde{\lambda}_1, \end{aligned} \tag{1.1.29}$$

with $z \in \mathbb{C}$, and $\tilde{\lambda}_1$ and λ_n are left unchanged. This changes the momenta,

$$\begin{aligned} p_1^{\alpha\dot{\alpha}} &\rightarrow \hat{p}_1^{\alpha\dot{\alpha}}(z) = (\lambda_1 - z\lambda_n)^\alpha \tilde{\lambda}_1^{\dot{\alpha}}, \\ p_n^{\alpha\dot{\alpha}} &\rightarrow \hat{p}_n^{\alpha\dot{\alpha}}(z) = \lambda_n^\alpha (\tilde{\lambda}_n + z\tilde{\lambda}_1)^{\dot{\alpha}}. \end{aligned} \tag{1.1.30}$$

As mentioned, this deformation preserves the on-shell conditions but it also preserves momentum conservation

$$\hat{p}_1^2(z) = 0, \quad \hat{p}_n^2(z) = 0, \quad \hat{p}_1(z) + \hat{p}_n(z) = p_1 + p_n, \tag{1.1.31}$$

and the deformed partial amplitude is written as

$$\mathscr{A}_n(z) = \delta^{(4)}\left(\sum_{i=1}^n p_i\right) A_n(z). \tag{1.1.32}$$

The BCFW recursion relation focusses on understanding the behaviour of the function $A_n(z)$ in the complex z plane. To this end we will first analyse the locations of the poles

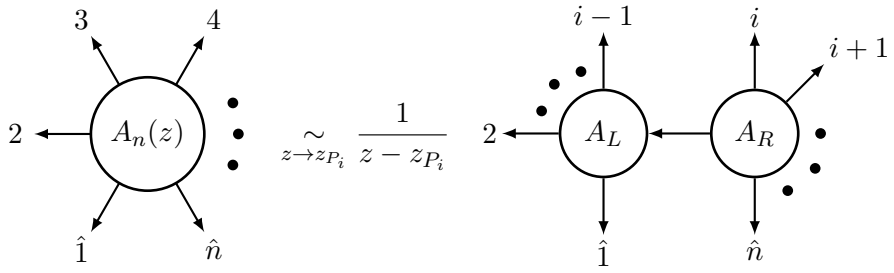

Figure 1.2: Factorisation of the z deformed amplitude on the pole $z = z_{P_i}$

of $A_n(z)$. We will then show that the residues of the poles correspond to products of lower point amplitudes. Finally, we will determine the large z behaviour of $A_n(z)$.

Our first step is to check that $A(z)$ only has poles where the Feynman propagators have poles. Due to colour-ordering, these propagators take the form

$$\frac{1}{(p_i + p_{i+1} + \cdots + p_j)^2}, \tag{1.1.33}$$

i.e. their denominators are formed by a sum of adjacent momenta. With the shifted momenta these propagators take the form

$$\begin{aligned}\frac{1}{\hat{P}_i(z)} \coloneqq& \frac{1}{(\hat{p}_1(z) + p_2 + \cdots + p_{i-1})^2} = \frac{1}{(p_i + p_{i+1} + \cdots + \hat{p}_n(z))^2} \\ =& \frac{1}{P_i^2 - z\,\langle n|\,P_i|1]},\end{aligned} \tag{1.1.34}$$

where $P_i \coloneqq p_1 + p_2 + \cdots + p_{i-1}$ and $\langle n|\,P_i|1] = \lambda_{n\alpha} P_i^{\alpha\dot{\alpha}} \tilde{\lambda}_{1\dot{\alpha}}$. Note that any region momenta containing both $\hat{p}_1$ and $\hat{p}_n$ is independent of z and so cannot contribute any poles. Therefore only the propagators considered above can produce poles. We can see that $A_n(z)$ only has simple poles in z at

$$z_{P_i} = \frac{P_i^2}{\langle n|\,P_i|1]}, \quad \forall\ i \in [3, n-1]. \tag{1.1.35}$$

Now we know where the poles are, we need to know the residues at these poles. It is known that tree-level amplitudes factorise when a propagator goes on-shell. The on-shell propagator splits the amplitude into two halves, one at each end of the propagator. The propagator going on-shell can also be represented as inserting a complete set of all on-shell states. Approaching the pole z_{P_i} is equivalent to a propagator going on-shell hence near it the amplitude $A_n(z)$ factorises into a product of lower-point amplitudes, which we label as "left" and "right" amplitudes A^L and A^R. We demonstrate this in Figure 1.2.

$$\lim_{z\to z_{P_i}} A_n(z) = \frac{1}{z - z_{P_i}} \frac{-1}{\langle n|\,P_i|1]} \sum_s A_L(\hat{1}(z_{P_i}), 2, \ldots, i-1, -\hat{P}_s(z_{P_i})) \tag{1.1.36}$$

$$\times A_R(\hat{P}_{\bar{s}}(z_{P_i}), i, \ldots, n-1, \hat{n}_s(z_{P_i})), \tag{1.1.37}$$

where the sum over s runs over all possible on-shell states propagating between A_L and A_R, and $\bar{s} = -s$. In general this will depend on the field content of the theory under consideration e.g. for gluons $s = \{+1, -1\}$.

We can now use complex analysis to construct $A_n(z = 0)$ from the knowledge of the

$$A_4^{\text{MHV}}(\hat{1}^-, 2^+, 3^+, \hat{4}^-) = \quad = \frac{\langle 14\rangle^4}{\langle 12\rangle\langle 23\rangle\langle 34\rangle\langle 41\rangle}$$

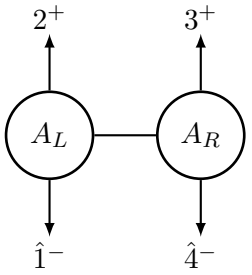

Figure 1.3: The four-point MHV amplitude with the intermediary BCFW step

poles of $A_n(z)$. We do this by looking at the function $A_n(z)/z$ and its behaviour in the limit

$$\lim_{z\to z_{P_i}} \frac{A_n(z)}{z} = -\frac{1}{z - z_{P_i}} \sum_s A_L^s(z_{P_i}) \frac{1}{P_i^2} A_R^{\bar{s}}(z_{P_i}), \tag{1.1.38}$$

where the A_L and A_R correspond to the A_L and A_R, respectively, in (1.1.37).

Using the residue theorem, we may write the original amplitude A_n as

$$\begin{aligned} A_n = A_n(z=0) &= \oint_{C_0} \frac{dz}{2\pi i} \frac{A_n(z)}{z} \\ &= \sum_{i=2}^{n-1} \sum_s A_L^s(z_{P_i}) \frac{1}{P_i^2} A_R^{\bar{s}}(z_{P_i}) + \text{Res}(z=\infty), \end{aligned} \tag{1.1.39}$$

where C_0 is a small circle around the origin at $z = 0$ that does not encompass any of the poles z_{P_i}. The step from the first line to the second line of (1.1.39) we have blown up C_0 to infinity, capturing all the poles in the complex plane z, now encircled in the opposite orientation. As $z \to \infty$ we need $A(z) \to 0$ as fast as $1/z \to 0$. This happens to be the case for gluon amplitudes but is not true in general. Hence we can drop the residue at infinity and we arrive at the BCFW recursion relation

$$A_n = \sum_{i=2}^{n-1} \sum_s A_L^s(z_{P_i}) \frac{1}{P_i^2} A_R^{\bar{s}}(z_{P_i}). \tag{1.1.40}$$

We stated above that we chose adjacent legs for simplicity, if we had chosen non-adjacent legs this would result in more BCFW diagrams. In general, different shifts in the momenta correspond to different, yet equivalent, representations of the same amplitude, which we will see later in this thesis.

In Figure 1.2 an n-point amplitude was factorised into sub-amplitudes. If we use the recursion relation repeatedly we can keep factorising sub-amplitudes until we have a series of three-point sub-amplitudes where at least one of the legs is an on-shell propagator. For example, the BCFW recursion of the four-point MHV amplitude is given in Figure 1.3.

1.1.4 Factorisation Poles

We have already seen that tree amplitudes factorise into the products of lower ones when taking the residues of the poles in propagators. However, one cannot take multiple residues in arbitrary channels. Mandelstams label different channels but they also correspond to an assignment of particles to incoming and outgoing states. Two channels are described

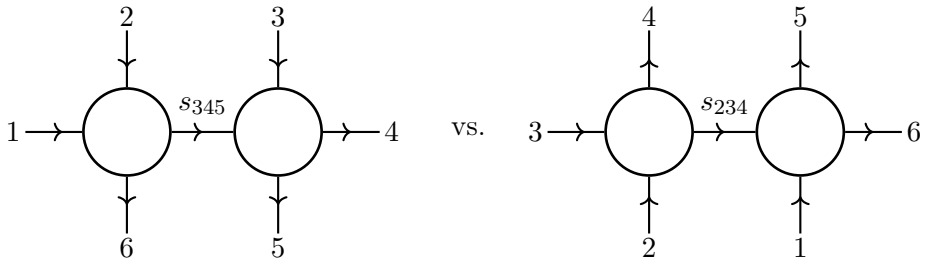

Figure 1.4: Two overlapping channels for six-point scattering. The discontinuity of an amplitude in the s_{345} channel (left) cannot be followed by a discontinuity in the s_{234} channel (right).

as overlapping if the four sets into which they divide the particles - (incoming, incoming), (incoming, outgoing), (outgoing, incoming), (outgoing, outgoing) - are all non-empty. An example of two overlapping channels is given in Figure 1.4. Hence taking consecutive residues in overlapping channels corresponds to the following condition

$$\text{Res}_{s_{jj+1j+2}}(\text{Res}_{s_{ii+1i+2}}A) = 0, \quad \text{for } j = i \pm 1, i \pm 2. \tag{1.1.41}$$

Similar conditions exists for loop amplitudes in the Steinmann conditions where an analogous statement restricts consecutive *discontinuities* in overlapping channels.

1.2 Scattering equations

In [80, 81], the authors described the Cachazo-He-Yuan (CHY) formalism, showing that any n-point tree-level amplitude, in an arbitrary number of dimensions, can be expressed as a multiple integral over the moduli space of n marked points on the Riemann sphere $\mathfrak{M}_{0,n}$

$$\mathcal{A}_n = \int \frac{\prod_{a=1}^n d\sigma_a}{\text{vol}SL(2,\mathbb{C})} \prod_a{}' \delta(f_a)\mathcal{I}_n. \tag{1.2.1}$$

Since tree-level amplitudes are rational functions, the integrand is completely localised by the delta functions, which are defined as

$$\prod_a{}' \delta(f_a) \equiv (\sigma_{rp}\sigma_{pq}\sigma_{qr}) \prod_{a\neq r,p,q} \delta(f_a), \tag{1.2.2}$$

where $\sigma_{ab} \equiv \sigma_a - \sigma_b$ and we are free to choose r, p, q at our convenience. The arguments of the delta functions are the so-called *scattering equations*, which establish a map from a configuration of n massless momenta to the moduli space $\mathfrak{M}_{0,n}$, and are given by

$$f_a = \sum_{b\neq a} \frac{k_a \cdot k_b}{\sigma_a - \sigma_b} = 0, \quad a = 1, 2, \ldots, n. \tag{1.2.3}$$

The integrand $\mathcal{I}_n$ contains the information on the dynamics of whichever massless theory one is considering. There are many so-called "special" theories that can be described using the CHY formalism including, but not limited to: Yang-Mills, Einstein Gravity, Einstein-Yang-Mills, Einstein-Maxwell, Born-Infeld, and Dirac-Born-Infeld. A full list and the relations between them can be found in [89].

One of these theories in particular will play a part in the second half of this thesis; the massless biadjoint ϕ^3 theory. A proof for the CHY formalism in an arbitrary number of dimensions was given in [90]. The authors first established a result for massless ϕ^3 theory using BCFW, then extending this to the gauge theory case. They also generalised CHY to massive particles.

As solving the scattering equations is infamously difficult, in later chapters we shall be examining ϕ^3 theory through the lens of *tropical geometry* by generalising the approach of summing over Feynman diagrams. This will also allow us to generalise the scattering equations beyond $\mathfrak{M}_{0,n}$.

1.3 $\mathcal{N} = 4$ super Yang-Mills theory

The majority of the research in this thesis involves a particular gauge theory - $\mathcal{N} = 4$ supersymmetric Yang-Mills theory (SYM). This is a superconformal field theory and the most symmetric gauge theory in four dimensions (without gravity) in which a substantial amount of progress has been made in the study of amplitudes. In this section we will review the symmetries and properties of this theory and how they affect the form of amplitudes within it, often simplifying calculations. The Lagrangian of $\mathcal{N} = 4$ super Yang-Mills theory is given by

$$\begin{aligned}\mathcal{L} = \frac{1}{g_{\text{YM}}^2}\,\text{Tr}\Big[-\frac{1}{4}F_{\mu\nu}^2 - D_\mu\phi_{AB}D^\mu\phi^{AB} - \frac{1}{2}\left[\phi_{AB},\phi_{CD}\right]\left[\phi^{AB},\phi^{CD}\right] \\ + i\bar{\psi}_{\dot{\alpha}}^A\sigma_\mu^{\alpha\dot{\alpha}}D^\mu\psi_{\alpha A} - \frac{i}{2}\psi_A^\alpha\left[\phi^{AB},\psi_{\alpha B}\right] - \frac{i}{2}\bar{\psi}_{\dot{\alpha}}^A\left[\phi_{AB},\bar{\psi}^{\dot{\alpha}B}\right]\Big],\end{aligned} \tag{1.3.1}$$

where $F_{\mu\nu} = \partial_\mu A_\nu - \partial_\nu A_\mu - ig[A_\mu, A_\nu]$ is the field strength tensor and $D_\mu = \partial_\mu - igA_\mu$ is the covariant derivative. This theory consists of a gluon, A_μ, four gluinos $\psi_{\alpha A}, \bar{\psi}^{\dot{\alpha}A}$, and six real scalars (or three complex) $\phi_{AB} = -\phi_{BA}$. The form of this theory is uniquely fixed by the $\mathcal{N} = 4$ supersymmetry and it only has two tunable parameters: the gauge coupling g_{YM} and the rank N of the gauge group $SU(N)$.

1.3.1 Supersymmetry

We can see from the interaction terms in (1.3.1), that a tree-level amplitude with only gluons as external states must *only* contain gluons. This tells us that all pure gluon tree-amplitudes in SYM are the same as those from pure Yang-Mills. It turns out the pure fermion and pure scalar tree-amplitudes are related to the purely gluonic ones by supersymmetry (SUSY) transformations. It has also been shown that one-loop gluon amplitudes can be written as a sum of scalar box integrals with rational coefficients [18, 38]. Hence SUSY allows us to exchange one, more complicated integral for a sum of simpler ones. These are just two ways in which the level of SUSY in SYM can simplify calculations and reveal more about pure YM. Here we will review $\mathcal{N} = 4$ supersymmetry.

Multiplicity	Field	
2	gluons	$g^-,\ g^+$
4	chiral fermions	$\psi_{\dot{\alpha}A}$
4	anti-chiral fermions	$\bar{\psi}^A_\alpha$
6	(real) scalars	ϕ_{AB}

Table 1.1: Field content of $\mathcal{N}=4$ SYM.

For SUSY with $\mathcal{N}$ supercharges, or generators, $Q^A_\alpha, \bar{Q}_{\dot{\alpha}A}$, the SUSY algebra is

$$\begin{aligned} \{Q^A_\alpha, \bar{Q}_{\dot{\alpha}B}\} &= 2\sigma^\mu_{\alpha\dot{\alpha}} P_\mu \delta^A_B, \\ \{Q^A_\alpha, Q^B_\beta\} &= 0, \\ \{\bar{Q}_{\dot{\alpha}A}, \bar{Q}_{\dot{\beta}B}\} &= 0, \end{aligned} \tag{1.3.2}$$

where $A, B = 1, \ldots, \mathcal{N}$ are R-symmetry indices. R-symmetry transforms the Q^A_α amongst themselves, and in the case of $\mathcal{N}=4$, this is an $SU(4)$ symmetry. The algebra in (1.3.2) is a Clifford algebra hence we can define Clifford vacua which are ground states for the supercharges

$$Q^A_\alpha \left|g^+\right\rangle = 0, \qquad \bar{Q}_{\dot{\alpha}A} \left|g^-\right\rangle = 0, \tag{1.3.3}$$

these ground states are associated with the positive and negative helicity gluons. The generators $\bar{Q}/Q$ act on these vacua as raising/lowering operators, generating a tower of helicity states, for example

$$Q^A_\alpha \left|g^-\right\rangle = \lambda_\alpha \left|\bar{\psi}\right\rangle^A, \qquad \bar{Q}_{\dot{\alpha}A} \left|g^+\right\rangle = \tilde{\lambda}_{\dot{\alpha}} \left|\psi\right\rangle_A. \tag{1.3.4}$$

Hence for $\mathcal{N}=4$ we have four left-handed and four right-handed fermions and continued acting of the generators produces a further six real scalars (or three complex scalars). We summarise these states in Table 1.1.

The only representation of this superalgebra is an on-shell vector supermultiplet which comprises all the states above which transform in the adjoint of the gauge group. This means we can collect these states together into one superfield [91]

$$\left|\Phi\right\rangle = \left|g^+\right\rangle + \eta^A \left|\psi_A\right\rangle + \frac{1}{2!}\eta^A\eta^B \left|\phi_{AB}\right\rangle + \frac{1}{3!}\eta^A\eta^B\eta^C \left|\psi_{ABC}\right\rangle + \eta^1\eta^2\eta^3\eta^4 \left|g^-\right\rangle, \tag{1.3.5}$$

where η^A is a Grassmann variable transforming in the $SU(4)$ fundamental representation.

The on-shell chiral superspace is parametrised by four fermionic coordinates $\{\theta^\alpha_A\}$. The state $\left|\Phi\right\rangle$ is an eigenstate of the generators

$$Q^A_\alpha \left|\Phi\right\rangle = q^A_\alpha \left|\Phi\right\rangle, \tag{1.3.6}$$

where the eigenvalue $q^A_\alpha = \lambda_\alpha \eta^A$ is the *supermomentum* carried by the state $\left|\Phi\right\rangle$ in the θ^α_A direction. We summarise the natural representation of the single-particle SUSY generators in on-shell superspace

$$P_{\alpha\dot{\alpha}} = \lambda_\alpha \tilde{\lambda}_{\dot{\alpha}}, \quad Q^A_\alpha = \lambda_\alpha \eta^A, \quad \bar{Q}_{\dot{\alpha}A} = \tilde{\lambda}_{\dot{\alpha}} \frac{\partial}{\partial \eta^A}, \tag{1.3.7}$$

where we have used $P_{\alpha\dot{\alpha}}$ as is convention when discussing generators.

1.3.2 Superamplitudes

We can see in (1.3.7) that the operators $p_{\alpha\dot{\alpha}}$ and Q_α^A are multiplicative while $\bar{Q}_{\dot{\alpha}A}$ is a first-order differential operator. The condition that superamplitudes be invariant under the multiplicative operators requires their general form to be

$$\mathcal{A}_n = \frac{\delta^{0|8}\left(\sum_{i=1}^n \lambda_i \eta_i\right) \delta^{(4)}\left(\sum_{i=1}^n \lambda_i \tilde{\lambda}_i\right)}{\langle 12\rangle\langle 23\rangle \cdots \langle n1\rangle} \mathcal{P}_n, \tag{1.3.8}$$

where $\delta^{a|b}$ corresponds to a bosonic constraints and b fermionic ones. The fermionic delta function enforces conservation of super-momentum and corresponds to an expansion

$$\delta^{0|8}\left(\sum_{i=1}^n \lambda_{i\alpha}\eta_i^A\right) = \prod_{\alpha=1,2}\prod_{A=1}^4 \sum_{i=1}^n \lambda_{i\alpha}\eta_i^A. \tag{1.3.9}$$

Due to the $SU(4)$ R-symmetry, the function $\mathcal{P}_n$ has an η-expansion of the form

$$\mathcal{P}_n = \mathcal{P}_n^{(0)} + \mathcal{P}_n^{(4)} + \mathcal{P}_n^{(8)} + \cdots + \mathcal{P}_n^{(4n-16)} \tag{1.3.10}$$

where $\mathcal{P}_n^{(k)} \sim \mathcal{O}(\eta^k)$. Each term in this expansion corresponds to a helicity configuration of the external particles

$$\mathcal{P}^{(4k)} \to \mathrm{N}^k\mathrm{MHV}, \tag{1.3.11}$$

where an N^kMHV amplitude has $k+2$ negative helicity particles and $n-k-2$ positive helicity particles. Hence the $k=0$ term corresponds to the MHV superamplitude. It can be shown that $\mathcal{P}^{(0)} = 1$, thus the MHV tree-superamplitude is given by the prefactor in (1.3.8)

$$\mathcal{A}_n^{\mathrm{MHV}} = \frac{\delta^{0|8}\left(\sum_{i=1}^n \lambda_i \eta_i\right) \delta^{(4)}\left(\sum_{i=1}^n \lambda_i \tilde{\lambda}_i\right)}{\langle 12\rangle\langle 23\rangle \cdots \langle n1\rangle}, \tag{1.3.12}$$

where the $\overline{\mathrm{MHV}}$ amplitude follows from parity ($\lambda \to \tilde{\lambda}, \eta \to \bar{\eta}$) and a Fourier transformation back to η-space. Integrating the superamplitude over the η's, in accordance with Grassmann calculus

$$\int d\eta^A \eta^A = 1, \quad \int d\eta^A = 0, \tag{1.3.13}$$

selects a specific state from (1.3.5)

$$\begin{aligned}
\int d^4\eta &\to |g^-\rangle\,, \\
\epsilon_{ABCD}\int d^4\eta\ \eta^A &\to |\psi\rangle_{BCD}\,, \\
\frac{1}{2!}\epsilon_{ABCD}\int d^4\eta\ \eta^A\eta^B &\to |\phi\rangle_{CD}\,, \\
\frac{1}{3!}\epsilon_{ABCD}\int d^4\eta\ \eta^A\eta^B\eta^C &\to |\psi\rangle_{D}\,, \\
\frac{1}{4!}\epsilon_{ABCD}\int d^4\eta\ \eta^A\eta^B\eta^C\eta^D &\to |g^+\rangle\,,
\end{aligned} \tag{1.3.14}$$

where $d^4\eta \equiv d\eta^1 d\eta^2 d\eta^3 d\eta^4$ and the Grassmann delta functions in the amplitudes ensure that the η's are localised. Thus SUSY reduces the number of calculations we have to

perform; once we have calculated a pure gluon amplitude in SYM we can generate the corresponding fermion and scalar amplitudes simply by SUSY transformations.

1.3.3 Super-BCFW

With the introduction of superamplitudes, we can now give a short review of the supersymmetric extension of the BCFW recursion relation. We begin by introducing a shift in the Grassmann variable η^A in a similar way as we did for the spinors in (1.1.29)

$$\hat{\eta}_1 = \eta_1, \quad \hat{\eta}_n = \eta_n + z\eta_1, \tag{1.3.15}$$

where we have dropped the $SU(4)$ index for clarity. Similarly, this shift conserves supermomentum

$$\begin{aligned} q_1 \to \hat{q}_1 &= (\lambda_1 - z\lambda_n)\hat{\eta}_1, \\ q_n \to \hat{q}_n &= \lambda_n \hat{\eta}_n, \\ \hat{q}_1 + \hat{q}_n &= q_1 + q_n. \end{aligned} \tag{1.3.16}$$

From here, the steps for deriving the super-BCFW recursion are the same as those given above. The amplitude is split into a left and right part and the knowledge of the poles of these parts allow us to derive a form for the unshifted superamplitude

$$\begin{aligned} \mathcal{A}_n = \sum_{i=3}^{n-1} \int d^4\eta_{\hat{P}_i} \mathcal{A}_i^L(\hat{1}(z_{P_i}), 2, \ldots, i-1, -\hat{P}(z_{P_i})) \\ \times \frac{1}{P_i^2} \mathcal{A}_{n-i+2}^R(\hat{P}(z_{P_i}), i, \ldots, n-1, \hat{n}(z_{P_i})), \end{aligned} \tag{1.3.17}$$

where A^L, A^R have their bosonic delta-functions $\delta^{(4)}(\sum_i \lambda_i \tilde{\lambda}_i)$ stripped-off but the fermionic ones remain included.

It will be useful for later discussions to review the NMHV derivation from super-BCFW which will closely follow that of [92].

One can decompose the super-BCFW recursion (1.3.17) into the different Grassmann degree contributions i.e. decomposing the superamplitudes into their various $\mathrm{N}^k\mathrm{MHV}$ parts as in (1.3.10). This results in a generalisation of the super-BCFW recursion

$$\begin{aligned} \mathcal{A}_n^{\mathrm{N}^k\mathrm{MHV}} = \int \frac{d^4\eta_P}{P^2} \mathcal{A}_3^{\overline{\mathrm{MHV}}}(z_P) \mathcal{A}_{n-1}^{\mathrm{N}^k\mathrm{MHV}}(z_P) \\ + \sum_{m=0}^{k-1} \sum_{i=4}^{n-1} \int \frac{d^4\eta_{P_i}}{P_i^2} \mathcal{A}_i^{\mathrm{N}^m\mathrm{MHV}}(z_{P_i}) \mathcal{A}_{n-i+2}^{\mathrm{N}^{(k-m-1)}\mathrm{MHV}}(z_{P_i}). \end{aligned} \tag{1.3.18}$$

This recursion relation demonstrates an iterative structure for helicity amplitudes. For example, in order to calculate an NMHV_n amplitude (where the subscript denotes the number of particles), we need to know the NMHV_{n-1}, $\mathrm{MHV}_{k<n}$, and $\overline{\mathrm{MHV}}_n$ amplitudes

$$\begin{aligned} \mathcal{A}_n^{\mathrm{NMHV}} &= \int \frac{d^4P}{P^2} \int d^4\eta_{\hat{P}} \mathcal{A}_3^{\overline{\mathrm{MHV}}}(z_P) \mathcal{A}_{n-1}^{\mathrm{NMHV}}(z_P) \\ &\quad + \sum_{i=4}^{n-1} \int \frac{d^4P_i}{P_i^2} \int d^4\eta_{P_i} \mathcal{A}_i^{\mathrm{MHV}}(z_{P_i}) \mathcal{A}_{n-i+2}^{\mathrm{MHV}}(z_{P_i}), \\ &\equiv A + B, \end{aligned} \tag{1.3.19}$$

where A, B are homogeneous and inhomogeneous terms respectively. The inhomogeneous term can be straightforwardly computed as it is built out of MHV amplitudes only, thus we have this contribution to the n-point NMHV amplitude

$$B = \frac{\delta^{(4)}(p)\delta^{(8)}(q)}{\prod_{j=1}^{n}\langle jj+1\rangle}\sum_{i=4}^{n-1} R_{n;2i}, \tag{1.3.20}$$

where p and q are total momentum and supermomentum respectively. Here $R_{r;st}$ is called an *R-invariant* (due to its invariance under the dual superconformal symmetry, something we shall discuss in more detail shortly) which has the form

$$R_{r;st} = \frac{\langle ss-1\rangle\langle tt-1\rangle\delta^{(4)}(\Xi_{r;st})}{x_{st}^2\,\langle r|\,x_{rs}x_{st}\,|t\rangle\,\langle r|\,x_{rs}x_{st}\,|t-1\rangle\,\langle r|\,x_{rt}x_{ts}\,|s\rangle\,\langle r|\,x_{rt}x_{ts}\,|s-1\rangle}, \tag{1.3.21}$$

where the Grassmann odd quantity $\Xi_{r;st}$ is given by

$$\Xi_{r;st} = \langle r|\,x_{rs}x_{st}\,|\theta_{tr}\rangle + \langle r|\,x_{rt}x_{ts}\,|\theta_{sr}\rangle\,, \tag{1.3.22}$$

and

$$x_{ij} \coloneqq p_i + p_{i+1} + \cdots + p_{j-1}, \qquad \theta_{ij} \coloneqq q_i + q_{i+1} + \cdots + q_{j-1}, \tag{1.3.23}$$

are the dual variables or region momenta which will play a more significant role in the next section.

The most trivial case for NMHV is five-points where $\text{NMHV}_5 = \overline{\text{MHV}}_5$ which we could calculate from (1.3.12) but it is an instructive case nevertheless. Since there is no four-point NMHV amplitude, the only contribution to NMHV_5 comes from the inhomogeneous term (1.3.20)

$$\mathcal{A}_5^{\text{NMHV}} = \frac{\delta^{(4)}(p)\delta^{(8)}(q)}{\prod_{j=1}^{5}\langle jj+1\rangle} R_{5;24}. \tag{1.3.24}$$

Requiring cyclic symmetry of the amplitude implies

$$R_{5;24} = R_{1;35} = R_{2;41} = R_{3;52} = R_{4;13}, \tag{1.3.25}$$

where we have dropped the supermomentum delta function for clarity. These identities are a first example of a general identity for n points

$$\sum_{s,t} R_{r;st} = \sum_{s,t} R_{r';st}, \tag{1.3.26}$$

where the sum is over all values of s, t such that r, s, t (or r', s, t) are ordered cyclically with $|r-s| \geq 2$ (or $|r'-s| \geq 2$).

The general n-point NMHV amplitude can be generated from the $(n-1)$-point one by assuming the ansatz

$$\mathcal{A}_n^{\text{NMHV}} = \mathcal{A}_n^{\text{MHV}}\mathcal{P}_n^{\text{NMHV}} = \frac{\delta^{(4)}(p)\delta^{(8)}(q)}{\langle 12\rangle\langle 23\rangle\cdots\langle n1\rangle}\sum_{2\leq s<t\leq n-1} R_{n;st}, \tag{1.3.27}$$

to be true and proving by induction. By assuming the above holds for $n-1$ we can

substitute it into the homogeneous term A in (1.3.19)

$$A = \int \frac{d^4P}{P^2} \int d^4\eta_{\hat{P}} \mathcal{A}_3^{\overline{\text{MHV}}}(z_P) \mathcal{A}_{n-1}^{\text{MHV}} \mathcal{P}_{n-1}^{\text{NMHV}}(\hat{P}, 3, \ldots, \bar{n}), \tag{1.3.28}$$

where we have used cyclic symmetry to identify the legs $\{1, 2, \ldots, n-1\}$ with the legs $\{\hat{P}, 3, 4, \ldots, n\}$. Due to the uniqueness of three-point kinematics and homogeneity of R-invariants, the explicit dependency on $\hat{P}$ can be removed, thus we find

$$A = \frac{\delta^{(4)}(p)\delta^{(8)}(q)}{\prod_{j=1}^{n}\langle jj+1\rangle} \sum_{3\leq s<t\leq n-1} R_{n;st}. \tag{1.3.29}$$

We can see that (1.3.20) is the missing $s = 2$ term to complete (1.3.29) into the ansatz (1.3.27)

$$A + B = \mathcal{A}_n^{\text{NMHV}} = \frac{\delta^{(4)}(p)\delta^{(8)}(q)}{\langle 12\rangle\langle 23\rangle \cdots \langle n1\rangle} \sum_{2\leq s<t\leq n-1} R_{n;st}. \tag{1.3.30}$$

It was also shown in [92] that one can *completely solve* the super-BCFW recursion, finding an exact analytic expression for all tree-level superamplitudes in $\mathcal{N} = 4$ SYM.

1.3.4 Dual conformal symmetry and twistors

It was shown in [3] that the colour-ordered partial amplitudes in planar $\mathcal{N} = 4$ super Yang-Mills exhibit a symmetry not present in the Lagrangian - dual superconformal symmetry. Introducing dual variables

$$p_i^{\alpha\dot{\alpha}} = \lambda_i^\alpha \tilde{\lambda}_i^{\dot{\alpha}} = x_{i+1}^{\alpha\dot{\alpha}} - x_i^{\alpha\dot{\alpha}}\,, \qquad q_i^{\alpha A} = \lambda_i^\alpha \eta_i^A = \theta_{i+1}^{\alpha A} - \theta_i^{\alpha A}\,, \tag{1.3.31}$$

it can be shown that amplitudes in SYM exhibit a formal superconformal invariance in the dual (x, θ) space. By the identification $x_{n+1} = x_1$, we can see that these dual variables automatically satisfy momentum conservation. This can be seen diagrammatically in Figure 1.5, where the dual variables form a closed, light-like polygon. This also demonstrates the duality between scattering amplitudes and Wilson loops in SYM at weak coupling. This duality has also been show to hold at strong coupling [50–55, 93–98]. This duality has very profound consequences for the scattering amplitudes. In particular, the scattering amplitude exhibits the anomalous conformal symmetry acting on the Wilson loop. The fact that the momenta are null means that the geometry in the dual space is associated with null lines, for which Penrose's (super)twistor variables are most appropriate [99],

$$\mathcal{Z}_i = (Z_i \,|\, \chi_i)\,, \qquad Z_i^{\alpha,\dot{\alpha}} = (\lambda_i^\alpha, x_i^{\beta\dot{\alpha}}\lambda_{i\beta})\,, \qquad \chi_i^A = \theta_i^{\alpha A}\lambda_{i\alpha}. \tag{1.3.32}$$

Hence the kinematics of scattering amplitudes or light-like Wilson-loops are naturally parametrised using n momentum twistors $Z_i \in \mathbb{CP}_3$ with $i = 1, \ldots, n$. The χ_i are Grassmann variables which complete the Z_i into supertwistors. They transform in the fundamental representation of the $su(4)$ R-symmetry and encode all the different possible choices of NMHV component amplitudes which may be extracted from the NMHV superamplitude. Each twistor also carries an index A which indicates the linear action of the sl_4 dual conformal symmetry. The basic sl_4 invariants are the Plücker coordinates $\langle ijkl\rangle$

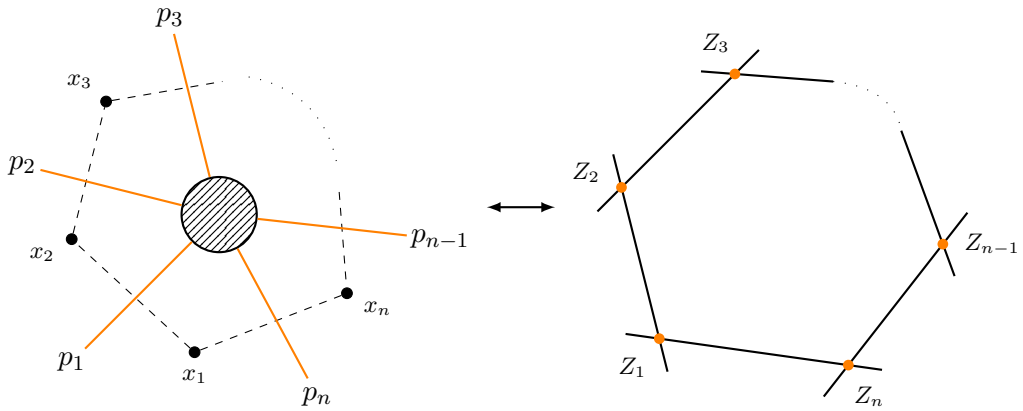

Figure 1.5: Equivalence between an amplitude in momentum space and a closed, light-like polygon in twistor space.

where

$$\langle ijkl\rangle = \epsilon_{ABCD} Z_i^A Z_j^B Z_k^C Z_l^D = \det(Z_i Z_j Z_k Z_l)\,. \tag{1.3.33}$$

These four-brackets are Plücker coordinates because the n twistors Z_i can be thought of as parameterising a Grassmannian $\mathrm{Gr}(4,n)$ modulo the rescaling of each of the Z_i individually. Since the global rescaling of all Z_i simultaneously is already taken into account in the definition of the Grassmannian, the kinematical space is identified with

$$\mathrm{Conf}_n(\mathbb{P}^3) = \mathrm{Gr}(4,n)/(\mathbb{C}^*)^{n-1}\,. \tag{1.3.34}$$

In Chapter 2, we will see that this space comes equipped with a very powerful mathematical structure called a *cluster algebra*.

In special cases where the four labels of the Plücker coordinate consists of two adjacent pairs, $\langle i-1\, i\, j-1\, j\rangle$, they correspond to multi-particle Mandelstam invariants

$$x_i = \frac{Z_{i-1}\wedge Z_i}{\langle i-1\, i\, I\rangle}\,, \qquad s_{i,\ldots,j-1} = x_{ij}^2 = \frac{\langle i-1\, i\, j-1\, j\rangle}{\langle i-1\, iI\rangle\langle j-1\, jI\rangle}\,, \tag{1.3.35}$$

where I is the 'infinity twistor' which is necessary to relate twistor brackets to non-conformally invariant quantities such as Mandelstam invariants. However, a dual-conformal object, examples of which we shall see shortly, depends only on the homogeneous rational combinations of these brackets such that the dependence on the infinity twistor cancels out.

When written in twistor variables [5], R-invariants (1.3.21) depend on five twistors and are defined as

$$[ijklm] = \frac{\delta^{(0|4)}(\chi_i\langle jklm\rangle + \text{cyclic})}{\langle ijkl\rangle\langle jklm\rangle\langle klmi\rangle\langle lmij\rangle\langle mijk\rangle}\,. \tag{1.3.36}$$

These are the basic invariants of the Yangian symmetry [100] of scattering amplitudes which combines both the superconformal and dual superconformal symmetries. The R-invariants are not all independent; there are $\binom{n-1}{4}$ linearly independent ones due to identities of the form

$$[abcde] - [bcdef] + [cdefa] - [defab] + [efabc] - [fabcd] = 0\,. \tag{1.3.37}$$

which is equivalent to the identity (1.3.26).

1.3.5 Loop amplitudes in SYM

Our discussion so far has only involved tree-amplitudes but calculating amplitudes at loop level can be much more challenging. Fortunately, dual conformal symmetry can simplify loop amplitude calculations quite substantially.

When studying loop amplitudes in SYM, it is useful to factor out the MHV tree-level amplitude

$$M_n^{(L)}(\epsilon) = \frac{A_n^{(L)}}{A_n^{(0)}}. \tag{1.3.38}$$

where ϵ is the dimensional regularisation parameter in $D = 4 - 2\epsilon$. The first indication of an underlying structure of loop amplitudes was found by Anastasiou, Bern, Dixon, and Kosower (ABDK) [101]. They observed that the four-particle, two-loop amplitude $M_4^{(2)}$ can be expressed in terms of the one-loop result. Motivated by the resummation and exponentiation of IR singularities in [102] and the connection to n-point amplitudes in [103], Bern, Dixon, and Smirnov (BDS) conjectured an exponentiation of the planar MHV n-point amplitudes at L-loops

$$\mathcal{M}_n^{\text{BDS}} = \frac{\mathcal{A}_n}{\mathcal{A}_n^{(0)}} = \exp\left[\sum_{L=1}^{\infty} a^L \left(f^{(L)}(\epsilon) M_n^{(1)}(L\epsilon) + C^{(L)} + \mathcal{O}(\epsilon)\right)\right]. \tag{1.3.39}$$

The remarkable fact about this formula is that kinematically it only depends on the one-loop scattering amplitude. This can be explained by realising that the *BDS ansatz* is the unique solution to the dual conformal Ward identities for $n < 6$ [104]. It also accounts for collinear factorisation to all orders in perturbation theory [105].

We shall now describe the various ingredients in the BDS-ansatz (1.3.39). The factor a keeps track of the loop order of perturbation theory and is given by

$$a = 2g^2 = \frac{g_{\text{YM}}^2 N}{8\pi^2}. \tag{1.3.40}$$

The quantity $M_n^{(1)}(L\epsilon)$ is the all-orders-in-ϵ one-loop amplitude and $f^{(L)}(\epsilon)$ is given by

$$f^{(L)}(\epsilon) = f_0^{(L)} + \epsilon f_1^{(L)} + \epsilon^2 f_2^{(L)}. \tag{1.3.41}$$

The constants $f_k^{(L)}$ and $C^{(L)}$ are independent of n and ϵ. They are both polynomials in the Riemann values ζ_m with rational coefficients. They also have uniform transcendentality, something we shall discuss in more detail shortly.

The BDS ansatz was successfully verified up to five-loops at four-points [106–108] and three-loops at five-points [105, 109, 110]. However starting at six-points one can define dual conformal invariant cross-ratios

$$U_{ijkl} = \frac{x_{ij}^2 x_{kl}^2}{x_{ik}^2 x_{jl}^2}, \tag{1.3.42}$$

where the number of algebraically independent cross-ratios at n-points is given by $3(n-5)$ hence there are none for $n < 5$. The BDS ansatz captures the IR divergent part of $M_6^{(2)}$ but there is a finite correction called the *remainder function* which depends on the cross-ratios

[54, 55]. Hence for $n > 5$ the BDS ansatz takes the form

$$\mathcal{A}_n^{\text{MHV}} = \mathcal{M}_n^{\text{BDS}} \exp[R_n], \tag{1.3.43}$$

where R_n is the remainder function. This ansatz captures all infrared and collinear divergences [102, 103, 111] of the planar amplitude, thus the remainder function is finite. It is also invariant under dual conformal transformations [50, 104, 112–114]. The remainder function can be a useful object when calculating amplitudes as the n-point remainder function smoothly tends to the $(n-1)$-point remainder function in its collinear limits, providing a consistency check of results. However, the remainder function has an altered dependence on three-particle Mandelstams and does not possess the correct discontinuity structure, namely it does not obey the Steinmann conditions [47]. For loop amplitudes, the Steinmann conditions take the form

$$\text{Disc}_{s_{jj+1j+2}}(\text{Disc}_{s_{ii+1i+2}} A) = 0, \quad \text{for } j = i \pm 1, i \pm 2, \tag{1.3.44}$$

and similar for higher-particle Mandelstam invariants. As we can see, these take the same form as (1.1.41) except here we are taking consecutive discontinuities instead of residues. For $n \neq 0 \bmod 4$ one can define an infrared finite and dual conformally invariant function Y_n, which can be removed from the one-loop amplitude allowing us to define a *BDS-like* ansatz [115]

$$\mathcal{A}_n^{\text{BDS-like}} = \mathcal{A}_n^{\text{BDS}} \exp\left[\frac{\Gamma_{\text{cusp}}}{4} Y_n\right], \tag{1.3.45}$$

where

$$\Gamma_{\text{cusp}} = \sum_{L=1}^{\infty} g^{2L} \Gamma_{\text{cusp}}^L = 4g^2 - \frac{4\pi^2}{3} g^4 + \frac{44\pi^4}{45} g^6 - 4\left(\frac{73\pi^6}{315} + 8\zeta_3^2\right) g^8 + \mathcal{O}(g^{10}), \tag{1.3.46}$$

is the cusp anomalous dimension in the normalisation of e.g. [58]. The BDS-like ansatz is the unique solution to the anomalous dual conformal Ward identity [104] dependent only on the two-particle invariants $(p_i + p_{i+1})^2 = x_{ii+2}^2$ (for $n \neq 0 \bmod 4$) thus obeying the Steinmann conditions.

The scattering (super)amplitude then can be decomposed into two parts

$$\mathcal{A}_n = \mathcal{A}_n^{\text{BDS-like}} \, \mathcal{E}_n \,, \tag{1.3.47}$$

where the remaining finite piece $\mathcal{E}_n$ can be written purely in terms of the supertwistors $\mathcal{Z}_i$ and has an expansion in Grassmann degree

$$\mathcal{E}_n = \mathcal{E}_{n,\text{MHV}} + \mathcal{E}_{n,\text{NMHV}} + \ldots, \tag{1.3.48}$$

and is invariant under the dual conformal symmetry.

The MHV term in (1.3.48) is of degree zero in the Grassmann χ_i variables and hence is just a function of the Z_i and is given by

$$\mathcal{E}_{n,\text{MHV}} = \exp\left[R_n - \frac{\Gamma_{\text{cusp}}}{4} Y_n\right]. \tag{1.3.49}$$

Dual conformal symmetry implies it is a function of the four-brackets $\langle ijkl \rangle$. It is homogeneous of degree zero in each Z_i and so is a function on the configuration space of n points

Object	Weight
π	1
ζ_n	n
$\log(x)$	1
$\mathrm{Li}_n(x)$	n

Table 1.2: Some examples of transcendental objects and their weights. $\mathrm{Li}_n(x)$ is the classical polylogarithm.

in $\mathbb{P}^3$, denoted $\mathrm{Conf}_n(\mathbb{P}^3)$.

The NMHV term in (1.3.48) is of Grassmann degree four and can be written in terms of R-invariants (1.3.36), which are multiplied by dual conformally invariant functions E_{ijklm} on $\mathrm{Conf}_n(\mathbb{P}^3)$,

$$\mathcal{E}_{n,\mathrm{NMHV}} = \sum_{i,j,k,l,m=1}^{n} [ijklm] E_{ijklm}(Z_1, \ldots, Z_n)\,, \tag{1.3.50}$$

The function $\mathcal{E}_{n,\mathrm{MHV}}$ depends only on the cross-ratios of the Wilson loop,

$$u_{ij} = \frac{x^2_{ij+1} x^2_{ji+1}}{x^2_{ij} x^2_{i+1,j+1}}\,. \tag{1.3.51}$$

For a seven-particle process, there are seven such cross-ratios satisfying a Gram determinant constraint which makes $\mathcal{E}_{7,\mathrm{MHV}}$ a six-variable function.

In what follows the functions $\mathcal{E}_{n,\mathrm{MHV}}$ and $\mathcal{E}_{n,\mathrm{NMHV}}$ (and hence the functions E_{ijklm}) admit perturbative expansions of the form

$$F = \sum_{L=0}^{\infty} g^{2L} F^{(L)}\,. \tag{1.3.52}$$

For the hexagon and heptagon amplitudes that we shall discuss later on we need only consider MHV and NMHV terms in the expansion (1.3.48) since other amplitudes are obtained by parity conjugation of these ones.

We refer the reader to [3, 5] for details on the structure of the supermultiplets and supertwistor variables.

1.3.6 Polylogarithms and symbols

In perturbation theory, it is conjectured that amplitudes in SYM are of uniform transcendentality i.e. the objects they are built out of all have the same *weight* k. Some examples of transcendental objects and their weights are given in Table 1.2. According to all current evidence, the functions appearing in six, seven, and eight-point SYM amplitudes are transcendental (or *pure*) functions of weight $2L$ where L is the loop order. These pure functions can be defined recursively by their derivatives

$$df^{(k)} = \sum_{a \in \mathcal{A}} f^{(k-1)}_{[a]} d\log a\,, \tag{1.3.53}$$

where the a are some rational (or algebraic) functions of some number of variables (called *letters*) and the sum runs over a finite set $\mathcal{A}$ of such functions (an *alphabet*). The space of functions of degree one is spanned by the set of logarithms of the letters a themselves.

The choice of the set $\mathcal{A}$ then determines a class of polylogarithmic functions recursively in the degree. For example, in the case of functions of a single variable x, the choice $\mathcal{A} = \{x, 1-x\}$ yields the class of harmonic polylogarithms [26] with indices 0 or 1. In particular, this example includes the classical polylogarithms $\mathrm{Li}_n(x)$

$$\mathrm{Li}_n(x) = \int_0^x \frac{dt}{t}\mathrm{Li}_{n-1}(t), \quad \mathrm{Li}_1(x) \equiv -\log(1-x) = \int_0^x \frac{dt}{1-t}, \tag{1.3.54}$$

where $\mathrm{Li}_n(x)$ can also be written as

$$\mathrm{Li}_n(x) = -\int_0^x d\log(1-t) \circ \underbrace{d\log(t) \circ d\log(t) \circ \cdots \circ d\log(t)}_{n-1 \text{ times}}. \tag{1.3.55}$$

Polylogarithms are iterated integrals over logarithmic singularities, a more general kind being Goncharov polylogarithms, also defined recursively

$$\begin{aligned} G(a_1, a_2, \ldots, a_n; x) &= \int_0^x \frac{dt}{t-a_1} G(a_2, \ldots, a_n; t), \\ G(a; x) &= \int_0^x \frac{dt}{t-a}, \quad a \neq 0, \quad G(\vec{0}_n; x) = \frac{1}{n!}\log^n(x). \end{aligned} \tag{1.3.56}$$

Thus the classical polylogarithms (1.3.54) are special cases of the Goncharov polylogarithms for $\{a_1, a_2, \ldots, a_n\} = \{0, 0, \ldots, 1\}$.

The formula (1.3.53) encodes the $(k-1, 1)$ part of the coproduct [62] of the function $f^{(k)}$. We write this as

$$f^{(k-1,1)} = \sum_{a \in \mathcal{A}} [f^{(k-1)}_{[a]} \otimes a], \tag{1.3.57}$$

where by convention we just record the argument of the $d\log$ in the second argument of the tensor product. The arguments of the $(k-1, 1)$ coproduct must obey the integrability relation

$$\sum_{a \in \mathcal{A}} df^{(k-1)}_{[a]} \wedge d\log a = 0, \tag{1.3.58}$$

which follows from $d^2 f^{(k)} = 0$.

If we continue applying the definition of the $(n, 1)$ coproduct iteratively to each of the functions $f^{(k-1)}_{[a]}$ all the way down to weight zero, we obtain the *symbol*, an element of the k-fold tensor product of the space of one-forms spanned by the $d\log a$ for $a \in \mathcal{A}$ (or more compactly a *word* in the alphabet $\mathcal{A}$),

$$S(f^{(k)}) = f^{(1,\ldots,1)} = \sum_{(a_1,\ldots,a_k)} c_{a_1,\ldots,a_k} [a_1 \otimes a_2 \otimes \ldots \otimes a_k], \quad c_{a_1,\ldots,a_k} \in \mathbb{Q}, \quad a_i \in \mathcal{A}. \tag{1.3.59}$$

Note that by common convention we write the letters a rather than $d\log a$ in the arguments of the tensor product. This leads to the property that symbols with products of functions in their arguments decompose as follows,

$$[a \otimes b\, b' \otimes c] = [a \otimes b \otimes c] + [a \otimes b' \otimes c], \tag{1.3.60}$$

and similarly that symbols with powers of functions in their arguments obey

$$[a \otimes b^p \otimes c] = p\,[a \otimes b \otimes c] \qquad p \in \mathbb{Q}. \tag{1.3.61}$$

Some symbol examples are given below

$$\begin{aligned}\mathcal{S}(\pi) &= 0,\\ \mathcal{S}(\zeta_n) &= 0,\\ \mathcal{S}(\log(x)) &= [x],\\ \mathcal{S}(\mathrm{Li}_n(x)) &= -[(1-x)\otimes \underbrace{x\otimes\cdots\otimes x}_{n-1 \text{ times}}],\end{aligned} \tag{1.3.62}$$

where we can see that the symbol for $\mathrm{Li}_n(x)$ mimics the integral over $d\log$ forms in (1.3.55). An example of the power of the symbol can be seen when looking at the five-term identity that the dilogarithms $\mathrm{Li}_2(x)$ satisfy

$$\begin{gathered}\sum_{i=1}^{5}\left(\mathrm{Li}_2(a_n)+\log(a_{n-1})\log(a_n)\right)=\frac{\pi^2}{6},\\ a_1=x,\quad a_2=\frac{1-x}{1-xy},\quad a_3=\frac{1-y}{1-xy},\quad a_4=y,\quad a_5=1-xy.\end{gathered} \tag{1.3.63}$$

It is not obvious that this identity holds when looking at the functions however if we take the symbol of the identity (and set $y=0$ for simplicity)

$$-[(1-x)\otimes x]-[x\otimes(1-x)]+[x\otimes(1-x)]+[(1-x)\otimes x]=0, \tag{1.3.64}$$

the identity is automatically satisfied. As we can see, the symbol does not capture zeta-values, or in other words, the symbol does not keep track of which Riemann sheet the multivalued functions are evaluated on. These *beyond the symbol* terms can be recovered numerically by demanding agreement before and after simplification.

The symbol $S[f^{(k)}]$ displays both the branch cut structure and the differential structure of the function $f^{(k)}$. From the definition of the symbol (1.3.59) and the behaviour of polylogarithms under derivative action (1.3.53) we see derivatives act on the symbol by action on the rightmost element of the tensor product,

$$d\,[a_1\otimes\ldots\otimes a_k]=[a_1\otimes\ldots\otimes a_{k-1}]\,d\log a_k\,. \tag{1.3.65}$$

In general, a linear combination of tensor products is not the symbol of a function. This is only the case if the symbol (1.3.59) obeys the integrability conditions,

$$\sum_{\vec{a}} c_{\vec{a}}\,[a_1\otimes\ldots\otimes a_{i-1}\otimes a_{i+2}\otimes\ldots\otimes a_k]\,(d\log a_i\wedge d\log a_{i+1})=0\,,\quad i=1,\ldots,k-1 \tag{1.3.66}$$

which follow from the fact that $d^2f=0$ for all functions of all weights and encode the commutativity of partial derivatives. These conditions also ensure that when integrating a symbol up to its function, one is free to choose a contour of integration since the functions depend only on the endpoints of integration.

Similarly, a logarithmic branch cut discontinuity around a singularity at $a_1=0$ is obtained from terms beginning with the letters a, assuming the alphabet is chosen so that no other letter vanishes at $a_1=0$,

$$\mathrm{Disc}_{a_1=0}[a_1\otimes a_2\otimes\ldots\otimes a_k]=(2\pi i)[a_2\otimes\ldots\otimes a_k]\,. \tag{1.3.67}$$

Above one-loop, scattering amplitudes built out of polylogarithms can be very complicated. For example, the two-loop hexagon Wilson loop (dual to the six-point two-loop remainder function [50–52]) was analytically calculated in [116]. The calculation was famous for being not only laborious but producing a 17-page long result, a combination of many weight-4 functions, many of which being Goncharov polylogarithms. However, in [66], the symbol was used to simplify this result down to an expression which fits on a single line! In using the symbol it was also shown that the six-point two-loop remainder function could be written in terms of classical polylogarithms only. We refer the reader to the many available references, e.g. [9, 25, 27, 28, 66, 117] for background on polylogarithms and symbols.

A first step in the bootstrap calculations of [40–48] is to build integrable words in a given alphabet. We quickly review here the method described in [48] for performing this task. The construction of integrable words can be done iteratively in weight. We suppose that we have a basis $\{f_i^{(k)}\}$ of integrable words up to weight k. This means that we know how to decompose integrable words of weight k into their $(k-1,1)$ coproducts

$$f_i^{(k)} = \sum_{a,j} M_{ija}^{(k)} [f_j^{(k-1)} \otimes a] \,. \tag{1.3.68}$$

Now we would like to construct integrable words of weight $(k+1)$. We build an ansatz for the $(k,1)$ coproduct with constants c_{ai},

$$f^{(k,1)} = \sum_{a,i} c_{ai} [f_i^{(k)} \otimes a] \,. \tag{1.3.69}$$

The constraints we have to solve come from the integrability condition (1.3.58),

$$\sum_{a,i} c_{ai} df^{(k)} \wedge d\log a = \sum_{a,i} c_{ai} \sum_{b,j} M_{ijb}^{(k)} f_j^{(k-1)} d\log b \wedge d\log a = 0 \,. \tag{1.3.70}$$

where the first equality expresses $df^{(k)}$ using (1.3.53).

The two-forms $d\log a \wedge d\log b$ are not generally all linearly independent. They satisfy linear relations known as Arnold relations which essentially come from partial fraction identities. We suppose that $\{\omega_m^{(2)}\}$ form a basis for the space of independent two forms. Then there exists a tensor Y which expresses each two-form $d\log a \wedge d\log b$ in terms of the independent basis

$$d\log a \wedge d\log b = \sum_m Y_{ab,m} \, \omega_m^{(2)} \,. \tag{1.3.71}$$

It follows that the condition (1.3.70) becomes

$$\sum_{a,i} c_{ai} \sum_{b,j} M_{ijb}^{(k)} f_j^{(k-1)} Y_{ab,m} \, \omega_m^{(2)} = 0 \,. \tag{1.3.72}$$

Since the $\omega_m^{(2)}$ form a basis for the independent two-forms and the $f_j^{(k-1)}$ form a basis for the integrable words of weight $(k-1)$ the condition becomes

$$\sum_{a,i} c_{ai} \sum_{b} M_{ijb}^{(k)} Y_{ab,m} = 0 \,. \tag{1.3.73}$$

In other words we need to compute the kernel of the matrix

$$\mathcal{M}_{AB} = \sum_b M^{(k)}_{ijb} Y_{ab,m}\,, \qquad A = (jm)\,,\, B = (ai)\,, \tag{1.3.74}$$

where we grouped indices into multi-indices A, B.

To obtain a solution to (1.3.74) is a linear algebra problem that can be helpfully addressed with available packages. The package SpaSM [118] for sparse modular linear algebra operations is particularly helpful as the matrices involved are typically sparse and all quantities involved can be chosen to be integer-valued. However it is solved, one obtains a basis for the kernel of $\mathcal{M}$, i.e. a set of linearly independent null vectors $\{v_{A,l}\}$ where $l = 1, \ldots, \dim(\ker \mathcal{M})$. Expanding the multi-index $A = (ai)$ we obtain the desired basis of weight $(k+1)$ words,

$$f^{(k+1)}_l = \sum_{a,i} M^{(k+1)}_{lia} [f^{(k)}_i \otimes a]\,, \qquad M^{(k+1)}_{lia} = v_{ai,l}\,. \tag{1.3.75}$$

The above procedure has been used extensively in several works as a first step in the analytic bootstrap programme for amplitudes.

1.3.7 The Bootstrap Program

Here we shall give a general overview of the symbol bootstrap program, providing some of the ingredients one would impose in order to calculate the symbol of an amplitude in SYM.

In the last section, we described how one can use linear algebra to iterative generate bases of integrable words of weight k. To compute the symbol of an L-loop amplitude we must find a linear combination of elements of the weight $2L$ basis such that the result matches the symbol one would get from taking the symbol of the explicit amplitude. This can be done by taking an ansatz built out of the basis elements and imposing conditions, which the amplitude is expected to obey, thus fixing the coefficients. We shall now discuss some typical conditions one could impose.

Initial entry condition

Locality requires that amplitudes only have singularities when an intermediate particle goes on-shell. For a planar theory the momenta of intermediate particles can always be expressed as a sum of cyclically adjacent momenta, and for massless theories the thresholds are always at the origin. Hence perturbative amplitudes in planar SYM theory can only have branch points when the corresponding Mandelstam $s_{i,\ldots,j-1} = x^2_{ij}$ vanishes. As shown in (1.3.67), the first entry of a symbol a_1 corresponds to the function having a branch point at $a_1 = 0$ or $a_1 = \infty$. Therefore the first entry of a symbol that corresponds to a physical n-point scattering amplitude must be one of the $3(n-5)$ cross-ratios [119].

Steinmann Conditions

We can impose the Steinmann conditions on the ansatz to ensure that the result has the correct discontinuity structure. For arbitrary n the Steinmann conditions take the form

$$\mathrm{Disc}_{s_{jj+1j+2}}(\mathrm{Disc}_{s_{ii+1i+2}} A) = 0, \quad \text{for } j = i \pm 1, i \pm 2, \tag{1.3.76}$$

with obvious generalisations to higher-particle Mandelstam invariants as well.

We shall see in the next chapter that so-called cluster algebras associated to Grassmannians $\mathrm{Gr}(k,n)$ provide more conditions beyond Steinmann which involve invariants other than Mandelstams.

Final entry condition

In [120], it was shown, as a result of dual conformal symmetry, that the total differential of the MHV remainder function is given by a linear combination of $d\log\langle ij-1jj+1\rangle$ forms. Since derivatives act on the final entry of a symbol, final entries of symbols of MHV amplitudes are given by twistor brackets of the form $\langle ij-1jj+1\rangle$.

The MHV final entry condition just described can be derived from an anomaly equation for the $\bar{Q}$ dual conformal generators [121], which is given by

$$\bar{Q}_a^A \mathcal{R}_{n,k} = a\mathrm{Res}_{\epsilon=0}\int_{\tau=0}^{\tau=\infty}\left(d^{2|3}\mathcal{Z}_{n+1}\right)_a^A [\mathcal{R}_{n+1,k+1} - \mathcal{R}_{n,k}\mathcal{R}^{\mathrm{tree}}_{n+1,1}] + \text{cyclic}, \tag{1.3.77}$$

where $\mathcal{R}_{n,k}$ is the infrared finite and regulator independent BDS-subtracted, n-point, N^kMHV amplitude, $a, A = 1,\ldots,4$ are momentum twistor indices, and ϵ,τ parametrise $\mathcal{Z}_{n+1}$ in the collinear limit (τ being related to the longitudinal momentum fraction). The operator $\bar{Q}_a^A$ is given by

$$\bar{Q}_a^A = (S_\alpha^A, \bar{Q}_{\dot{\alpha}}^A) \coloneqq \sum_{i=1}^{n} \chi_i^A \frac{\partial}{\partial Z_i^a}, \tag{1.3.78}$$

where the form of the operators $S_\alpha^A, \bar{Q}_{\dot{\alpha}}^A$ and the algebra they obey are given in Appendix B.

This same anomaly equation can also be used to constrain the final entries of the symbol of the NMHV superamplitude. For example, using the leading singularities of the N^2MHV eight-point amplitude obtained from the Grassmannian [2] as input, and redefining the $\bar{Q}$ equation to act on the BDS-like normalised amplitude rather than the BDS-normalised one, Caron-Huot found 147 distinct (R-invariant) $\times$ (final entry) combinations which are given in [48] [1].

Discrete symmetries

Scattering amplitudes usually possess certain discrete symmetries, for example, dihedral symmetry and parity are common. Dihedral symmetry consists of cyclic symmetry $Z_i \to Z_{i+1}$ and reflection symmetry $Z_i \to Z_{1-i}$. Parity is a more involved transformation, acting on the twistors as

$$Z_i \to W_i = *(Z_{i-1} \wedge Z_i \wedge Z_{i+1}). \tag{1.3.79}$$

These discrete transformations can be imposed on the ansatz of integrable words in order to fix more coefficients.

[1] In the reference [48] it was stated that the list of 147 final entry combinations was from a private conversation with Caron-Huot.

Collinear limit

As mentioned above, the remainder function tends smoothly in the collinear limit, namely

$$R_n \to R_{n-1}, \quad \text{for } i||i+1. \tag{1.3.80}$$

In terms of (super)twistors, for $n||n-1$ this limit takes the form

$$\mathcal{Z}_n \to \mathcal{Z}_{n-1} + \epsilon \frac{\langle n-3\, n-1\, 12\rangle}{\langle n-3\, n-2\, 12\rangle}\mathcal{Z}_{n-2} + \frac{\langle n-3\, n-2\, n-1\, 2\rangle}{\langle n-3\, n-2\, 12\rangle}\epsilon\tau\mathcal{Z}_1 + \frac{\langle n-3\, n-2\, n-1\, 1\rangle}{\langle n-3\, n-2\, 12\rangle}\eta\mathcal{Z}_2, \tag{1.3.81}$$

although there are many other collinear limits one could choose from.

Multi-Regge kinematics

Useful information about amplitudes can be extracted by analysing them in particular kinematics. One such kinematic regime is the *multi-Regge* kinematics.

Multi-Regge kinematics (MRK) is defined as a 2-to-$(n-2)$ scattering of particles (for our purposes we need only consider gluons) where the produced particles in the final state are strongly ordered in rapidity while having comparable transverse momenta

$$y_3 \gg y_4 \gg \cdots \gg y_n \quad \text{and} \quad |p_3^\perp| \simeq |p_4^\perp| \simeq \cdots \simeq |p_n^\perp|, \tag{1.3.82}$$

where $p_i^\perp = p_i^1 + ik_i^2$ is the complexified transverse momenta. This strong ordering in rapidity is equivalent to a strong ordering in lightcone +-coordinates

$$p_3^+ \gg p_4^+ \gg \cdots \gg p_n^+, \tag{1.3.83}$$

where

$$p_i = (p_i^+, p_i^-; p_i^\perp), \quad p^\pm = p_i^0 \pm p_i^3. \tag{1.3.84}$$

The mass-shell condition $p_i^2 = p_i^+ p_i^- - |p_i^\perp|^2 = 0$ implies that

$$p_n^- \gg p_{n-1}^- \gg \cdots \gg p_4^- \gg p_3^-. \tag{1.3.85}$$

In lightcone coordinates, the two-particle invariants become

$$\begin{aligned} s_{12} &= 2p_1 \cdot p_2 \simeq p_3^+ p_n^-, \\ s_{1i} &= 2p_1 \cdot p_i \simeq -p_i^+ p_n^-, \\ s_{2i} &= 2p_2 \cdot p_i \simeq -p_3^+ p_i^-, \\ s_{ij} &= 2p_i \cdot p_j \simeq p_i^+ p_j^-, \quad 3 \le i < j \le n. \end{aligned} \tag{1.3.86}$$

The last line of (1.3.86) shows that all Mandelstams made of k consecutive final state momenta $s_{ii+1\cdots i+k} \simeq s_{ii+k}$ will be comparable in size and much larger than invariants made of $k-1$ consecutive momenta. Thus the ordering of the lightcone coordinates in (1.3.83) leads to a hierarchy of Mandelstams

$$\begin{aligned} s_{12} \gg s_{3\cdots n-1}, s_{4\cdots n} \gg s_{3\cdots n-2}, s_{4\cdots n-1}, s_{5\cdots n} \gg \cdots \\ \cdots \gg s_{34}, \cdots, s_{n-1n} \gg -t_1, \cdots, -t_{n-3}, \end{aligned} \tag{1.3.87}$$

where $t_{i+1} \equiv q_i^2$ and $q_i \equiv -p_2 - \cdots - p_{i+3} = x_{i+3,1}^2$. It is conjectured that in MRK every gluon amplitude factorises into a set of universal building blocks, as shown in Figure 1.6,

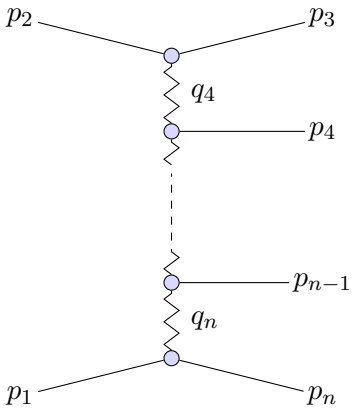

Figure 1.6: The factorised form of a tree-level scattering amplitude in multi-Regge kinematics.

describing the emission of gluons along a t-channel ladder

$$\mathcal{A}_n \simeq sC(2;3)\frac{-1}{|q_4^\perp|^2}V(q_4;4;q_5)\cdots\frac{-1}{|q_{n-1}^\perp|^2}V(q_{n-1};n-1;q_n)\frac{-1}{|q_n^\perp|^2}C(1;n), \tag{1.3.88}$$

where $q_i = \sum_{j=2}^{i-1} p_j$ with $4 \leq i \leq n$ are the momenta exchanged in the t-channel. Certain terms in (1.3.88) are power-suppressed in the kinematic limit hence the use of $\simeq$. The various building blocks on the right-hand side of (1.3.88) are the *impact factors* [72, 122]

$$\begin{aligned} C(2^+;3^+) &= C(2^-;3^-) = 0, \\ C(2^-;3^+) &= C(2^+;3^-) = 1, \\ C(1^+;n^+) &= C(1^-;n^-) = 0, \\ C(1^-;n^+) &= C(1^+;n^-) = \frac{(p_n^\perp)^*}{p_n^\perp}, \end{aligned} \tag{1.3.89}$$

and the *Lipatov vertices* [122–124]

$$V(q_i;i^+;q_{i+1}) = V(q_i;i^-;q_{i+1})^* = \frac{(q_i^\perp)^* q_{i+1}^\perp}{p_i^\perp}. \tag{1.3.90}$$

The impact factors conserve helicity thus forcing certain helicity combinations in (1.3.89) to vanish. They, along with the Lipatov vertices, are completely determined by the four and five-point amplitudes. Since all helicity configurations for four and five particles are MHV (or $\overline{\text{MHV}}$), any amplitude in MRK is determined by MHV-type building blocks, independently of the helicity configuration.

The factorisation of the amplitude in MRK (1.3.88) is consistent with all available results for tree amplitudes but has only been rigorously proven for arbitrary multiplicity for the simplest helicity configurations [122].

In SYM, we can pick a set of $3n-15$ dual conformal invariant cross-ratios (1.3.42) of the form

$$u_{1i} = \frac{x_{i+1,i+5}^2 x_{i+2,i+4}^2}{x_{i+1,i+4}^2 x_{i+2,i+5}^2}, \quad u_{2i} = \frac{x_{n,i+3}^2 x_{1,i+2}^2}{x_{n,i+2}^2 x_{1,i+3}^2}, \quad u_{3i} = \frac{x_{1,i+4}^2 x_{2,i+3}^2}{x_{1,i+3}^2 x_{2,i+4}^2}, \tag{1.3.91}$$

which can be associated to the t-channel invariants (1.3.87) with transverse momentum

$|\mathbf{q}_i|^2$ [125, 126]. In MRK these cross-ratios take the form

$$\begin{aligned} u_{1i} &= 1 - \delta_i \frac{|\mathbf{k}_i + \mathbf{k}_{i+1}|^2}{|\mathbf{k}_{i+1}|^2} + \mathcal{O}(\delta_i^2), \\ u_{2i} &= \delta_i \frac{|\mathbf{q}_{i-1}|^2}{|\mathbf{q}_i|^2} + \mathcal{O}(\delta_i^2), \\ u_{3i} &= \delta_i \frac{|\mathbf{q}_{i+1}|^2 |\mathbf{k}_i|^2}{|\mathbf{q}_i|^2 |\mathbf{k}_{i+1}|^2} + \mathcal{O}(\delta_i^2), \end{aligned} \tag{1.3.92}$$

where $k_i \equiv p_{i+3}, 1 \leq i \leq n-4$ denote the momenta of the gluons emitted along the t-channel ladder and $\delta_i \equiv k_{i+1}^+ / k_i^+$. From (1.3.83) it is evident that $\delta_i \to 0$ in MRK hence

$$u_{1i} \to 1, \quad u_{2i} \to 0, \quad u_{3i} \to 0, \tag{1.3.93}$$

all at the same rate. It is convenient to define reduced cross-ratios [125, 126]

$$\begin{aligned} v_{2i} &= \frac{u_{2i}}{1-u_{1i}} = \frac{|\mathbf{q}_{i-1}|^2 |\mathbf{k}_{i+1}|^2}{|\mathbf{q}_i|^2 |\mathbf{k}_i \mathbf{k}_{i+1}|^2} + \mathcal{O}(\delta_i), \\ v_{3i} &= \frac{u_{3i}}{1-u_{1i}} = \frac{|\mathbf{q}_{i+1}|^2 |\mathbf{k}_i|^2}{|\mathbf{q}_i|^2 |\mathbf{k}_i \mathbf{k}_{i+1}|^2} + \mathcal{O}(\delta_i). \end{aligned} \tag{1.3.94}$$

In Chapter 3, we will employ the bootstrap program in order to calculate the four-loop, seven-point, NMHV amplitude in SYM and we shall use these reduced cross-ratios to perform an MRK analysis of the result.

We shall now give a very short example of the bootstrap program, computing the symbol of Y_6 for the BDS-like ansatz (1.3.45) at six-points.

The alphabet for six-point scattering in SYM is given by

$$\begin{aligned} u &= \frac{\langle 1236\rangle\langle 3456\rangle}{\langle 1346\rangle\langle 2356\rangle}, & v &= \frac{\langle 1234\rangle\langle 1456\rangle}{\langle 1245\rangle\langle 1346\rangle}, & w &= \frac{\langle 1256\rangle\langle 2345\rangle}{\langle 1245\rangle\langle 2356\rangle}, \\ 1-u &= \frac{\langle 1356\rangle\langle 2346\rangle}{\langle 1346\rangle\langle 2356\rangle}, & 1-v &= \frac{\langle 1246\rangle\langle 1345\rangle}{\langle 1245\rangle\langle 1346\rangle}, & 1-w &= \frac{\langle 1235\rangle\langle 2456\rangle}{\langle 1245\rangle\langle 2356\rangle}, \\ y_u &= \frac{\langle 1236\rangle\langle 1345\rangle\langle 2456\rangle}{\langle 1235\rangle\langle 1246\rangle\langle 3456\rangle}, & y_v &= \frac{\langle 1235\rangle\langle 1456\rangle\langle 2346\rangle}{\langle 1234\rangle\langle 1356\rangle\langle 2456\rangle}, & y_w &= \frac{\langle 1246\rangle\langle 1356\rangle\langle 2345\rangle}{\langle 1256\rangle\langle 1345\rangle\langle 2346\rangle}. \end{aligned} \tag{1.3.95}$$

The first entries of the symbol can only be the cross-ratios themselves

$$a_i \in \{u, v, w\}, \tag{1.3.96}$$

and the final entries of the symbol can only be taken from the set

$$b_i \in \left\{ \frac{u}{1-u}, \frac{v}{1-v}, \frac{w}{1-w}, y_u, y_v, y_w \right\}, \tag{1.3.97}$$

hence we have a $3 \times 6 = 18$ dimensional ansatz for which we need to solve

$$\mathcal{S}(Y_6) = \sum_{i=1}^{3} \sum_{j=1}^{6} c_{ij} [a_i \otimes b_j]. \tag{1.3.98}$$

Imposing integrability is our first step which reduces our 18 free coefficients down to 3

$$\mathcal{S}(Y_6) = c_{11}([u\otimes u]-[u\otimes 1-u])+c_{22}([v\otimes v]-[v\otimes 1-v])+c_{33}([w\otimes w]-[w\otimes 1-w]). \tag{1.3.99}$$

We are now free to impose another condition such as a discrete symmetry like cyclic symmetry, under which $u \to v, v \to w, w \to u$, which fixes 2 coefficients leaving us with one function up to an overall constant which we can ignore

$$\mathcal{S}(Y_6) = [u \otimes u] - [u \otimes 1 - u] + [v \otimes v] - [v \otimes 1 - v] + [w \otimes w] - [w \otimes 1 - w] \quad (1.3.100)$$

which turns out to be the symbol of

$$Y_6 = -\mathrm{Li}_2\left(1 - \frac{1}{u}\right) - \mathrm{Li}_2\left(1 - \frac{1}{v}\right) - \mathrm{Li}_2\left(1 - \frac{1}{w}\right). \quad (1.3.101)$$

This function is removed from the one-loop amplitude, capturing three-particle (and higher) invariants such that the function $\mathcal{E}_n$ only depends on two-particle invariants. In fact, as the remainder function starts at two loops

$$\mathcal{E}_n^{(1)} = -Y_n \quad (1.3.102)$$

where $\mathcal{E}_n^{(1)}$ is the BDS-like-normalised one-loop amplitude.

Chapter 2

Cluster Algebras and Adjacency

In this chapter we will introduce cluster algebras and how they relate to the singularities of scattering amplitudes in SYM.

In [6] the important observation was made that the symbols of the two-loop MHV remainder functions constructed in [120] were written in terms of alphabets that exclusively contained $\mathcal{A}$-coordinates of cluster algebras associated to Grassmannians $\mathrm{Gr}(4,n)$, or more precisely, the $(3n-15)$-dimensional spaces $\mathrm{Conf}_n(\mathbb{P}^3) = \mathrm{Gr}(4,n)/(\mathbb{C}^*)^{n-1}$. From here on we will abuse notation slightly and refer to $\mathrm{Conf}_n(\mathbb{P}^{k-1})$ as $\mathrm{Gr}(k,n)$ unless it is required to distinguish between them. Beyond two loops, great progress has been made in understanding the hexagon ($n=6$) and heptagon ($n=7$) amplitudes via the analytic bootstrap programme. All current evidence is compatible with the hypothesis that the hexagon and heptagon amplitudes are polylogarithmic at all orders in perturbation theory and moreover that their symbol alphabets are given by the set of $\mathcal{A}$-coordinates for the cases $\mathrm{Gr}(4,6)$ and $\mathrm{Gr}(4,7)$ respectively. The associated cluster algebras are isomorphic to the ones based on A_3 and E_6 respectively. Here we will review some of the important aspects of cluster algebras. Many of the points we recall here are covered already in [6] but we review them as we will need many of the ideas to explain the notion of adjacency for the cluster polylogarithms appearing in the expressions for scattering amplitudes.

We will develop the connection between singularities and cluster algebras further. We emphasise that, although the connection to cluster algebras is phrased in algebraic terms, there is also a very geometric picture to the structure of relations between branch point singularities. The geometry in question is that of cluster polytopes and in particular the intricate structure of their boundaries, which captures the possible nested sequences of cluster subalgebras. The picture which emerges is different from, but shares many features with, the positive geometry arising in the description of integrands in [23, 24]. Before introducing cluster algebras, it will first be useful for our purposes to introduce the Grassmannian.

2.1 The Grassmannian

The Grassmannian $\mathrm{Gr}(k,n)$ is the space of k-planes in n dimensions. The Grassmannian can therefore be parametrised by a $k \times n$ complex matrix with the k rows specifying a

k plane. Since the plane is invariant under the action of $GL(k)$ transformations one must mod out by the action of $GL(k)$, leaving a space of dimension $k(n-k)$.

The Grassmannian may also be specified in terms of the minors of the matrix. The $(k \times k)$ minors $p_{i_1,\ldots,i_k}$ (Plücker coordinates) of any matrix obey homogeneous quadratic relations (Plücker relations) obtained by antisymmetrising $(k+1)$ indices,

$$p_{i_1,\ldots,i_r,[i_{r+1},\ldots i_k}p_{j_1,\ldots,j_{r+1}],j_{r+2},\ldots,j_k} = 0\,. \tag{2.1.1}$$

In the $\mathrm{Gr}(2,n)$ case the Plücker relations are given by the familiar $\binom{n}{4}$ three-term equations

$$p_{ij}p_{kl} - p_{ik}p_{jl} + p_{il}p_{jk} = 0\,, \qquad 1 \le i < j < k < l \le n\,. \tag{2.1.2}$$

The Plücker relations define a subspace in the Plücker space parametrised by the $\binom{n}{k}$ Plücker coordinates $p_{i_1,\ldots,i_k}$. Algebraically this space may be thought of as the ideal generated by the quadratic Plücker relations inside the ring of polynomials in the Plücker coordinates. After quotienting by a global rescaling of all Plücker coordinates the subspace satisfying the Plücker relations can be identified with the Grassmannian $\mathrm{Gr}(k,n)$ of dimension $k(n-k)$.

The original Plücker relations are actually homogeneous in n independent rescalings $p_{i_1,\ldots,i_k} \to t_{i_1}\ldots t_{i_k}p_{i_1,\ldots,i_k}$ with $t_i \in \mathbb{C}^*$. If we quotient by all of these scalings instead of just the overall scaling we obtain a smaller space,

$$\mathrm{Conf}_n(\mathbb{P}^{k-1}) = \mathrm{Gr}(k,n)/(\mathbb{C}^*)^{n-1}\,, \tag{2.1.3}$$

which has dimension $m = (k-1)(n-k-1)$ and corresponds to taking the columns of our original $(k \times n)$ to be elements of $\mathbb{P}^{k-1}$ instead of $\mathbb{C}^k$.

2.2 Cluster Algebras

Cluster algebras are commutative associative algebras with generators referred to as cluster coordinates which arise in families called clusters. They can be specified by giving an initial cluster with a set of $\mathcal{A}$-coordinates together with a mutation rule which allows the generation of further clusters and cluster coordinates. To each cluster can be associated a quiver diagram with $\mathcal{A}$-coordinates associated to the nodes. Such a quiver is described by the exchange matrix b_{ij} defined via

$$b_{ij} = (\text{no. of arrows } i \to j) - (\text{no. of arrows } j \to i)\,. \tag{2.2.1}$$

A $\mathrm{Gr}(k,n)$ cluster is identified by its $m = (k-1)(n-k-1)$ unfrozen nodes, n frozen nodes, and an $(m+n)\times(m+n)$ exchange matrix B which encodes the connectivity of the nodes within the cluster. The first m rows and columns correspond to the arrows between the unfrozen nodes. Mutating an unfrozen node k transforms B to B' given by

$$b'_{ij} = \begin{cases} -b_{ij} & \text{if } i = k \text{ or } j = k. \\ b_{ij} + [-b_{ik}]_+ b_{kj} + b_{ik}[b_{kj}]_+ & \text{otherwise.} \end{cases} \tag{2.2.2}$$

where $[x]_+ = \max(x,0)$.

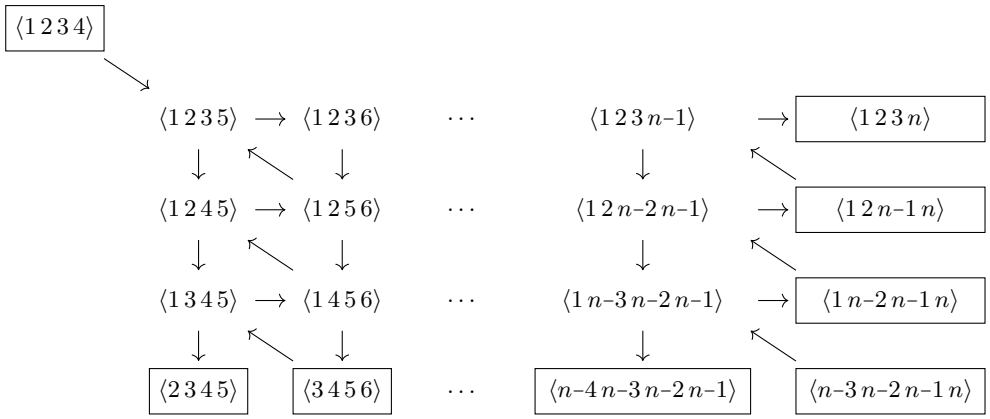

Figure 2.1: The initial cluster of the Grassmannian series $\mathrm{Gr}(4,n)$.

The mutated node also transforms, given by

$$a_k' = \frac{1}{a_k}\left[\prod_{i=1}^{m+n} a_i^{[b_{ik}]_+} + \prod_{i=1}^{m+n} a_i^{[-b_{ik}]_+}\right]. \tag{2.2.3}$$

For the set of cluster algebras associated to $\mathrm{Gr}(4,n)$ we take the initial cluster depicted in Figure 2.1. The boxed nodes are the frozen nodes and the remainder are the unfrozen ones. Other clusters (and hence other $\mathcal{A}$-coordinates) are obtained by mutating on the unfrozen nodes according to the above rules. In the cases of $n = 6, 7$ the number of distinct clusters obtained is finite. For $n = 6$ all $\mathcal{A}$-coordinates are Plücker coordinates of the form $\langle ijkl\rangle$ while $n = 7$ some $\mathcal{A}$-coordinates are quadratic in Plückers.

Note that while $\mathcal{A}$-coordinates are called 'coordinates' they are not strictly coordinates on $\mathrm{Conf}_n(\mathbb{P}^3)$ because they are not homogeneous under rescalings of the twistors. A natural set of homogeneous coordinates for $\mathrm{Conf}_n(\mathbb{P}^3)$ are the cluster $\mathcal{X}$-coordinates. They are defined with respect to a given cluster for each unfrozen node j and are related to the $\mathcal{A}$-coordinates and the adjacency matrix of the cluster via

$$x_j = \prod_i a_i^{b_{ij}}\,, \tag{2.2.4}$$

where the product runs over all nodes (frozen and unfrozen) labelled by i. Under mutation on an unfrozen node k the $\mathcal{X}$-coordinates change according to

$$x_i' = \begin{cases} 1/x_i & k = i\,, \\ x_i\big(1 + x_k^{\mathrm{sgn}(b_{ik})}\big)^{b_{ik}} & k \neq i\,. \end{cases} \tag{2.2.5}$$

Note that if node i is not connected to node k then $b_{ik} = 0$ and $x_i' = x_i$.

The adjacency matrix b_{ij} actually defines a Poisson structure on the space $\mathrm{Gr}(k,n)$ via the formula

$$\{x_i, x_j\} = b_{ij} x_i x_j. \tag{2.2.6}$$

The choice of cluster is irrelevant since the formula (2.2.6) is preserved under mutation. Note that only the restriction of the adjacency matrix to the unfrozen nodes actually

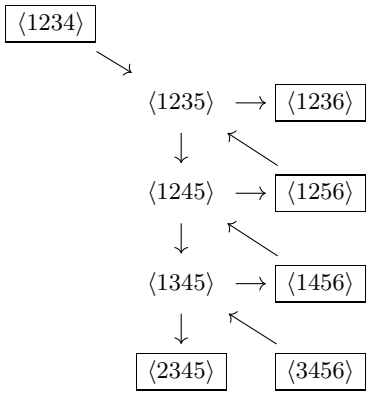

Figure 2.2: The quiver diagram for the initial cluster for the algebra associated to $\mathrm{Gr}(4,6)$.

appears in (2.2.6). We recall that a Poisson structure can be described in terms of a bivector b such that $b(df, dg) = \{f, g\}$. The adjacency matrix of a cluster then gives the components of the Poisson bivector in the coordinate system given by the (logarithms of the) cluster $\mathcal{X}$-coordinates for that cluster.

If we restrict attention to the real case then the condition that all $\mathcal{X}$-coordinates obey $0 < x < \infty$ defines a region inside $\mathrm{Conf}_n(\mathbb{RP}^3)$. The region should be visualised as a polytope with a boundary that is made of facets corresponding to codimension-one subalgebras of the original cluster algebra (which, as we described before are associated to individual $\mathcal{A}$-coordinates). Each facet has boundaries corresponding to codimension-two subalgebras (associated to admissible pairs of $\mathcal{A}$-coordinates) and so on. If we continue all the way down we arrive at dimension-zero subalgebras given by the clusters themselves and corresponding to corners of the polytope in the sense that the corner is the origin in the associated set of $\mathcal{X}$-coordinates.

The cluster $\mathcal{X}$-coordinates are edge coordinates in that they can be associated to the one-dimensional edges (axes) which meet at the vertex corresponding to the cluster. On each edge the associated $\mathcal{X}$-coordinate runs over $0 < x < \infty$, in correspondence with the fact that the $\mathcal{X}$-coordinate associated to a given edge inverts under the mutation along that edge.

2.2.1 Hexagons and the A_3 associahedron

For $\mathrm{Gr}(4,6)$, the initial cluster is represented by the quiver diagram given in Figure 2.2 with Plücker coordinates at each of the nodes. The unfrozen $\mathcal{A}$-coordinates of this cluster are

$$a_1 = \langle 1235 \rangle\,, \qquad a_2 = \langle 1245 \rangle\,, \qquad a_3 = \langle 1345 \rangle\,. \tag{2.2.7}$$

By repeated mutation of the above data according to 2.2.2 and 2.2.3 one obtains 14 distinct clusters arranged in the topology of the Stasheff polytope or associahedron illustrated in Figure 2.3. In total nine distinct unfrozen $\mathcal{A}$-coordinates are obtained, corresponding to the nine faces of the polytope, in addition to the six frozen ones present in every cluster. Three are square faces and six are pentagonal. Each cluster corresponds to a vertex, with

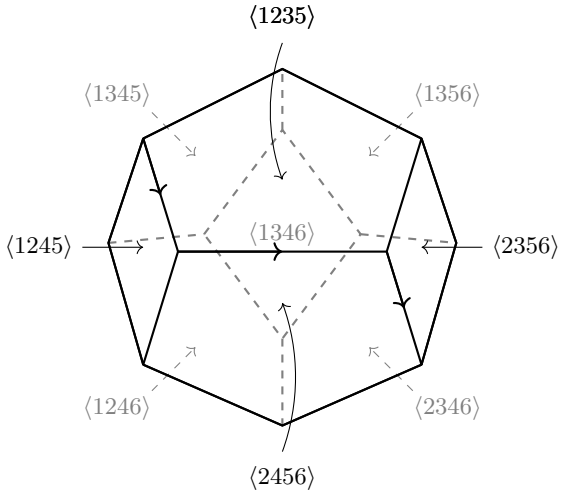

Figure 2.3: The A_3 Stasheff polytope with six pentagonal faces and three square faces, each labelled with the corresponding $\mathcal{A}$-coordinate. The initial cluster corresponds to the vertex at the top left corner at the intersection of the faces labelled by $\langle 1235\rangle$, $\langle 1245\rangle$, $\langle 1345\rangle$. The three-step path leads from the initial cluster to one obtained by a cyclic rotation by one unit.

the unfrozen $\mathcal{A}$-coordinates of the cluster corresponding to the faces of the polytope which meet at the vertex. The frozen $\mathcal{A}$-coordinates $\langle i\, i+1\, i+2\, i+3\rangle$, being present in every cluster, are not shown in Figure 2.3. The initial cluster drawn in Figure 2.2 corresponds to the cluster in the top left of Figure 2.3. The edges between clusters correspond to mutation operations.

Figure 2.3 also makes manifest the discrete symmetries of the $\mathrm{Gr}(4,6)$ cluster algebra. A cyclic rotation of the initial cluster can be generated by a threefold sequence of mutations, as indicated by the arrows. This corresponds to mutating on the three unfrozen nodes in Figure 2.2 in turn, starting at the bottom and moving to the top. A threefold cyclic rotation corresponds to a reflection in the equatorial plane of Figure 2.3 and also corresponds to the parity transformation $Z_i \mapsto Z_{i-1} \wedge Z_i \wedge Z_{i+1}$ when applied to homogeneous quantities. Finally, the reflection $Z_i \mapsto Z_{7-i}$ corresponds to a left-right reflection of Figure 2.3 together with a reflection in the equatorial plane.

The space $\mathrm{Conf}_6(\mathbb{P}^3)$ can be identified with the space $\mathrm{Conf}_6(\mathbb{P}^1) \cong \mathcal{M}_{0,6}$, that is the moduli space of six points on the Riemann sphere modulo sl_2 transformations. At the level of Plücker coordinates this can be achieved by identifying an ordered four-bracket $\langle ijkl\rangle$ (such that $i<j<k<l$) with an ordered two-bracket $\langle mn\rangle$ (with $m<n$) made of the absent labels from the set $\{1,\ldots,6\}$. In other words we make the identifications $\langle 1345\rangle = \langle 26\rangle$, $\langle 1245\rangle = \langle 36\rangle$, $\langle 1235\rangle = \langle 46\rangle$ and so on. In this way the nodes of each quiver diagram can be identified with chords of a hexagon. The edges of the hexagon correspond to adjacent two-brackets, e.g. $\langle 12\rangle = \langle 3456\rangle$. Such an identification is described in Figure 2.4. With the triangulation labelling of clusters to hand we may illustrate all triangulations on the Stasheff polytope, as shown in Figure 2.5.

It is important to stress again that Figure 2.3 is not just a pictorial representation of a set of topological relations between clusters. If we restrict attention to the case of real

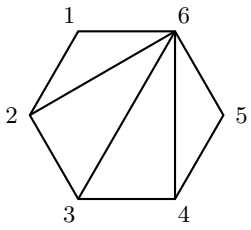

Figure 2.4: The two-brackets $\langle ij \rangle$ can be identified with chords on a hexagon between the vertices i and j. A triangulation of the hexagon then corresponds to a cluster of the A_3 or $\mathrm{Gr}(4,6)$ polytope. Above is shown the triangulation corresponding to the initial cluster of Figure 2.2 comprised of the chords $\langle 26 \rangle = \langle 1345 \rangle$, $\langle 36 \rangle = \langle 1245 \rangle$ and $\langle 46 \rangle = \langle 1235 \rangle$ together with the six edges which correspond to the frozen nodes.

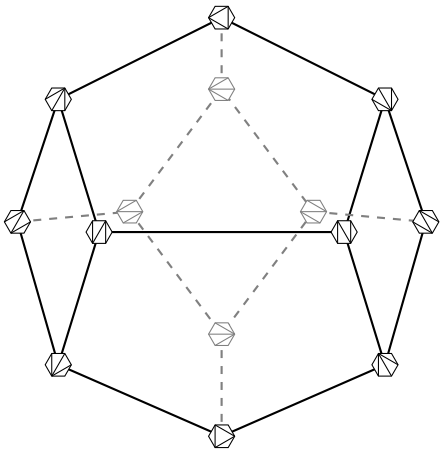

Figure 2.5: The Stasheff polytope for $\mathrm{Gr}(4,6) \cong \mathcal{M}_{0,6}$ with the clusters labelled by the different triangulations of a hexagon.

twistors then $\mathrm{Conf}_6(\mathbb{RP}^3) \cong \mathcal{M}_{0,6}(\mathbb{R})$ is a three-dimensional space. The interior of the polytope in Figure 2.3 is precisely the region inside $\mathrm{Conf}_6(\mathbb{P}^3)$ where all the cluster $\mathcal{X}$-coordinates obey $0 < x < \infty$. Each corner is the origin in the set of $\mathcal{X}$-coordinates defined by the corresponding cluster. As an example, the $\mathcal{X}$-coordinates of the initial cluster for the $\mathrm{Conf}_6(\mathbb{P}^3)$ polytope are

$$\begin{aligned} x_1 &= \frac{\langle 1234\rangle\langle 1256\rangle}{\langle 1236\rangle\langle 1245\rangle} = \frac{\langle 56\rangle\langle 34\rangle}{\langle 45\rangle\langle 36\rangle}\,, \\ x_2 &= \frac{\langle 1235\rangle\langle 1456\rangle}{\langle 1256\rangle\langle 1345\rangle} = \frac{\langle 46\rangle\langle 23\rangle}{\langle 34\rangle\langle 26\rangle}\,, \\ x_3 &= \frac{\langle 1245\rangle\langle 3456\rangle}{\langle 2345\rangle\langle 1456\rangle} = \frac{\langle 36\rangle\langle 12\rangle}{\langle 16\rangle\langle 23\rangle}\,. \end{aligned} \tag{2.2.8}$$

The vertex corresponding to the initial cluster is the origin $x_1 = x_2 = x_3 = 0$ in this coordinate system. The cluster coordinates run from 0 to ∞ along the three one-dimensional edges which meet at the vertex. This is in accord with the fact that under a mutation (which corresponds to moving along an edge to an adjacent vertex) the associated $\mathcal{X}$-coordinate inverts.

The adjacency matrix for the unfrozen nodes of the initial cluster is

$$b = \begin{pmatrix} 0 & 1 & 0 \\ -1 & 0 & 1 \\ 0 & -1 & 0 \end{pmatrix}\,. \tag{2.2.9}$$

We recall that the $\mathcal{X}$-coordinates are (log) canonical coordinates for the Poisson bracket. The adjacency matrix b in (2.2.9) is singular and has rank two. This means that there is a coordinate Δ which Poisson commutes with every function $\{\Delta, f\} = 0$. It is the product of two of the x_i above,

$$\Delta = x_1 x_3 = \frac{\langle 12\rangle\langle 34\rangle\langle 56\rangle}{\langle 16\rangle\langle 23\rangle\langle 45\rangle} = \frac{\langle 1234\rangle\langle 1256\rangle\langle 3456\rangle}{\langle 1236\rangle\langle 1456\rangle\langle 2345\rangle}\,. \tag{2.2.10}$$

Equivalently, there is a canonical (up to a constant rescaling) one-form $d\log\Delta$ which is null under the action of the Poisson bivector,

$$b(d\log\Delta, \cdot) = 0\,. \tag{2.2.11}$$

Note that Δ is built purely from frozen $\mathcal{A}$-coordinates.

Another natural set of coordinates are *dihedral* coordinates [28] which can be defined (here with respect to the trivial ordering $\{1, \ldots, n\}$) for all the moduli spaces $\mathcal{M}_{0,n}$ (or A_{n-3} cluster algebras) via

$$u_{ij} = \frac{\langle i\, j+1\rangle\langle i+1\, j\rangle}{\langle i\, j\rangle\langle i+1\, j+1\rangle}\,. \tag{2.2.12}$$

We require that the labels i and j are separated by at least two (as for unfrozen two-brackets). For the case $n = 6$ this implies that there are nine such dihedral coordinates, each labelled by the chords of the hexagon.

The interior of the Stasheff polytope is the region where all nine u_{ij} obey $0 < u_{ij} < 1$. A face of the polytope is the locus defined by $u_{ij} = 0$ where $\langle ij\rangle$ is the chord associated to that

face. When a particular $u_{ij} = 0$ then all the u_{kl} such that the chord $\langle kl \rangle$ intersects the chord $\langle ij \rangle$ take the value 1. The vertices of the polytope are then the origin in the coordinate system defined by taking the dihedral coordinates associated to the triangulation of the corresponding cluster. For example, the initial cluster is associated to the origin in the coordinates $\{u_{26}, u_{36}, u_{46}\}$ and the equations $u_{26} = 0$, $u_{36} = 0$ and $u_{46} = 0$ define the faces labelled by $\langle 1345 \rangle = \langle 26 \rangle$, $\langle 1245 \rangle = \langle 36 \rangle$ and $\langle 1235 \rangle = \langle 46 \rangle$ respectively in Figure 2.3. These dihedral coordinates are related to the $\mathcal{X}$-coordinates above via

$$u_{26} = \frac{x_3}{1+x_3}\,, \qquad u_{36} = \frac{x_2(1+x_3)}{1+x_2+x_2x_3}\,, \qquad u_{46} = \frac{x_1(1+x_2+x_2x_3)}{1+x_1+x_1x_2+x_1x_2x_3}\,. \tag{2.2.13}$$

From the above relations it is clear that the three faces meeting at the vertex are equivalently defined either by vanishing of dihedral coordinates or by vanishing of cluster $\mathcal{X}$-coordinates.

The dihedral coordinates form a complete set of nine multiplicatively independent homogeneous combinations of the $\mathcal{A}$-coordinates. They can therefore be taken as an alphabet for the construction of polylogarithms on $\mathrm{Conf}_6(\mathbb{P}^3) = \mathcal{M}_{0,6}$. They are related to the nine letters taken in e.g. [41] for the construction of hexagon functions as follows,

$$\begin{aligned}
u &= u_{26}u_{35}u_{25}u_{36}\,, & 1-u &= u_{14}\,, & y_u &= \frac{u_{35}}{u_{26}}\,,\\
v &= u_{13}u_{46}u_{36}u_{14}\,, & 1-v &= u_{25}\,, & y_v &= \frac{u_{13}}{u_{46}}\,,\\
w &= u_{24}u_{15}u_{14}u_{25}\,, & 1-w &= u_{36}\,, & y_w &= \frac{u_{15}}{u_{24}}\,.
\end{aligned} \tag{2.2.14}$$

The null Poisson coordinate Δ is given by

$$\Delta = \frac{u_{24}u_{26}u_{46}}{u_{13}u_{15}u_{35}} = \frac{1}{y_u y_v y_w}\,. \tag{2.2.15}$$

There are two distinct types of codimension-one subalgebras in the A_3 polytope. Each pentagonal face of Figure 2.3 corresponds to an A_2 subalgebra. For example, freezing the node labelled by $\langle 1235 \rangle = \langle 46 \rangle$ in the initial cluster, and mutating the other nodes generates the pentagon of clusters around the edge of the corresponding face of the polytope. The condition $u_{46} = 0$ corresponds to restricting to the pentagonal boundary. Physically, taking the limit $u_{46} \to 0$ corresponds to taking the double scaling limit where $v \to 0$ on the branch where $y_v \to \infty$. Its parity conjugate version is the limit $u_{13} \to 0$ which corresponds to $v \to 0$ on the branch where $y_v \to 0$. These double-scaling limits are highlighted in red in Figure 2.6.

The other type of codimension-one subalgebra is $A_1 \times A_1$, corresponding to a square face, as can be obtained from freezing the node $\langle 1245 \rangle = \langle 36 \rangle$ in the initial cluster and mutating the others. The condition $u_{36} = 0$ defines this face and taking the limit $u_{36} \to 0$ corresponds to taking the soft limit where $u \to 0$, $v \to 0$, $w \to 1$. Note that this limit is a limit to a codimension one (i.e. dimension two) subspace. This is important because, although the soft limit itself (of the remainder function) is independent of the location approached on the face, after analytic continuation the same limit corresponds to a Regge limit which is not independent of where on the face is being approached. The remaining transverse kinematic dependence of the amplitude in the Regge limit is precisely

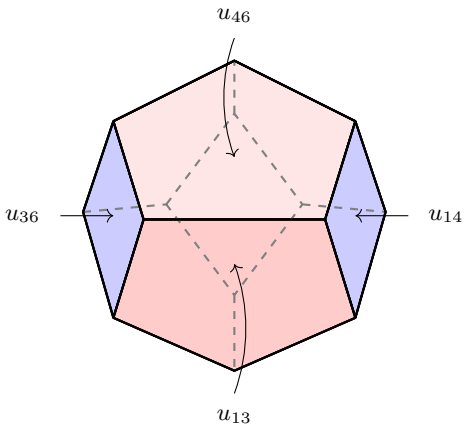

Figure 2.6: The A_3 polytope with four faces labelled by their dihedral coordinates. The double scaling limits $u_{46} \to 0$ and its parity conjugate version $u_{13} \to 0$ are are the highlighted red pentagons. The soft limits $u_{36} \to 0$ and $u_{14} \to 0$ are the blue squares. The line joining the two squares corresponds to the collinear limit $u_{13} = u_{46} = 0$.

parametrised by the two-dimensional square face. The limit $u_{36} \to 0$ and a cyclically rotated one $u_{14} \to 0$ are highlighted as blue squares in Figure 2.6.

The full space $\mathrm{Conf}_6(\mathbb{RP}^3) \cong \mathcal{M}_{0,6}(\mathbb{R})$ is tiled by 60 regions identical to the Stasheff polytope of Figure 2.3. In general [28], the moduli spaces $\mathcal{M}_{0,n}(\mathbb{R})$ are tiled by $n!/(2n)$ regions which are $(n-3)$-dimensional polytopes, each corresponding to a choice of dihedral structure (i.e. an ordering modulo cyclic transformations and reflections) on the n points in $\mathbb{RP}^1$.

Each vertex of the polytope provides a natural base point for the contour of integration over which a symbol made of homogeneous combinations of the $\mathcal{A}$-coordinates can be iteratively integrated to produce a polylogarithmic function [28].

2.2.2 Heptagons and the E_6 polytope

For $\mathrm{Gr}(4,7)$, the initial cluster is represented by the quiver diagram of Figure 2.7. Each cluster contains six unfrozen nodes as well as the seven frozen ones labelled by the adjacent four-brackets $\langle i\, i{+}1\, i{+}2\, i{+}3\rangle$. Repeated mutation generates a total of 833 distinct clusters containing a total of 42 distinct unfrozen $\mathcal{A}$-coordinates in addition to the 7 frozen ones.

A useful feature of cases of $\mathrm{Gr}(k,n)$ where the pair (k,n) is coprime (such as the heptagon case) is that one may use the frozen $\mathcal{A}$-coordinates to render the unfrozen ones homogeneous [45]. In this way one can make a natural set of 42 homogeneous letters labelled in one-to-one correspondence with the 42 unfrozen $\mathcal{A}$-coordinates. They are given by the following six quantities together with their cyclic rotations,

$$\begin{aligned} a_{11} &= \frac{\langle 1234\rangle\langle 1567\rangle\langle 2367\rangle}{\langle 1237\rangle\langle 1267\rangle\langle 3456\rangle} & a_{21} &= \frac{\langle 1234\rangle\langle 2567\rangle}{\langle 1267\rangle\langle 2345\rangle} \\ a_{31} &= \frac{\langle 1567\rangle\langle 2347\rangle}{\langle 1237\rangle\langle 4567\rangle} & a_{41} &= \frac{\langle 2457\rangle\langle 3456\rangle}{\langle 2345\rangle\langle 4567\rangle} \\ a_{51} &= \frac{\langle 1(23)(45)(67)\rangle}{\langle 1234\rangle\langle 1567\rangle} & a_{61} &= \frac{\langle 1(34)(56)(72)\rangle}{\langle 1234\rangle\langle 1567\rangle}\,, \end{aligned} \tag{2.2.16}$$

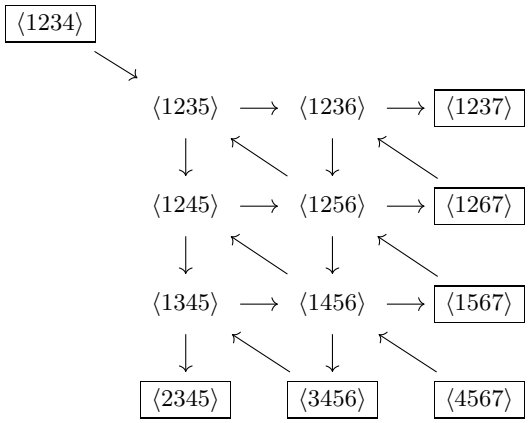

Figure 2.7: The initial cluster of the $\mathrm{Gr}(4,7)$ cluster algebra, relevant for heptagon amplitudes.

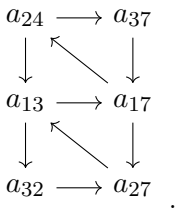

Figure 2.8: The initial cluster for $\mathrm{Gr}(4,7)$ labelled by homogenised $\mathcal{A}$-coordinates.

where the cyclic copies are defined as $a_{i,j+r} = a_{ij}\big|_{Z_k \mapsto Z_{k+r}}$ and we use the notation

$$\langle a(bc)(de)(fg)\rangle = \langle abcd\rangle\langle efga\rangle - \langle abce\rangle\langle dfga\rangle\,. \tag{2.2.17}$$

By labelling the nodes of the quiver diagram with the homogenised $\mathcal{A}$-coordinates, the initial cluster can be illustrated as in Figure 2.8.

Just as in the hexagon case we should try to visualise the 833 clusters being connected together in a polytope (the E_6 polytope). The polytope is a six-dimensional space with 42 codimension one (i.e dimension five) boundary faces, corresponding to the 42 unfrozen $\mathcal{A}$-coordinates. As with the hexagon case, this polytope corresponds to the 'postive' region in kinematical space. Considering the dimension and the number of vertices it is not as visually instructive to plot the full polytope as a graph. Nevertheless similar general features are present as in the hexagon case.

To illustrate the structure of possible subalgebras it is helpful to bring the initial cluster to a cluster with the topology of an E_6 Dynkin diagram by a sequence of mutations as shown in Figure 2.9. A helpful feature of the E_6-shaped cluster is that its homogenised $\mathcal{A}$-coordinates contain one representative of each of the six cyclically related classes given in (2.2.16). The codimension-one subalgebras obtained by freezing any given letter are then obvious. Freezing a_{13} and mutating on the other nodes generates an A_5 subalgebra. Freezing a_{25} or a_{33} will generate a D_5 subalgebra. Freezing a_{41} or a_{51} generates an $A_4 \times A_1$ subalgebra. Finally freezing a_{62} generates an $A_2 \times A_2 \times A_1$ subalgebra. The E_6-shaped cluster is special in this regard. For example, the initial cluster contains only a_{1i}, a_{2i}

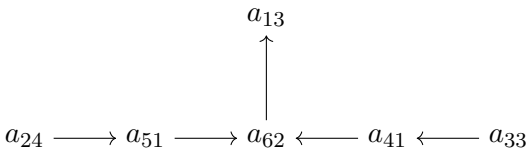

Figure 2.9: The initial cluster of $\mathrm{Gr}(4,7)$ does not have the topology of an E_6 Dynkin diagram but it is possible to mutate it to one which does. This cluster contains homogenised $\mathcal{A}$-coordinates of all six types given in (2.2.16).

and a_{3i} types of coordinates and therefore is at the intersection only of D_5 and A_5 type subalgebras.

Each cluster (or dimension zero subalgbera) corresponds to a vertex on the boundary of the E_6 polytope and the six associated cluster $\mathcal{X}$-coordinates define a local coordinate system such that the vertex is the origin. Once again the $\mathcal{X}$-coordinates can be associated to the one-dimensional edges of the polytope and the interior of the polytope is the region where all $\mathcal{X}$-coordinates obey $0 < x < \infty$. The six $\mathcal{X}$-coordinates for the E_6-shaped cluster are shown in Figure 2.10. The five-dimensional face corresponding to the A_5 subalgebra is the boundary component defined by $x_6 = 0$ with all other x_i obeying $0 < x_i < \infty$. The condition $x_4 = 0$ defines a face corresponding to an $A_4 \times A_1$ subalgebra and so on.

As in the A_3 case we may define another set of coordinates u_{ij} such that the $u_{ij} = 0$ defines the codimension one face labelled by a_{ij}. In terms of the cluster $\mathcal{X}$-coordinates of the E_6 shaped cluster we have the following six face coordinates[2],

$$\begin{aligned}
u_{13} &= \frac{x_1}{1+x_1} & u_{62} &= \frac{x_6(1+x_1)}{1+x_6+x_1x_6} \\
u_{51} &= \frac{x_5(1+x_6+x_1x_6)}{1+x_5+x_5x_6+x_1x_5x_6} & u_{41} &= \frac{x_4(1+x_6+x_1x_6)}{1+x_4+x_4x_6+x_1x_4x_6} \\
u_{24} &= \frac{x_2(1+x_5+x_5x_6+x_1x_5x_6)}{1+x_2+x_2x_5+x_2x_5x_6+x_1x_2x_5x_6} & u_{33} &= \frac{x_3(1+x_4+x_4x_6+x_1x_4x_6)}{1+x_3+x_3x_4+x_3x_4x_6+x_1x_3x_4x_6}\,.
\end{aligned} \tag{2.2.18}$$

Again the origin in the cluster $\mathcal{X}$-coordinates coincides with the origin in the face coordinates. In terms of the homogenised $\mathcal{A}$-coordinates we have

$$\begin{aligned}
u_{13} &= \frac{a_{62}}{a_{11}a_{13}} & u_{62} &= \frac{a_{11}a_{41}a_{51}}{a_{62}a_{67}} \\
u_{51} &= \frac{a_{24}a_{67}}{a_{46}a_{51}} & u_{41} &= \frac{a_{33}a_{67}}{a_{41}a_{56}} \\
u_{24} &= \frac{a_{46}}{a_{24}a_{31}} & u_{33} &= \frac{a_{56}}{a_{22}a_{33}}\,.
\end{aligned} \tag{2.2.19}$$

Again we clearly have $0 < u_{ij} < 1$ in the interior of the polytope from (2.2.18). From the equations (2.2.19) and cyclically related equations one can define a complete set of 42 homogeneous coordinates u_{ij} which makes an alternative multiplicatively independent set to the a_{ij}. The variables u_{ij} have the property that $u_{ij} = 0$ implies $u_{kl} = 1$ if the face labelled by a_{kl} is not adjacent to the face labelled by a_{ij}. In other words, setting one u_{ij} to zero for a given face means that all the u_{kl} corresponding to non-adjacent faces go to 1.

[2]Such variables have already been derived by Arkani-Hamed and collaborators [127] for finite cluster algebras from a different perspective. Here we obtain them from the cluster $\mathcal{X}$-coordinates. We would like to thank Nima Arkani-Hamed for discussions of this point.

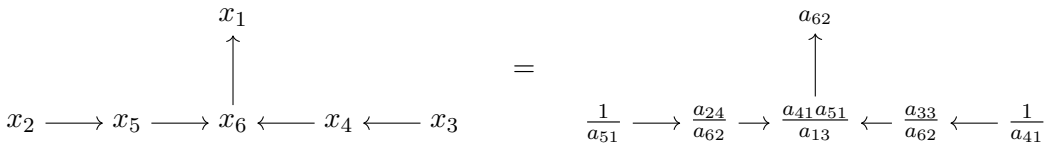

Figure 2.10: The E_6-shaped cluster with $\mathcal{X}$-coordinates shown at each of the nodes.

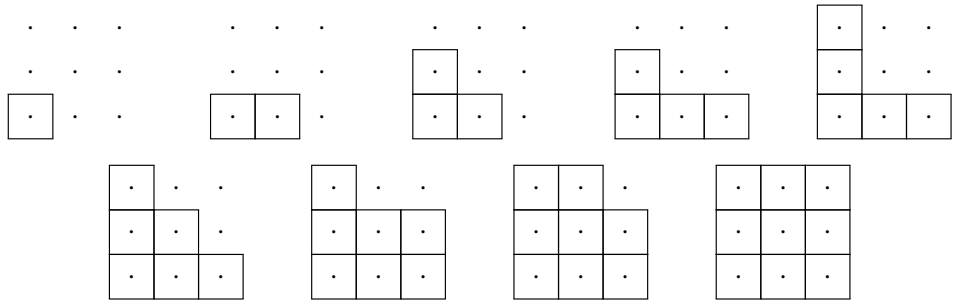

Figure 2.11: A series of mutations which result in a rotation of the $\mathrm{Gr}(4,8)$ initial cluster by one unit. The dots represent unfrozen nodes (arrows have been removed for clarity) and the squares represent the mutated nodes. Note there are no gaps between mutated nodes and we always mutate from the bottom up and from left to right.

Just as in the A_3 case there are specific sequences of mutations which generate a cyclic transformation of the $\mathcal{A}$-coordinates in a given cluster. Rather than describe it here for E_6 we give a general discussion for $\mathrm{Gr}(k,n)$ in the next section.

2.2.3 General cyclic mutations for $n > 7$

For $n > 7$, the $\mathrm{Gr}(4,n)$ cluster algebra is infinite. We can still define a positive region where all $\mathcal{X}$-coordinates are positive but the structure of its boundary is much less clear. We can still, however, understand certain finite aspects of these infinite algebras. For instance we can mutate from the initial cluster in Figure 2.1 to another one in which all the $\mathcal{A}$-coordinate labels have been rotated by one unit. We do this by mutating in a manner that mirrors building Young tableaux, instead building from the bottom-left to the top-right (as opposed from top-left to bottom-right) as demonstrated in Figure 2.11.

We can use this method to rotate initial-type sub-algebras within a cluster in order to search for clusters with specific Plückers. In fact we will use this method later to prove that all R-invariants are cluster adjacent. An example is given in Figure 2.12. As we can see, the $\mathrm{Gr}(3,6)$ sub-topology remains unchanged but the labels have all been rotated by one unit. The other nodes have rearranged themselves such that the frozen nodes connected to the sub-algebra have shifted round the cluster. Mutating on $\langle 156\rangle$ followed by $\langle 126\rangle$ will result in the same topology as the left cluster but with each label rotated by one unit. We can repeat this process any number of times to achieve the desired number of rotations.

2.3 Adjacency rules from $\mathrm{Gr}(4,n)$ clusters

Steinmann relations [67, 68] are the requirement that a scattering amplitude does not have consecutive discontinuities in overlapping channels. In the context of amplitudes in

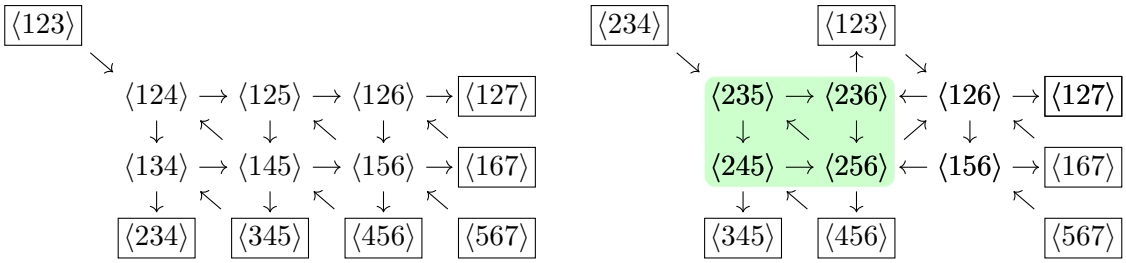

Figure 2.12: The $\mathrm{Gr}(3,7)$ initial cluster (left) and the cluster resulting from a cyclic mutation of a $\mathrm{Gr}(3,6)$ subalgebra, highlighted in green (right). $\mathrm{Gr}(3,7) \sim \mathrm{Gr}(4,7)$ but we have given this example to demonstrate this procedure is valid for $\mathrm{Gr}(k,n)\ \forall\ k,n$.

planar $\mathcal{N}=4$ super Yang-Mills theory their importance was emphasised in [128] and they have been usefully employed to construct amplitudes in [47, 48].

In order to see the appearance of Steinmann relations in massless amplitudes it is useful to define an appropriate infrared finite quantity [47]. In planar $\mathcal{N}=4$ this quantity is the *BDS-like subtracted amplitude* [115] which exists for n-point amplitudes with $n \geq 6$ and $n \neq 0 \bmod 4$. These amplitudes do not have consecutive branch cuts in overlapping three-particle or higher Mandelstam invariants. For example, a discontinuity around $s_{123}=0$ cannot itself have a discontinuity around $s_{234}=0$.

While mutations of clusters generate the letters of the symbol alphabet, the alphabet itself does not contain information on the details of which clusters contain which $\mathcal{A}$-coordinates nor which clusters are linked by mutations. However, a survey of all known MHV and NMHV BDS-like subtracted heptagon amplitudes reveals that only certain pairs of letters appear in neighbouring slots. This leads us to conjecture a much more general set of adjacency relations for BDS-like subtracted amplitudes:

> *Two distinct $\mathcal{A}$-coordinates can appear consecutively in a symbol only if there exists a cluster where they both appear.*

We believe that the above conjecture will apply to any BDS-like subtracted amplitude which is expressed in terms of cluster polylogarithms. It has been conjectured that all MHV and NMHV amplitudes in planar $\mathcal{N}=4$ super Yang-Mills will have a polylogarithmic form [23], though it has not yet been tested whether the alphabets are dictated by the $\mathrm{Gr}(4,n)$ cluster structures for $n \geq 8$ beyond two-loop MHV amplitudes.

For eight-point amplitudes, a BDS-like subtracted amplitude in the sense of [115], which uses only two-particle Mandelstam invariants to provide a solution to the conformal Ward identity of [104], does not exist. Proceeding to nine points, one again has a canonical BDS-like subtracted amplitude, constructible from the two-loop results in [120] and we have verified directly that it does obey the above conjecture. That is, for each neighbouring pair appearing in the symbol we can find a cluster containing that pair.

We can go back and look at the geometric interpretation of this conjecture. If we pick a particular $\mathcal{A}$-coordinate a and look at all clusters containing a we obtain a cluster subalgebra. Such clusters may be generated by starting in one cluster containing a and performing all possible combinations of mutations on the other nodes. In this way, to each

$\mathcal{A}$-coordinate we associate a codimension-one subalgebra. Similarly we may pick a pair of coordinates $\{a, b\}$ and, as long as there is at least one cluster where they both appear, associate to them a codimension-two subalgebra by performing all possible mutations on the other nodes. If there is no cluster where a and b appear together then there is no such subalgebra. The fact that some pairs can be found together (we call them 'admissible' or 'adjacent') while other pairs cannot is at the heart of the cluster adjacency property describing the behaviour of singularities of scattering amplitudes. Note that frozen nodes are present in every cluster and hence are always admissible with any other $\mathcal{A}$-coordinate.

We can continue further and associate codimension-three subalgebras with admissible triplets $\{a, b, c\}$ where a, b and c can all be found together in some cluster and so on. Finally when we have fixed an admissible set of $(3n - 15)$ $\mathcal{A}$-coordinates we uniquely specify a cluster which we could alternatively describe as a dimension-zero subalgebra.

Using the hexagon case as an example, admissible pairs of unfrozen nodes are pairs of faces of the Stasheff polytope which intersect on the boundary, e.g. the pair $\{\langle 1235\rangle, \langle 2456\rangle\} = \{\langle 46\rangle, \langle 13\rangle\}$ is admissible and intersects in a codimension-two (i.e. dimension-one) A_1 subalgebra corresponding to the shared edge of those two faces. The edge in question is defined by $u_{46} = u_{13} = 0$ and corresponds to taking the collinear limit of the hexagon amplitudes. Note that the collinear limit indeed interpolates between two soft limits corresponding to the square faces labelled by $\langle 36\rangle$ and $\langle 14\rangle$.

The pair $\{\langle 1245\rangle, \langle 2356\rangle\} = \{\langle 36\rangle, \langle 14\rangle\}$ on the other hand is not admissible as the corresponding faces do not intersect on the boundary of Figure 2.3. The absence of such an intersection is directly related to the Steinmann relations, or even more basically, to the absence of overlapping factorisation poles in tree-level amplitudes. In general we can describe admissible pairs as non-intersecting chords $\langle ij\rangle$ of the polygon while intersecting chords give non-admissible pairs. Frozen $\mathcal{A}$-coordinates correspond to the edges of the polygon and therefore do not intersect any chord and hence are admissible with every other $\mathcal{A}$-coordinate.

Finally, admissible triples correspond to corners of Figure 2.3, i.e. to clusters themselves. They are codimension-three or dimension-zero subalgebras and as an example we could take the triplet $\{\langle 1235\rangle, \langle 1245\rangle, \langle 1345\rangle\}$ which defines the initial cluster.

Admissible pairs in the E_6 case correspond to codimension two subalgebras, i.e. dimension four subalgebras. For example the admissible pair $\{a_{13}, a_{62}\}$ corresponds to an $A_2 \times A_2$ subalgebra while the pair $\{a_{51}, a_{41}\}$ corresponds to an $A_2 \times A_1 \times A_1$ subalgebra. Admissible triplets correspond to dimension three subalgebras and so on.

It is important to emphasise that the above adjacency conjecture introduces a much more detailed role for the cluster structure over and above the fact that the alphabet can be obtained from the union over all cluster $\mathcal{A}$-coordinates. It is the structure of the individual clusters which constrains both sequences of discontinuities (reading the symbol from the left) and successive derivatives (reading from the right).

In the case of planar $\mathcal{N} = 4$ heptagon amplitudes there are 840 distinct admissible ordered pairs of letters out of the 1764 possible ordered pairs one can make from the 42 letters. We summarise this information in Table 2.1, where we also distinguish whether the

	a_{1i}	a_{2i}	a_{3i}	a_{4i}	a_{5i}	a_{6i}
a_{11}	●○○◆◆○○	◆◆○●◆●○	◆○●◆●○◆	●○◆○○◆○	●○◆○○◆○	◇◆○○○○◆
a_{21}	◆○●◆●○◆	●○●◆◆●○	◆○◆◆○◆●	◆○◆○●◆○	○◆●○◆○◆	○◆○●○◆○
a_{31}	◆◆○●◆●○	◆●◆○◆◆○	●○●◆◆●○	◆○◆●○◆○	○◆○◆○●◆	○○◆○●○◆
a_{41}	●○◆○○◆○	◆○◆●○◆○	◆○◆○●◆○	●◇◆○○◆◇	●○○○○○○	◇◆◇○○◇◆
a_{51}	●○◆○○◆○	○◆○◆○●◆	○◆●○◆○◆	●○○○○○○	●◇◆○○◆◇	◇◆◇○○◇◆
a_{61}	◇◆○○○○◆	○○◆○●○◆	○◆○●○◆○	◇◆◇○○◇◆	◇◆◇○○◇◆	●◇○◇◇○◇

Table 2.1: The neighbourhood and connectivity relations of the coordinates a_{i1} with the 42-letter alphabet. Other relations can be inferred by cyclic symmetry. The relations in the dashed box imply the Steinmann conditions.
◆: There are clusters where the coordinates appear together connected by an arrow.
●: There are clusters where the coordinates appear together but they are never connected.
○: The coordinates never appear in the same cluster but there is a mutation that links them.
◇: The coordinates do not appear in the same cluster nor there is a mutation that links them.

pairs that appear together in a cluster are connected by a quiver arrow as well as whether two letters that never appear together mutate into each other. If one letter mutates into another, this pair never appear together in a third cluster.

The Steinmann constraints on the symbol are a subset of the cluster adjacency conditions: The letters a_{12}, a_{13}, a_{16} or a_{17} never share a cluster with a_{11}. In fact, four dihedral copies of the initial cluster mutate to another cluster where a_{11} is replaced by one of these four letters which cannot appear after an initial a_{11}. While the Steinmann condition [47] only applies to the first two letters of the symbol, it has been observed [70, 129] that for the hexagon amplitudes the same condition applies everywhere in the symbol, which is consistent with cluster adjacency.

Only 784 of the 840 allowed adjacencies actually occur in the known 7-particle amplitudes, while the pairs

$$[a_{11} \otimes a_{41}] \qquad \& \text{ cyclic} + \text{parity} \tag{2.3.1a}$$

$$[a_{21} \otimes a_{64}] \qquad \& \text{ cyclic} + \text{reflection} \tag{2.3.1b}$$

and their reverses do not appear even though they are permitted by our conjecture. Nevertheless, in the following section we compute the symbol of a three-loop integral by constraining the space of weight-six Steinmann functions and find that its symbol has, consistently with our conjecture, adjacent pairs of the form (2.3.1a).

2.4 Heptagon integrals

Let us consider the following finite double pentaladder integral (drawn in Figure 2.13)

$$I^{(3)} = \int d\tilde{Z} \frac{N\langle AB13\rangle\langle EF46\rangle}{\langle CD34\rangle\langle ABCD\rangle\langle CDEF\rangle\langle CD67\rangle \prod_{i=1}^{4}\langle AB\, i-1\, i\rangle \prod_{i=4}^{7}\langle EF\, i-1\, i\rangle} \,. \tag{2.4.1}$$

The measure is $d\tilde{Z} = \frac{d^4 Z_{AB}}{i\pi^2} \frac{d^4 Z_{CD}}{i\pi^2} \frac{d^4 Z_{EF}}{i\pi^2}$ and the numerator $N = \langle 2345\rangle\langle 3467\rangle\langle 7(12)(34)(56)\rangle$ ensures that the integral has unit leading singularity [130].

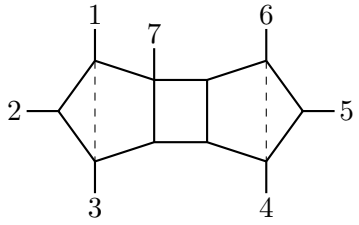

Figure 2.13: Seven-point, three-loop, massless integral.

There exists a set of four second-order differential operators which relate $I^{(3)}$ to two-loop integrals [131]. Using the notation $O_{ij} = Z_i \cdot \frac{\partial}{\partial Z_j}$ they are

$$\langle 4567\rangle N O_{45} O_{34} N^{-1} I^{(3)} = -\langle 3467\rangle I^{(2)}\,, \tag{2.4.2}$$

$$\langle 3456\rangle N O_{65} O_{76} N^{-1} I^{(3)} = -\langle 3467\rangle I^{(2)}\,, \tag{2.4.3}$$

$$\langle 1237\rangle N O_{32} O_{43} N^{-1} I^{(3)} = +\langle 1347\rangle \tilde{I}^{(2)}\,, \tag{2.4.4}$$

$$\langle 1234\rangle N O_{12} O_{71} N^{-1} I^{(3)} = -\langle 1347\rangle \tilde{I}^{(2)}\,. \tag{2.4.5}$$

The two-loop integrals $I^{(2)}$ and $\tilde{I}^{(2)}$ are shown in Figure 2.14.

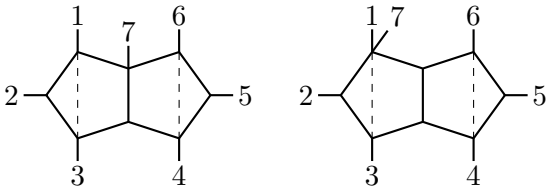

Figure 2.14: The seven-point, two-loop integrals $I^{(2)}$ and $\tilde{I}^{(2)}$.

The second-order operators above reduce the weight by two, therefore they must annihilate the final entries in the symbol of $I^{(3)}$. Using this condition we can construct a set of ten multiplicative combinations out the 42 possible heptagon letters for the final entries.

The integral $I^{(2)}$ obeys a similar set of differential equations, except that the integrals on the RHS are the one-loop hexagons $I^{(1)}$ and $\tilde{I}^{(1)}$ depicted in Figure 2.15.

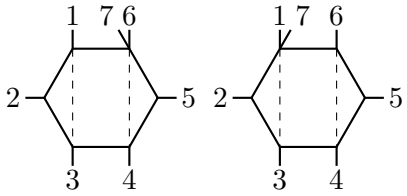

Figure 2.15: The one-loop hexagon integrals $I^{(1)}$ and $\tilde{I}^{(1)}$.

Therefore the integral $I^{(2)}$ can also only have the same ten possible final entries as $I^{(3)}$. Of the 322 weight-4 Steinmann heptagon symbols constructed in [48], there is a unique linear combination with the correct final entries for $I^{(2)}$ which we conclude must be the result up to a scale. The details of the RHS differential equations were not required to

obtain it, and indeed they can be used to derive formulas for the one-loop hexagons in Figure 2.15.

Returning to $I^{(3)}$, we find that of the 3192 weight-6 Steinmann heptagon symbols constructed in [48], seven of them have good final entries. However, only one of these produces our result for $I^{(2)}$ on the RHS of equations (2.4.2) and (2.4.3) and we conclude this is the symbol of $I^{(3)}$. Either of the equations (2.4.4) or (2.4.5) can then be used to derive a result for $\tilde{I}^{(2)}$. We quote all symbols in a file attached to the arXiv submission.

When analysing the symbol of the three-loop integral $I^{(3)}$, pairs not present in the MHV and NMHV heptagon data were found, namely $[a_{11} \otimes a_{41}]$ and $[a_{41} \otimes a_{11}]$. Their cyclic and parity copies will therefore be found in the associated cyclic and parity copies of the integral, completing the set (2.3.1a). This evidence supports our conjecture that it is the cluster structure which controls the appearance of consecutive letters.

The results for these integrals were later confirmed in [132].

2.5 Cluster adjacent polylogarithms

In [47] it was realised that the Steinmann relations were employed to greatly increase the power of the hexagon bootstrap programme and in [48] the same conditions were extended to the heptagon case. In fact the Steinmann conditions can be extended to hold on all adjacent pairs in the symbol [70, 129], not only in the first two entries. The cluster adjacency property outlined above implies the Steinmann conditions, including the extended ones. In the hexagon (or A_3) case this is simply the statement that the square faces of the associahedron in Figure 2.3 are not adjacent to each other. In the heptagon (E_6) case it follows from the fact that the face labelled by a_{11} only intersects those labelled by a_{14} and a_{15} but not those labelled by the other a_{1i}. What is less obvious but nevertheless appears to hold for the hexagon and heptagon symbols is that the extended Steinmann relations *together with the physical initial entry conditions* actually imply cluster adjacency.

Note that the property of cluster adjacency is described in terms of the inhomogeneous $\mathcal{A}$-coordinates. The polylogarithms describing the known dual conformal invariant amplitudes are functions on the space $\mathrm{Gr}(4, n)$ and their symbols are normally described in terms of homogeneous multiplicative combinations of $\mathcal{A}$-coordinates. Such combinations can be expanded out into non-manifestly homogeneous combinations by the identities (1.3.60) and (1.3.61). The resulting expressions are the ones which obey the adjacency criterion.

In the heptagon case we may take the homogenised $\mathcal{A}$-coordinates (2.2.16) as our symbol alphabet and the statement of adjacency becomes very direct. In the hexagon case this is not possible, essentially due to the existence of the purely frozen homogeneous combination Δ defined eq. (2.2.10).

In general, beyond the hexagon and heptagon amplitudes we discuss here, we expect a number of new features whose interplay with cluster adjacency is not yet clear. Firstly there will exist algebraic symbol letters with square roots which are not immediately related to $\mathcal{A}$-coordinates which are all polynomials in the Plücker coordinates. These already appear in the N^2MHV octagon at one loop in the four-mass box contributions. Moreover at high enough multiplicity and loop order there will appear non-polylogarithmic functions,

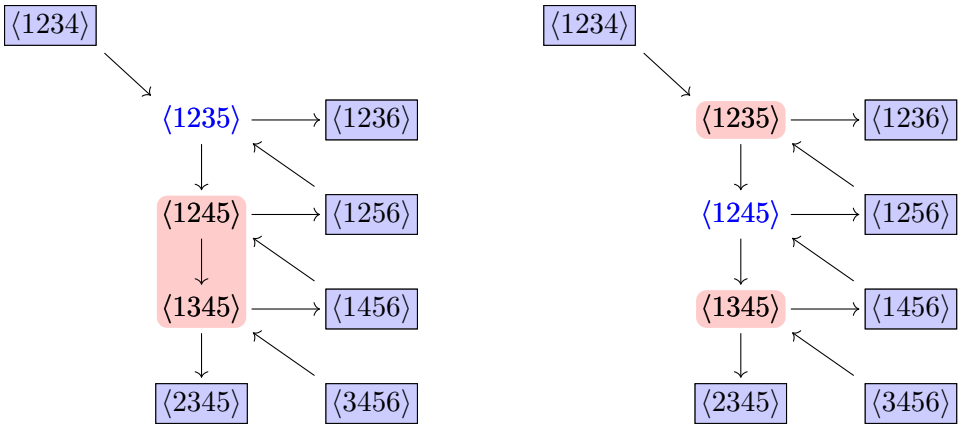

Figure 2.16: The initial cluster of $\mathrm{Gr}(4,6)$ has the topology of an A_3 Dynkin diagram. Freezing $\langle 1235\rangle = \langle 46\rangle$ results in a A_2 subalgebra whereas freezing $\langle 1245\rangle = \langle 36\rangle$ results in a $A_1 \times A_1$ subalgebra. These subalgebras generate the letters in $\mathrm{ns}[\langle 1235\rangle]$ and $\mathrm{ns}[\langle 1245\rangle]$, respectively.

e.g. in the ten-point N^{3}MHV amplitude at two loops [30]. Nevertheless we believe that some suitably extended notion of cluster adjacency will also hold beyond the hexagon and heptagon amplitudes.

2.5.1 Neighbour sets

We define the *neighbour set* $\mathrm{ns}[a]$ of a given $\mathcal{A}$-coordinate a as the set of $\mathcal{A}$-coordinates b such that $\{a, b\}$ form an admissible pair together with a itself. This set automatically includes all the frozen $\mathcal{A}$-coordinates. In terms of the polytope the unfrozen nodes in the neighbour set correspond to all faces that share a codimension-two boundary with the face labelled by a (i.e. are adjacent to a) together with the face labelled by a itself. One way of systematically constructing neighbour sets is to go to a convenient cluster and freeze the $\mathcal{A}$-coordinate whose neighbour set is being considered. The neighbour set then consists of all unfrozen $\mathcal{A}$-coordinates generated in this codimension-one subalgebra, the frozen coordinates and the coordinate a itself. This is demonstrated in Figure 2.16. Note that the notion of a neighbour set depends on the cluster algebra in question, as well as the choice of $\mathcal{A}$-coordinate a.

Through this procedure we find the following neighbour sets for the unfrozen hexagon $\mathcal{A}$-coordinates:

$$\begin{aligned}\mathrm{ns}[\langle 1235\rangle] &= \{\langle 1235\rangle, \langle 2456\rangle, \langle 2356\rangle, \langle 1356\rangle, \langle 1345\rangle, \langle 1245\rangle, \text{ \& frozen coordinates.}\}\\ \mathrm{ns}[\langle 1245\rangle] &= \{\langle 1245\rangle, \langle 2456\rangle, \langle 1345\rangle, \langle 1246\rangle, \langle 1235\rangle, \text{ \& frozen coordinates.}\}\,.\end{aligned} \tag{2.5.1}$$

As stated above, apart from a itself, the unfrozen elements of the neighbour set of a are associated with the faces of the Stasheff polytope which neighbour the face associated with a. The edges where these faces intersect correspond to the remaining A_1 algebra in a cluster containing the two letters associated with the two faces, cf. Figure 2.3.

An equivalent way to state the neighbouring principle for the A_3 case (and more generally for the A_n case) is that $\mathcal{A}$-coordinates corresponding to chords on the hexagon which

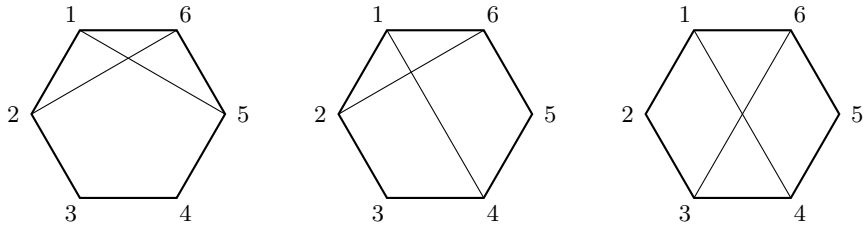

Figure 2.17: Forbidden pairs correspond to crossing chords of the hexagon.

cross are non-neighbouring, i.e. are forbidden to appear next to each other in the symbol. Examples are shown in Figure 2.17.

There are 12 coordinates in the neighbour set of the $\mathcal{A}$-coordinate $\langle 2456\rangle = \langle 13\rangle$ including itself and the 6 frozen coordinates. When writing down homogeneous functions, it convenient to work with a homogeneous alphabet and there are 6 homogeneous combinations that can be constructed using the allowed neighbours of $\langle 1235\rangle = \langle 46\rangle$. Such a *homogeneous neighbour set* can be chosen as the five $\mathcal{X}$-coordinates associated to the edges of the pentagonal face labelled by $\langle 46\rangle$ together with Δ from eq. (2.2.10) as follows:

$$\text{hns}[\langle 46\rangle] = \left\{ \frac{\langle 13\rangle\langle 46\rangle}{\langle 16\rangle\langle 34\rangle}, \frac{\langle 24\rangle\langle 16\rangle}{\langle 12\rangle\langle 46\rangle}, \frac{\langle 36\rangle\langle 12\rangle}{\langle 23\rangle\langle 16\rangle}, \frac{\langle 14\rangle\langle 23\rangle}{\langle 12\rangle\langle 34\rangle}, \frac{\langle 26\rangle\langle 34\rangle}{\langle 23\rangle\langle 46\rangle}, \frac{\langle 12\rangle\langle 34\rangle\langle 56\rangle}{\langle 23\rangle\langle 45\rangle\langle 16\rangle} \right\} . \quad (2.5.2)$$

Similarly, there are five homogeneous combinations that are made out of the 11 allowed neighbours of $\langle 2356\rangle = \langle 14\rangle$. They may be taken as the two $\mathcal{X}$-coordinates associated to the square (opposite edges on a square have the same $\mathcal{X}$-coordinate) as well as any three of the four $\mathcal{X}$-coordinates which are associated to the edges which lead away from the square face. A choice is as follows:

$$\text{hns}[\langle 14\rangle] = \left\{ \frac{\langle 14\rangle\langle 23\rangle}{\langle 12\rangle\langle 34\rangle}, \frac{\langle 14\rangle\langle 56\rangle}{\langle 16\rangle\langle 45\rangle}, \frac{\langle 13\rangle\langle 24\rangle}{\langle 12\rangle\langle 34\rangle}, \frac{\langle 15\rangle\langle 46\rangle}{\langle 16\rangle\langle 45\rangle}, \frac{\langle 13\rangle\langle 45\rangle}{\langle 34\rangle\langle 15\rangle} \right\} . \quad (2.5.3)$$

For the cases of the cluster algebras associated to $\text{Gr}(k,n)$ with (k,n) coprime, one has the advantage of using frozen coordinates to homogenise all remaining letters to construct a homogeneous alphabet. Since frozen coordinates appear in every cluster by definition, they cannot spoil cluster adjacency. Hence for (k,n) coprime, it is possible to talk about the cluster adjacency directly in terms of homogeneous letters such as those in equation (2.2.16) for seven-particle scattering and ignore the frozen coordinates altogether.

The E_6-shaped cluster contains one of each of the six cyclic classes of letters given in (2.2.16). If we freeze the node a_{13} the cluster algebra reduces to an A_5 algebra which generates 20 letters all of which are in a cluster with a_{13}. Including a_{13} itself we find 21 possible neighbours for a_{13}. The letters a_{16} and a_{17} are in the neighbour set of a_{13} but a_{11}, a_{12}, a_{14} and a_{15} are not, which implies the Steinmann conditions. The analysis applies similarly to all a_{1i} type letters and is in accordance with the first line of Table 2.1. If we freeze either of the nodes a_{24} or a_{37} the cluster algebra reduces to a D_5 algebra, generating 25 allowed neighbours in addition to the letter itself. Likewise freezing either a_{41} or a_{51} leads to an $A_4 \times A_1$ algebra which generates $14 + 2 = 16$ neighbouring letters in addition to the letter itself. Finally if we freeze the node a_{62} we obtain an $A_2 \times A_2 \times A_1$ subalgebra

which generates $5+5+2=12$ allowed neighbours in addition to a_{62} itself. Each subalgebra responsible for generating the allowed neighbour set of a given letter corresponds to a subpolytope in the whole E_6 polytope. One finds the following homogeneous neighbour sets for the letters a_{11}, a_{21}, a_{41} and a_{61}:

$$\begin{aligned}
\text{hns}[a_{11}] &= \{a_{11}, a_{14}, a_{15}, a_{21}, a_{22}, a_{24}, a_{25}, a_{26}, a_{31}, a_{33}, a_{34}, a_{35}, a_{37}, a_{41}, a_{43}, a_{46}, a_{51}, \\
&\qquad a_{53}, a_{56}, a_{62}, a_{67}\} \\
\text{hns}[a_{21}] &= \{a_{11}, a_{13}, a_{14}, a_{15}, a_{17}, a_{21}, a_{23}, a_{24}, a_{25}, a_{26}, a_{31}, a_{33}, a_{34}, a_{36}, a_{37}, a_{41}, a_{43}, \\
&\qquad a_{45}, a_{46}, a_{52}, a_{53}, a_{55}, a_{57}, a_{62}, a_{64}, a_{66}\} \\
\text{hns}[a_{41}] &= \{a_{11}, a_{13}, a_{16}, a_{21}, a_{23}, a_{24}, a_{26}, a_{31}, a_{33}, a_{35}, a_{36}, a_{41}, a_{43}, a_{46}, a_{51}, a_{62}, a_{67}\} \\
\text{hns}[a_{61}] &= \{a_{12}, a_{17}, a_{23}, a_{25}, a_{27}, a_{32}, a_{34}, a_{36}, a_{42}, a_{47}, a_{52}, a_{57}, a_{61}\}\,.
\end{aligned} \tag{2.5.4}$$

All other homogeneous neighbour sets for $\text{Gr}(4,7)$ can be obtained as cyclic rotations, reflections or parity conjugates of these.

2.5.2 Definition of cluster adjacent polylogarithms

We recall a polylogarithm of weight k obeys

$$df^{(k)} = \sum_{a\in\mathcal{A}} f^{(k-1)}_{[a]} d\log a\,, \tag{2.5.5}$$

where for us $\mathcal{A}$ is the set of all $\mathcal{A}$-coordinates of our cluster algebra. A cluster adjacent polylogarithm is one where the $f^{(k-1)}_{[a]}$ above additionally obey

$$df^{(k-1)}_{[a]} = \sum_{b\in\text{ns}[a]} f^{(k-2)}_{[b],a} d\log b\,, \tag{2.5.6}$$

where the sum is only over b in the neighbour set of a. We also insist that the $f^{(k-1)}_{[a]}$ are themselves cluster adjacent polylogarithms in the same sense, i.e.

$$df^{(k-2)}_{[b],a} = \sum_{c\in\text{ns}[b]} f^{(k-3)}_{[c],ba} d\log c\,, \tag{2.5.7}$$

and so on all the way down to weight zero. It follows from the above that all adjacent pairs in the symbol of a cluster adjacent polylogarithm $[\ldots\otimes a\otimes b\otimes\ldots]$ are such that $a\in\text{ns}[b]$ or equivalently $b\in\text{ns}[a]$.

Note that the above discussion is phrased in terms of the inhomogeneous $\mathcal{A}$-coordinates, even though we are always interested in homogeneous functions $f^{(k)}$. This simply means that all the $df^{(k)}$ above can be rewritten purely in terms of homogeneous combinations of $\mathcal{A}$-coordinates and the sum in (2.5.6) could be taken over the homogeneous neighbour set of a. In general, not all the cluster adjacency properties will be manifest in such a homogeneous representation, as happens in the hexagon case. In particular if we choose to write take sum in (2.5.6) over the homogeneous neighbour set of a, then each homogeneous b should be expanded in terms of the inhomogeneous $\mathcal{A}$-coordinates in order to then reveal the cluster adjacent nature of the expression (2.5.7).

In the heptagon case one can phrase the whole discussion in terms of the homogenised unfrozen coordinates and the sum in (2.5.6) can be taken over the homogeneous neighbour

sets given in (2.5.4). Since the frozen factors play no role in cluster adjacency this property can be made manifest at the same time as homogeneity.

In Table 2.2 we record the dimensions of the spaces of cluster adjacent symbols. Up to weight three all Steinmann symbols are cluster adjacent. At weight four there are 14 Steinmann symbols which fail to be cluster adjacent. They are of the form $[u \otimes (1-u) \otimes u \otimes u]$ for $u = \frac{a_{11}a_{12}}{a_{15}}$ or $u = a_{11}a_{13}$ and cyclic copies. The failure of adjacency comes in the last two slots as in either case the letter u may not appear next to itself. Interestingly, if we apply just the Steinmann conditions on the a_{1i}, but everywhere in the symbol as in [70, 129], then up to weight six the dimensions come out to be the same as with the cluster condition i.e. the 'extended' Steinmann condition and initial entry condition imply cluster adjacency. We do not yet know if this pattern continues.

Function space	1	2	3	4	5	6	7	8
7gon	7	42	237	1288	6763	?	?	?
Steinmann 7gon	7	28	97	322	1030	3192	9570	?
Cluster 7gon	7	28	97	308	911	2555	6826	?

Table 2.2: Dimensions of various spaces constructed from the $\mathcal{A}$-coordinates of the $\mathrm{Gr}(4,7)$ cluster algebra.

2.5.3 Neighbour-set functions

When constructing integrable cluster-adjacent functions, it is natural to introduce the concept of *neighbour-set functions*. They are defined as polylogarithms which satisfy

$$df^{(k)} = \sum_{b \in \mathrm{ns}[a]} f^{(k-1)}_{[b]} d\log b \tag{2.5.8}$$

for a given choice of $\mathcal{A}$-coordinate a. The final entries of the symbols of such functions are selected only from the neighbour set of a given $\mathcal{A}$-coordinate. As can be seen from (2.5.6) above, any cluster adjacent weight-k function only requires neighbour set functions in its $(k-1,1)$ coproduct. Hence, when constructing cluster adjacent functions of weight k one can use a reduced ansatz for the $(k-1,1)$ coproduct

$$f^{(k-1,1)} = \sum_{a \in \mathcal{A}} \sum_{i=1}^{d^{(k-1)}_{[a]}} c_{ai} \left[f^{(k-1)}_{[a],i} \otimes a \right], \tag{2.5.9}$$

where $f^{(k-1)}_{[a],i}$ are elements of a basis for the space of homogeneous weight-$(k-1)$ functions whose final entries are in the neighbour-set of a and $d^{(k-1)}_{[a]}$ is the dimension of this space. If the $\mathcal{A}$-coordinates a in (2.5.9) above cannot be chosen as unfrozen ones homogenised purely in terms of frozen ones, then the coefficients c_{ai} are assumed to be constrained to ensure homogeneity of the resulting expression. Eliminating any cluster-adjacency violation in the ansatz reduces the size of the resulting linear algebra problem. The notion of a neighbour set function is compatible with any possible choices of constraints in the initial entries, for

Weight	2	3	4	5	6	7	8	9	10	11	12	13	14
hns[$\langle 13\rangle$]	3	6	11	21	39	73	132	237	415	717	1216	2036	3358
hns[$\langle 14\rangle$]	3	5	10	19	36	66	120	213	374	644	1096	1835	3041
Full A_3	6	13	26	51	98	184	340	613	1085	1887	3224	5431	9014

Table 2.3: Dimensions of the spaces of integrable words in the hexagon alphabet with hexagon initial entries $\{u, v, w\}$ only and final entries drawn from the neighbour sets hns[$\langle 13\rangle$], hns[$\langle 14\rangle$] or from the full nine-letter A_3 alphabet.

Weight	2	3	4	5	6	7
hns[a_{1i}]	10	29	83	229	612	1577
hns[a_{2i}]	15	43	117	311	804	2025
hns[a_{4i}]	6	14	34	87	224	570
hns[a_{6i}]	4	11	29	76	193	476
Full E_6	28	97	308	911	2555	6826

Table 2.4: Dimensions of the neighbour-set function spaces of the heptagon alphabet with initial entries a_{1i} and the dimensions of the full cluster-adjacent heptagon functions

example when constructing hexagon symbols to describe six-point amplitudes in planar $\mathcal{N} = 4$ super Yang-Mills theory.

We now illustrate neighbour set functions for $\mathrm{Gr}(4, 6)$. In this case, there are two types of unfrozen $\mathcal{A}$-coordinates with neighbour set functions: $\langle 13\rangle$ & cyclic and $\langle 14\rangle$ & cyclic. The neighbour-set functions for the hexagon are then defined as homogeneous, cluster-adjacent functions that obey the initial entry condition, i.e. begin with the three-cross ratios of the hexagon (u, v or w from (2.2.14), and end with aforementioned homogeneous combinations that are cluster-adjacent to $\langle 13\rangle$ or $\langle 14\rangle$. The dimensions of such spaces for a few weights are compared to the full space of cluster-adjacent hexagon symbols is given in Table 2.3.

We have also computed the neighbour-set functions of the heptagon letters up to weight seven. The dimensions of the neighbour-set function spaces depend on the letter and they are summarised in Table 2.4. For weights 2-7 we find the span of all a_{2i} and a_{3i} neighbour-set function spaces covers the entire cluster-adjacent function space of the corresponding weight.

2.5.4 Integrability

It is interesting to investigate in low weights the spaces of cluster adjacent functions without any initial entry condition. At weight two we may split the space of integrable words into those which are symmetric in the two entries of the symbol and those which are antisymmetric. The symmetric ones are trivially integrable: any word of the form $[a \otimes b] + [b \otimes a]$ is the symbol of $\log a \log b$. Adjacency however constrains the possible choices of a and b - they must come from a common cluster, i.e. they must not correspond to distant faces on the polytope. The antisymmetric words on the other hand are not trivially integrable. However, they do automatically obey the adjacency condition, in the

sense that all antisymmetric integrable weight two words are cluster adjacent, even if that condition was not imposed in constructing them. Actually they obey a stronger condition, namely that the $\mathcal{A}$-coordinates appearing in the two slots can be found in some cluster together where they are connected by an arrow. The antisymmetric words correspond to combinations of dilogarithms.

The cluster adjacency criterion is therefore really a constraint on the *symmetric* and trivially integrable part. It implies that, even though any symmetric pair $[a \otimes b] + [b \otimes a]$ is integrable, to be admissible a and b must still appear together in some cluster. Moreover admissible pairs which are never connected by an arrow in any cluster must appear symetrically.

When we investigate weight three words we find that the associated triplets of $\mathcal{A}$-coordinates are of two possible types. Each term $[a \otimes b \otimes c]$ is either of the form where a, b and c can all be found together in the same cluster or we have $c = a'$ where a' is the result of mutating on a in some cluster. In fact there is an even stronger condition in this latter case: if we find triplets of the form $[a \otimes b \otimes a']$ then they can always be combined so that the intermediate letter becomes the $\mathcal{X}$-coordinate associated with the mutation pair (a, a'). Recall that $\mathcal{X}$-coordinates are associated to one-dimensional edges of the polytope which are also associated to mutations. Moreover if there is more than one edge between the two faces labelled by a and a' those edges are associated to the same $\mathcal{X}$-coordinate. In other words $\mathcal{X}$-coordinates are associated to mutation pairs of $\mathcal{A}$-coordinates, hence we may denote them by $x(a, a')$. So we have triplets of the form $[a \otimes x(a, a') \otimes a']$ or triplets $[a \otimes b \otimes c]$ where all three letters can be found together in some cluster. This implies that some pairs of letters such as a_{11} and a_{61} which neither share a cluster nor mutate into each other never appear together in a triplet - there must be at least two letters appearing between them in an admissible symbol.

Chapter 3

BCFW and NMHV

In this chapter we will develop the notion of cluster adjacency further. Since the monodromies of analytic functions in general and amplitudes in particular are typically non-abelian in nature, the cluster adjacency controlling their appearance has a non-abelian character; the order in which $\mathcal{A}$-coordinates appear in the symbol is important. Here we also develop an abelian version of adjacency which controls the poles of individual terms in tree-level amplitudes. We find that precisely the same notion of adjacency holds for individual BCFW terms, NMHV amplitudes and beyond. Since poles multiply in a commutative fashion the adjacency constraints apply to all poles in a given term.

When considering NMHV loop amplitudes we have expressions which simultaneously exhibit non-trivial poles and branch cuts. We find that the cluster structure also imposes relations between the two. Specifically we find that the derivatives of individual terms in NMHV loop amplitudes are constrained in such a way that they are compatible with the poles of the multiplying rational function. The cluster adjacency we find actually comprises a subset of the constraints which follow from dual superconformal symmetry [3]. At loop level these constraints are expressed through the $\bar{Q}$ equation of [121, 133]. So the cluster adjacency structure simultaneously implies both branch cut relations, e.g. the Steinmann relations, and derivative relations such as those following from dual superconformal symmetry.

As an example of the power and utility of the cluster adjacency principle we show here how it can be used to construct the four-loop NMHV heptagon amplitude from a rather minimal and manifestly cluster adjacent ansatz.

3.1 Cluster adjacency in hexagon and heptagon loop amplitudes

We have confirmed that all the currently available results for hexagon and heptagon functions appearing in the loop expansion of MHV and NMHV amplitudes are cluster adjacent polylogarithms. That is, the functions $\mathcal{E}^{\mathrm{MHV},(L)}$ and $E^{(L)}_{ijklm}$ are weight $2L$ polylogarithms whose symbols obey the cluster adjacency conditions and whose initial entries are constrained to be compatible with the physical branch cut conditions. In the hexagon case this means the initial entries are drawn from the set $\{u, v, w\}$ from (2.2.14) and in the

heptagon case that they are of the form a_{1i} from the heptagon alphabet given in (2.2.16).

In the MHV case the $(2L-1,1)$ coproduct of the polylogarithmic functions which appear is constrained in the final entries which are drawn only from $\mathcal{A}$-coordinates of the form $\langle i\, j-1\, j\, j+1\rangle$. This behaviour follows from an analysis of the $\bar{Q}$-equation of [121, 133]. This has the consequence that the $(n-1,1)$ coproduct of the MHV amplitudes is heavily constrained,

$$\mathcal{E}^{(2L-1,1)} = \sum_{i,j} [\mathcal{E}_{ij} \otimes \langle i\, j-1\, j\, j+1\rangle]\,, \tag{3.1.1}$$

where $\mathcal{E}_{ij}$ is a neighbour set function of the $\mathcal{A}$-coordinate $\langle i\, j-1\, j\, j+1\rangle$, i.e. it is a weight $(2L-1)$ polylogarithm whose symbol's final entries are drawn from the neighbour set of $\langle i\, j-1\, j\, j+1\rangle$.

In the NMHV case there is an interplay between the R-invariants and the final entries of the symbols of the polylogarithms which appear. We will address this point in greater detail in Section 3.3.

3.2 Cluster adjacency of tree-level BCFW recursion

It is clear from the above discussion that cluster adjacency of polylogarithms or symbols has a non-abelian character. Two $\mathcal{A}$-coordinates a and a' which cannot appear next to each other are allowed to appear in the same word if they are appropriately separated by intermediate $\mathcal{A}$-coordinates. For example, if they are separated by one step only the $\mathcal{X}$-coordinate associated to the relevant mutation appears between them, as discussed above. This non-abelian behaviour is due to the fact that the symbol comes with an ordering which ultimately reflects the fact that monodromies of the associated iterated integrals do not commute with each other.

However we now discuss a setting where an abelian form of cluster adjacency holds. It is in the context of the poles of rational functions contributing to tree-level amplitudes. Here we will restrict our discussion to the cluster adjacency properties of BCFW tree-amplitudes for NMHV and N^2MHV helicity configurations. The superconformal and dual superconformal symmetries are known to combine into a Yangian structure [100]. BCFW expansions for tree amplitudes are solved in terms of Yangian invariants. These quantities can be found as residues in the Grassmannian integral of [2, 5].

The pattern we find can be stated as follows: *every Yangian invariant in the BCFW expansion of tree amplitudes has poles given by $\mathcal{A}$-coordinates which can be found together in a common cluster.*

Expressions for BCFW expansions may be generated directly in momentum twistor variables using the `bcfw.m` package provided in [134]. We give explicit examples showing all BCFW terms obey the cluster adjacency property up to eight points. As well as providing another example in which the cluster algebra structure plays a role in controlling the singularities of amplitudes, the discussion of R-invariants will be relevant later when we consider NMHV loop amplitudes.

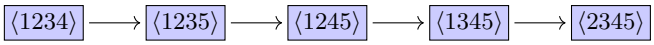

Figure 3.1: The single $\mathrm{Conf}_5(\mathbb{P}^3) \sim A_0$ cluster. All nodes are frozen.

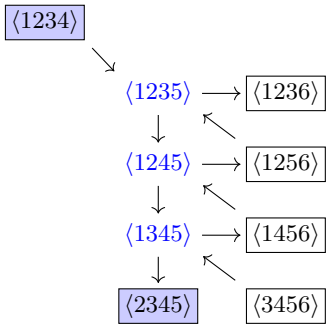

Figure 3.2: The cluster containing the poles of [12345] in $\mathrm{Conf}_6(\mathbb{P}^3)$.

3.2.1 NMHV

The BCFW expansion of the n-point NMHV tree amplitude of $\mathcal{N} = 4$ SYM (divided by the MHV tree) can be written as a linear combination of R-invariants

$$\mathcal{A}_{n,1}^{\text{tree}} = \sum_{1<i<j<n} [1ii+1jj+1] \tag{3.2.1}$$

We will now show that the $\mathcal{A}$-coordinates which describe the poles of R-invariants obey an abelian form of cluster adjacency: it is always possible to find a cluster where all the poles of an R-invariant appear together. Since the poles multiply in a commutative fashion there is no ordering to them and it is natural therefore that adjacency simply requires them all to appear together in some cluster.

Five points

Five-points is a trivial example as there is just one R-invariant and hence the amplitude is simply

$$\mathcal{A}_{5,1} = [12345], \tag{3.2.2}$$

also $\mathrm{Conf}_5(\mathbb{P}^3)$ contains just one cluster containing all frozen nodes. The nodes in Fig. 3.1 are coloured blue to indicate that they are present as poles in the R-invariant [12345]. The basic R-invariant (3.2.2) and its associated cluster will be the starting point for analysing all other NMHV R-invariants.

Six points

At six-points there is only one type of R-invariant, [12345] and its cyclic rotations, which make up the six-point, NMHV, tree given as

$$\mathcal{A}_{6,1} = [12345] + [12356] + [13456] = [12346] + [12456] + [23456]. \tag{3.2.3}$$

Since every R-invariant at six points is a rotation of (3.2.2) in $\mathrm{Conf}_6(\mathbb{P}^3)$ we can identify each one with a single cluster in the polytope, one of which is given in Fig. 3.2. One would obtain the other five R-invariants and their associated clusters through cyclic rotations of

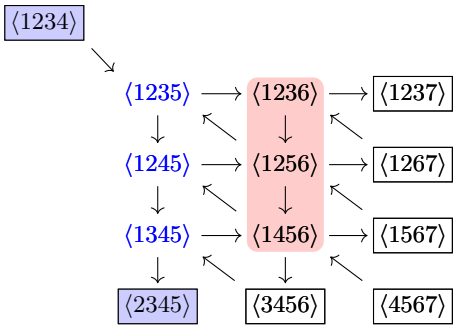

Figure 3.3: A cluster containing the poles of [12345] in $\mathrm{Conf}_7(\mathbb{P}^3)$. The unfrozen nodes highlighted in red generate an A_3 subalgebra by repeated mutation.

this cluster. This can be achieved by applying the sequence of mutations illustrated in Figure 2.3 which generates a cyclic rotation. The clusters associated to the R-invariants are the six associated to the top and bottom corners of the square faces in Figure 2.3.

Note that while the full tree amplitude (3.2.3) only contains physical poles of the form $\langle 1245\rangle \sim 1/x_{25}^2 = 1/(p_2+p_3+p_4)^2$ and rotations, the adjacency property holds term by term in the BCFW expansion. Hence it also constrains the way in which the spurious poles at $\langle 1235\rangle = 0$ and its cyclic rotations may appear. A consequence of the adjacency property is the well-known fact that the tree amplitude cannot have simultaneous poles in two different factorisation channels. For example, there is no term with both $\langle 1245\rangle$ and $\langle 2356\rangle$ in the denominator. This statement is the analogue of the fact that the Steinmann relations follow from cluster adjacency in the loop amplitudes.

Seven points and beyond

At seven points there are three types of R-invariant,

$$[12345]\ \&\ \text{cyclic}, \quad [12346]\ \&\ \text{cyclic}, \quad [12356]\ \&\ \text{cyclic}. \tag{3.2.4}$$

The tree amplitude takes the form

$$\mathcal{A}_{7,1} = [12345] + [12356] + [12367] + [13456] + [13467] + [14567]\,. \tag{3.2.5}$$

As with (3.2.3), the BCFW representation of this amplitude is not unique due to the identity among the R-invariants (1.3.37). At seven points multiple clusters contain the poles of a given R-invariant and hence R-invariants are associated to sub-algebras in the full $\mathrm{Conf}_7(\mathbb{P}^3)$ cluster algebra. For example, the initial cluster in Figure 2.7 contains all the poles of [12345]. It also contains three more unfrozen nodes in the second column. Performing all possible mutations in the second column generates an entire A_3 subalgebra, all of whose clusters contain the poles of [12345]. This is illustrated in Fig. 3.3. The other two types of R-invariants in (3.2.4) appear respectively in A_2 and A_1 subalgebras.

One form of the eight-point NMHV tree amplitude is given by

$$\begin{aligned}\mathcal{A}_{8,1} =&[12345] + [12356] + [12367] + [12378] + [13456]\\ &+[13467] + [13478] + [14567] + [14578] + [15678].\end{aligned} \tag{3.2.6}$$

n	5	6	7	8
[12345]	A_0	A_0	A_3	E_6
[12356]	–	A_0	A_1	A_4
[12346]	–	A_0	A_2	A_5
[13467]	–	–	A_1	$A_2 \times A_1 \times A_1$
[12357]	–	–	A_2	A_4

Table 3.1: Various R-invariants and their subalgebras in $\text{Conf}_n(\mathbb{P}^3)$ at different multiplicities n.

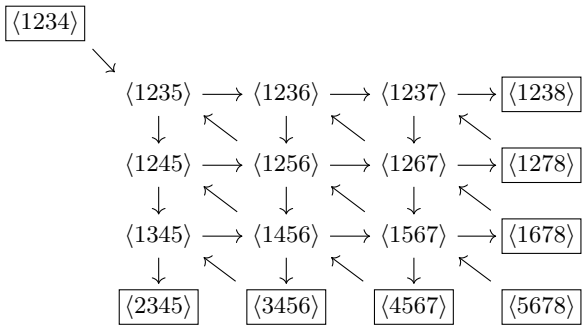

Figure 3.4: A cluster containing the poles of [12345] in $\text{Conf}_8(\mathbb{P}^3)$.

As we can see, more types of R-invariants begin to appear at eight points so we have presented their subalgebras in Table 3.1 below along with their subalgebras at lower points. The notation A_0 in Table 3.1 indicates that a single cluster is associated to that R-invariant. The last R-invariant [12357] does not appear in the BCFW expansion of any tree in formula (3.2.1) amplitude but we can nevertheless associate a sub-algebra to this Yangian invariant object.

As described in Section 2.2.3 above, one can rotate the nodes in an initial-type cluster by mutating up all consecutive columns. Using this we can show that one can obtain any R-invariant by starting with the initial cluster, which we associate to [12345], and mutating in different $\text{Conf}_n(\mathbb{P}^3)$ sub-algebras. We illustrate this procedure with the following eight-point example: we will find a cluster in $\text{Conf}_8(\mathbb{P}^3)$ which contains the poles of [13467].

Starting from [12345], the sequence of rotations to get [13467] is

$$[12345] \xrightarrow{+4} [12356] \xrightarrow{+5} [13467] \tag{3.2.7}$$

where the rotations are in $\text{Conf}_6(\mathbb{P}^3)$ and $\text{Conf}_7(\mathbb{P}^3)$ respectively. To find a cluster in $\text{Conf}_8(\mathbb{P}^3)$ with all the $\mathcal{A}$-coordinates we need we start from the initial cluster (shown in Fig. 3.4) and mutate in the $\text{Conf}_7(\mathbb{P}^3)$ subalgebra (the first two columns) such that its nodes rotate by five to arrive at the cluster shown in Fig. 3.5. Then we mutate in the $\text{Conf}_6(\mathbb{P}^3)$ subalgebra (the first column only) such that its nodes rotate by four. Beginning with the $\text{Conf}_8(\mathbb{P}^3)$ initial cluster we employ our mutation prescription by mutating up the first column, followed by the second column, repeating this another four times which results in the cluster shown in Fig. 3.5 where the unchanged topology of the $\text{Conf}_7(\mathbb{P}^3)$ subalgebra is given in green. We now mutate up the first column in the green section

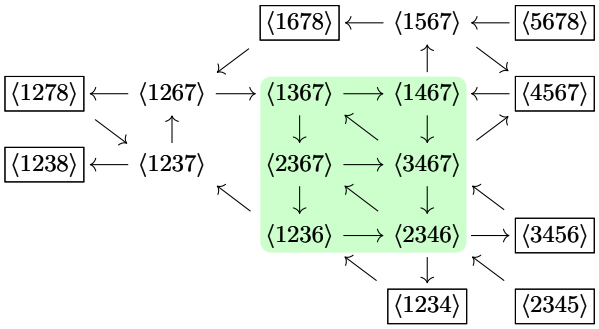

Figure 3.5: The cluster obtained after five cyclic mutations of Fig. 3.4 in the first two columns.

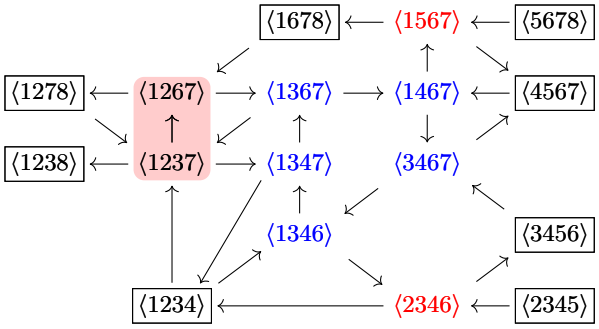

Figure 3.6: A cluster containing the poles of the R-invariant [13467].

four times, resulting in the final cluster shown in Fig. 3.6 where the poles of [13467] are in blue and the $A_2 \times A_1 \times A_1$ subalgebra is in red in agreement with Table 3.1. Using this procedure one can locate a cluster which contains the poles of any R-invariant for an arbitrary number of points.

3.2.2 Beyond NMHV

Beyond NMHV, terms in BCFW tree amplitudes are more complicated than simple R-invariants so it is less obvious that one could associate subalgebras of $\text{Conf}_n(\mathbb{P}^3)$ cluster algebras to individual terms. We show, up to eight points, that one can do this in much the same way as for NMHV.

Six points

At six points the N^{2}MHV amplitude is equivalent to the $\overline{\text{MHV}}$ amplitude. It is given by

$$\mathcal{A}_{6,2} = \frac{\langle\langle 123456\rangle\rangle}{\langle 1234\rangle\langle 1236\rangle\langle 1256\rangle\langle 1456\rangle\langle 2345\rangle\langle 3456\rangle} \tag{3.2.8}$$

where

$$\langle\langle ijklmn\rangle\rangle = \frac{\langle\langle ijkmn\rangle\rangle\langle\langle jklmn\rangle\rangle}{\langle jkmn\rangle^4} \tag{3.2.9}$$

is cyclically invariant and polynomial although not manifestly so in this form. The five-index object is given by $\langle\langle ijklm\rangle\rangle = \delta^{0|4}(\chi_i\langle jklm\rangle + \text{cyclic})$.

Identifying a cluster with (3.2.8) is trivial since every pole is an adjacent bracket and hence appears in every cluster in $\text{Conf}_6(\mathbb{P}^3)$ i.e. one can associate this amplitude with the entire A_3 cluster algebra. The blue nodes correspond to poles in the amplitude and the

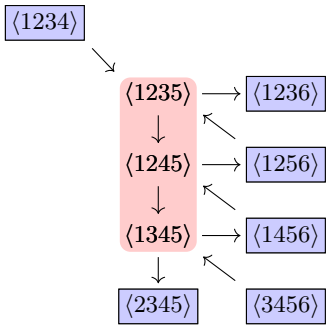

Figure 3.7: A cluster in A_3 corresponding to the six-point N^{2}MHV amplitude.

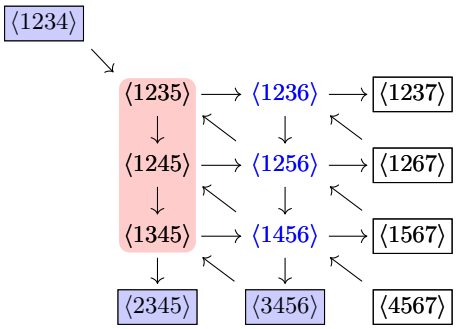

Figure 3.8: A cluster containing the poles of $\mathcal{A}_{6,2}$ in $\text{Conf}_7(\mathbb{P}^3)$.

nodes highlighted in red correspond to the full A_3 algebra in which the amplitude lives.

Seven points

The seven-point, N^{2}MHV, tree-amplitude is equivalent to the $\overline{\text{NMHV}}$ amplitude

$$\begin{aligned}\mathcal{A}_{7,2} = \mathcal{A}_{6,2} &\\ &+ \frac{\langle\langle 134567\rangle\rangle}{\langle 1345\rangle\langle 1347\rangle\langle 1367\rangle\langle 1567\rangle\langle 3456\rangle\langle 4567\rangle}\\ &+ \frac{\langle\langle 123467\rangle\rangle}{\langle 1234\rangle\langle 1237\rangle\langle 1267\rangle\langle 1467\rangle\langle 2346\rangle\langle 3467\rangle}\\ &+ \frac{\langle\langle 12345\rangle\rangle\langle\langle 14567\rangle\rangle}{\langle 1234\rangle\langle 1245\rangle\langle 1345\rangle\langle 1456\rangle\langle 1457\rangle\langle 1567\rangle\langle 2345\rangle\langle 4567\rangle\langle 1(23)(45)(67)\rangle}\\ &+ \frac{\langle\langle 12367\rangle\rangle\langle\langle 23456\rangle\rangle}{\langle 1236\rangle\langle 1237\rangle\langle 1267\rangle\langle 2345\rangle\langle 2346\rangle\langle 2356\rangle\langle 2367\rangle\langle 3456\rangle\langle 6(23)(45)(17)\rangle}\\ &+ \frac{\langle\langle 12367\rangle\rangle\langle\langle 14567\rangle\rangle}{\langle 1237\rangle\langle 1267\rangle\langle 1367\rangle\langle 1467\rangle\langle 1567\rangle\langle 4567\rangle\langle 1(23)(45)(67)\rangle\langle 6(23)(45)(17)\rangle}.\end{aligned} \tag{3.2.10}$$

The first term is equal to the expression (3.2.8) for the six-point amplitude. It is now in $\text{Conf}_7(\mathbb{P}^3) \sim E_6$ therefore some of the poles are now unfrozen and the A_3 algebra is now a subalgebra of the full E_6 algebra, as shown in Fig. 3.8. As before, the blue nodes correspond to poles in the term while the nodes highlighted in red correspond to an A_3 subalgebra inside the full E_6 algebra in which all the poles of (3.2.8) can be found. The second and third terms of (3.2.10) can be obtained by rotating the momentum twistors in (3.2.8) by two and five units respectively and hence one can obtain clusters containing

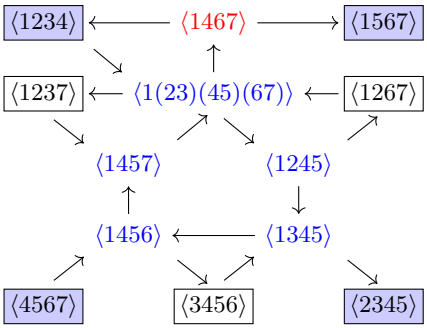

Figure 3.9: A cluster corresponding to the 4^{th} term in $\mathcal{A}_{7,2}$.

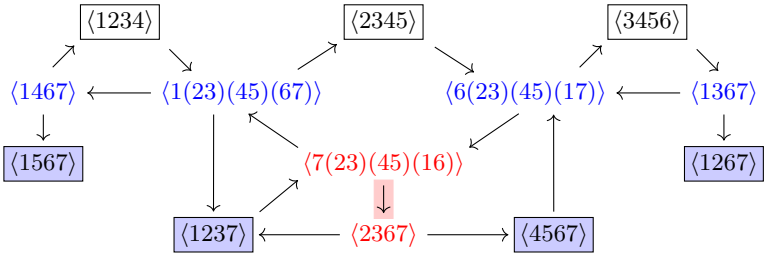

Figure 3.10: A cluster corresponding to the 6^{th} term in $\mathcal{A}_{7,2}$.

their poles by rotating Fig. 3.8 by the same amounts. We can associate the fourth term of (3.2.10) with an A_1 subalgebra as shown in Fig. 3.9. One can obtain the fifth term by rotating the fourth term by five units hence it also lives in an A_1 subalgebra found by rotating Fig. 3.9 by five units. Finally, the sixth term can be associated to an A_2 subalgebra as illustrated in Fig. 3.10.

Eight points

The eight-point N^2MHV amplitude is the first true N^2MHV amplitude in that it is not equivalent to the parity conjugate of another $\text{N}^{k<2}\text{MHV}$ amplitude. Explicitly it is given by

Term	Sub-Algebra	Term	Sub-Algebra	Term	Sub-Algebra	Term	Sub-Algebra
1	$A_3 \times A_3$	6	A_2	11	$A_3 \times A_1$	16	$A_1 \times A_1$
2	$A_3 \times A_2$	7	$A_3 \times A_3$	12	$A_1 \times A_1$	17	$A_2 \times A_1$
3	$A_3 \times A_1$	8	A_3	13	$A_1 \times A_1$	18	$A_3 \times A_2$
4	$A_2 \times A_1$	9	$A_3 \times A_3$	14	$A_2 \times A_1$	19	$A_2 \times A_1$
5	$A_1 \times A_1$	10	A_3	15	$A_1 \times A_1$	20	A_2

Table 3.2: Subalgebras associated to terms in $\mathcal{A}_{8,2}$.

$$
\begin{aligned}
\mathcal{A}_{8,2} = \mathcal{A}_{7,2}
&+ \frac{\langle\langle 123478\rangle\rangle}{\langle 1234\rangle\langle 1238\rangle\langle 1278\rangle\langle 1478\rangle\langle 2347\rangle\langle 3478\rangle} \\
&+ \frac{\langle\langle 134578\rangle\rangle}{\langle 1345\rangle\langle 1348\rangle\langle 1378\rangle\langle 1578\rangle\langle 3457\rangle\langle 4578\rangle} \\
&+ \frac{\langle\langle 145678\rangle\rangle}{\langle 1456\rangle\langle 1458\rangle\langle 1478\rangle\langle 1678\rangle\langle 4567\rangle\langle 5678\rangle} \\
&+ \frac{\langle\langle 12345\rangle\rangle\langle\langle 15678\rangle\rangle}{\langle 1234\rangle\langle 1235\rangle\langle 1245\rangle\langle 1345\rangle\langle 1567\rangle\langle 1568\rangle\langle 1578\rangle\langle 1678\rangle\langle 2345\rangle\langle 5678\rangle} \\
&- \frac{\langle\langle 12378\rangle\rangle\langle\langle 23456\rangle\rangle}{\langle 1237\rangle\langle 1238\rangle\langle 1278\rangle\langle 2345\rangle\langle 2346\rangle\langle 2356\rangle\langle 2378\rangle\langle 3456\rangle\langle 23\bar{5}\cap\bar{8}\rangle} \\
&+ \frac{\langle\langle 12345\rangle\rangle\langle\langle 14578\rangle\rangle}{\langle 1234\rangle\langle 1245\rangle\langle 1345\rangle\langle 1457\rangle\langle 1458\rangle\langle 1578\rangle\langle 2345\rangle\langle 4578\rangle\langle 1(23)(45)(78)\rangle} \\
&+ \frac{\langle\langle 12356\rangle\rangle\langle\langle 15678\rangle\rangle}{\langle 1235\rangle\langle 1256\rangle\langle 1356\rangle\langle 1567\rangle\langle 1568\rangle\langle 1678\rangle\langle 2356\rangle\langle 5678\rangle\langle 1(23)(56)(78)\rangle} \\
&+ \frac{\langle\langle 13456\rangle\rangle\langle\langle 15678\rangle\rangle}{\langle 1345\rangle\langle 1356\rangle\langle 1456\rangle\langle 1567\rangle\langle 1568\rangle\langle 1678\rangle\langle 3456\rangle\langle 5678\rangle\langle 1(34)(56)(78)\rangle} \\
&+ \frac{\langle\langle 12378\rangle\rangle\langle\langle 23467\rangle\rangle}{\langle 1237\rangle\langle 1238\rangle\langle 1278\rangle\langle 2346\rangle\langle 2347\rangle\langle 2367\rangle\langle 2378\rangle\langle 3467\rangle\langle 7(23)(46)(18)\rangle} \\
&+ \frac{\langle\langle 13478\rangle\rangle\langle\langle 34567\rangle\rangle}{\langle 1347\rangle\langle 1348\rangle\langle 1378\rangle\langle 3456\rangle\langle 3457\rangle\langle 3467\rangle\langle 3478\rangle\langle 4567\rangle\langle 7(34)(56)(18)\rangle} \\
&+ \frac{\langle\langle 12378\rangle\rangle\langle\langle 14578\rangle\rangle}{\langle 1238\rangle\langle 1278\rangle\langle 1378\rangle\langle 1478\rangle\langle 1578\rangle\langle 4578\rangle\langle 1(23)(45)(78)\rangle\langle 7(23)(45)(18)\rangle} \\
&+ \frac{\langle\langle 12378\rangle\rangle\langle\langle 15678\rangle\rangle}{\langle 1238\rangle\langle 1278\rangle\langle 1378\rangle\langle 1578\rangle\langle 1678\rangle\langle 5678\rangle\langle 1(23)(56)(78)\rangle\langle 7(23)(56)(18)\rangle} \\
&+ \frac{\langle\langle 13478\rangle\rangle\langle\langle 15678\rangle\rangle}{\langle 1348\rangle\langle 1378\rangle\langle 1478\rangle\langle 1578\rangle\langle 1678\rangle\langle 5678\rangle\langle 1(34)(56)(78)\rangle\langle 7(34)(56)(18)\rangle} \\
&+ \frac{\langle\langle 12378\rangle\rangle\Delta^{0|4}}{\langle 1237\rangle\langle 1238\rangle\langle 1378\rangle\langle 2378\rangle\langle 4567\rangle\langle 23\bar{5}\cap\bar{8}\rangle\langle 7(23)(45)(18)\rangle\langle 7(23)(46)(18)\rangle\langle 7(23)(56)(18)\rangle}
\end{aligned}
\tag{3.2.11}
$$

where in the last term we have the quantity $\Delta^{0|4} = \delta^{0|4}(\chi_2\langle 1378\rangle\langle 4567\rangle - \chi_3\langle 1278\rangle\langle 4567\rangle - \chi_4\langle 7(23)(56)(18)\rangle + \chi_5\langle 7(23)(46)(18)\rangle - \chi_6\langle 7(23)(45)(18)\rangle - \chi_7\langle 23\bar{5}\cap\bar{8}\rangle)$.

At eight points, $\mathrm{Conf}_8(\mathbb{P}^3)$ is an infinite cluster algebra, however we can still associate finite subalgebras to each of the 20 terms in the amplitude. These subalgebras are displayed in Table 3.2 where terms 1-6 are those in (3.2.10). Although the subalgebras shown in Table 3.2 are all finite, at higher points they may become infinite. For example, the subalgebra associated to (3.2.8) at ten points will be $A_3 \times \mathrm{Conf}_8(\mathbb{P}^3)$ which is infinite as $\mathrm{Conf}_8(\mathbb{P}^3)$ is infinite.

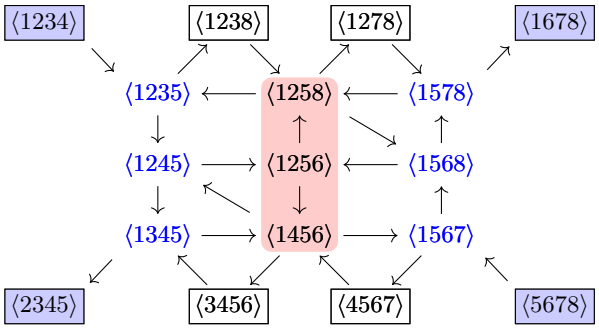

Figure 3.11: A cluster containing the poles of [12345][56781] in $\text{Conf}_8(\mathbb{P}^3)$.

The tenth term is a new type of term of the form

$$[12345][56781]\,, \tag{3.2.12}$$

to which we can associate an A_3 subalgebra, a cluster belonging to which takes the form shown in Fig. 3.11 below. The left and right columns of blue nodes in Fig. 3.11 correspond to the poles of [12345] and [56781] respectively while the red column signifies the A_3 subalgebra to which we associate this term.

3.2.3 Discussion

We have shown that all NMHV R-invariants obey the cluster adjacency property in that their poles can all be found together in some cluster. We have also shown that the BCFW terms in the expansion of N^{2}MHV trees also obey cluster adjacency for six, seven, and eight points. To each term is associated some subalgebra in the full polytope where every cluster contains all of the poles. Similar structures have emerged in the study of the Grassmannian integrals of [2, 5] and on-shell diagrams [23]. The difference here is that the properties we observe between poles (both physical and spurious) are phrased in the same language that we have found relates the branch cuts (symbol entries) of the integrated amplitudes.

The results for tree-level NMHV and N^{2}MHV are highly suggestive that there should exist a general relation between the singularities of the Yangian invariant leading singularities and the cluster algebras associated to $\text{Conf}_n(\mathbb{P}^3)$. A natural question is whether an extension of the notion of cluster adjacency holds for all Yangian invariants. This would lead us to consider quantities which go beyond $\mathcal{A}$-coordinates for $\text{Conf}_n(\mathbb{P}^3)$ such as the four-mass box leading singularity which exhibits square root branch cuts in momentum twistor variables. Studying such quantities should lead to insight on what cluster adjacency has to say beyond rational $\mathcal{A}$-coordinates and should have implications for understanding the boundary structure of higher polytopes and the type of transcendental functions which appear beyond seven-point amplitudes.

Certain operations can also be performed on Yangian invariants [86], e.g. the 'fusing' of two Yangian invariants is also a Yangian invariant. Could one find a cluster interpretation of such an operation? The cluster shown in Fig. 3.11 contains the poles of the product of two Yangian invariants and could also be indicative of the amalgamation procedure [23] whereby two clusters can be joined together to produce a cluster in a larger algebra.

3.3 NMHV loop amplitudes

Now we are in a position to relate the cluster adjacency properties described in the two previous sections. The first amplitudes which exhibit both poles and cuts non-trivially are the NMHV loop amplitudes.

3.3.1 Hexagons

The BDS-like subtracted NMHV hexagon is often written in terms of a parity even function $E(u,v,w) = E(Z_1,\ldots,Z_6)$ and a parity odd function[3] $\tilde{E}(y_u,y_v,y_w) = \tilde{E}(Z_1,\ldots,Z_6)$, where we have drawn attention to their dependence on the twistor variables. Here we will adopt a shorthand notation which makes reference to the which of the cyclically ordered twistors Z_i sits in the first argument,

$$\begin{aligned} &E_1 = E(u,v,w)\,, && E_2 = E(v,w,u)\,, && E_3 = E(w,u,v)\,, \\ &\tilde{E}_1 = E(y_u,y_v,y_w)\,, && \tilde{E}_2 = -\tilde{E}(y_v,y_w,y_u)\,, && \tilde{E}_3 = E(y_w,y_u,y_v)\,. \end{aligned} \tag{3.3.1}$$

The parity properties of E and $\tilde{E}$ imply

$$E_4 = E_1\,, \qquad \tilde{E}_4 = -\tilde{E}_1\,. \tag{3.3.2}$$

With this notation the hexagon NMHV amplitude takes the form

$$\begin{aligned} \mathcal{E}_{6,\mathrm{NMHV}} =& E_1[(1)+(4)] + E_2[(2)+(5)] + E_3[(3)+(6)] \\ &+\tilde{E}_1[(1)-(4)] + \tilde{E}_2[(2)-(5)] + \tilde{E}_3[(3)-(6)]\,. \end{aligned} \tag{3.3.3}$$

Here we have adopted a common shorthand notation for the R-invariants: we write $(1) = [23456]$ and cyclically related formulae. The function $\tilde{E}$ is taken to obey

$$\tilde{E}_1 - \tilde{E}_2 + \tilde{E}_3 = 0\,. \tag{3.3.4}$$

We may equivalently write $\mathcal{E}_6^{\mathrm{NMHV}}$ as follows,

$$\mathcal{E}_{6,\mathrm{NMHV}} = (1)F_1 + \text{ cyc.} \qquad F_1 = E_1 + \tilde{E}_1\,. \tag{3.3.5}$$

In (3.3.5) the notation 'cyc' refers to all cyclic rotations of the momentum twistors. At L loops the functions E and $\tilde{E}$ are weight $2L$ polylogarithms.

To discuss the cluster adjacency properties of the hexagon NMHV amplitudes we should consider the $(2L-1,1)$ coproduct of $\mathcal{E}_{6,\mathrm{NMHV}}$,

$$\mathcal{E}^{(2L-1,1)}_{6,\mathrm{NMHV}} = (1)\sum_{i<j<k<l} [F_1^{\langle ijkl\rangle} \otimes \langle ijkl\rangle] + \text{ cyc.} \tag{3.3.6}$$

Cluster adjacency manifest itself in two ways in the above expression. Firstly the $F^{\langle ijkl\rangle}$ are neighbour set functions for $\langle ijkl\rangle$. This is the statement that F and hence E and $\tilde{E}$ cluster adjacent polylogarithms in the sense described in Section 2.5.2. Secondly we find that the different functions $F_1^{\langle ijkl\rangle}$ appearing in (3.3.6) are constrained by the fact that F_1 appears with the R-invariant (1) in (3.3.5).

[3]Sometimes $\tilde{E}(y_u,y_v,y_w)$ denoted simply as $\tilde{E}(u,v,w)$, in which case one should in addition take care to remember its odd parity.

In order to reveal the additional constraints that cluster adjacency places on the form of F we exploit the fact that the R-invariants obey the identity

$$(1) - (2) + (3) - (4) + (5) - (6) = 0\,. \tag{3.3.7}$$

This allows us to modify the presentation of $\mathcal{E}^{(2L-1,1)}_{6,\text{NMHV}}$ by adding to it a vanishing term of the form

$$[(1) - (2) + (3) - (4) + (5) - (6)]Z_1\,, \tag{3.3.8}$$

where Z is given by

$$Z_1 = \sum_{i<j<k<l} [Z_1^{\langle ijkl\rangle} \otimes \langle ijkl\rangle]\,. \tag{3.3.9}$$

Here (by cyclically symmetrising (3.3.8) if necessary) we can require that Z is anti-cyclic,

$$Z_2 = -Z_1\,. \tag{3.3.10}$$

This means that the presentation of $\mathcal{E}^{(2L-1,1)}_{6,\text{NMHV}}$ is still manifestly cyclic,

$$\mathcal{E}^{(2L-1,1)}_{6,\text{NMHV}} = (1) \sum_{i<j<k<l} [(F_1^{\langle ijkl\rangle} + Z_1^{\langle ijkl\rangle}) \otimes \langle ijkl\rangle] + \text{ cyc.} \tag{3.3.11}$$

We find the following additional cluster adjacency property of all hexagon NMHV loop amplitudes: *there exists a Z such that the only $\mathcal{A}$-coordinates $\langle ijkl\rangle$ appearing in (3.3.11) are in the neighbour set of every $\mathcal{A}$-coordinate in the denominator of the R-invariant* (1).

As we have discussed in Section 3.2.1, the R-invariant $(1) = [23456]$ is associated to a single cluster in $\text{Conf}_6(\mathbb{P}^3)$ (in fact it is the one whose triangulation involves all the chords of the form $(1i)$). It follows that the only unfrozen $\mathcal{A}$-coordinates allowed in the final entries are the ones of that cluster, namely $\langle 2346\rangle = (15)$, $\langle 2356\rangle = (14)$ and $\langle 2456\rangle = (13)$. The following unfrozen $\mathcal{A}$-coordinates,

$$\{\langle 1235\rangle, \langle 1245\rangle, \langle 1246\rangle, \langle 1345\rangle, \langle 1346\rangle, \langle 1356\rangle\}\,, \tag{3.3.12}$$

are therefore forbidden in the sum in (3.3.11) above.

Note that since Z is multiplied by zero in (3.3.8) we do not need to require that it is integrable, nor even that it is homogeneous. Nevertheless, the fact that it exists and obeys (3.3.10) has the following implications for the final entries (or $(n-1,1)$ coproduct) of F,

$$\begin{aligned}
F_1^{\langle 1235\rangle} &= -Z_1^{\langle 1235\rangle}\,,\\
F_1^{\langle 1246\rangle} &= -Z_1^{\langle 1246\rangle}\,,\\
F_1^{\langle 1345\rangle} &= -Z_1^{\langle 1345\rangle}\,,\\
F_1^{\langle 1356\rangle} &= -Z_1^{\langle 1356\rangle}\,,\\
F_1^{\langle 1245\rangle} &= -Z_1^{\langle 1245\rangle}\,,\\
F_1^{\langle 1346\rangle} &= -Z_1^{\langle 1346\rangle}\,.
\end{aligned} \tag{3.3.13}$$

The anti-cyclicity of Z implies[4]

$$\begin{aligned} Z_1^{\langle 1246\rangle} &= -Z_6^{\langle 1235\rangle}\,, \\ Z_1^{\langle 1345\rangle} &= +Z_3^{\langle 1235\rangle}\,, \\ Z_1^{\langle 1356\rangle} &= +Z_5^{\langle 1235\rangle}\,, \\ Z_1^{\langle 1346\rangle} &= +Z_3^{\langle 1245\rangle}\,. \end{aligned} \tag{3.3.14}$$

Combining the above two sets of relations we deduce that adjacency implies the following relations among the coproducts of F,

$$\begin{aligned} F_1^{\langle 1246\rangle} &= -F_6^{\langle 1235\rangle}\,, \\ F_1^{\langle 1345\rangle} &= +F_3^{\langle 1235\rangle}\,, \\ F_1^{\langle 1356\rangle} &= +F_5^{\langle 1235\rangle}\,, \\ F_1^{\langle 1346\rangle} &= +F_3^{\langle 1245\rangle}\,. \end{aligned} \tag{3.3.15}$$

The equations (3.3.15) are the consequences of cluster adjacency between the final entries of the coproduct of $F = E + \tilde{E}$ and the R-invariants.

As discussed in [46], similar coproduct relations follow from the $\bar{Q}$-equation of [121, 133]. We may ask how the $\bar{Q}$ conditions are related to the adjacency ones. To do this it is simplest to count how many homogeneous (final entry)$\otimes$(R-invariant) combinations are allowed by cluster adjacency. To do this one may choose five independent R-invariants, say $(1), (2), (3), (4), (5)$, and nine $d\log$'s of multiplicatively independent homogeneous letters and make an arbitrary linear combination of all 45 possible products. We expand the resulting expression into the $d\log\langle ijkl\rangle$ and eliminate all pairs $(m)\, d\log\langle ijkl\rangle$ which obey adjacency (taking care to remember that some $\mathcal{A}$-coordinates are compatible with the R-invariant $(6) = (1) - (2) + (3) - (4) + (5)$) and require the resulting combination to vanish. This yields 27 conditions, leaving 18 linearly independent homogeneous (final entry)$\otimes$(R-invariant) combinations. This is exactly the same number of linearly independent combinations which are compatible with the $\bar{Q}$ final entry conditions described in [46].

We conclude that for the NMHV hexagon, the cluster adjacency property is equivalent to the $\bar{Q}$ final entry conditions. One should nevertheless stress that the $\bar{Q}$ equation itself is stronger than just the final entry conditions as it expresses the $(2L-1, 1)$ coproduct entries in terms of and integral over a limit of certain heptagon amplitudes. We find it remarkable that cluster adjacency property in its various forms encompasses both the (extended) Steinmann conditions as well as some of the implications of dual superconformal symmetry.

3.3.2 Heptagons

In the case of heptagons it is possible to write down 21 R-invariants,

$$(12) = [34567]\,, \qquad (13) = [24567]\,, \qquad (14) = [23567] \quad \& \text{ cyclic}\,. \tag{3.3.16}$$

[4]We remind the reader that the subscripts refer to the arguments of functions. For example, $Z_6^{\langle 1235\rangle}$ means $Z_1^{\langle 1235\rangle}|_{Z_i \to Z_{i-1}}$ and not the $\langle 1235\rangle$ coproduct element of Z_6.

They satisfy seven six-term identities of the form

$$(12) - (13) + (14) - (15) + (16) - (17) = 0 \quad \& \text{ cyclic}\,. \tag{3.3.17}$$

Only six of these identities are linearly independent and the number of independent R-invariants is therefore 15, which can be chosen as [121]

$$\begin{aligned} &\mathcal{E}^{(0)}_{7,\text{NMHV}} = (12) + (14) + (34) + (16) + (36) + (56)\,, \\ &(12) \qquad \& \text{ cyclic}\,, \\ &(14) \qquad \& \text{ cyclic}\,. \end{aligned} \tag{3.3.18}$$

In this basis the BDS-like-normalised amplitude is expressed as follows:

$$\mathcal{E}_{7,\text{NHMV}} = \mathcal{A}_{7,1} E_0 + \big[(12)\, E_{12} + \text{cyclic} + (14)\, E_{14} + \text{cyclic}\big]\,, \tag{3.3.19}$$

where $\mathcal{A}_{7,1}$ is equal to the NMHV tree amplitude, given in (3.2.5).

The property of cluster adjacency again manifests itself in the heptagon NMHV amplitudes. It is possible to find a representation of the $(2L-1,1)$ coproduct of the form

$$\mathcal{E}^{(2L-1,1)}_{7,\text{NMHV}} = \sum_{a\in\mathcal{A}} \big[[(12)e^a_{12} + (13)e^a_{13} + (14)e^a_{14}] \otimes a\big] + \text{ cyc.} \tag{3.3.20}$$

Here the sum is over the heptagon alphabet (2.2.16). As in the hexagon case, adjacency manifests itself in two ways in (3.3.20). Firstly each of the e^a_{ij} is a weight $(2L-1)$ heptagon neighbour set function for the letter a. This implies that the functions E_0 and E_{ij} in (3.3.19) are cluster adjacent polylogarithms. Secondly, only some of the e^a_{ij} are non-zero: the ones where the letter a is cluster adjacent to all of the poles of the R-invariant (ij). For example, the R-invariant (12) contains three poles that are non-frozen cluster $\mathcal{A}$ coordinates, namely $\langle 3567\rangle \sim a_{34}$, $\langle 3467\rangle \sim a_{15}$, and $\langle 3457\rangle \sim a_{26}$:

$$(12) = \frac{\delta^{0|4}\big(\chi_7\langle 3456\rangle + \text{cyclic}\big)}{\langle 4567\rangle\langle 3567\rangle\langle 3467\rangle\langle 3457\rangle\langle 3456\rangle}\,. \tag{3.3.21}$$

The intersection of the homogeneous neighbour sets of these coordinates defines the neighbour set of the R-invariant (12), and similarly for the other R-invariants:

$$\begin{aligned} \text{hns}[(12)] &= \text{hns}[a_{34}] \cap \text{hns}[a_{15}] \cap \text{hns}[a_{26}] \\ &= \{a_{11}, a_{12}, a_{15}, a_{21}, a_{22}, a_{26}, a_{31}, a_{32}, a_{34}, a_{53}, a_{55}, a_{57}\}\,, \\ \text{hns}[(13)] &= \text{hns}[a_{21}] \cap \text{hns}[a_{33}] \cap \text{hns}[a_{41}] \cap \text{hns}[a_{43}] \\ &= \{a_{11}, a_{13}, a_{21}, a_{23}, a_{31}, a_{33}, a_{41}, a_{43}, a_{62}\}\,, \\ \text{hns}[(14)] &= \text{hns}[a_{11}] \cap \text{hns}[a_{14}] \cap \text{hns}[a_{21}] \cap \text{hns}[a_{34}] \cap \text{hns}[a_{46}] \\ &= \{a_{11}, a_{14}, a_{21}, a_{24}, a_{31}, a_{34}, a_{46}\}\,. \end{aligned} \tag{3.3.22}$$

Only the (final entry)$\otimes$(R-invariant) combinations compatible with the above and their cyclic rotations are allowed by cluster adjacency.

Note that the representation (3.3.20) employs the full redundant set of R-invariants. Upon elimination of the redundant R-invariants, the coproducts of the functions E_0 and

E_{ij} in (3.3.19) above are seen to be related to the quantities e_{ij} via

$$E_0^a = \sum_i e_{i,i+2}^a \,, \qquad E_{12}^a = e_{12}^a - e_{16}^a - e_{24}^a - e_{46}^a \,, \qquad E_{14}^a = e_{14}^a - e_{16}^a - e_{46}^a \,. \tag{3.3.23}$$

As in the hexagon case, we do not require that the combinations $\sum_a [e_{ij}^a \otimes a]$ are integrable; only $\sum_a [E_0^a \otimes a]$ and $\sum_a [E_{ij}^a \otimes a]$ are integrable. Nevertheless, just as in the hexagon case, the existence and adjacency properties of the e_{ij}^a imply relations on the coproducts of the functions E_0 and E_{ij}.

Out of the $7 \times (7 + 9 + 12) = 196$ cluster adjacent (final entry)$\otimes$(R-invariant) combinations allowed by (3.3.22). The following linear combinations of cluster adjacent (final entry)$\otimes$(R-invariant) products vanish due to identities,

$$[(12) - (13) + (14) - (15) + (16) - (17)] \otimes \{a_{11}, a_{21}, a_{31}\} \tag{3.3.24}$$

as do their cyclic rotations. This allows us to eliminate 21 such combinations leaving 175 independent cluster adjacent combinations.

The 175 combinations form a larger set than the more restricted set of 147 NMHV (final entry)$\otimes$(R-invariant) combinations derived by Caron-Huot which are compatible with the $\bar{Q}$ equation. These 147 combinations are listed in [48]. Using the identities 1.3.37, these NMHV final entries can be rewritten in the following manifestly cluster-adjacent way in which the final entries of the function multiplying the R-invariant (ij) are in the set $\text{hns}_{\bar{Q}}[(ij)]$ where:

$$\begin{aligned}
&\text{hns}_{\bar{Q}}[(12)] = \{a_{15}, a_{21}, a_{26}, a_{32}, a_{34}, a_{53}, a_{57}\} \subset \text{hns}[(12)] \\
&\text{hns}_{\bar{Q}}[(13)] = \{a_{21}, a_{23}, a_{31}, a_{33}, a_{41}, a_{43}, a_{62}\} \subset \text{hns}[(13)] \\
&\text{hns}_{\bar{Q}}[(14)] = \{a_{11}, a_{14}, a_{21}, a_{24}, a_{31}, a_{34}, a_{46}\} \subset \text{hns}[(14)] \qquad \& \text{ cyclic} \,.
\end{aligned} \tag{3.3.25}$$

The above set of $7 \times 3 \times 7 = 147$ (final entry)$\otimes$(R-invariant) pairs are equivalent up to using identities to the set presented in [48]. In contrast to the form presented in [48], the $\bar{Q}$-compatible final entries are monomials in the letters, which makes it trivial to verify cluster adjacency properties. Note that the list of (final entry)$\otimes$(R-invariant) pairs (3.3.2) is not unique since it is possible to trade some combinations with others using the six-term identities (1.3.37).

We will make use of the above cluster adjacent form for the NMHV heptagon amplitude to allow for an efficient implementation of the bootstrap programme at four loops.

3.4 The four-loop NMHV heptagon

In Table 2.4, we reproduce the dimensions of the spaces in which various types of heptagon neighbour-set functions with physical branch cuts live. The dimensions of these spaces depend on the letter the neighbours of which are allowed in the final entry. The neighbour-set functions will play a central role in parameterising the four-loop NMHV amplitude.

3.4.1 NMHV loop amplitudes and $\overline{Q}$ final entries

The observations above extend from individual symbols and R-invariants to NMHV amplitudes in a way in which poles and symbol final entries are related by cluster adjacency. We use this to construct a simplified ansatz for the NMHV heptagon and comment in the next section on how one can fix all its parameters using simple physical constraints at four loops.

This means that the L-loop NMHV heptagon amplitude can be written in the following form

$$\mathcal{E}^{(L)}_{7,\text{NMHV}} = E^{(L)}_0 \mathcal{E}^{(0)}_{7,\text{NMHV}} + \big(E^{(L)}_{12}\,(12) + E^{(L)}_{14}\,(14) + \text{cyclic}\big), \tag{3.4.1}$$

where E_0, E_{12} and E_{14} are all cluster adjacent polylogarithms built on the heptagon alphabet (2.2.16). Here we use

$$g^2 = \frac{a}{2} = \frac{\lambda}{16\pi^2} \tag{3.4.2}$$

as a loop-counting parameter, where λ is the usual 't Hooft coupling.

As mentioned above, there are 15 independent R-invariants however, to fully exploit the cluster adjacency in the final entries, we are required to write an ansatz of a different form from (3.4.1), employing all 21 invariants. We start with the following manifestly cluster adjacent and $\overline{Q}$ satisfying ansatz for the L-loop BDS-like normalised NMHV amplitude,

$$\mathcal{E}^{(L)}_{7,\text{NMHV}} = e^{(L)}_{12}\,(12) + e^{(L)}_{13}\,(13) + e^{(L)}_{14}\,(14) + \text{cyclic}. \tag{3.4.3}$$

The e_{ij} are tensor products of the form

$$e^{(L)}_{ij} = \sum_{\phi_\alpha \,\in\, \text{hns}_{\bar{Q}}[(ij)]} \;\sum_k \; c^{(ij)}_{k,\alpha}\; f^{(2L-1)}_{\text{hns}[\phi_\alpha],k} \otimes \phi_\alpha\,, \tag{3.4.4}$$

conforming to the coproduct structure of cluster-adjacent functions described in equation (2.5.9) and with final entries ϕ_α are chosen from the set $\text{hns}_{\bar{Q}}[(ij)]$ defined in equation (3.3.2).

Note that adjacency (and $\overline{Q}$) helps in two ways in the above ansatz. It reduces the possible final entries next to each R-invariant and it also reduces the possible next-to-final entries for a given final entry. This means that we do not even need a full weight seven basis of cluster adjacent functions, we only need the much smaller spaces whose final entries are compatible with each ϕ_α in turn.

We stress that the form (3.4.3) is not unique due to the six-term identities that the heptagon R-invariants satisfy and the amplitude $\mathcal{E}^{(L)}$ needs to be integrable only on the support of these identities. In order to obtain a manifestly integrable amplitude one should express the 21 (ij) in terms of a non-redundant set of 15, e.g. those in equation (3.3.18). In that basis, the integrable coefficient functions are expressed in terms of $e^{(L)}_{ij}$ as follows:

$$E^{(L)}_0 = \sum_{i=1}^{7} e^{(L)}_{i\,i+2}, \qquad E^{(L)}_{14} = e^{(L)}_{14} - e^{(L)}_{16} - e^{(L)}_{46}, \qquad E^{(L)}_{12} = e^{(L)}_{12} - e^{(L)}_{16} - e^{(L)}_{24} - e^{(L)}_{46}\,. \tag{3.4.5}$$

It is possible to remove some redundancies of this ansatz using the appropriate reflection symmetries of the coproducts $e^{(L)}_{ij}$. For example $e^{(L)}_{12}$ is invariant under $Z_i \mapsto Z_{3-i}$, which

relates the terms ending with a_{21}, a_{26} and a_{53} to those ending with a_{32}, a_{34} and a_{57}, respectively. Moreover, in $e_{12}^{(L)}$, a_{15} is preceded by a function which is invariant under the reflections of the twistors that leave Z_5 invariant.

In the following section we will focus on the technical details of the four-loop computation.

3.5 The four-loop computation

We will first give an account of the free parameters in the cluster-adjacent ansatz with dihedral symmetry (3.4.3) at four loops. We then describe the steps we took to find the values of these parameters to determine the NMHV amplitude. We also explain how one can use the ancillary files to construct the symbol of the amplitude in explicit form.

Following the dimensions listed in Table 2.4, we can work out the dimensions of weight-$\{7,1\}$ tensor-product spaces in which we are looking for the symbols e_{ij}. For example, consider the neighbour-set functions associated with the seven final entries $\{a_{15}, a_{21}, a_{26}, a_{32}, a_{34}, a_{53}, a_{57}\}$ of the symbol e_{12}, as given in equation (3.3.2). The weight-7 neighbour set functions that come before a_{15} live in a 1577-dimensional space, those that come before a_{21},a_{26} a_{32} and a_{34} live in a 2025-dimensional space and those that come before a_{53} and a_{57} live in a 570-dimensional one. This amounts to a total of 10,817 unknown coefficients in the coproduct $e_{12}^{(L)}$ but taking the reflection symmetry into account reduces this number to 5426. With a similar counting, one has 4867 and 5919 unfixed coefficients for $e_{13}^{(4)}$ and $e_{14}^{(4)}$, respectively, so that the undetermined coefficients in (3.4.3) number 16,212 in total. Requiring that $\mathcal{E}_{7,\text{NMHV}}^{(4)}$ is integrable, free of spurious poles and has the correct collinear limits uniquely fixes all of these coefficients.

We have implemented these constraints in separate stages. One can start by requiring the integrability of the symbol $E_{14} = e_{14} - e_{16} - e_{46}$. This leaves 8,444 unfixed coefficients. Then one can impose the integrability of $E_{12} = e_{12} - e_{16} - e_{24} - e_{46}$ bringing this number down to 56. Once the integrability of E_{12} and E_{14} is imposed, there are no new constraints coming from the integrability of E_0. In this 56-dimensional space, one can then look for combinations for which the amplitude is free of spurious poles. These are poles that could potentially appear in the limit where one of the 4-brackets in the denominator of the R-invariants vanishes. However in physical amplitudes such poles are only allowed when the 4-bracket is of the form $\langle i-1ij-1j\rangle$, corresponding to an intermediate particle becoming on shell. In all other cases, this potential pole must be cancelled by a vanishing of its transcendental component, which, after also taking into account cyclic symmetry, implies the following conditions:

$$\text{Spurious I:} \quad E_{47}|_{\langle 1356\rangle=0} = 0\,, \tag{3.5.1}$$

$$\text{Spurious II:} \quad E_{23}|_{\langle 1467\rangle=0} = E_{25}|_{\langle 1467\rangle=0}\,, \tag{3.5.2}$$

which have been worked out in [48, 135]. Imposing both conditions described in equation (3.5.1), one is left with only five coefficients to be determined by imposing a kinematic limit, such as the collinear limits.

In the collinear limit, two of the neighbouring particles in a colour-ordered amplitude

become proportional to each other with an unspecified proportionality constant. We follow [48] to describe the collinear limit in the momentum twistor. In a generic configuration, the momentum twistor Z_7 can be parametrised as a linear combination of four other momentum twistors as follows:

$$Z_7 = Z_1 + \epsilon \frac{\langle 1456\rangle}{\langle 2346\rangle} Z_2 + \tau \frac{\langle 1245\rangle}{\langle 2456\rangle} Z_6 + \eta \frac{\langle 1256\rangle}{\langle 2456\rangle} Z_4 \,. \tag{3.5.3}$$

A collinear configuration is obtained when one sends first $\eta \to 0$ followed by $\epsilon \to 0$. The parameter τ then relates the momentum fraction.

Scattering amplitudes in planar $\mathcal{N} = 4$ super Yang-Mills have a well-known collinear behaviour and they can be related to the amplitude with one fewer particle. Usually the BDS-normalised amplitude [101, 105] $\mathcal{B}_n$ is used to consider collinear kinematics, as opposed to the BDS-like normalised one, because the former is finite in this limit and directly reduces to the quantity of one fewer particle $\mathcal{B}_{n-1}$. The two quantities are related via

$$\mathcal{B}_n = \exp\left(-\frac{\Gamma_{\text{cusp}}}{4} Y_n\right) \mathcal{E}_n, \qquad Y_n \equiv -\mathcal{E}^{(1)}_{n,\text{MHV}} \,. \tag{3.5.4}$$

In other words a BDS-like normalised quantity "$\mathcal{E}$", which may be the full superamplitude (1.3.47), or a given MHV sector $\mathcal{E}_{\text{N}^k\text{MHV}}$ thereof (1.3.48), or a particular transcendental component of the latter such as E_0, E_{ij} in (3.4.1), is related to the corresponding BDS-normalised quantity "$\mathcal{B}$" by an exponential factor involving the one-loop MHV amplitude and the cusp anomalous dimension Γ_{cusp}.

Explicitly for $n = 6, 7$, the functions Y_n are given by:

$$\begin{aligned} Y_6 &= -\sum_{i=1}^{3} \left[\text{Li}_2\left(1 - \frac{1}{u_i}\right)\right], \\ Y_7 &= -\sum_{i=1}^{7} \left[\text{Li}_2\left(1 - \frac{1}{u_i}\right) + \frac{1}{2}\log\left(\frac{u_{i+2}u_{i-2}}{u_{i+3}u_i u_{i-3}}\right)\log u_i \right], \end{aligned} \tag{3.5.5}$$

where $u_i = u_{i,i+3}$ in terms of the cross-ratios defined in (1.3.51).

For seven particle scattering, there are two types of combinations of the NMHV superamplitude components that produce six-point amplitudes. The "k-decreasing" combination of BDS-normalised functions produces the six-point MHV superamplitude, whereas the "k-preserving" ones produce the five independent components of the six-point NMHV superamplitude [45].

For example, in the k-decreasing collinear limit, the MHV (ξ^0) component of the six-particle amplitude receives contribution from a number of functions multiplying different R-invariants. More precisely, the combination

$$B_0 + B_{23} + B_{34} = \exp\left(-\frac{\Gamma_{\text{cusp}}}{4} Y_7\right)\left(E_0 + E_{23} + E_{34}\right), \tag{3.5.6}$$

where Γ_{cusp} is the cusp anomalous dimension, is what is expected to reproduce the BDS-normalised six-point MHV amplitude $\mathcal{B}_{6,\text{MHV}}$.

Especially at four loops, it is cumbersome to compute the BDS-normalised functions, which contain redundant information in that they involve a large number of known prod-

ucts. However, with the knowledge of the MHV heptagon amplitude, it is not necessary to convert between the different normalisations of the amplitude. Instead, one can consider the difference

$$E_0 + E_{23} + E_{34} - \mathcal{E}_{7,\text{MHV}}\,, \tag{3.5.7}$$

where $\mathcal{E}_{7,\text{MHV}}$ is the known BDS-like normalised heptagon amplitude. Since $\mathcal{E}_{7,\text{MHV}}$ and the combination $E_0 + E_{23} + E_{34}$ both reduce to the same quantity

$$E_0 + E_{23} + E_{34}\,,\ \mathcal{E}_{7,\text{MHV}} \ \to\ \left[\exp\left(\frac{\Gamma_{\text{cusp}}}{4}(Y_6 - Y_7)\right)\mathcal{E}_{6,\text{MHV}}\right]\Bigg|_L \tag{3.5.8}$$

in the collinear limit, where $\mathcal{E}_{6,\text{MHV}}$ is the six particle amplitude, one can impose the vanishing of the difference (3.5.7) which only contains relatively simple, cluster-adjacenct quantities.

While the vanishing of (3.5.7) in the collinear limit is a sufficient constraint to uniquely fix the amplitude, constraints that relate $\mathcal{E}^{(4)}_{7,\text{NMHV}}$ to another amplitude are not strictly necessary. One can still explicitly construct the BDS-normalised amplitude in either k-decreasing or k-preserving collinear limit and determine $\mathcal{E}^{(4)}_{7,\text{NMHV}}$ only by requiring the finiteness of the limit, without prior knowledge of $\mathcal{E}^{(4)}_7$.

Integrability and the cancellation of spurious poles are linear constraints on the space of coproducts and finding their solution spaces can be formulated as null-space problems for integer-valued matrices encoding these constraints (see [48] for details). We found that an efficient way of computing these kernels is to work modulo a prime number and feed the constraint matrices into SpaSM [118], a sparse linear solver that employs modular arithmetic. One can then compute these null-spaces modulo p for various prime numbers p and reconstruct the exact amplitude using the Chinese Remainder Theorem. However, it was possible to guess the answer that satisfies all constraints exactly by only repeating the calculation mod 43051 and mod 46153.

3.5.1 Explicit results

The explicit tensor products $e^{(4)}_{ij}$ are too large to be included as supplementary material to this thesis and therefore we provide them encoded as {6,1,1} coproducts. In this section we describe how one can use the provided data to reconstruct the amplitude.

The file `e74.m` , provided in [10], contains a 4-index tensor of dimensions $3 \times 2555 \times 42 \times 42$ in `Mathematica` `SparseArray` format. The first index enumerates the tensors $e^{(4)}_{12}$, $e^{(4)}_{13}$ and $e^{(4)}_{14}$. Once the first index is specified, the remaining array contains the coefficients $c^{k\alpha\beta}_{ij}$ in the coproduct representation of $e^{(4)}_{ij}$:

$$e^{(4)}_{ij} = \sum_{k=1}^{2555}\sum_{\alpha=1}^{42}\sum_{\beta=1}^{42} c^{k\alpha\beta}_{ij}\ f^{(6)}_k \otimes \phi_\alpha \otimes \phi_\beta\,. \tag{3.5.9}$$

We also provide bases spanning the spaces of weight-w $f^{(w)}_k$ in terms of $\{w-1,1\}$ coproducts:

$$f^{(w)}_k = \sum_{\ell}^{\dim_{w-1}}\sum_{\alpha}^{42} M^{(w)}_{k\ell\alpha}\ f^{(w-1)}_\ell \otimes \phi_\alpha\,, \tag{3.5.10}$$

using which one can recursively construct the symbols of functions $f_k^{(w)}$ in order to convert the coproducts (3.5.9) to symbols. The coefficients $M_{k\ell\alpha}^{(w)}$ are encoded in the files `mw.m` as `SparseArray` objects for $2 \leq w \leq 6$. These files can be found in [10].

Due to the cyclic symmetry of the superamplitude, the coefficients $c_{1j}^{k\alpha\beta}$ for $j = 2, 3, 4$ are sufficient to describe the amplitude. The remaining symbols $c_{ij}^{k\alpha\beta}$ with $i \neq 1$ can be constructed by rotating the coproduct form (3.5.9). For example $e_{23}^{(4)}$ can be constructed as

$$e_{23}^{(4)} = \sum_{k=1}^{2555} \sum_{\alpha=1}^{42} \sum_{\beta=1}^{42} c_{12}^{k\alpha\beta}\, \mathcal{C}\big[f_k^{(6)}\big] \otimes \mathcal{C}\big[\phi_\alpha\big] \otimes \mathcal{C}\big[\phi_\beta\big]\,, \tag{3.5.11}$$

where the cyclic rotation operator $\mathcal{C}$ acts on the letters as

$$\mathcal{C}\big[a_{i\,j}\big] = a_{i\,j+1} \tag{3.5.12}$$

while its action on the functions is a linear transformation in the corresponding function space:

$$\mathcal{C}\big[f_k^{(w)}\big] = \sum_{\ell=1}^{\dim_w} \mathcal{C}_{k\ell}^{(w)}\, f_\ell^{(w)}\,. \tag{3.5.13}$$

The matrices $\mathcal{C}_{k\ell}^{(w)}$ are given as a Mathematica `List` in the file `rotationmatrices.m` for $2 \leq w \leq 6$, found in [10].

Following this procedure one obtains three 8-dimensional Mathematica `SparseArray` objects encoding the symbols of $e_{ij}^{(4)}$ which enter the coefficient functions $E_*^{(4)}$. These then can be used to perform various analyses of our result, such as the investigation of its behaviour in the multi-Regge kinematics.

3.6 Multi-Regge limit

In this section, we will consider the multi-Regge limit of our $n = 7$, 4-loop NMHV symbol, with a two-fold aim: First, to check our calculation against independent results available for the amplitude in this limit up to NLLA [76, 78]. And second, to obtain new predictions up to N^{3}LLA, which we hope will play an important role in further elucidating the perturbative structure of the heptagon in the limit, and guide its finite-coupling determination, similarly to the hexagon case. We start by briefly reviewing the kinematics and the most natural amplitude normalisation for our purposes in subsections 3.6.1 and 3.6.2, before describing the evaluation of the amplitude in subsection 3.6.3. The reader interested in the final result and comparison may just skip directly to subsection 3.6.4.

3.6.1 Kinematics

We will focus on $2 \to 5$ scattering, for which multi-Regge kinematics (MRK) is defined as the limit where the produced particles are strongly ordered in rapidity. For $\mathcal{N} = 4$ SYM, the nontrivial kinematic dependence is encoded in dual conformal cross ratios, and in [125, 126] it was shown that in the following convenient choice of six algebraically independent

cross ratios, the limit becomes[5]

$$v_{1i} \equiv u_{i+2i+5} \to 1\,, \quad v_{2i} \equiv u_{1i+3} \to 0\,, \quad v_{3i} \equiv u_{2i+4} \to 0\,, \tag{3.6.1}$$

with

$$\frac{v_{2i}}{1-v_{1i}} \equiv \frac{1}{|1-z_i|^2}\,, \quad \frac{v_{3i}}{1-v_{1i}} \equiv \frac{|z_i|^2}{|1-z_i|^2}\,, \quad i=1,2\,, \tag{3.6.2}$$

held fixed. The right hand-side defines the four real, or two complex, finite cross ratios z_1, z_2 that parametrise the limit, whereas the two cross ratios that become infinitesimal may be chosen as

$$\tau_i \equiv \sqrt{v_{2i}v_{3i}}\,, \quad i=1,2\,. \tag{3.6.3}$$

From the above equations, we may also deduce the behaviour of all heptagon symbol letters, (2.2.16), in MRK, which is a necessary step before evaluating the corresponding amplitude. Let us therefore record it here before closing this subsection,

$$\begin{array}{lllll}
a_{14} \to \frac{1}{a_{12}} & a_{15} \to a_{11}a_{12} & a_{16} \to \frac{1}{a_{11}} & a_{24} \to \frac{a_{13}}{a_{23}} & a_{27} \to \frac{a_{17}}{a_{21}} \\
a_{32} \to \frac{a_{12}a_{13}}{a_{23}} & a_{33} \to \frac{a_{23}}{a_{12}} & a_{36} \to \frac{a_{21}}{a_{11}} & a_{37} \to \frac{a_{11}a_{17}}{a_{21}} & a_{41} \to \frac{a_{23}a_{26}}{a_{12}} \\
a_{42} \to \frac{a_{17}a_{34}}{a_{21}} & a_{43} \to a_{11}a_{23} & a_{44} \to \frac{a_{34}}{a_{11}} & a_{45} \to \frac{a_{11}a_{17}a_{23}}{a_{21}} & a_{46} \to \frac{a_{26}}{a_{12}} \\
a_{47} \to \frac{a_{11}a_{12}a_{17}}{a_{21}} & a_{51} \to \frac{a_{13}a_{35}}{a_{23}} & a_{52} \to \frac{a_{21}a_{25}}{a_{11}} & a_{53} \to \frac{a_{11}a_{12}a_{13}}{a_{23}} & a_{54} \to \frac{a_{25}}{a_{11}} \\
a_{55} \to \frac{a_{12}a_{13}a_{21}}{a_{23}} & a_{56} \to \frac{a_{35}}{a_{12}} & a_{57} \to a_{12}a_{21} & a_{61} \to a_{12}a_{17} & a_{62} \to a_{11}a_{13} \\
a_{63} \to \frac{a_{25}a_{34}}{a_{11}} & a_{64} \to a_{11}a_{12}a_{13} & a_{65} \to \frac{1}{a_{11}a_{12}} & a_{66} \to a_{11}a_{12}a_{17} & a_{67} \to \frac{a_{26}a_{35}}{a_{12}}\,,
\end{array} \tag{3.6.4}$$

where we see that only 12 out of the 42 letters remain multiplicatively independent in the limit. These 12 letters may in turn be expressed in terms of the variables (3.6.1)-(3.6.3) as

$$\begin{array}{lll}
a_{11} \to \frac{\tau_1}{z_2\bar{z}_2\sqrt{z_1\bar{z}_1}} & a_{12} \to \tau_2 z_1 \bar{z}_1 \sqrt{z_2\bar{z}_2} & a_{13} \to \frac{\sqrt{z_2\bar{z}_2}}{\tau_1^2\tau_2} \\
a_{17} \to \frac{1}{\tau_1\tau_2^2\sqrt{z_1\bar{z}_1}} & a_{21} \to -\frac{1}{\tau_2 z_1\sqrt{z_2\bar{z}_2}} & a_{22} \to \frac{\tau_1\tau_2\,(\bar{z}_2 - \bar{z}_1\bar{z}_2 - 1)}{\sqrt{z_2\bar{z}_2}}\sqrt{\frac{z_1}{\bar{z}_1}} \\
a_{23} \to -\frac{z_2\sqrt{z_1\bar{z}_1}}{\tau_1} & a_{25} \to -\frac{\tau_1\,(1-z_1)}{\bar{z}_2\sqrt{z_1\bar{z}_1}} & a_{26} \to \tau_2\bar{z}_1\,(1-z_2)\sqrt{\frac{\bar{z}_2}{z_2}} \\
a_{31} \to \frac{\tau_1\tau_2\,(z_2 - z_1z_2 - 1)}{\sqrt{z_2\bar{z}_2}}\sqrt{\frac{\bar{z}_1}{z_1}} & a_{34} \to -\frac{\tau_1\,(1-\bar{z}_1)}{z_2\sqrt{z_1\bar{z}_1}} & a_{35} \to \tau_2 z_1\,(1-\bar{z}_2)\sqrt{\frac{z_2}{\bar{z}_2}}\,.
\end{array} \tag{3.6.5}$$

3.6.2 BDS normalisation and analytic continuation

While in the previous sections we determined the heptagon superamplitude in the BDS-like normalisation[6] $\mathcal{E}_{\text{NMHV}}$, in MRK it is most conveniently described in the BDS normalisation, introduced in (3.5.4). Here we are exclusively dealing with symbols, and since $\mathcal{S}(\Gamma_{\text{cusp}}) = 4g^2$, we may write each term in the weak coupling expansion of (3.5.4) at symbol level as

$$\mathcal{E}^{(L)} = \sum_{k=0}^{L} \mathcal{B}^{(k)} \frac{(-Y)^{L-k}}{(L-k)!}\,. \tag{3.6.6}$$

Given the conformal equivalence of MRK with the double soft limit for the heptagon, all loop corrections to the corresponding BDS-normalised superamplitude will vanish in the

[5] In the notations of [76, 78], $u_{i+1,j_1} = U_{ij}$, due to different numbering of momentum twistors.

[6] In what follows, we will drop the particle multiplicity index n, since we will be focusing on $n = 7$.

Euclidean region. In order to obtain a nontrivial result, we therefore need to analytically continue the latter amplitude to different kinematic regions, and here we will chose the region where we analytically continue the energy components of all produced particles to opposite sign. In terms of the conformally invariant cross ratios, this amounts to

$$u_{73} \xrightarrow{\mathcal{C}} e^{-2\pi i} u_{73}\,, \tag{3.6.7}$$

and given the relation of the latter to the a_{1i} letters,

$$a_{11} = \frac{u_{14}u_{51}}{u_{36}u_{62}u_{73}} \quad + \text{ cyclic}\,, \tag{3.6.8}$$

it is evident that the amplitude in this region will differ from its value in the Euclidean region by

$$\begin{aligned}\Delta\mathcal{B} \equiv \mathcal{B}^{\mathcal{C}} - \mathcal{B} &= -2\pi i \text{Disc}_{u_{73}}\mathcal{B} \\ &= -2\pi i \left(-\text{Disc}_{a_{11}}\mathcal{B} - \text{Disc}_{a_{12}}\mathcal{B} + \text{Disc}_{a_{13}}\mathcal{B} - \text{Disc}_{a_{15}}\mathcal{B} + \text{Disc}_{a_{17}}\mathcal{B}\right)\,.\end{aligned} \tag{3.6.9}$$

Note that the above equation also holds for each component of the superamplitude separately, since the R-invariants (1.3.36) are rational functions of the kinematics, and thus they will remain unchanged under the analytic continuation.

3.6.3 Evaluating the gluon amplitude in the limit

So far our discussion was at the level of the entire superamplitude, however in MRK the natural object to consider are its gluon amplitude components, since the theoretical framework for describing the limit was born out of the study of strong interactions. Focusing on $1+2 \to 3+\ldots+7$ scattering in all-outgoing momenta conventions, and denoting the helicities of the produced gluons as h_1, h_2, h_3, without loss of generality can define the relevant BDS-normalised gluon amplitudes as

$$\mathcal{R}_{h_1,h_2,h_3} \equiv \frac{A(-,-,+,h_1,h_2,h_3,+)}{A^{\text{BDS}}(-,-,+,h_1,h_2,h_3,+)}\Big|_{\text{MRK}}\,, \tag{3.6.10}$$

since the high energy of the incoming gluons implies that helicity is preserved along their lines in the limit. Particularly for the NMHV case, which is our focus here, there exist two inequivalent helicity configurations, $\mathcal{R}_{-++}$ and $\mathcal{R}_{+-+}$, since $\mathcal{R}_{++-}$ may be obtained from the former by a discrete parity and target-projectile (a particular dihedral flip that commutes with the limit) transformation.

The gluon amplitudes (3.6.10) can be extracted from the superamplitude, as coefficients of particular monomials of the fermionic variables χ_i^I entering in the R-invariants (1.3.36), with the latter being polynomials in these variables due to the fermionic delta function. We will not demonstrate the details of this calculation here and just quote the final answer[7],

$$\begin{aligned}\mathcal{R}_{-++} &= \hat{B}_0 + \hat{B}_{67} + \hat{B}_{71} + R_{234}\Big(\hat{B}_{51} - \hat{B}_{71}\Big) + R_{235}\Big(\hat{B}_{56} - \hat{B}_{51}\Big)\,, \\ \mathcal{R}_{+-+} &= \hat{B}_0 + \hat{B}_{14} + \hat{B}_{47} + \hat{B}_{73} + \overline{R}_{234}\Big(\hat{B}_{12} - \hat{B}_{14} - \hat{B}_{47}\Big) \\ &\quad + R_{345}\Big(\hat{B}_{36} - \hat{B}_{14}\Big) + \overline{R}_{234}R_{345}\Big(\hat{B}_{14} + \hat{B}_{62} - \hat{B}_{12}\Big)\,,\end{aligned} \tag{3.6.11}$$

[7] The result of this calculation was also reported in [76], but with the $\hat{B}_{ij}$ components cyclically permuted up by two compared to here, as a result of inconsistent conventions for momentum twistors.

expressing the gluon amplitude as a linear combination of the independent, integrable components of the BDS-normalised NMHV superamplitude $\hat{B}_*$ with index $*$ equal to 0 or ij, after we analytically continue it and take its multi-Regge limit, times the independent rational factors coming from the R-invariants in the limit,

$$R_{234} = -\frac{z_1}{1-z_1}\,, \quad R_{235} = \frac{z_1 z_2}{1-z_2+z_1 z_2}\,, \quad R_{345} = -\frac{z_2}{1-z_2}\,, \tag{3.6.12}$$

with the corresponding barred quantities being their complex conjugates.

In principle we now have everything laid out for extracting the symbol of the 4-loop NMHV gluon amplitudes in MRK from the corresponding superamplitude in general kinematics, however in the current order the computation requires the tedious step of converting from the BDS-like to BDS normalisation in general kinematics, eq. (3.6.6). Instead, we have found it significantly more efficient to obtain the final result directly from the discontinuity of E as follows: From the definition in the first line of (3.6.9), it is evident that the discontinuity of a product of symbols F, G obeys the Leibniz rule,

$$\Delta(F\cdot G) = (F+\Delta F)\cdot(G+\Delta G) - (F\cdot G) = \Delta F\cdot G + F\cdot \Delta G\,, \tag{3.6.13}$$

since the $\Delta F\cdot\Delta G$ term has an additional factor of π, and is thus beyond the symbol. With the help of this property, and eq. (3.6.6), is is straightforward to relate the discontinuities of the symbols of the BDS and BDS-like amplitudes in MRK,

$$\Delta\hat{\mathcal{E}}^{(L)} = \sum_{k=1}^{L}\left(\hat{\mathcal{B}}^{(k)} - \delta_{k1}\Delta\hat{Y}\right)\frac{(-\hat{Y})^{L-k}}{(L-k)!}\,, \tag{3.6.14}$$

where also we also used the fact that in MRK $\mathcal{B}^{(k)} \to \delta_{k0}$ before analytic continuation, and thus $\Delta\hat{\mathcal{B}}^{(k)} = \hat{\mathcal{B}}^{(k)}$ for $k \geq 1$. In the above relation, the function Y and its discontinuity evaluate in the limit to

$$\begin{aligned}\hat{Y} =& 2(\log^2\tau_1 + \log^2\tau_2 + \log\tau_1\log\tau_2) + \log\tau_2\log|z_1|^2 - \log\tau_1\log|z_2|^2 \\ &+ \frac{1}{2}(\log^2|z_1|^2 + \log^2|z_2|^2 + \log|z_1|^2\log|z_2|^2) \\ \Delta\hat{Y} =& -2\pi i\left[-2\log\tau_1 - 2\log\tau_2 + \log|z_2|^2 - \log|1-z_2+z_1z_2|^2\right]\,,\end{aligned} \tag{3.6.15}$$

and $|z|^2 = z\bar{z}$ etc.

This completes our method for obtaining the BDS-normalised gluon amplitudes (3.6.10), focusing on the NMHV configurations $\mathcal{R}_{-++}$ and $\mathcal{R}_{+-+}$. To summarise, starting with the symbol of $\mathcal{E}^{(L)}_{\text{NMHV}}$, eq. (3.4.3), we take the linear combinations of its transcendental components, eq. (3.4.5), that appear in the right-hand side of (3.6.11) upon replacing $\hat{B}_* \to E_*$. For each such component, we take its discontinuity as in the second line of (3.6.9), and then its multi-Regge limit as in (3.6.4) and (3.6.5), sequentially. Finally, we plug the result on the left-hand side of (3.6.14), which is valid not only for the entire superamplitude, but also for its components separately, and solve for $\hat{\mathcal{B}}^{(L)}$ recursively, starting from $L=1$. For example, at 4 loops we will have

$$\hat{\mathcal{B}}^{(4)} = \Delta\hat{\mathcal{E}}^{(4)} + \frac{1}{6}\hat{Y}^3\left(\hat{\mathcal{B}}^{(1)} - \Delta\hat{Y}\right) - \frac{\hat{Y}^2}{2}\hat{\mathcal{B}}^{(2)} + \hat{Y}\hat{\mathcal{B}}^{(3)}\,. \tag{3.6.16}$$

3.6.4 Comparison with BFKL approach and new predictions

In this final subsection, we will compare our findings for the 4-loop NMHV heptagon in MRK with independent results obtained for the latter to LLA [76] and NLLA [78], based on the Balitsky-Fadin-Kuraev-Lipatov (BFKL) approach [136–138]. We will also discuss our new predictions for the amplitude in question up to N^3LLA.

Let us start by reviewing what has been previously known for the heptagon in the limit. Building on earlier work at LLA, in [78] an all-loop dispersion integral was presented, yielding the $2 \to 5$ amplitude in MRK to arbitrary logarithmic accuracy. It reads,

$$\mathcal{R}_{h_1 h_2 h_3} e^{i\delta_7(z_1,z_2)} = 2\pi i f_{h_1 h_2 h_3} \,, \tag{3.6.17}$$

where the right-hand side has the form of a Fourier-Mellin transform,

$$\begin{aligned} f_{h_1 h_2 h_3} =& \frac{a}{2} \sum_{n_1,n_2=-\infty}^{\infty} \left(\frac{z_1}{\bar{z}_1}\right)^{\frac{n_1}{2}} \left(\frac{z_2}{\bar{z}_2}\right)^{\frac{n_2}{2}} \int \frac{d\nu_1 d\nu_2}{(2\pi)^2} |z_1|^{2i\nu_1} |z_2|^{2i\nu_2} \tilde{\Phi}(\nu_1, n_1) \tilde{\Phi}(\nu_2, n_2) \\ & \times e^{-L_1 \omega(\nu_1,n_1) - L_2 \omega(\nu_2,n_2)} I^{h_1}(\nu_1, n_1) \tilde{C}^{h_2}(\nu_1, n_1, \nu_2, n_2) \bar{I}^{h_3}(\nu_2, n_2) \,, \end{aligned} \tag{3.6.18}$$

with

$$L_i = \log \tau_i + i\pi \,, \quad \delta_7(z_1, z_2) = \frac{\pi \Gamma_{\text{cusp}}}{4} \log \frac{|z_1 z_2|^2}{|1 - z_2 + z_1 z_2|^4} \,, \tag{3.6.19}$$

which we see evidently depends on the variables (3.6.1)-(3.6.3) that naturally describe the limit. Following the conventions of the relevant literature, in this section we have also switched our coupling normalisation to

$$a = 2g^2 \,. \tag{3.6.20}$$

The remaining quantities in the integral (3.6.18) are associated to the effective particle whose exchange governs the multi-Regge limit, known as the reggeised gluon or reggeon. In the kinematic region characterised by the analytic continuation (3.6.7), we have in particular a two-reggeon bound state, whose energy is the BFKL eigenvalue $\omega(\nu, n)$, and whose creation (annihilation) with a simultaneous emission a new final-state gluon of helicity h_1 (h_3) is encoded in the combined quantity $\tilde{\Phi} I^{h_1}$ ($\tilde{\Phi} \bar{I}^{h_2}$) known as the BFKL impact factor. These building blocks also appear in the hexagon amplitude, and they can be determined from first principles at weak coupling [128, 139], or even to all loops with the help of integrability [77].

Finally, the genuinely heptagonal quantity $\tilde{C}^{h_2}$, known as the central emission vertex, describes the emission of a gluon of helicity h_2 from the reggeon bound state in the middle of the ladder[8]. It was originally determined at leading order in [136], whereas its next-to-leading order correction was extracted from the 2-loop MHV heptagon, after promoting its known symbol [140] to a function, in [78]. Plugging this correction back to the integral (3.6.18) it is then possible to compute the amplitude at higher loops to NLLA, and this was indeed carried out for $\mathcal{R}^{(4)}_{-++}$. In more detail, at weak coupling the amplitude in MRK also has a natural expansion in large logarithms in the infinitesimal τ_i variables, whose

[8] In (3.6.18), the impact factor and central emission block have been rescaled compared to their original definition, so as to better expose their analytic properties, but this does not alter their physical interpretation.

perturbative coefficients may be defined as

$$\mathcal{R}_{h_1,h_2,h_3}(\tau_1,z_1,\tau_2,z_2)\,e^{i\delta_7(z_1,z_2)} = 1 + 2\pi i \sum_{\ell=1}^{\infty}\sum_{i_1,i_2=0}^{\ell-1} a^\ell \left(\prod_{k=1}^{2}\frac{1}{i_k!}\log^{i_k}\tau_k\right) \times \left(\tilde{g}^{(\ell;i_1,i_2)}_{h_1,h_2,h_3}(z_1,z_2) + 2\pi i\,\tilde{h}^{(\ell;i_1,i_2)}_{h_1,h_2,h_3}(z_1,z_2)\right). \tag{3.6.21}$$

The maximal logarithmic order amounts to $i_1+i_2=\ell-1$, as a consequence of the fact that all building blocks of the integrand (3.6.18) start at $\mathcal{O}(1)$, except for $\omega(\nu,n)$, which starts at $\mathcal{O}(a)$. These coefficients have already been determined in [76], in the notation

$$\tilde{g}^{(\ell;i_1,i_2)}_{h_1,h_2,h_3} \to g^{(i_1,i_2)}_{h_1,h_2,h_3} = \texttt{LL[\{i1,i2\},\{h1,h2,h3\}]}\,, \tag{3.6.22}$$

where the naming is provided in the ancillary files `NMHVLL7.m` and `NMHVLL6.m` accompanying the paper [10]. The latter file is needed because of the interesting factorisation property

$$g^{(i_1,0)}_{-++}(\rho_1,\rho_2) = g^{(i_1)}_{-+}(\rho_1)\,, \tag{3.6.23}$$

reducing heptagon perturbative coefficients to hexagon ones, after one first expresses them in so-called simplicial MRK coordinates,

$$\rho_1 = -\frac{z_1 z_2}{1-z_2}\,, \quad \rho_2 = (1-z_1)\,z_2\,. \tag{3.6.24}$$

Similarly, NLLA corresponds to $i_1+i_2=\ell-2$, and the relevant coefficients that are visible at the level of the symbol (imaginary part) may be found in the file `gTilde.m` attached to [78]. Note that since both $\mathcal{R}$ and δ_7 are proportional to π, beyond one loop we can completely neglect the contribution of the phase in the left-hand side of (3.6.21) to the symbol, so that

$$\mathcal{S}\left(\tfrac{1}{2\pi i}\mathcal{R}^{(\ell)}_{h_1,h_2,h_3}\right) = \sum_{i_1=0}^{\ell-1}\sum_{i_2=0}^{\ell-1-i_1}\left(\prod_{k=1}^{2}\frac{1}{i_k!}\log^{i_k}\tau_k\right)\mathcal{S}\left(\tilde{g}^{(\ell;i_1,i_2)}_{h_1,h_2,h_3}\right), \quad \ell\geq 2\,. \tag{3.6.25}$$

The perturbative coefficients belong to the class of single-valued multiple polylogarithms (SVMPL) [76, 141, 142], which enjoy the important property that they can be uniquely determined from the knowledge of their holomorphic part, defined as their $\bar{z}_i \to 0$ limit, also with any divergent $\log\bar{z}_i$ terms removed. Thus, in order to simplify our comparison even further, we may consider the holomorphic part of (3.6.25), which for the left-hand side amounts to setting all $\bar{z}$-dependent factors to one in the limit (3.6.5).

In this manner, we observe perfect agreement between the previously known results for the NMHV heptagon, up to (N)LLA for the $\mathcal{R}^{(4)}_{+-+}$ ($\mathcal{R}^{(4)}_{-++}$) helicity configuration, and the corresponding multi-Regge limit of our 4-loop symbol with general kinematic dependence. We view this as strong evidence for the correctness of our result for the latter, as well as of the all-loop dispersion integral (3.6.17)-(3.6.18).

Perhaps more importantly, from our calculation we have obtained new predictions for the symbols of the remaining perturbative coefficients in (3.6.21) or (3.6.25), namely up to $\mathrm{N^3LLA}$ at 4 loops. These predictions are included as the computer-readable file `gTilde4L.m` in [10]. These predictions will be useful for determining the central emission block beyond NLO, and may provide significant insight towards its structure to all loops.

Part II

Tropical Geometry

Chapter 4

Tropical Geometry

In this chapter we will review the recent connection between scattering amplitudes and tropical geometry [7, 143]. Namely how tree-level biadjoint ϕ^3 amplitudes can be calculated as volumes of the positive region of tropical Grassmannians. We describe here the tropical formulation of the Grassmannian spaces and how to select the positive region. We will see that this coincides with the criteria recently used in [7, 143] to determine the generalised ϕ^3 amplitudes for $\mathrm{Gr}(3,6)$ and $\mathrm{Gr}(3,7)$. These amplitudes also have a formulation in terms of a set of scattering equations which generalise the usual scattering equations of [79–81].

Once the positive region is obtained, the generalised biadjoint ϕ^3 amplitudes can be constructed as its volume in a direct generalisation of the picture described in [82]. Such a volume can be obtained additively via a triangulation of the region into simplexes. One such triangulation is provided by the (dual of the) associated cluster polytope. For the $\mathrm{Gr}(2,n)$ cases these polytopes are the A_{n-3} associahedra. In the $\mathrm{Gr}(3,6)$ case this corresponds to the D_4 polytope while in the $\mathrm{Gr}(3,7)$ case it is the E_6 polytope discussed above. For the $\mathrm{Gr}(3,8)$ case we can obtain a triangulation from the E_8 cluster polytope. The above cases exhaust the list of finite Grassmannian cluster algebras.

A feature of the polytopes arising as positive tropical Grassmannians is that in general their facets are not all simplexes. This means that there is a redundancy in parametrising their volumes since they may be triangulated (or cut into simplexes) in multiple ways, each yielding a seemingly different but actually equivalent way of obtaining the volume. In physical language this means there are multiple ways of writing the amplitude which are in fact equivalent due to non-trivial identities between different contributions.

We will demonstrate how the corresponding cluster algebra provides one such triangulation as well as other powerful tools to calculate these amplitudes. We will then use these methods to reproduce the results in [7, 143] for $\mathrm{Gr}(3,6)$ and $\mathrm{Gr}(3,7)$, extending to the case of $\mathrm{Gr}(3,8)$.

Since all these cluster algebras are finite, the triangulation procedure works in exactly the same way for all of them. Nevertheless the correspondence between the cluster algebra and the fan for each case contains intricacies of different nature with valuable lessons and we elaborate on these in sections dedicated to different Grassmannians.

Before this we review the interpretation of the biadjoint ϕ amplitude as the volume of the dual to a kinematic realisation of the associahedron. We then illustrate all the main

principles of the tropical Grassmannian, its positive part and the connection to cluster algebras in the example of $\mathrm{Gr}(2,5)$.

4.1 Amplitudes from volumes of dual associahedra

In [82] a connection between biadjoint scalar amplitudes and volumes was made. The main idea is to introduce a kinematic realisation of the associahedron. This is done as follows. Given an ordered set of light-like momenta $p_1, \ldots, p_n$ satisfying momentum conservation one introduces dual coordinates,

$$x_{i+1} - x_i = p_i \,, \tag{4.1.1}$$

as defined in (1.3.31), with all indices treated modulo n. The $\frac{1}{2}n(n-3)$ square distances $(x_i - x_j)^2 = X_{ij}$ can be related to Mandelstam invariants via

$$X_{ij} = s_{i,i+1,\ldots,j-1} = (p_i + p_{i+1} + \ldots p_{j-1})^2 \,. \tag{4.1.2}$$

Note that the momenta being null implies $X_{i,i+1} = 0$. The two-particle Mandelstam invariants $s_{ij} = (p_i + p_j)^2$ can be related to the dual variables via

$$s_{ij} = X_{i,j+1} + X_{i+1,j} - X_{ij} - X_{i+1,j+1} \,. \tag{4.1.3}$$

To define the *kinematic associahedron* we take all X_{ij} positive and choose $(n-3)$ coordinates, e.g. the $X_{1,i}$ for $i = 3, \ldots, (n-1)$. The remaining $\frac{1}{2}(n-2)(n-3)$ independent variables need to be constrained in order to obtain a space of dimension $(n-3)$. To do this we impose $\frac{1}{2}(n-2)(n-3)$ conditions which we take to be of the form

$$s_{ij} = -c_{ij} \,, \qquad 2 \leq i < j \leq n \,, \quad i \leq j-2 \,, \tag{4.1.4}$$

for *positive* constants c_{ij}. The coordinates $X_{1,i}$ are then constrained to run only over a certain region: the kinematic associahedron.

For the $n = 5$ example the conditions (4.1.4) become

$$\begin{aligned} X_{35} &= c_{35} + X_{13} - X_{14} \,, \\ X_{25} &= c_{25} + c_{35} - X_{14} \\ X_{24} &= c_{24} + c_{25} - X_{13} \,. \end{aligned} \tag{4.1.5}$$

The coordinates (X_{13}, X_{14}) then run over a region with the shape of a pentagon as shown in Fig. 4.1.

To obtain the dual of the kinematic associahedron it is helpful to embed it into projective space $\mathbb{P}^{n-3}$. We introduce the auxiliary point $Y = (1, X_{13}, X_{14}, \ldots, X_{1,n-1})$. The boundary conditions $X_{ij} = 0$ of the kinematic associahedron become $Y \cdot W_{ij} = 0$ with W_{ij} given by projective dual vectors determined by the conditions (4.1.4).

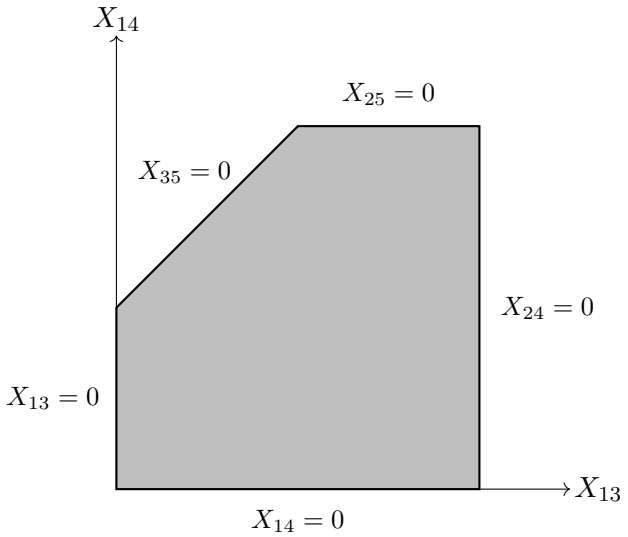

Figure 4.1: The shaded area is the kinematic associahedron for $n = 5$.

In the case $n = 5$ we have $Y = (1, X_{13}, X_{14})$ and

$$\begin{aligned} W_{13} &= (0, 1, 0)\,, \\ W_{14} &= (0, 0, 1)\,, \\ W_{24} &= (c_{24} + c_{25}, -1, 0)\,, \\ W_{25} &= (c_{25} + c_{35}, 0, -1)\,, \\ W_{35} &= (c_{35}, 1, -1)\,. \end{aligned} \tag{4.1.6}$$

These dual vectors define the dual to the $\mathrm{Gr}(2,5)$ kinematic associahedron. Its volume may be computed by first triangulating it, e.g. by picking the reference point $W_* = (1, 0, 0)$ and adding the volume of the five triangles formed by W_* and two adjacent dual vectors according to

$$\mathrm{Vol}(W_1, W_2, W_3) = \frac{\langle W_1 W_2 W_3 \rangle}{(Y \cdot W_1)(Y \cdot W_2)(Y \cdot W_3)}\,. \tag{4.1.7}$$

In this way we obtain the sum of five terms,

$$\begin{aligned} \mathrm{Vol}(\mathcal{A}^*) &= \frac{1}{X_{13}X_{14}} + \frac{1}{X_{14}X_{24}} + \frac{1}{X_{24}X_{25}} + \frac{1}{X_{25}X_{35}} + \frac{1}{X_{35}X_{13}}\,, \\ &= \frac{1}{s_{12}s_{45}} + \frac{1}{s_{45}s_{23}} + \frac{1}{s_{23}s_{15}} + \frac{1}{s_{15}s_{34}} + \frac{1}{s_{34}s_{12}} \end{aligned} \tag{4.1.8}$$

and we recognise the obtained representation as the Feynman diagram expansion for the canonically ordered biadjoint ϕ^3 amplitude.

4.2 Tropical Grassmannians and amplitudes

In Chapter 2 we defined the Grassmannian in terms of the minors of the matrix that paramatrises it. There exists a *tropical* version of the above construction. In tropical geometry one takes the generating relations of the ideal and replaces multiplication with addition and addition with minimum. For example the generating quadratic polynomials

of the $\mathrm{Gr}(2,n)$ Plücker relations (2.1.2) become the tropical polynomials

$$\min(w_{ij}+w_{kl}, w_{ik}+w_{jl}, w_{il}+w_{jk})\,, \tag{4.2.1}$$

which are piecewise linear maps on the space of $\binom{n}{2}$ variables $w_{ij}\in\mathbb{R}$.

Piecewise linear maps have special surfaces between one region of linearity and another. Such surfaces are called tropical hypersurfaces and are attained when at least two of the terms of the tropical polynomial simultaneously attain the minimum. In other words the tropical polynomial (4.2.1) defines the following tropical hypersurfaces,

$$\begin{aligned} & w_{ij}+w_{kl} = w_{ik}+w_{jl} \leq w_{il}+w_{jk} \\ \text{or}\quad & w_{ij}+w_{kl} = w_{il}+w_{jk} \leq w_{ik}+w_{jl} \\ \text{or}\quad & w_{ik}+w_{jl} = w_{il}+w_{jk} \leq w_{ij}+w_{kl}\,. \end{aligned} \tag{4.2.2}$$

When we have many polynomial relations we must simultaneously satisfy the conditions arising from each polynomial relation. In the case of $\mathrm{Gr}(2,n)$ we must simultaneously satisfy the hypersurface relations coming from every Plücker relation, i.e. for every choice of $\{i,j,k,l\}$ in (2.1.2).

Note that for any solution $\{w_{ij}\}$, any global *positive* rescaling of the w_{ij} will also obey the conditions. Solutions therefore form rays emanating from the origin and can be represented by an $\binom{n}{2}$-component vector, or more generally for $\mathrm{Gr}(k,n)$ an $\binom{n}{k}$-component vector. Note also that if $\{w_{ij}\}$ are solutions of the above conditions then so are $\{w_{ij}+a_i+a_j\}$ for any set of n constants $a_i\in\mathbb{R}$. Such a shift symmetry is referred to as *lineality*. In the context of generalised biadjoint scattering amplitudes it corresponds to momentum conservation.

Quotienting the space of solutions of the tropical hypersurface conditions (4.2.2) by a single global shift with $a_i=a$ corresponds to the tropical version of the Grassmannian. Quotienting by all shifts corresponds to the tropical version of the space $\mathrm{Conf}_n(\mathbb{P}^{k-1})$. Here we are interested in the latter case where we quotient by all shifts. Despite this we will refer to the space obtained simply as the tropical Grassmannian and we use the notation $\mathrm{Tr}(k,n)$ to denote it.

The sign of the individual terms of the Plücker relations (2.1.2) is lost through tropicalisation. We can recover the information by identifying *positive* hypersurfaces as those whose defining terms in (2.1.2) have *opposite* signs [144]. This prescription defines the *positive tropical Grassmannian*. The positive part of $\mathrm{Tr}(2,n)$ (denoted $\mathrm{Tr}^+(2,n)$) is closely related to the dual of the kinematic associahedron that we described above and hence can be identified with the canonically ordered amplitude of the bi-adjoint ϕ^3 theory. This fact is at the heart of the recent generalisation of the biadjoint amplitudes to general $\mathrm{Tr}(k,n)$ [7]. In Sect. 4.3 we give a more detailed introduction to the positive tropical Grassmannian following [83].

Such generalised biadjoint amplitudes can also be related to a generalisation of the scattering equations [7, 79, 80] to $\mathbb{CP}^{k-1}$ and through them to amplitudes of a generalised scalar bi-adjoint theory [81]. Focusing for simplicity to $k=3$, we consider homogenous

coordinates of n particles on $\mathbb{CP}^2$ and form the $3 \times n$ matrix

$$m = \begin{pmatrix} 1 & 1 & \cdots & 1 \\ x_1 & x_2 & \cdots & x_n \\ y_1 & y_2 & \cdots & y_n \end{pmatrix}. \tag{4.2.3}$$

We then define the potential function

$$S_3 = \sum_{1 \le i < j < k \le n} s_{ijk} \log[ijk], \tag{4.2.4}$$

where $[ijk]$ represent minors of m and s_{ijk} are generalized Mandelstam variables that satisfy $\sum_{j \neq k} s_{ijk} = 0, \ \forall i$. We can now write down the amplitude of a generalised scalar theory as

$$A_n^{(3)}(\alpha|\beta) = \frac{1}{\text{vol}(\text{SL}(3,\mathbb{C}))} \int \prod_i \mathrm{d}x_i \mathrm{d}y_i \delta(S_{3,x_i}) \delta(S_{3,y_i}) \text{PT}(\alpha) \text{PT}(\beta), \tag{4.2.5}$$

where S_3, i denotes derivative with respect to i and the generalized Parke-Taylor factors involve two orderings α and β and are given by

$$\text{PT}(\mathbb{I}) = \frac{1}{[123][234]\cdots[n12]}. \tag{4.2.6}$$

The positive region of the tropical computation should then equal (4.2.5) for the canonical ordering $\alpha = \beta = \mathbb{I}$.

Let us consider explicit examples of the tropical Grassmannian [145]. The simplest case is $\text{Gr}(2,4)$, defined by the single Plücker relation,

$$p_{12}p_{34} - p_{13}p_{24} + p_{14}p_{23} = 0\,. \tag{4.2.7}$$

In this case the tropical hypersurface conditions have three solutions (modulo lineality), given by the three possibilities in (4.2.2) with $\{i,j,k,l\} = \{1,2,3,4\}$. They are represented by the following six component vectors corresponding to the canonical ordering of the $\{w_{12}, w_{13}, w_{14}, w_{23}, w_{24}, w_{34}\}$,

$$\begin{aligned} e_{12} &= (1,0,0,0,0,0)\,, \\ e_{13} &= (0,1,0,0,0,0)\,, \\ e_{14} &= (0,0,1,0,0,0)\,. \end{aligned} \tag{4.2.8}$$

Of these only the first and third are positive. Note that one may not generally add solutions to obtain other solutions, the above vectors represent three distinct solutions. Note also that because of the shift symmetry $w_{ij} \mapsto w_{ij} + a_i + a_j$ the following vectors

$$\begin{aligned} e_{34} &= (0,0,0,0,0,1)\,, \\ e_{24} &= (0,0,0,0,1,0)\,, \\ e_{23} &= (0,0,0,1,0,0) \end{aligned} \tag{4.2.9}$$

are equivalent to the original three. This shift symmetry has the interpretation of momentum conservation once the solution vectors e_{ij} are contracted with a canonically ordered vector of Mandelstam invariants $y = (s_{12}, \ldots, s_{34})$ entering the massless biadjoint scatter-

ing amplitudes.

Let us now describe the $\mathrm{Gr}(2,5)$ case. In this case we have ten Plücker coordinates p_{ij} and the Plücker relations are given by (4.2.7) and four more relations obtained from cyclic rotation of the labels. These relations give rise to the tropical hypersurface conditions (4.2.2) for $\{i,j,k,l\}$ given by $\{1,2,3,4\}$, $\{1,2,3,5\}$, $\{1,2,4,5\}$, $\{1,3,4,5\}$ and $\{2,3,4,5\}$. Each of these five cases must be simultaneously satisfied.

We arrange the coordinates in the standard, lexicographical order,

$$\{w_{12}, w_{13}, w_{14}, w_{15}, w_{23}, w_{24}, w_{25}, w_{34}, w_{35}, w_{45}\} \tag{4.2.10}$$

and define ray vectors as

$$\begin{aligned} e_{12} &= (1,0,0,0,0,0,0,0,0,0)\,, \\ e_{13} &= (0,1,0,0,0,0,0,0,0,0)\,, \\ &\vdots \\ e_{45} &= (0,0,0,0,0,0,0,0,0,1) \end{aligned} \tag{4.2.11}$$

and so on. The vectors e_{ij} so defined are simultaneously solutions to all five of the tropical hypersurface conditions.

In this case we can also combine certain solutions. For example we find that any positive linear combination $ae_{12} + be_{34}$ with $a, b > 0$ is also a solution. However no positive linear combination $ae_{12} + be_{13}$ is a solution. We thus obtain a notion of *connectivity* of solutions: two solutions are connected if any positive linear combination of them is a solution. We say that there is an *edge* between such solutions. In the case of $\mathrm{Gr}(2,5)$ we can never combine three or more solutions to obtain another solution. In higher dimensional examples one can obtain triangles of solutions and higher dimensional faces.

Performing permutations on the indices leads us to find 15 edges between the 10 vertices given by the e_{ij}. The full set of solutions corresponding to the tropical Grassmannian $\mathrm{Tr}(2,5)$ can be depicted by the Petersen graph shown in Fig. 4.2.

The positive part $\mathrm{Tr}^+(2,5)$ is identified with those solutions where only the first and third possibilities in (4.2.2) are allowed in each of the five cases. This picks out the solutions $\{e_{12}, e_{23}, e_{34}, e_{45}, e_{15}\}$. The positive part is then given by the positive rays and the edges between them (any positive linear combination of connected positive solutions is a positive solution). The positive part is highlighted in Fig. 4.2.

4.3 The positive tropical Grassmannian from webs

In [83] an alternative way of describing just the positive part $\mathrm{Tr}^+(k,n)$ was given. In this approach one introduces a grid called a *web diagram* with labels $\{1,\ldots,k\}$ on the horizontal edge and labels $\{(k+1),\ldots,n\}$ on the vertical edge. The squares of the grid are populated with variables x_i. In Fig. 4.3 we illustrate the general procedure in the case of $\mathrm{Tr}(3,7)$.

A Plücker coordinate is indexed by a set K of k distinct labels chosen from $\{1,\ldots,n\}$. We denote the set $\{1,\ldots,k\}$ by $[k]$. We may then associate a Plücker coordinate p_K to

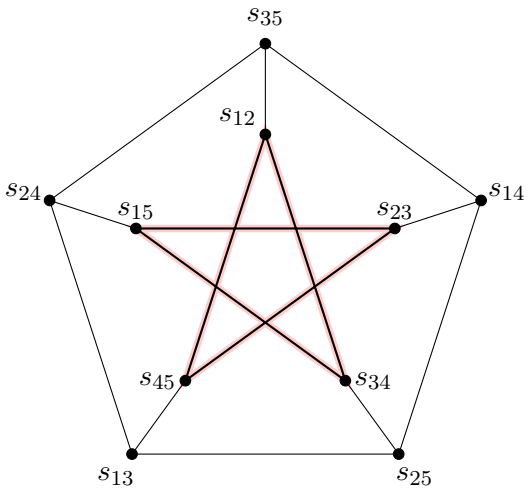

Figure 4.2: The 10 vertices and 15 edges of the full $\mathrm{Tr}(2,5)$ space. The highlighted star is the positive region. It corresponds to the canonical order amplitude of the scalar bi-adjoint ϕ^3 theory.

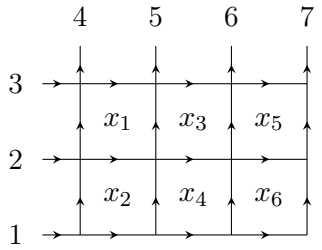

Figure 4.3: Example web diagram for $\mathrm{Gr}(3,7)$.

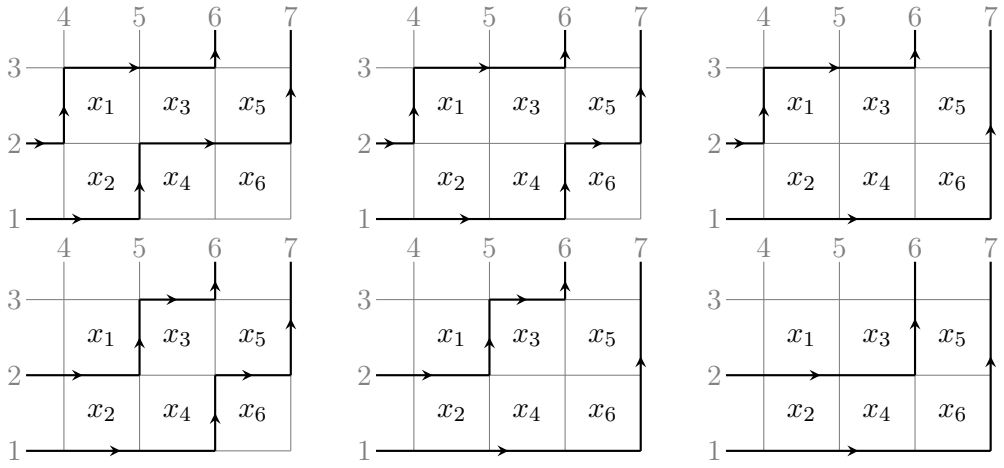

Figure 4.4: Possible sets of non-intersecting paths from $\{1,2\}$ to $\{6,7\}$ describing the representation (4.3.1) of the Plücker coordinate p_{367} in $\mathrm{Gr}(3,7)$.

a set of paths on the web diagram as follows. Consider sets S of non-intersecting paths consistent with the arrows which go from $[k]\setminus([k]\cap K)$ to $K\setminus([k]\cap K)$. We denote the set of all such sets as $\mathrm{Path}(K)$. For each path in a given set S we record the product of the variables in the squares above the path (if there are no squares above the path we record the value 1). For a set S of paths we take the product over all paths in the set which we denote by $\mathrm{Prod}_S(x)$ (if the set is empty we record the value 1). Finally we sum over all possible choices of sets S of such non-intersecting paths, i.e. we sum over $S\in\mathrm{Path}(K)$,

$$p_K = \sum_{S\in\mathrm{Path}(K)} \mathrm{Prod}_S(x)\,. \tag{4.3.1}$$

The procedure is best illustrated with an example: consider the Plücker coordinate p_{367} in the case illustrated in Fig. 4.3. We need to consider sets of non-intersecting paths from $\{1,2\}$ to $\{6,7\}$. We find the possible choices illustrated in Fig. 4.4. The final result for the Plücker coordinate is therefore,

$$\begin{aligned} p_{367} &= x_1x_2x_3x_5 + x_1x_2x_3x_4x_5 + x_1x_2x_3x_4x_5x_6 \\ &\quad + x_1^2x_2x_3x_4x_5 + x_1^2x_2x_3x_4x_5x_6 + x_1^2x_2x_3^2x_4x_5x_6\,. \end{aligned} \tag{4.3.2}$$

To consider the tropical Grassmannian we tropicalise the resulting polynomial, replacing multiplication with addition and addition with minimum to obtain w_K.

Following exactly the same logic for the simpler example of $\mathrm{Gr}(2,5)$ we obtain (as in [83])

$$\begin{aligned} p_{1i} &= p_{23} = 1\,, & w_{1i} &= w_{23} = 0\,,\\ p_{24} &= 1+x_1, & w_{24} &= \min(0,\tilde{x}_1)\,,\\ p_{25} &= 1+x_1+x_1x_2\,, & w_{25} &= \min(0,\tilde{x}_1,\tilde{x}_1+\tilde{x}_2)\,,\\ p_{34} &= x_1\,, & w_{34} &= \tilde{x}_1\,,\\ p_{35} &= x_1+x_1x_2\,, & w_{35} &= \min(\tilde{x}_1,\tilde{x}_1+\tilde{x}_2)\,,\\ p_{45} &= x_1x_2\,, & w_{45} &= \tilde{x}_1+\tilde{x}_2\,. \end{aligned}$$

The resulting tropical minors are piecewise linear functions in the space parametrised by $(\tilde{x}_1, \tilde{x}_2)$. Each such function defines tropical hypersurfaces in exactly the same way as before. Taking the union over the tropical hypersurfaces gives rise to a fan with five domains of linearity separated by five rays as illustrated in Fig. 4.5a. We may label the five rays by

$$\{\mathbf{e}_1, \mathbf{e}_2, -\mathbf{e}_1, -\mathbf{e}_2, \mathbf{e}_1 - \mathbf{e}_2\} \tag{4.3.3}$$

where $\mathbf{e}_1$ and $\mathbf{e}_2$ are the two-component vectors,

$$\mathbf{e}_1 = (1, 0)\,, \qquad \mathbf{e}_2 = (0, 1)\,. \tag{4.3.4}$$

More generally, the tropical minors in $\mathrm{Tr}^+(k, n)$ define a polyhedral fan in the $(k-1)(n-k-1)$-dimensional space of $\tilde{x}_i$ variables with many domains of linearity separated by walls of codimension one. The walls intersect in surfaces of codimension two and so on all the way down to individual rays of dimension one defined by the multiple intersection of (at least) $((k-1)(n-k-1)-1)$ walls. We illustrate the fan obtained in the case of $\mathrm{Tr}^+(2, 6)$ in Fig. 4.5b.

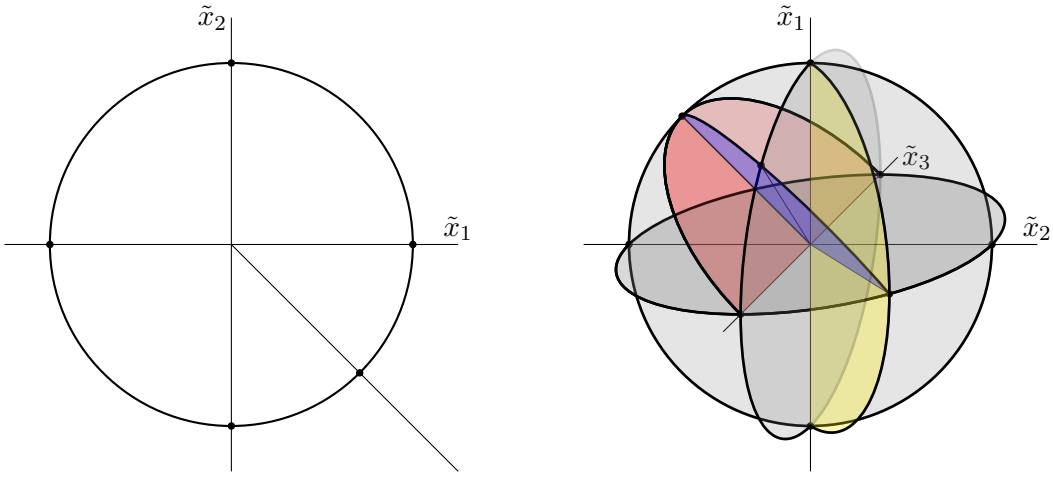

(a) The $\mathrm{Tr}^+(2, 5)$ polyhedral fan

(b) The $\mathrm{Tr}^+(2, 6)$ polyhedral fan

Figure 4.5: The intersection of the $\mathrm{Tr}^+(2, n)$ fan with the unit sphere S^{n-4} gives the dual of the $\mathrm{Gr}(2, n)$ associahedron. Notice the $\mathrm{Tr}^+(2, 5)$ subfan on the $(\tilde{x}_1, \tilde{x}_2)$ plane of $\mathrm{Tr}^+(2, 6)$.

The five rays we have obtained correspond to the five positive rays among the set (4.2.11). We may verify this by evaluating the tropical minors w_{ij} in (4.3.3) on the five rays $\{\mathbf{e}_1, \mathbf{e}_2, -\mathbf{e}_1, -\mathbf{e}_2, \mathbf{e}_1 - \mathbf{e}_2\}$. For example if we evaluate the ten-component vector of the w_{ij} on $\mathbf{e}_1$ we obtain the vector

$$\mathbf{e}_1 \mapsto \mathrm{ev}(\mathbf{e}_1) = (0,0,0,0,0,0,0,1,1,1) \sim (1,0,0,0,0,0,0,0,0,0) = e_{12}\,. \tag{4.3.5}$$

where the equivalence corresponds to the lineality shift $w_{ij} \to w_{ij}+a_i+a_j$ with $(a_1, a_2, a_3, a_4, a_5) = \frac{1}{2}(1, 1, -1, -1, -1)$. Doing the same for each of the five rays in (4.3.3) we indeed obtain the ten-component vectors $\{e_{12}, e_{45}, e_{23}, e_{15}, e_{34}\}$, precisely the five positive rays in the list of ten solutions given in (4.2.11). The regions between the rays in Fig. 4.5a then correspond to the edges between the positive rays in Fig. 4.2.

We may also recover the rays (4.3.3) from $\{e_{12}, e_{45}, e_{23}, e_{15}, e_{34}\}$ by tropically evaluating the coordinates x_1 and x_2 which are given by

$$\begin{aligned} x_1 &= \frac{p_{12}p_{34}}{p_{14}p_{23}}\,, \quad \longrightarrow \quad \tilde{x}_1 = w_{12} + w_{34} - w_{14} - w_{23}\,, \\ x_2 &= \frac{p_{13}p_{45}}{p_{15}p_{34}}\,, \quad \longrightarrow \quad \tilde{x}_2 = w_{13} + w_{45} - w_{15} - w_{34}\,. \end{aligned} \tag{4.3.6}$$

So for example the vector e_{12} evaluates to $(1, 0) = \mathbf{e}_1$ and the vector e_{34} evaluates to $(1, -1) = \mathbf{e}_1 - \mathbf{e}_2$.

Note that the rays (4.3.3) we have obtained from the tropical minors (4.3.3) correspond to the dual vectors (4.1.6) after dropping their first components. For example we have

$$W_{24} = (c_{24} + c_{25}, -1, 0) \sim -\mathbf{e}_1\,. \tag{4.3.7}$$

The first component of the dual vector W_{24} may be recovered by demanding for example

$$Y \cdot W_{24} = y \cdot \mathrm{ev}(-e_1) = s_{23} = X_{24}\,, \tag{4.3.8}$$

where we recall $Y = (1, X_{13}, X_{14})$ and $y = (s_{12}, \ldots, s_{45})$. Since the dual vectors are equivalent to the defining constraints of the kinematic associahedron, this gives us a way to recover the kinematic associahedron from the tropical minors.

The expressions of the web variables x_i in terms of Plücker coordinates in fact identifies them with the cluster $\mathcal{X}$-variables of [63, 64] for the initial cluster of the $\mathrm{Gr}(2, 5)$ cluster algebra. Indeed more generally the web variables are identified with the $\mathcal{X}$-coordinates of the initial cluster for any $\mathrm{Gr}(k, n)$. As we now outline, we can use the algebraic machinery of the cluster algebra to generate all the ray vectors describing the positive tropical Grassmannian $\mathrm{Tr}^+(k, n)$.

4.4 The tropical Grassmannian and cluster algebras

As mentioned above, we can identify cluster $\mathcal{X}$-coordinates with web variables. As we shall see we can also identify the ray vectors with cluster $\mathcal{A}$-coordinates. This allows us to generalise the notion of mutation to these rays such that we can generate all rays in the fan in a cluster algebraic way [146]. For a description of the relation between cluster algebras and polyhedral fans, see also [147].

When we described cluster algebras in Chapter 2, one piece of information that each cluster is equipped with is the exchange matrix B. Generalising mutations to rays requires additional information, namely an additional matrix C (the coefficient matrix), its mutation given by [9]

$$c'_{ij} = \begin{cases} -c_{ij} & \text{if } j = k. \\ c_{ij} - [c_{ik}]_+ b_{kj} + c_{ik}[b_{kj}]_+ & \text{otherwise.} \end{cases} \tag{4.4.1}$$

To each unfrozen $\mathcal{A}$-coordinate we associate a ray vector $\mathbf{g}$. We start by constructing the initial cluster such that the m unfrozen nodes are the m basis vectors for $\mathbb{R}^m$ and C is the

[9] Note that we have modified slightly the mutation rule of the coefficient matrix of [146] so that the $\mathbf{g}$ vectors defined by (4.4.2,4.4.3) match precisely the ray vectors for $\mathrm{Tr}^+(k, n)$ as defined in Sect. 4.3.

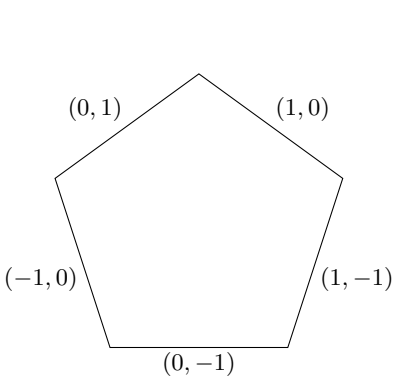

(a) The $\mathrm{Tr}^+(2,5)$ polytope labelled by rays.

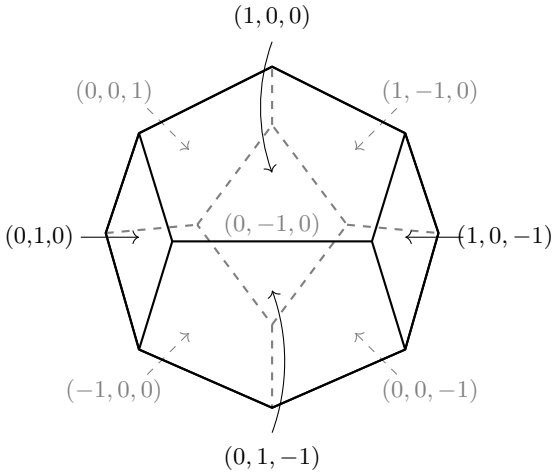

(b) The $\mathrm{Tr}^+(2,6)$ polytope with the faces labelled by rays.

Figure 4.6: The cluster polytopes pictured here are the dual polyhedra of those arising from the fans shown in Fig. 4.5.

identity

$$\mathbf{g}_l = \mathbf{e}_l, \quad l = (1, \ldots, m), \quad C = \mathbb{I}_m. \tag{4.4.2}$$

We then select a node k to mutate on, following the mutation rule

$$\begin{aligned} \mathbf{g}'_l &= \mathbf{g}_l, \quad \text{for} \quad l \neq k \\ \mathbf{g}'_k &= -\mathbf{g}_k + \sum_{i=1}^{n} [-b_{ik}]_+ \mathbf{g}_i + \sum_{j=1}^{n} [c_{jk}]_+ \mathbf{b}^0_j \end{aligned} \tag{4.4.3}$$

where $\mathbf{b}^0_j$, $j \in \{1, \ldots, m\}$ corresponds to the jth column of B^0, the exchange matrix for the initial cluster. We can then repeat this process as many times as required to generate a vector for each unfrozen $\mathcal{A}$-coordinate. In the cases where the cluster algebra is of finite type (in this context the cases are $\mathrm{Gr}(2,n)$, $\mathrm{Gr}(3,6)$, $\mathrm{Gr}(3,7)$ and $\mathrm{Gr}(3,8)$) we obtain a finite cluster polytope by performing all mutations where each vertex is associated to a cluster. Each face of the polytope is associated to an unfrozen $\mathcal{A}$-coordinate a and also by the above procedure a vector $\mathbf{g}$.

The advantage of having the relation of the positive tropical fan to the cluster algebra is that it gives us a very easy algebraic way to generate the relevant ray vectors to describe the fan. Once we have the fan we can embed it into the original Plücker space using the tropical minors and compute its volume to obtain the generalised scattering amplitude.

The resulting polytope in the simplest case is given in Figure 4.6a. It has five clusters connected in the shape of a pentagon. This pentagon is the dual of the pentagon obtained from intersecting the fan illustrated in Fig. 4.5a with the unit circle; its edges are labelled with ray vectors (4.3.3).

In fact for $\mathrm{Gr}(2,n)$ the polytope obtained by intersecting the positive tropical fan with the unit sphere is always the dual polytope of the $\mathrm{Gr}(2,n)$ associahedron or Stasheff

polytope. For example in Fig. 4.6b we show the vectors associated to the faces of the A_3 associahedron. The dual polytope coincides with the intersection of the $\mathrm{Gr}(2,6)$ positive tropical fan with the unit sphere given in Fig. 4.5b.

For the other finite cases the tropical positive fan gives polytopes that are closely related to the duals of the cluster polytopes as we now describe.

4.5 $\mathrm{Tr}^+(3,6)$

Let us now consider the first case of the generalised biadjoint amplitudes which was addressed in [7]. In analogy to the $\mathrm{Gr}\,(2,n)$ cases of the previous section, the generalised amplitude for higher k and n can be interpreted as the volume of the computed by triangulating the relevant $\mathrm{Tr}^+(3,6)$ fan.

Following [145] we start by considering by the Plücker relations of $\mathrm{Gr}(3,6)$, of which there are two kinds, three-term relations and four-term relations,

$$\begin{aligned} p_{123}p_{145} + p_{125}p_{134} - p_{124}p_{135} &= 0, \dots \\ p_{123}p_{456} - p_{156}p_{234} + p_{146}p_{235} - p_{145}p_{236} &= 0, \dots \end{aligned} \tag{4.5.1}$$

While one can combinatorially generate many relations, only 35 of them are linearly independent.

We then tropicalise these polynomials in Plückers to obtain

$$\begin{aligned} &\min(w_{123} + w_{145}, w_{125} + w_{134}, w_{124} + w_{135}), \dots \\ &\min(w_{123} + w_{456}, w_{156} + w_{234}, w_{146} + w_{235}, w_{145} + w_{236}), \dots . \end{aligned} \tag{4.5.2}$$

As before the tropical polynomials define regions of linearity in the tropical Plücker space $\mathbb{R}^{20}$ separated by hypersurfaces defined as the set of points at which the two smallest arguments of the min functions are equal. Consider for instance, the first tropical polynomial in (4.5.2). It gives rise to a boundary between two cones if one of the following is satisfied:

$$w_{123} + w_{145} = w_{125} + w_{134} \leq w_{124} + w_{135} \tag{4.5.3a}$$

$$\text{or} \qquad w_{123} + w_{145} = w_{124} + w_{135} \leq w_{125} + w_{134} \tag{4.5.3b}$$

$$\text{or} \qquad w_{124} + w_{135} = w_{125} + w_{134} \leq w_{123} + w_{145}. \tag{4.5.3c}$$

This polytope contains 65 vertices [145]. As above we denote the unit vectors in the w_{ijk} directions by e_{ijk}. These vectors give 20 of the vertices. A further 15 are of the form

$$f_{ijkl} = e_{ijk} + e_{jil} + e_{ikl} + e_{jkl}\,. \tag{4.5.4}$$

The remaining 30 are of the form (for $\{i,j,k,l,m,n\}$ distinct)

$$g_{ij,kl,mn} = f_{ijkl} + e_{klm} + e_{kln}\,. \tag{4.5.5}$$

The part of the polytope that is relevant for a planar ordering is its *positive part* $\mathrm{Tr}^+(3,6)$. In [7] the positive vertices were determined by requiring compatibility with a planar ordering for the scattering amplitude. Here we identify the positive rays by

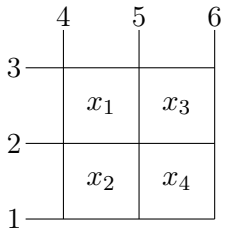

Figure 4.7: The web diagram for $\mathrm{Gr}(3,6)$.

requiring that they satisfy the hypersurface conditions generated by monomials in the Plücker coordinates with opposite signs as we described in Sect. 4.2. This leaves us with 16 rays out of 65, coinciding precisely with the set of [7]. They are e_{123} and cyclic, f_{1234} and cyclic and $g_{12,34,56}$, $g_{23,45,61}$, $g_{34,12,56}$ and $g_{45,23,61}$.

The $\mathrm{Gr}^+(3,6)$ web diagram shown in Fig. 4.7 produces a matrix with following piecewise linear tropical minors [83, 144],

$$
\begin{aligned}
&w_{12i} = w_{134} = w_{234} = 0\,,\\
&w_{135} = \min(0,\tilde{x}_1),\\
&w_{136} = \min(0,\tilde{x}_1,\tilde{x}_1+\tilde{x}_3),\\
&w_{145} = \tilde{x}_1\,,\\
&w_{146} = \min(\tilde{x}_1,\tilde{x}_1+\tilde{x}_3)\,,\\
&w_{156} = \tilde{x}_1+\tilde{x}_3\,,\\
&w_{235} = \min(0,\tilde{x}_1,\tilde{x}_1+\tilde{x}_2)\,,\\
&w_{236} = \min(0,\tilde{x}_1,\tilde{x}_1+\tilde{x}_2,\tilde{x}_1+\tilde{x}_3,\tilde{x}_1+\tilde{x}_2+\tilde{x}_3,\tilde{x}_1+\tilde{x}_2+\tilde{x}_3+\tilde{x}_4)\,,\\
&w_{245} = \min(\tilde{x}_1,\tilde{x}_1+\tilde{x}_2)\,,\\
&w_{246} = \min(\tilde{x}_1,\tilde{x}_1+\tilde{x}_2,\tilde{x}_1+\tilde{x}_3,\tilde{x}_1+\tilde{x}_2+\tilde{x}_3,\tilde{x}_1+\tilde{x}_2+\tilde{x}_3+\tilde{x}_4)\,,\\
&w_{256} = \min(\tilde{x}_1+\tilde{x}_3,\tilde{x}_1+\tilde{x}_2+\tilde{x}_3,\tilde{x}_1+\tilde{x}_2+\tilde{x}_3+\tilde{x}_4)\,,\\
&w_{345} = \tilde{x}_1+\tilde{x}_2\,,\\
&w_{346} = \min(\tilde{x}_1+\tilde{x}_2,\tilde{x}_1+\tilde{x}_2+\tilde{x}_3,\tilde{x}_1+\tilde{x}_2+\tilde{x}_3+\tilde{x}_4)\,,\\
&w_{356} = \min(\tilde{x}_1+\tilde{x}_2+\tilde{x}_3,\tilde{x}_1+\tilde{x}_2+\tilde{x}_3+\tilde{x}_4,2\tilde{x}_1+\tilde{x}_2+\tilde{x}_3+\tilde{x}_4)\,,\\
&w_{456} = 2\tilde{x}_1+\tilde{x}_2+\tilde{x}_3+\tilde{x}_4\,.
\end{aligned}
\tag{4.5.6}
$$

The regions of linearity of the tropical minors (4.5.6) define the fan for $\mathrm{Tr}^+(3,6)$ and its intersection with the unit sphere S^3 is a polytope with 16 vertices, 66 edges, 98 triangles and 48 three-dimensional facets. The tropical $\mathcal{X}$-coordinates are given by

$$
\begin{aligned}
&\tilde{x}_1 = w_{123}+w_{145}-w_{125}-w_{134}\,, \quad \tilde{x}_3 = w_{124}+w_{156}-w_{126}-w_{145}\,,\\
&\tilde{x}_2 = w_{124}+w_{345}-w_{145}-w_{234}\,, \quad \tilde{x}_4 = w_{134}+w_{125}+w_{456}-w_{124}-w_{156}-w_{345}\,.
\end{aligned}
\tag{4.5.7}
$$

With the above relations (4.5.6) and (4.5.7) we can go back and forth between the representation of the 16 positive vertices in terms of the e_{ijk} and in terms of a four-component representation which we can also obtain from cluster mutations as we now describe.

4.5.1 Triangulating $\mathrm{Tr}^+(3,6)$ with clusters

Unlike in $\mathrm{Gr}(2,5)$, the $\mathrm{Tr}^+(3,6)$ fan contains facets that are not simplicial. In particular, it contains 46 simplicial facets and two bipyramids defined by five vertices. This is a common feature of $k > 2$ (tropical) Grassmannians.

To see this, first recall that $(k-1)(n-k+1)$ rays define a facet of the fan if an arbitrary positive linear combination of them solves the positive versions of inequalities derived from the Plücker relations. In particular $\mathrm{Tr}^+(3,6)$ has 2 such facets with *five* vertices that form bipyramids. These non-simplicial bipyramids are arranged inside the fan $\mathrm{Tr}^+(3,6)$ as sketched in Figure 4.8.

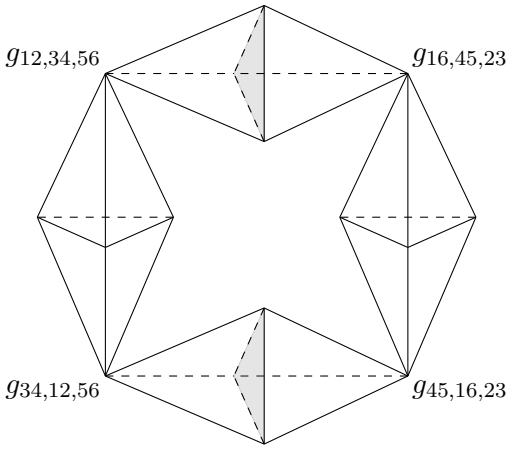

Figure 4.8: The arrangement of bipyramids inside $\mathrm{Tr}^+(3,6)$. The vertices represent the intersections of the rays r_i with the unit sphere S^4. Two triangles are shaded to emphasize that they are actual 2-faces of the polytope.

The fan $\mathrm{Tr}^+(3,6)$ is closely related to the dual of the $\mathrm{Gr}^+(3,6)$ associahedron in that the latter provides a natural triangulation of the former [144]. The vertices of the dual of the associahedron correspond to cluster $\mathcal{A}$-coordinates. Two vertices are connected by an edge when the corresponding pair of $\mathcal{A}$-coordinates appear together in a cluster, i.e. are cluster-adjacent. By definition, a pairwise connected quadruplet of vertices of the dual $\mathrm{Gr}^+(3,6)$ associahedron corresponds to a cluster, which in turn can be identified as a simplex triangulating $\mathrm{Tr}^+(3,6)$.

We begin with the initial cluster

$$\begin{array}{ccc} (124) & \to & (125) \\ \downarrow & \nwarrow & \downarrow \\ (134) & \to & (145) \end{array}$$

and associate its unfrozen $\mathcal{A}$-coordinates with the unit vectors $\mathbf{e}_1, \ldots, \mathbf{e}_4$ in the tropical $\tilde{x}_i$ coordinates,

$$(124) \leftrightarrow \mathbf{e}_1 = (1,0,0,0), \qquad (125) \leftrightarrow \mathbf{e}_2 = (0,1,0,0), \tag{4.5.8}$$

$$(134) \leftrightarrow \mathbf{e}_3 = (0,0,1,0), \qquad (145) \leftrightarrow \mathbf{e}_4 = (0,0,0,1)\,. \tag{4.5.9}$$

Performing all possible mutations generates the full set of 16 ray vectors which arise from

50 distinct clusters.

Among the 16 rays we find the following five,

$$\begin{aligned}
\mathbf{e}_3 &\mapsto (\,0\;\;0\;\;0\;\;0\;\;0\;\;0\;\;0\;\;0\;\;1\;\;0\;\;0\;\;0\;\;0\;\;0\;\;1\;\;0\;\;0\;\;1\;\;1\,) \sim f_{1234}\\
-\mathbf{e}_1 &\mapsto (\,0\;\;0\;\;0\;\;0\;\;0\;\;\text{-}1\;\text{-}1\;\text{-}1\;\text{-}1\;\text{-}1\;\;0\;\;\text{-}1\;\text{-}1\;\text{-}1\;\text{-}1\;\text{-}1\;\text{-}1\;\text{-}1\;\text{-}2\;\text{-}2\,) \sim f_{1256}\\
\mathbf{e}_2 &\mapsto (\,0\;\;0\;\;0\;\;0\;\;0\;\;0\;\;0\;\;0\;\;0\;\;0\;\;0\;\;0\;\;0\;\;0\;\;0\;\;1\;\;1\;\;1\;\;1\,) \sim f_{3456}\\
\mathbf{e}_2+\mathbf{e}_3-\mathbf{e}_4 &\mapsto (\,0\;\;0\;\;0\;\;0\;\;0\;\;0\;\;0\;\;0\;\;1\;\;0\;\;0\;\;0\;\;0\;\;0\;\;1\;\;1\;\;1\;\;1\;\;1\,) \sim g_{12,34,56}\\
\mathbf{e}_4-\mathbf{e}_1 &\mapsto (\,0\;\;0\;\;0\;\;0\;\;0\;\;\text{-}1\;\text{-}1\;\text{-}1\;\text{-}1\;\text{-}1\;\;0\;\;\text{-}1\;\text{-}1\;\text{-}1\;\text{-}1\;\text{-}1\;\text{-}1\;\text{-}1\;\text{-}1\;\text{-}1\,) \sim g_{34,12,56}
\end{aligned}$$

where we have also given their evaluations through the tropical minors (4.5.6) and the corresponding positive solutions given above. The fact that these five vertices form a single bipyramid rather than two tetrahedral facets can be seen from the linear relation,

$$f_{1234}+f_{1256}+f_{3456}=g_{12,34,56}+g_{34,12,56}\,. \tag{4.5.10}$$

Note that the cluster algebra provides a canonical way of determining a triangulation. In particular the bipyramid formed by the five rays described above is triangulated by two clusters whose vertices are given by $\{f_{1234},f_{1256},f_{3456},g_{12,34,56}\}$ and $\{f_{1234},f_{1256},f_{3456},g_{34,12,56}\}$.

Equipped with the cluster triangulation, we can express the scattering amplitude as a sum over clusters,

$$m_3^6(\mathbb{I}|\mathbb{I})=\sum_{c\in\substack{\text{clusters of}\\ \text{Gr}^+(3,\,6)}}\;\prod_{a\in\,\mathcal{A}\text{-coords of }c}\frac{1}{y\cdot\text{ev}(r_a)}\,, \tag{4.5.11}$$

where as before $y=(s_{123},\ldots,s_{456})$ is the lexicographically ordered vector of Mandelstam invariants, r_a is the representation of the $\mathcal{A}$-coordinate a as a ray in $\tilde{x}$ coordinates and ev means the evaluation using the tropical minors in (4.5.6).

Using this identification, we can read off the two terms in the amplitude directly from the two clusters as[10]

$$\frac{1}{t_{1234}t_{1256}t_{3456}}\left[\frac{1}{R_{12,34,56}}+\frac{1}{R_{34,12,56}}\right]. \tag{4.5.12}$$

Note that using the identity between kinematic invariants

$$R_{12,34,56}+R_{34,12,56}=t_{1234}+t_{3456}+t_{5612} \tag{4.5.13}$$

we can write these two terms as

$$(4.5.12)=\frac{1}{R_{12,34,56}R_{34,12,56}}\left[\frac{1}{t_{1256}t_{3456}}+\frac{1}{t_{1234}t_{3456}}+\frac{1}{t_{1234}t_{1256}}\right] \tag{4.5.14}$$

which was noted in [7] to correspond to a different triangulation of the bipyramid. However the cluster algebra prefers a particular one of these triangulations.

[10]Here we use the notation $t_{ijkl}=s_{ijk}+s_{ijl}+s_{ikl}+s_{jkl}$ and $R_{ij,kl,mn}=t_{ijkl}+s_{klm}+s_{kln}$.

4.6 $\mathrm{Tr}(3,7)$: the amplitude from E_6 clusters

In this section we explicitly demonstrate how the triangulation of the fan associated to the positive tropical Grassmannian $\mathrm{Tr}^+(3,7)$ can be worked out from the $\mathrm{Gr}(3,7)$ cluster algebra.

As in the previous section, one can either compute $F_{3,7}$ from the web $\mathrm{Web}_{3,7}$ or run the cluster-algebra machinery to obtain the generalised amplitude without even referring to $\mathrm{Tr}(3,7)$. Nevertheless let us first describe $\mathrm{Tr}^+(3,7)$ starting from $\mathrm{Tr}(3,7)$ and elaborate on a situation that is not encountered in Grassmannians of lower dimension.

The tropical Grassmannian $\mathrm{Tr}(3,7)$ has 721 rays which come in six types,[11]

$$b_{1,1234567} = e_{123}, \tag{4.6.1a}$$

$$b_{2,1234567} = e_{123} + e_{124} + e_{134} + e_{234}, \tag{4.6.1b}$$

$$b_{3,1234567} = e_{123} + e_{124} + e_{125} + e_{126} + e_{127}, \tag{4.6.1c}$$

$$b_{4,1234567} = e_{123} + e_{124} + e_{125} + e_{126} + e_{127} + e_{134} + e_{234}, \tag{4.6.1d}$$

$$b_{5,1234567} = e_{123} + e_{124} + e_{125} + e_{126} + e_{127} + e_{134} + e_{156} + e_{234} + e_{256} \tag{4.6.1e}$$

$$b_{6,1234567} = b_{3,1234567} + b_{3,3456712} + b_{3,6712345}\,, \tag{4.6.1f}$$

where as before the lexicographically-ordered e_{ijk} are identified with unit vectors in $\mathbb{R}^{\binom{7}{3}}$. Other rays are obtained by the permutations of those that are written out above. For the types $b_1, \ldots, b_5$ and b_6, the permutations generate the six symmetry classes of respective sizes 35, 35, 21, 210, 315 and 105. These rays have also been tabulated in [148] with their explicit Plücker coordinates. Henceforth we will drop the labels in $b_{i,1234567}$ and just write b_i unless the order of the indices is not canonical.

To compute positive Grassmannian $\mathrm{Tr}^+(3,7)$, we select out of the 721 rays above those which solve the positive versions of tropicalised Plücker relations. One finds that 49 of them satisfy such relations. This seems incompatible with the fact that the cluster algebra has 42 distinct unfrozen $\mathcal{A}$-coordinates.

The resolution to this discrepancy is that seven positive rays of the type b_6 are linear combinations of three mutually-connected rays of type b_3, any positive linear combination of which is a solution. In other words, $b_{6,1234567}$ is in the middle of a triangular 2-face of $\mathrm{Tr}^+(3,7)$ and is not necessary to define a cone of the fan.

As explained by Speyer and Williams [83], the $\mathrm{Tr}^+(3,7)$ fan has 693 facets. While 595 of these facets are simplicial, there are also 63 facets with 7 vertices, 28 with 8 vertices and 7 with with 9 vertices. These non-simplicial facets are the $\mathrm{Gr}(3,7)$ analogues of the bipyramids of $\mathrm{Tr}^+(3,6)$.

We again resort to the relevant cluster algebra E_6 to obtain a triangulation on which we evaluate the amplitude. The E_6 cluster algebra has 833 clusters that give the vertices of the associahedron. These 833 clusters make up the simplexes of the triangulation each of which contain six vertices.

If we employ the duality between $\mathrm{Gr}(3,7)$ and $\mathrm{Gr}(4,7)$ and work in terms of the latter,

[11] This form was also given in [143].

we can relate the positive vertices above to the established notation for $\mathcal{A}$-coordinates in the literature on $\mathcal{N}=4$ amplitudes [8, 45]. The different types of rays classified in (4.6.1a)-(4.6.1f) nicely match the conventional cluster $\mathcal{A}$-coordinates:

$$\begin{aligned} a_{11} &\leftrightarrow b_{2,7123456} & a_{41} &\leftrightarrow b_{4,7156234} \\ a_{21} &\leftrightarrow b_{1,7123456} & a_{51} &\leftrightarrow b_{4,2345671} \\ a_{31} &\leftrightarrow b_{3,5671234} & a_{61} &\leftrightarrow b_{5,1234675}\,, \end{aligned} \tag{4.6.2}$$

where the rest of the correspondence can be worked out by cyclic rotations of the second indices of the a_{ij} and the arguments of the b_i. With this correspondence, we find that the E_6 initial cluster

$$\begin{array}{ccccc} a_{24} & \longrightarrow & a_{37} \\ \downarrow & \nwarrow & \downarrow \\ a_{13} & \longrightarrow & a_{17} \\ \downarrow & \nwarrow & \downarrow \\ a_{32} & \longrightarrow & a_{27} \end{array} \tag{4.6.3}$$

produces the following term in the amplitude

$$\frac{1}{(y\cdot b_{1,1234567})(y\cdot b_{3,1234567})(y\cdot b_{2,1234567})(y\cdot b_{2,4567123})(y\cdot b_{3,6712345})(y\cdot b_{1,5671234})}\,, \tag{4.6.4}$$

with $y=(s_{123},\ldots,s_{567})$. We then mutate these rays iteratively according to (4.4.3) until we cover all 833 clusters of the E_6 polytope. Recovering the corresponding kinematic invariants using (4.6.2), we can construct the $\mathrm{Gr}(3,7)$ amplitude as the volume of the positive tropical Grassmannian. An expression for this amplitude is provided in the ancillary file `Gr37amp.m` provided with [11].

4.7 $\mathrm{Gr}(3,8)$: redundant triangulations

In this section we will run the same construction in $\mathrm{Gr}(3,8)$ to provide a conjecture for the canonically-ordered part of the generalised biadjoint amplitude that one would obtain by solving the scattering equations for this Grassmannian.

We start with the initial cluster of $\mathrm{Gr}(3,8)$

$$\begin{array}{ccccccccc} (124) & \longrightarrow & (125) & \longrightarrow & (126) & \longrightarrow & (127) \\ \downarrow & \nwarrow & \downarrow & \nwarrow & \downarrow & \nwarrow & \downarrow \\ (134) & \longrightarrow & (145) & \longrightarrow & (156) & \longrightarrow & (167) \end{array} \tag{4.7.1}$$

and identify its $\mathcal{A}$-coordinates with the rays $(124)\leftrightarrow\mathbf{e_1}$, $(134),\leftrightarrow\mathbf{e_2}$, $(125)\leftrightarrow\mathbf{e_3}$, …, $(167)\leftrightarrow\mathbf{e_8}$ in $\mathbb{R}^8$. Using the map explained in Sect. 4.3.3 we recover the Plücker coordinates for the Speyer-Williams rays $\mathbf{e}_1,\ldots,\mathbf{e}_8$ and deduce that the initial cluster produces the following for the first term in the amplitude

$$\begin{aligned} &1/\big((y\cdot b_{1,12345678})(y\cdot b_{3,12345678})(y\cdot b_{2,12345678})(y\cdot b_{5,67548123}) \\ &\quad\times(y\cdot b_{5,34215678})(y\cdot b_{2,56781234})(y\cdot b_{3,78123456})(y\cdot b_{1,67812345})\big)\,, \end{aligned} \tag{4.7.2}$$

where the b vertices are given below in (4.7.4) and as before $y = (s_{123}, \ldots, s_{678})$.

We then generate all 25,080 clusters using the mutation rules of [146] which we have adapted in equation (4.4.3). These clusters contain 128 distinct vectors in $\mathbb{R}^8$, identified with the 128 $\mathcal{A}$-coordinates of $\mathrm{Gr}(3,8)$. As usual, the Plücker coordinates of these vectors provides us the factors in the denominator of every term in the amplitude. All 25080 terms are provided in the ancillary file `Gr38amp.m` in [11].

Let us comment further on the correspondence between the $\mathrm{Tr}^+(3,8)$ fan and the $\mathrm{Gr}(3,8)$ cluster algebra. We find that, out of the 128 vectors generated by the cluster algebra, only 120 are rays of the corresponding fan. The extra 8 vectors have the form

$$b_{\mathrm{e}} = b_{8,12345678} + b_{8,78564123} \tag{4.7.3}$$

and cyclic rotations thereof. These too are positive vectors but being linear combinations of two genuine rays they lie on an edge of the fan. In other words, they separate only 7 regions of piecewise linearity for the tropical minors instead of 8. This can be interpreted as the $\mathrm{Gr}(3,7)$ cluster algebra producing *redundant triangulation* of the fan which decomposes already simplicial facets into even smaller simplexes.

We can compare the Plücker coordinates of the vectors we obtain to the rays of another object called the Dressian $\mathrm{Dr}(3,8)$, studied in [149]. $\mathrm{Dr}(3,8)$ is a non-simplicial fan that consists of 15470 rays which split into 12 symmetry classes of size (56, 70, 28, 420, 56, 1260, 420, 560, 1680, 840, 5040, 5040). These define facets in groups of sizes ranging from 8 to 12. While all rays of $\mathrm{Dr}(k,n)$ are expected to be rays of $\mathrm{Gr}(k,n)$, the converse is not true. Indeed the Dressian $\mathrm{Dr}(3,8)$ does not capture the rays b_8 which give rise to "superfluous" triangulations.

The rays of $\mathrm{Dr}(3,8)$, positive and non-positive, are explicitly given as:

$$\begin{aligned}
b_1 &= e_{123},\\
b_2 &= e_{123}+e_{124}+e_{134}+e_{234},\\
b_3 &= e_{123}+e_{124}+e_{125}+e_{126}+e_{127}+e_{128},\\
b_4 &= e_{123}+e_{124}+e_{125}+e_{126}+e_{127}+e_{128}+e_{134}+e_{234},\\
b_5 &= e_{123}+e_{124}+e_{125}+e_{134}+e_{135}+e_{145}+e_{234}+e_{235}+e_{245}+e_{345},\\
b_6 &= e_{123}+e_{124}+e_{125}+e_{126}+e_{127}+e_{128}+e_{136}+e_{145}+e_{236}+e_{245},\\
b_7 &= e_{123}+e_{124}+e_{125}+e_{126}+e_{127}+e_{128}+e_{138}+e_{147}+e_{156}+e_{238}\\
&\quad +e_{247}+e_{256},\\
b_8 &= e_{123}+e_{124}+e_{125}+e_{126}+e_{127}+e_{128}+e_{134}+e_{135}+e_{145}+e_{234}\\
&\quad +e_{235}+e_{245}+e_{345},\\
b_9 &= e_{123}+e_{124}+e_{125}+e_{126}+e_{127}+e_{128}+e_{134}+e_{135}+e_{145}+e_{167}\\
&\quad +e_{234}+e_{235}+e_{245}+e_{267}+e_{345},\\
b_{10} &= e_{123}+e_{124}+e_{125}+e_{134}+e_{135}+e_{145}+e_{146}+e_{147}+e_{148}+e_{234}\\
&\quad +e_{235}+e_{236}+e_{237}+e_{238}+e_{245}+e_{345},\\
b_{11} &= e_{123}+e_{124}+e_{125}+e_{126}+e_{127}+e_{128}+e_{134}+e_{137}+e_{147}+e_{156}\\
&\quad +e_{234}+e_{237}+e_{247}+e_{256}+e_{345}+e_{346}+e_{347}+e_{348},\\
b_{12} &= e_{123}+e_{124}+e_{125}+e_{126}+e_{127}+e_{128}+e_{134}+e_{138}+e_{148}+e_{157}\\
&\quad +e_{234}+e_{238}+e_{248}+e_{257}+e_{345}+e_{346}+e_{347}+e_{348}+e_{356}+e_{456}.
\end{aligned} \tag{4.7.4}$$

Out of these, the 120 vectors defined by

$$\begin{aligned}
&\{b_{1,12345678}, b_{2,12345678}, b_{3,12345678}, b_{4,12345678}, b_{4,23184567}, b_{5,23184567},\\
&b_{6,12378456}, b_{8,12345678}, b_{8,34128567}, b_{9,12345786}, b_{9,23178456}, b_{10,13482567},\\
&b_{11,34185627}, b_{11,12457836}, b_{12,12457683}\}
\end{aligned} \tag{4.7.5}$$

and their cyclic copies lie in the positive region in the sense that they satisfy the positive version of the inequalities (4.2.2). These vectors are in one-to-one correspondence with the 120 non-redundant rays generated by the cluster algebra.

Note that the redundant vectors b_{e} that we encountered in $\mathrm{Gr}(3,8)$ are of different nature to the b_6 of $\mathrm{Gr}(3,7)$. While both types of vectors are not rays of the relevant fan, unlike the b_{e}, the b_6 are not generated by the cluster algebra.

It is clear that tropical geometry offers significant information regarding scattering amplitudes. We will expand on the interplay explored here in the following chapters.

Chapter 5

Finite Fans

In this chapter we will study further the connection between cluster algebras and the positive tropical Grassmannian, a link already partly explored in [83]. We will identify a whole range of tropical fans which can be associated with the positive tropical Grassmannian, one of which is the fan of [83] and another is the **g**-vector fan of the cluster algebra. In the finite cases the **g**-vector fan (which we refer to as the 'cluster' fan) is the most refined fan and other fans we consider, including the fan of [83], can be obtained as projections of it.

These considerations lead us to propose new scattering equations which are more general than those of [7] and involve a more general set of Mandelstam invariants. We can obtain generalised amplitudes which depend on the generalised Mandelstam invariants in a similar fashion by considering volumes of facets of the corresponding tropical fan. This construction can also be used to describe the dual cluster polytope by providing a direct route to determining the face variables, which define the codimension-one boundaries of these polytopes. In this regard the tropical fans we study and their associated generalised ϕ^3 ampliutudes are very closely related to the notion of stringy canonical forms introduced in [150–152]. Indeed the integrals considered there provide in principle a deformation of the ϕ^3 amplitude in the same way that tree-level superstring amplitudes are effectively derived from the α' deformation of biadjoint ϕ^3 amplitudes. In fact a range of techniques explored in recent papers are effectively different languages to describe the same (or closely related) underlying mathematics, namely the tropical Grassmannians discussed in [7], the cluster algebras, mutations and **g**-vector fans as studied in Chapter 4 and in [153], the Minkowski sums of Newton polytopes [150, 154, 155] (which are dual to tropical fans), the planar arrangements of [156, 157] and matroid subdivisions, as studied in [158, 159].

With a selection of different tropical fans to hand we discuss how such differences may show up in the singularities of loop amplitudes in $\mathcal{N} = 4$ super Yang-Mills theory. This leads us to a generalisation of cluster adjacency. Here we define a natural set of polylogarithms satisfying adjacency criteria (not only pairs but also triplets, and in general longer consecutive sequences). The cluster adjacent polylogarithms discussed in Chapter 2 correspond to the cluster fan, while less refined fans lead to stronger sets of adjacency criteria. We examine the known loop amplitudes and compare them at the level of pairs and triplets to establish a tentative correspondence between amplitudes of different MHV degree and classes of tropical fans.

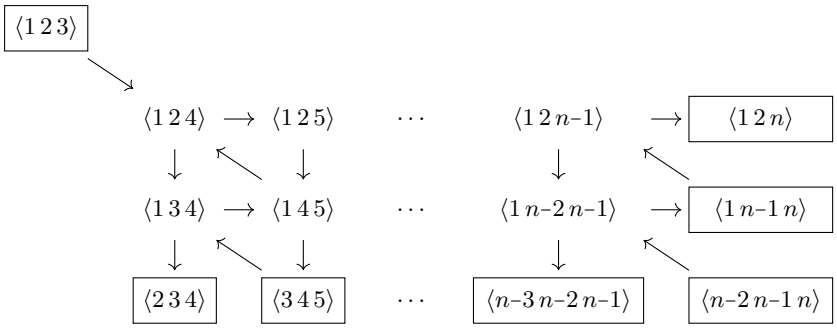

Figure 5.1: The initial cluster of the Grassmannian cluster algebra $\mathrm{Gr}(3,n)$.

5.1 Grassmannian cluster algebras and tropical fans

Let us begin by recalling the construction of Speyer and Williams [83] to describe the positive part of the tropical Grassmannian $\mathrm{Gr}(k,n)$. We will focus on $\mathrm{Gr}(3,6)$ as our motivating example and later consider also $\mathrm{Gr}(3,7)$ and $\mathrm{Gr}(3,8)$. Apart from the Grassmannians $\mathrm{Gr}(2,n)$ these cases (and their duals) exhaust the list of finite cluster Grassmannian cluster algebras. Of particular relevance to planar amplitudes in $\mathcal{N}=4$ super Yang-Mills theory is the case $\mathrm{Gr}(3,7)$ which is dual to $\mathrm{Gr}(4,7)$.

We recall the structure of the initial cluster of the Grassmannian cluster algebra $\mathrm{Gr}(k,n)$. The example of $\mathrm{Gr}(3,n)$ is shown in Fig. 5.1. From the initial cluster we obtain a $(k-1)\times(n-k-1)$ array of cluster $\mathcal{X}$-coordinates x_{rs} given by the product of incoming $\mathcal{A}$-coordinates over the product of outgoing ones to the node in row r and column s.

Given the $\mathcal{X}$-coordinates we can form the $(k\times n)$ web matrix

$$W=(\mathbb{1}_k|M)\,, \tag{5.1.1}$$

where M is the $k\times(n-k)$ matrix with entries

$$m_{ij}=(-1)^{i+k}\sum_{\underline{\lambda}\in Y_{ij}}\prod_{r=1}^{k-i}\prod_{s=1}^{\lambda_r}x_{rs}\,. \tag{5.1.2}$$

The sum in (5.1.2) is over the range Y_{ij} given by $0\le\lambda_{k-i}\le\ldots\le\lambda_1\le j-1$ which is equivalent to a sum over Young tableaux of at most $(k-i)$ rows $\underline{\lambda}=\{\lambda_1,\ldots,\lambda_{k-i}\}$ with at most $(j-1)$ columns. We can then evaluate all the $\mathcal{A}$-coordinates as polynomials in the $\mathcal{X}$-coordinates with positive coefficients by identifying the Plücker coordinates $\langle i_1\ldots i_k\rangle$ with the maximal minors formed by taking the columns $i_1,\ldots,i_k$ of the web matrix W.

In the case of $\mathrm{Gr}(3,6)$ we have the initial cluster shown in Fig 5.2. For this cluster we have the following cluster $\mathcal{X}$-coordinates,

$$\begin{aligned}
x_{11}&=\frac{\langle123\rangle\langle145\rangle}{\langle125\rangle\langle134\rangle}\,, & x_{12}&=\frac{\langle124\rangle\langle156\rangle}{\langle126\rangle\langle145\rangle}\,,\\
x_{21}&=\frac{\langle124\rangle\langle345\rangle}{\langle234\rangle\langle145\rangle}\,, & x_{22}&=\frac{\langle134\rangle\langle456\rangle\langle125\rangle}{\langle124\rangle\langle345\rangle\langle156\rangle}\,.
\end{aligned} \tag{5.1.3}$$

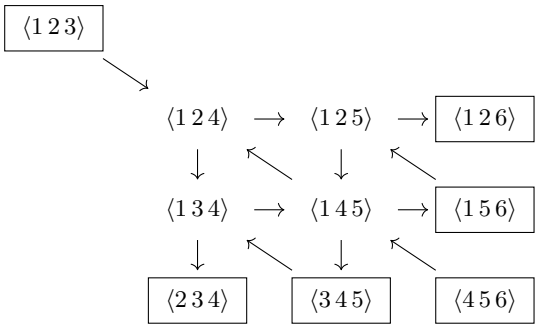

Figure 5.2: The initial cluster of the Grassmannian cluster algebra $\mathrm{Gr}(3,6)$.

The web matrix then takes the form $W = (\mathbb{1}_3|M)$ with

$$M = \begin{bmatrix} 1 & 1+x_{11}+x_{11}x_{21} & 1+x_{11}+x_{11}x_{21}+x_{11}x_{12}+x_{11}x_{12}x_{21}+x_{11}x_{12}x_{21}x_{22} \\ -1 & -1-x_{11} & -1-x_{11}-x_{11}x_{12} \\ 1 & 1 & 1 \end{bmatrix} \tag{5.1.4}$$

If we identify the Plücker coordinate $\langle ijk\rangle$ with the minor formed by taking columns i, j and k of the web matrix then we find that all the $\mathcal{A}$ coordinates of the $\mathrm{Gr}(3,6)$ cluster algebra are expressed as polynomials in the $\mathcal{X}$-coordinates. To emphasise this point we also use the notation $p_{ijk} = \langle ijk\rangle$. The frozen $\mathcal{A}$-coordinates are in fact monomials,

$$\begin{aligned} &p_{123} = 1\,, && p_{234} = 1\,, && p_{345} = x_{11}x_{21}\,, \\ &p_{456} = x_{11}^2x_{21}x_{12}x_{22}\,, && p_{156} = x_{11}x_{12}\,, && p_{126} = 1\,. \end{aligned} \tag{5.1.5}$$

The remaining $\mathcal{A}$-coordinates of the initial cluster and their cyclic images are

$$\begin{aligned} &p_{124} = 1\,, && p_{235} = 1+x_{11}+x_{11}x_{21}\,, && p_{346} = x_{11}x_{21}(1+x_{12}+x_{12}x_{22})\,, \\ &p_{145} = x_{11}\,, && p_{256} = x_{11}x_{12}(1+x_{21}+x_{21}x_{22})\,, && p_{136} = 1+x_{11}+x_{11}x_{12}\,, \end{aligned} \tag{5.1.6}$$

and

$$\begin{aligned} &p_{134} = 1\,, \quad p_{245} = x_{11}(1+x_{21})\,, \quad p_{356} = x_{11}x_{21}x_{12}(1+x_{22}+x_{11}x_{22})\,, \\ &p_{146} = x_{11}(1+x_{12})\,, \qquad\qquad p_{125} = 1\,, \\ &p_{236} = 1+x_{11}+x_{11}x_{12}+x_{11}x_{21}+x_{11}x_{21}x_{12}+x_{11}x_{21}x_{12}x_{22}\,. \end{aligned} \tag{5.1.7}$$

There are two remaining minors which appear as the central nodes of D_4-shaped clusters

$$\begin{aligned} &p_{135} = 1+x_{11}\,, \\ &p_{246} = x_{11}(1+x_{12}+x_{21}+x_{12}x_{21}+x_{12}x_{21}x_{22})\,. \end{aligned} \tag{5.1.8}$$

In addition we have the two quadratic $\mathcal{A}$-coordinates (which also appear in the central node of D_4-shaped clusters),

$$\begin{aligned} q_1 &= \langle 12[34]56\rangle = x_{11}x_{12}x_{21}(1+x_{22})\,, \\ q_2 &= \langle 23[45]61\rangle = x_{11}(1+x_{11}+x_{11}x_{12}+x_{11}x_{21}+x_{11}x_{12}x_{21})\,, \end{aligned} \tag{5.1.9}$$

where $\langle ab[cd]ef\rangle = \langle abd\rangle\langle cef\rangle - \langle abc\rangle\langle def\rangle$ obeys the symmetry properties $\langle ab[cd]ef\rangle =$

$\langle cd[ef]ab\rangle = -\langle cd[ab]ef\rangle$. Under a cyclic transformation $q_1 \to q_2$ and $q_2 \to q_1$.

With the expressions of the $\mathcal{A}$-coordinates to hand we may now define a number of different tropical fans. The fan defined by Speyer and Williams to describe the positive part of the tropical Grassmannian is obtained by replacing the polynomial expressions for the Plücker coordinates $p_{ijk} = \langle ijk\rangle$ by their tropical counterparts $\tilde{p}_{ijk}$. For example, the tropical versions of the minors (5.1.8) are

$$\begin{aligned}\tilde{p}_{135} &= \min(0, \tilde{x}_{11})\,,\\ \tilde{p}_{246} &= \min(\tilde{x}_{11}, \tilde{x}_{11}+\tilde{x}_{12}, \tilde{x}_{11}+\tilde{x}_{21}, \tilde{x}_{11}+\tilde{x}_{12}+\tilde{x}_{21}, \tilde{x}_{11}+\tilde{x}_{12}+\tilde{x}_{21}+\tilde{x}_{22})\,,\end{aligned} \tag{5.1.10}$$

where we have used the notation $\tilde{x}$ to remind the reader that these are tropical counterparts to the original polynomials. Each tropically evaluated minor defines distinct regions of piecewise linearity. For example, the regions of piecewise linearity of the tropical minor

$$\tilde{p}_{346} = \min(\tilde{x}_{11}+\tilde{x}_{21}, \tilde{x}_{11}+\tilde{x}_{21}+\tilde{x}_{12}, \tilde{x}_{11}+\tilde{x}_{21}+\tilde{x}_{12}+\tilde{x}_{22})\,, \tag{5.1.11}$$

are separated by the following tropical hypersurfaces,

$$\begin{aligned}\tilde{x}_{12} = 0 \leq \tilde{x}_{22}\,,\\ \text{or } \tilde{x}_{12}+\tilde{x}_{22} = 0 \leq \tilde{x}_{12}\,,\\ \text{or } \tilde{x}_{12}+\tilde{x}_{22} = \tilde{x}_{12} \leq 0\,.\end{aligned} \tag{5.1.12}$$

Note that the tropically evaluated frozen variables are simply linear (instead of piecewise linear) as the frozen minors are expressed as monomials in terms of the $\mathcal{X}$-coordinates. Taking all minors together defines the fan of Speyer and Williams [83]. More precisely, each tropical minor defines a fan via the boundaries of its distinct regions of piecewise linearity. The Speyer-Williams fan is then the common refinement of all the fans defined by the set of tropical minors. The maximal cones of the fan are four-dimensional regions in the $\tilde{x}$ space in which all minors are linear. The intersection of each maximal cone with the unit sphere is a three-dimensional facet of some polyhedral complex. As described in [83] there are 48 facets of which 46 are tetrahedra and 2 are bipyramids. The facets have boundaries where some minor is between two different regions of linearity. Such boundaries are of dimension two and in this case there are 98 of them and they are all triangles. The triangles themselves are bounded by edges of dimension one, with 66 edges in total. The edges are then bounded by points (corresponding to intersections of rays of the fan with the unit sphere). The $\mathrm{Gr}(3,6)$ Speyer-Williams fan has the following 16 rays (with the coordinates ordered as $(\tilde{x}_{11}, \tilde{x}_{21}, \tilde{x}_{12}, \tilde{x}_{22})$),

$$\begin{array}{llll}(1,0,0,0), & (-1,0,0,0), & (1,-1,0,0), & (0,0,1,-1),\\ (0,1,0,0), & (0,-1,0,0), & (1,0,-1,0), & (-1,0,0,1),\\ (0,0,1,0), & (0,0,-1,0), & (1,0,0,-1), & (0,1,1,-1),\\ (0,0,0,1), & (0,0,0,-1), & (0,1,0,-1), & (1,-1,-1,0)\,.\end{array} \tag{5.1.13}$$

In fact one may generalise the above discussion and consider multiple different tropical fans associated to a given Grassmannian. We could consider a fan defined by only a subset

of minors, for example only those minors of the form $\langle i\, i+1\, j\rangle$. Or we could refine the fan further by including tropical evaluations of cluster $\mathcal{A}$-coordinates which are polynomials in minors, as well as the minors themselves. More generally we will define a fan by choosing some subset $\mathcal{S}$ of tropically evaluated $\mathcal{A}$-coordinates and we denote the fan by $F(\mathcal{S})$.

It is important to emphasise that for any given choice of the set $\mathcal{S}$, the resulting fan is finite and in particular has a finite number of rays. One may systematically solve the tropical hypersurface conditions to find all the rays of some fan $F(\mathcal{S})$. In Chapter 4 we described another approach which makes use of the associated cluster algebra. In the case of finite cluster algebras the cluster algebra also defines a fan by means of its **g**-vectors. In fact the **g**-vector fan coincides with the fan obtained by considering $\mathcal{S}$ to be given by the set of all $\mathcal{A}$-coordinates (not just all minors). It is therefore in general a refinement of the Speyer-Williams fan. In the case of $\mathrm{Gr}(2,n)$ the $\mathcal{A}$-coordinates are all minors $\langle ij\rangle$ and the **g**-vector fan coincides with the Speyer-Williams fan.

In the case of $\mathrm{Gr}(3,6)$ we may refine the fan by tropically evaluating also the quadratic $\mathcal{A}$-coordinates (5.1.9),

$$\begin{aligned}\tilde{q}_1 &= \min(\tilde{x}_{11}+\tilde{x}_{12}+\tilde{x}_{21}, \tilde{x}_{11}+\tilde{x}_{12}+\tilde{x}_{21}+\tilde{x}_{22})\,,\\ \tilde{q}_2 &= \min(\tilde{x}_{11}, 2\tilde{x}_{11}, 2\tilde{x}_{11}+\tilde{x}_{12}, 2\tilde{x}_{11}+\tilde{x}_{21}, 2\tilde{x}_{11}+\tilde{x}_{12}+\tilde{x}_{21})\,.\end{aligned} \tag{5.1.14}$$

Alternatively we can make a less refined fan by not considering the minors $\langle 135\rangle$ and $\langle 246\rangle$. One motivation for considering these different fans is that the fan of Speyer and Williams breaks a discrete symmetry of the $\mathrm{Gr}(3,6)$ (or D_4) cluster algebra while both the more refined one and the less refined one manifest it.

As we have seen only unfrozen $\mathcal{A}$-coordinates are relevant in defining the fan since the frozen coordinates are all monomials in the $\mathcal{X}$-coordinates and therefore they do not produce tropical hypersurfaces. The three fans we consider in the context of $\mathrm{Gr}(3,6)$, from least refined to most refined are recorded in Table 5.1 along with their f-vectors. As we will describe in more detail below, the most refined fan (the third in the Table 5.1) is the dual of the D_4 cluster polytope and it is simplicial. For this reason we sometimes refer to it as the 'cluster fan'. The Speyer-Williams fan is not simplicial in that two pairs of tetrahedra from the cluster fan have been combined into bipyramids. The least refined fan then has two more pairs of tetrahedra combined into bipyramids. When two tetrahedra are combined into a bipyramid, the triangle at the interface is removed.

$\mathcal{S}$	f-vector	tetrahedra	bipyramids
$\{\langle i\, i+1\, j\rangle\}$	(16, 66, 96, 46)	42	4
$\{\langle ijk\rangle\}$	(16, 66, 98, 48)	46	2
$\{\langle ijk\rangle\}\cup\{q_1,q_2\}$	(16, 66, 100, 50)	50	0

Table 5.1: Different possible fans for $\mathrm{Gr}(3,6)$ with their f-vectors as well as a characterisation of the dimension two faces.

Another way of encoding all the data listed in Table 5.1 is to split up the f-vectors for

the three fans as follows,

$$\{16_1, 66_2, 96_3, 42_4 + 4_5\},$$
$$\{16_1, 66_2, 98_3, 46_4 + 2_5\},$$
$$\{16_1, 66_2, 100_3, 50_4\}.$$

Here the subscript notation refers to the number of vertices of each component, i.e. the 2_5 in the final entry of the middle vector refers to the two five-vertex bipyramids, while the 46_4 refers to the 46 tetrahedra.

All three fans described above share the same set of 16 rays (and also the same set of 66 edges between rays). As we described in Chapter 4, the rays may be obtained as $\mathbf{g}$-vectors from the associated cluster algebra. Each $\mathbf{g}$-vector is associated to a cluster $\mathcal{A}$-coordinate, which in turn is associated to a codimension one subalgebra and hence a codimension one boundary of the cluster polytope, as mentioned above and in [6]. This implies that the above fans should all be interpreted as duals of polytopes related to the cluster polytope. In the final case (the cluster fan) the corresponding polytope is exactly the D_4 cluster polytope whose codimension one (i.e dimension three) boundary components correspond to the vertices arising from the rays of the fan. The codimension one boundary components are either 14-vertex Stasheff polytopes or 8-vertex cubes. The edges of the fan correspond to intersections of the polytope boundary components and are either 5-vertex pentagons or 4-vertex squares. The triangles of the fan correspond to edges in the polytope and the facets correspond to vertices of the polytope which correspond to individual clusters of the D_4 cluster algebra. The fact that the facets of the cluster fan are all tetrahedra corresponds to the fact that the clusters of the D_4 cluster algebra all have four active nodes.

In Fig. 5.3 we illustrate relevant parts of the cluster fan and its dual D_4 cluster polytope. The left figure shows all sixteen rays but only eight of the tetrahedal facets. The facets shown come in pairs in which the two tetrahedra intersect on a common triangle. The right figure shows the connectivity of the subset of clusters in the D_4 cluster polytope which have the topology of the D_4 Dynkin diagram. Only the four codimension one boundaries with the topology of cubes are therefore shown fully. The cubes are dual to the rays at the four marked corners of the left figure. Each cube is connected to its two neighbours by a single edge, dual to the corresponding shaded triangle in the left figure.

The polytope dual to the Speyer-Williams fan can be obtained from the D_4 cluster polytope by shrinking the two vertical grey edges connecting the cubes in the right half of Figure 5.3 so that two pairs of vertices become six-valent. These then correspond to the two bipyramidal facets of the Speyer-Williams fan. To obtain the polytope dual to the first fan listed in Table 5.1 one should also shrink the two horizontal grey edges connecting corners of distinct cubes. The edges which are shrunk in this procedure therefore do not belong to the cubes but only the Stasheff polytopes and moreover only belong to pentagonal faces, not square faces. When an edge is shrunk the corresponding dual triangle is deleted from the fan and the associated pair of tetrahedra combine into a bipyramid. The triangles that can be removed in this way have a special property: the vertices are all *disconnected* neighbours in the sense discussed in Chapter 2. That is the $\mathcal{A}$-coordinates associated to any pair do appear in clusters together, but never connected by an arrow of the quiver

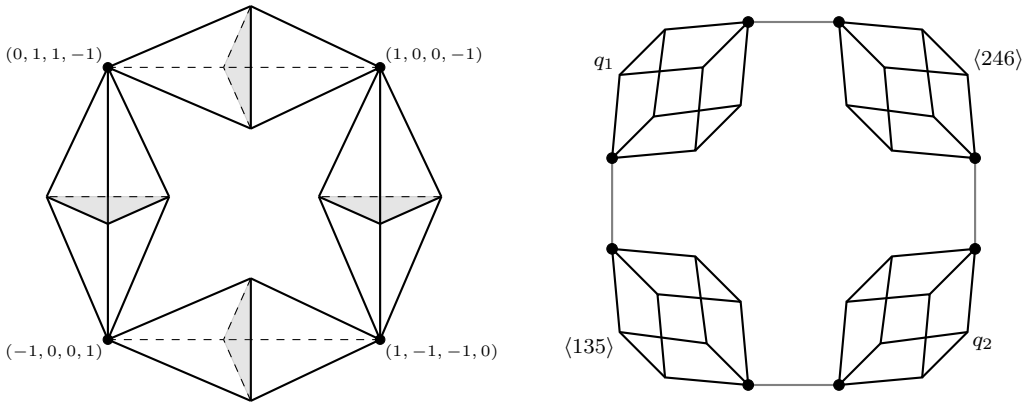

Figure 5.3: Left: a subset of the cluster fan (or more precisely its intersection with the unit sphere) showing eight tetrahedral facets and four highlighted triangles. The highlighted vertices correspond to the four rays given. Right: the subgraph of the D_4 cluster polytope formed by keeping only the clusters whose active nodes are connected in the shape of a D_4 Dynkin diagram. The cubes correspond to the $\mathcal{A}$-coordinates shown and are dual to the four highlighted vertices of the left figure. The grey edges connecting the four cubes are dual to the highlighted triangles of the left figure. The highlighted vertices (clusters) are dual to the eight tetrahedra of the left figure.

diagram.

Finally let us point out that there is also a fan, topologically equivalent to the Speyer-Williams fan, which can be obtained by taking $\mathcal{S}$ to be the set of all $\mathcal{A}$-coordinates, except $\langle 135\rangle$ and $\langle 246\rangle$. The dual polytope to this fan would the simply be obtained from the cluster polytope by shrinking only the horizontal grey edges of Fig. 5.3 and not the vertical ones.

The above statements can also be encoded in the splitting of the f-vectors of the dual polytopes as follows,

$$\{46_1, 96_2, 42_4 + 24_5, 4_8 + 12_{13}\},$$
$$\{48_1, 98_2, 36_4 + 30_5, 4_8 + 6_{13} + 6_{14}\},$$
$$\{50_1, 100_2, 30_4 + 36_5, 4_8 + 12_{14}\}.$$

Here the final line again corresponds to the cluster polytope with the 12_{14} in the final line referring to the twelve Stasheff polytope codimension-one boundaries and the 4_8 the four cubes. After shrinking the first pair of edges we obtain the middle line (dual to the Speyer-Williams fan) where the 50 vertices have become 48, the two shrunk edges are missing leaving only 98 of the original 100, 6 of the 36 pentagons have become squares and 6 of the Stasheff polytopes have been shrunk to 13-vertex objects.

It is clear that the relation between Grassmannian cluster algebras and tropical Grassmannians is really related to a whole family of possible fans and their dual polytopes with the cluster fan being the most refined and the dual of the cluster polytope. The other fans, including that of Speyer and Williams describing the positive part of the tropical Grassmannian are obtained by shrinking edges in the cluster polytope or equivalently removing data from the corresponding tropical fan. As we will see in the next section, this will lead to a generalised set of scattering equations associated to each fan.

We may similarly describe different fans in the case of $\mathrm{Gr}(3,7)$. The fans and their

dual polytopes are harder to picture but we can describe the relevant features by means of the notation introduced above. Let us first introduce a notation for the 42 unfrozen $\mathcal{A}$-coordinates of the Gr(3, 7) cluster algebra which come in six cyclic classes,

$$\begin{aligned} &a_{11} = \langle 347 \rangle, && a_{21} = \langle 134 \rangle, && a_{31} = \langle 156 \rangle, \\ &a_{41} = \langle 257 \rangle, && a_{51} = \langle 12[34]56 \rangle, && a_{61} = \langle 61[23]45 \rangle \,. \end{aligned} \tag{5.1.15}$$

The remaining a_{ij} are obtained by cyclic rotations of the above.[12]

The fans we wish to consider in this case are given by choosing four possibilities for the set $\mathcal{S}$ of $\mathcal{A}$-coordinates as described in Table 5.2. The second fan in Table 5.2 corresponds to the Speyer-Williams fan since the set $\{a_{1i}, a_{2i}, a_{3i}, a_{4i}\}$ corresponds to taking all minors to define the fan. There is one less refined fan where we omit the a_{4i} from $\mathcal{S}$. There are two more refined fans, one where we include also the a_{5i} and a final one where we take all $\mathcal{A}$-coordinates, which we will again refer to as the cluster fan.

Once again the cluster fan ($\{a_{1i}, \ldots, a_{6i}\}$) is simplicial. To obtain the $\{a_{1i}, \ldots, a_{5i}\}$ fan, seven triangles are removed, indicating the presence of seven bipyramids in dimension three. To then obtain the Speyer-Williams fan ($\{a_{1i}, \ldots, a_{4i}\}$) seven edges are removed indicating that seven pairs of triangles combine into squares. The remaining triangles (49 of them) including these missing edges are then removed as well as 21 further triangles which do not involve the removed edges, leaving 1456 triangles and 7 squares in dimension two. To obtain the least refined fan ($\{a_{1i}, \ldots, a_{3i}\}$) one then removes a further 7 edges meaning another seven pairs of triangles combine into squares and another 42 triangles involving the removed edges are lost. In addition a further 21 triangles are removed leaving 1379 triangles and 14 squares in dimension two.

$\mathcal{S}$	f-vector	triangles	squares
$\{a_{1i}, a_{2i}, a_{3i}\}$	(42, 385, 1393, 2373, 1918, 595)	1379	14
$\{a_{1i}, a_{2i}, a_{3i}, a_{4i}\}$	(42, 392, 1463, 2583, 2163, 693)	1456	7
$\{a_{1i}, a_{2i}, a_{3i}, a_{4i}, a_{5i}\}$	(42, 399, 1540, 2821, 2443, 805)	1540	0
$\{a_{1i}, a_{2i}, a_{3i}, a_{4i}, a_{5i}, a_{6i}\}$	(42, 399, 1547, 2856, 2499, 833)	1547	0

Table 5.2: Different possible fans for Gr(3, 7) with their f-vectors as well as a characterisation of the dimension two faces.

Using the same notation introduced in Gr(3, 6) we can compactly include the above information and more into refined f-vectors which split up repsectively as,

$$\begin{aligned} &\{42_1, 385_2, 1379_3 + 14_4, 2240_4 + 133_5, 1659_5 + 196_6 + 63_7, 455_6 + 84_7 + 28_8 + 28_9\}, \\ &\{42_1, 392_2, 1456_3 + 7_4, 2506_4 + 77_5, 1995_5 + 140_6 + 28_7, 595_6 + 63_7 + 28_8 + 7_9\}, \\ &\{42_1, 399_2, 1540_3, 2814_4 + 7_5, 2415_5 + 28_6, 777_6 + 28_7\}, \\ &\{42_1, 399_2, 1547_3, 2856_4, 2499_5, 833_6\}. \end{aligned} \tag{5.1.16}$$

Here we remind the reader that the notation n_m means n faces, each one consisting of m

[12] The notation has been chosen to match existing notation on $\mathcal{A}$-coordinates for Gr(4, 7) which we will study further in Sect. 5.4.

vertices (rays), with the dimension of the face increasing from zero to five as we proceed from left to right along the f-vector.

Also as in the $\mathrm{Gr}(3,6)$ case we can think of all of the fans as being dual to polytopes. The cluster fan is dual to the $\mathrm{Gr}(3,7)$ (or E_6) cluster polytope. The other polytopes are then successively obtained by shrinking edges in this polytope. We can capture a lot of information about the shrinking by splitting the f-vectors of the dual polytopes which are respectively,

$$\begin{aligned}
&\{595_1, 1918_2, 1848_4 + 525_5, 651_8 + 448_{10} + 14_{12} + 252_{13} + 28_{14},\\
&\ 91_{16} + 70_{20} + 7_{25} + 98_{26} + 14_{33} + 42_{34} + 28_{37} + 21_{38} + 14_{46},\\
&\ 7_{32} + 14_{68} + 7_{98} + 14_{138}\},\\
&\{693_1, 2163_2, 1841_4 + 742_5, 525_8 + 574_{10} + 7_{12} + 161_{13} + 196_{14},\\
&\ 42_{16} + 112_{20} + 7_{25} + 49_{26} + 49_{28} + 7_{33} + 7_{34} + 56_{37} + 14_{40} + 28_{42} + 14_{48} + 7_{49},\\
&\ 7_{40} + 14_{74} + 7_{112} + 7_{144} + 7_{170}\},\\
&\{805_1, 2443_2, 1834_4 + 987_5, 406_8 + 658_{10} + 28_{12} + 84_{13} + 364_{14},\\
&\ 7_{16} + 112_{20} + 14_{24} + 21_{25} + 28_{26} + 70_{28} + 56_{40} + 56_{42} + 7_{48} + 14_{49} + 14_{50},\\
&\ 7_{50} + 14_{80} + 7_{128} + 14_{178}\},\\
&\{833_1, 2499_2, 1785_4 + 1071_5, 357_8 + 714_{10} + 476_{14},\\
&\ 119_{20} + 21_{25} + 112_{28} + 112_{42} + 35_{50}, 7_{50} + 14_{84} + 7_{132} + 14_{182}\}.
\end{aligned}$$

As an example of the information captured in the above splittings, we see in the final entry of the final line the codimension one subalgebras of the E_6 polytope: with 7_{50} corresponding to the 7 $A_2 \times A_2 \times A_1$ subalgebras, 14_{84} to the 14 $A_4 \times A_1$, 7_{132} to the 7 A_5 and 14_{182} to the 14 D_5.

In the above computations, the computer package `polymake` [160] was used.

5.2 Generalised scattering equations

In [7] Cachazo, Early, Guevara and Mizera proposed a relation between the tropical Grassmannians $\mathrm{Gr}(k,n)$ and a set of scattering equations which generalise the scattering equations introduced in [79–81] for $\mathrm{Gr}(2,n)$. Here we would like to emphasise the point that there is a set of generalised scattering equations for each choice of tropical fan $F(\mathcal{S})$ described in the previous section, with the equations of [7] corresponding to the Speyer-Williams fans. In the finite cases, the most refined fan (the cluster fan) is associated to the most general set of scattering equations.

Let us first review the scattering equations of [7] before introducing their generalisations. One starts with the potential function

$$F = \sum_{i_1<i_2<\ldots<i_k} s_{i_1 i_2 \ldots i_k} \log\langle i_1 i_2 \ldots i_k\rangle\,. \tag{5.2.1}$$

Here $\langle i_1 i_2 \ldots i_k\rangle$ are minors of the Grassmannian (k,n) matrix which depend on $(k-1)(n-k-1)$ variables[13], and $s_{i_1 i_2 \ldots i_k}$ are generalised Mandelstam variables, totally symmetric

[13]For example by choosing coordinates via the web matrix W defined in (5.1.4).

in their k indices. The generalised Mandelstam variables satisfy generalised momentum conservation relations

$$\sum_{i_2<\ldots<i_k} s_{i_1 i_2 \ldots i_k} = 0, \quad \forall\, i_1. \tag{5.2.2}$$

The generalised momentum conservation relations guarantee the homogeneity of the potential F under the rescalings of the n columns of the $k \times n$ matrix. The scattering equations are then defined to be

$$dF = 0\,. \tag{5.2.3}$$

These equations are to be interpreted as equations for the coordinates parametrising the matrix (e.g. the cluster $\mathcal{X}$ coordinates) in terms of the generalised Mandelstam variables $s_{i_1 \ldots i_k}$. The ϕ^3 amplitude is then evaluated as a localised integral of Parke-Taylor factors (see [7]).

The ϕ^3 amplitude thus obtained can also be identified with the volume of the fan (or its intersection with the unit sphere), which itself can be computed by triangulating and adding the volume of all simplicial facets. This picture generalises the kinematic associahedron picture of [82] which computes the volume of the $\mathrm{Gr}(2, n)$ fan, in which the volume of each facet is simply a tree-level ϕ^3 Feynman diagram. As we stressed in Chapter 4, in the cases where the Grassmannian cluster algebra is finite, the cluster algebra provides a useful way to immediately obtain a triangulation of the Speyer-Williams fan and thus obtain the amplitude as a function of the generalised Mandelstam invariants $s_{i_1 i_2 \ldots i_k}$ via its volume.

Also discussed in Chapter 4 was the fact that we can recover the rays in the positive part of the tropical Grassmannian of Speyer and Sturmfels [145] by simply evaluating all the tropical minors on the rays of the Speyer-Williams fan. Such rays can be expressed in terms of the generalised Mandelstam invariants if we form the scalar product of the vector of generalised Mandelstam invariants with the vector of tropical minors. For example, in the case of $\mathrm{Gr}(3, 6)$ we have

$$(\tilde{x}_{11}, \tilde{x}_{21}, \tilde{x}_{12}, \tilde{x}_{22}) \mapsto \sum s_{i_1 i_2 i_3} \tilde{p}_{i_1 i_2 i_3}(\tilde{x}_{11}, \tilde{x}_{21}, \tilde{x}_{12}, \tilde{x}_{22})\,. \tag{5.2.4}$$

More explicitly, if we take the rays describing the vertices of the bipyramid on the left side of the left figure in Fig. 5.3 and evaluate the quantity (5.2.4) we find

$$\begin{aligned}
(0, 0, 1, 0) &\mapsto t_{1234}\,, \\
(-1, 0, 0, 0) &\mapsto t_{1256}\,, \\
(0, 1, 0, 0) &\mapsto t_{3456}\,, \\
(0, 1, 1, -1) &\mapsto r_{123456}\,, \\
(-1, 0, 0, 1) &\mapsto r_{341256}\,.
\end{aligned} \tag{5.2.5}$$

Here we use the notation

$$\begin{aligned}
t_{ijkl} &= s_{ijk} + s_{ijl} + s_{ikl} + s_{jkl}\,, \\
r_{ijklmn} &= t_{ijkl} + s_{klm} + s_{kln}\,.
\end{aligned} \tag{5.2.6}$$

The full set of sixteen rays becomes the set of s_{123} (and its five cyclic cousins), t_{1234} (and its five cyclic cousins), r_{123456} (and one cyclic cousin), r_{341256} (and one cyclic cousin). The fact that these five rays form a bipyramid is reflected in the fact that the Mandelstam form of the rays obeys

$$t_{1234} + t_{1256} + t_{3456} = r_{123456} + r_{341256} \,. \tag{5.2.7}$$

The reverse map from the kinematic expression to the Speyer-Williams ray consists of tropically evaluating the $\mathcal{X}$-coordinates in terms of minors [83].

The above description corresponds to the choice of the Speyer-Williams fan. To obtain the less refined $\mathrm{Gr}(3,6)$ fan described in Sect. 5.1 we simply set $s_{135} = s_{246} = 0$ in the above discussion. This suggests that there should also be a further generalisation of the scattering equations which corresponds the more refined cluster fan. Indeed we propose a further generalisation of the potential function,

$$F = \sum_{i_1<i_2<i_3} s_{i_1 i_2 i_3} \log\langle i_1 i_2 i_3\rangle + s_{q_1} \log q_1 + s_{q_2} \log q_2 \,. \tag{5.2.8}$$

Here we have added two more terms corresponding to the two quadratic $\mathcal{A}$-coordinates (5.1.9) and introduced new generalised Mandelstam variables s_{q_1} and s_{q_2}. The momentum conservation relation now reads

$$\sum_{i_2<i_3} s_{i_1 i_2 i_3} + s_{q_1} + s_{q_2} = 0, \quad \forall\ i_1. \tag{5.2.9}$$

The relation (5.2.9) again guarantees the homogeneity of the potential function (5.2.8). The scattering equations are the same as in (5.2.3). To return to the system corresponding to the Speyer-Williams fan we simply set $s_{q_1} = s_{q_2} = 0$ in the new system. If we do not set s_{q_1} and s_{q_2} to zero then the expressions for the sixteen rays become modified as follows,

$$\begin{aligned} s_{123} &\mapsto s_{123} \,, \\ t_{1234} &\mapsto t_{1234} + s_{q_1} \,, \\ r_{123456} &\mapsto r_{123456} + s_{q_1} \,, \\ r_{341256} &\mapsto r_{341256} + s_{q_1} \,. \end{aligned} \tag{5.2.10}$$

As before the rays above generated cyclic classes of size six, six, two and two respectively (where $s_{q_1} \to s_{q_2}$ and $s_{q_2} \to s_{q_1}$ under a cyclic transformation).

If we perform the above replacements we see that the relation (5.2.7) will no longer hold since the LHS acquires an additional $3s_{q_1}$ while the RHS only acquires $2s_{q_1}$. This is in accordance with the fact that these five rays no longer form a bipyramid in the cluster fan but rather two tetrahedra separated by a triangle.

We can then form a generalised ϕ^3 amplitude computed from the volume of each facet, just as in the Speyer-Williams case. We obtain a sum over 50 terms (one for each facet - now all tetrahedra) which now depend also on s_{q_1} and s_{q_2}. For example, the two tetrahedra

described above contribute two of the 50 terms:

$$\frac{1}{(t_{1234}+s_{q_1})(t_{1234}+s_{q_1})(t_{1234}+s_{q_1})(r_{123456}+s_{q_1})} + \frac{1}{(t_{1234}+s_{q_1})(t_{1234}+s_{q_1})(t_{1234}+s_{q_1})(r_{341256}+s_{q_1})}\,. \tag{5.2.11}$$

By construction the amplitude obtained this way reduces to the amplitude of [7] upon setting $s_{q_1} = s_{q_2} = 0$. The amplitude described above should be equivalent to the lowest order contribution to the integrals over the stringy canonical forms discussed in [150].

In order to justify the equivalence of the generalised scattering equations and tropical fans beyond the Speyer-Williams case considered in [7], we consider an example. We focus on the cluster fan of $\mathrm{Gr}(3,6)$ and choose the special kinematics where $s_{ijk} = s_{ij} + s_{ik} + s_{jk}$, $s_{i,i+1} = 1$, $s_{i,i+2} = -1$. Analogous kinematics was also considered for the $(2,n)$ case in [81], where it was shown that each term of the amplitude (each Feynman diagram) contributes 1, thus the scattering amplitude equals the number of all possible diagrams which is the Catalan number. In $\mathrm{Gr}(3,6)$ our special kinematics does not have the effect that each of the 50 terms of the amplitude contributes 1, but it does simplify the scattering equations obtained from the potential (5.2.8).

Let us choose coordinates for the (3×6) matrix as follows

$$m_{36} = \begin{pmatrix} 1 & 0 & 0 & 1 & 1 & 1 \\ 0 & 1 & 0 & 1 & x_5 & x_6 \\ 0 & 0 & 1 & 1 & y_5 & y_6 \end{pmatrix}, \tag{5.2.12}$$

with $\langle ijk\rangle$ now being the minors of m_{36}. The scattering equations to be solved are

$$\frac{\partial F}{\partial x_5} = \frac{\partial F}{\partial x_6} = \frac{\partial F}{\partial y_5} = \frac{\partial F}{\partial y_6} = 0\,, \tag{5.2.13}$$

with F given in (5.2.8). For our chosen kinematics, the generalised momentum conservation relations imply $s_{q_1} = -s_{q_2} \equiv t$. The expected amplitude evaluated from adding up the volume of the 50 facets is

$$A_{36} = -\frac{2(3t^4 - 68t^2 + 288)}{(t^2-4)^3}. \tag{5.2.14}$$

Choosing numerical values for t we are able to solve the scattering equations. Generically, we find 8 solutions. Then we consider the sum over the solutions of the scattering equations

$$A_{36} = \sum_{\text{slns}} \frac{1}{\det'\Phi'} \frac{1}{\prod_{i=1}^{6}\langle i\, i+1\, i+2\rangle}, \tag{5.2.15}$$

where

$$\Phi = \begin{pmatrix} \phi_1 & \phi_3 \\ \phi_3^{\mathrm{T}} & \phi_2 \end{pmatrix}, \qquad \phi_1 = \frac{\partial^2 F}{\partial x_a \partial x_b},\ \phi_2 = \frac{\partial^2 F}{\partial y_a \partial y_b},\ \phi_3 = \frac{\partial^2 F}{\partial x_a \partial y_b}, \tag{5.2.16}$$

and Φ' the matrix Φ after the removal of rows and columns 1,2,3,4,7,8,9,10. Explicitly

$$\det'\Phi' = \frac{\det\Phi'}{(\langle 123\rangle\langle 234\rangle\langle 341\rangle\langle 412\rangle)^2}. \tag{5.2.17}$$

We have solved the scattering equations for various values of t and found agreement with

the expected answer.

The extension of the generalised ϕ^3 amplitude to more refined fans clearly also generalises to higher $\mathrm{Gr}(k,n)$. For $\mathrm{Gr}(3,7)$ one can introduce a new set of Mandelstam variables $s_{q_{5i}}$ corresponding to the a_5-type quadratic $\mathcal{A}$-coordinates and also $s_{q_{6i}}$ for the a_6 type. The potential F now reads

$$F = \sum_{i<j<k} s_{ijk} \log\langle ijk\rangle + \left[(s_{q_{51}}\langle 23[45]67\rangle + s_{q_{61}}\langle 56[72]34\rangle) + \text{cyc.}\right]. \tag{5.2.18}$$

The generalised momentum conservation relation reads,

$$\sum_{j<k} s_{ijk} + \sum_{j\neq i}(s_{q_{5j}} + s_{q_{6j}}) = 0\,. \tag{5.2.19}$$

The above system corresponds to the $\{a_{1i},\ldots,a_{6i}\}$ fan described in Sect. 5.1. To obtain the $\{a_{1i},\ldots,a_{5i}\}$ fan one simply imposes $s_{q_{6i}} = 0$. To obtain the Speyer-Williams fan one imposes also $s_{q_{5i}} = 0$. To then obtain the $\{a_{1i},\ldots,a_{3i}\}$ fan one imposes further that $s_{135} = 0$ and the cyclically related relations.

One can similarly make a generalisation of the scattering equations corresponding to the $\mathrm{Gr}(3,8)$ cluster fan (or E_8 cluster fan). To do so one needs new Mandelstam variables corresponding to the quadratic and cubic $\mathcal{A}$-coordinates. We will return to this case later. For $k = 3$ and $n > 8$ there does not exist an analogue of the cluster fan but there are certainly fans which are more refined than the Speyer-Williams fans which therefore introduce new Mandelstam variables beyond the $s_{i_1\ldots i_k}$.

5.3 Cluster polytopes and face variables

The cluster polytopes can be defined in terms of face variables. We discussed such variables in Chapter 3 and they have also been discussed in many recent papers [150, 152] and generalise the dihedral coordinates of $\mathrm{Gr}(2,n)$ (see e.g. [28]) to more general cluster polytopes. Face variables have the property that they are valued between 0 and 1 in the positive region (which is also the region where all cluster $\mathcal{X}$-coordinates are positive. Each codimension one boundary a of the cluster polytope has an associated face variable u_a and $u_a = 0$ defines the boundary. Furthermore on every other codimension one boundary b that does not intersect the defining boundary a the variables u_a takes the value 1.

In Chapter 3, a method to systematically construct the face variables from a cluster quiver diagram was described and given explicitly in the E_6 (or $\mathrm{Gr}(3,7)$) case. First, one has to find a Dynkin diagram shaped quiver. There are many quivers of this shape. In figure (5.4a) we show an example from the $\mathrm{Gr}(3,7)$ case. If we denote by x_i the $\mathcal{X}$-coordinates in node i of the quiver, then the corresponding u-coordinates take the form

$$u_i = \frac{x_i f_i}{1 + x_i f_i}, \tag{5.3.1}$$

where

$$f_1 = 1, \quad f_2 = 1 + x_1, \quad f_3 = f_4 = 1 + x_2(1 + x_1),$$
$$f_5 = 1 + x_3(1 + x_2(1 + x_1)), \quad f_6 = 1 + x_4(1 + x_2(1 + x_1)).$$

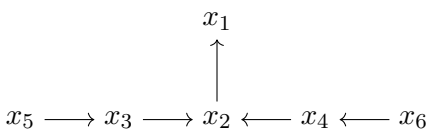

(a) Dynkin diagram shaped quiver in $\mathrm{Gr}(3,7)$.

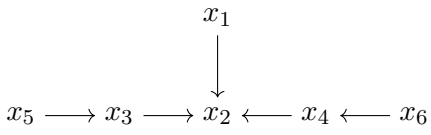

(b) Tree shaped quiver.

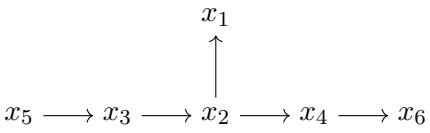

(c) Quiver with bifurcations.

Figure 5.4: Examples of cluster quivers.

In fact, we can generalise the method described in Chapter 3 to include any tree shaped cluster. Then, the u-coordinate of node i can be found by following the path of the arrow that starts from node i and follow the recursive formula $f_i = 1 + x_j f_j$, where j is the first node we land by following the path of the arrow. As an example, we have for figure (5.4b)

$$f_1 = f_3 = f_4 = 1 + x_2, \quad f_2 = 1, \quad f_5 = 1 + x_3(1 + x_2), \quad f_6 = 1 + x_4(1 + x_2).$$

When there is a bifurcation we consider the product of paths. For example, for figure (5.4c) we have

$$f_1 = f_6 = 1, \quad f_2 = (1 + x_1)(1 + x_4(1 + x_6)), \quad f_4 = 1 + x_6,$$
$$f_3 = 1 + x_2(1 + x_1)(1 + x_4(1 + x_6)), \quad f_5 = 1 + x_3(1 + x_2(1 + x_1)(1 + x_4(1 + x_6))).$$

The method is valid when the quiver contains loops, if the chosen node does not contain any path that forms a loop.

We would now like to outline a different method for finding the face variables which is more directly related to the tropical fans and their associated scattering equations discussed in the preceding sections. Let us recall that the general form for the potential function is

$$F = \sum_a s_a \log a \,, \tag{5.3.2}$$

where we have used a very compact notation, with the sum being over all the $\mathcal{A}$-coordinates a of the cluster algebra (including the frozen ones) and s_a the corresponding generalised Mandelstam variable. For the minors $\langle i_1 \dots i_k \rangle$ the associated Mandelstams are the $s_{i_1 \dots i_k}$ but the s_a also include the Mandelstams associated to e.g. the quadratic $\mathcal{A}$-coordinates (5.1.9).

We claim that the potential can also be written

$$F = \sum_a v_a \log u_a \,, \tag{5.3.3}$$

where the sum is over only the *unfrozen* $\mathcal{A}$-coordinates a, v_a is the ray (evaluated in

terms of Mandelstam variables) and u_a is the corresponding face variable. Note that, due to the generalised momentum conservation relations, (5.3.2) is homogeneous, even if each term individually is not. The expression (5.3.3) is manifestly homogeneous since the u_a are homogeneous combinations of $\mathcal{A}$-coordinates. Once one has solved the tropical problem and found the rays, equating (5.3.2) and (5.3.3) gives a simple linear system to solve for the $\log u_a$ in terms of the $\log a$. The solution is exactly the face variables. Thus the tropical geometry provides a simple map from $\mathcal{A}$-coordinates to face variables. The method described above is closely related to the discussion of face variables in [150] based on Minkowski sums of Newton polytopes arising from considering generalisations of string worldsheet integrals to $\mathrm{Gr}(k,n)$.

5.3.1 $\mathrm{Gr}(3,6)$

As described above, the $\mathrm{Gr}(3,6)$ cluster fan consists of 16 rays which are divided into four cyclic classes of size 6,6,2 and 2. Written in terms of generalised Mandelstam invariants, the generators of these four classes are

$$\{v_a\} = \{s_{123}, t_{1234} + s_{q_1}, r_{341256} + s_{q_1}, r_{123456} + s_{q_1}\}. \tag{5.3.4}$$

For each of the 16 rays v_a we can associate the $\mathcal{A}$-coordinate a, which can be found from mutations as described in Chapter 4. For the rays in (5.3.4) we associate

$$\{\langle 124\rangle, \langle 125\rangle, \langle 135\rangle, \langle 12[34]56\rangle\}, \tag{5.3.5}$$

where we recall $\langle 12[34]56\rangle \equiv \langle 124\rangle \langle 356\rangle - \langle 123\rangle \langle 456\rangle$.

In addition, to each ray v_a we can associate the face variable u_a. As described above we may derive them from the equality of the two ways of writing the potential F in (5.2.8),

$$\sum_{i<j<k} s_{ijk} \log\langle ijk\rangle + \sum_{i=1}^{2} s_{q_i} \log q_i = \sum_a v_a \log u_a \,. \tag{5.3.6}$$

All 22 $\mathcal{A}$-coordinates appear in (5.3.6), including the frozen ones, however the generalised momentum conservation relations (5.2.9) imply the LHS can be written as a combination of 16 homogeneous combinations of $\mathcal{A}$-coordinates. Equation (5.3.6) therefore reduces to a linear system for of the 16 unknowns $\log u_a$ with a unique solution. For the rays in (5.3.4) we find the corresponding u-coordinates,

$$\left\{ \frac{\langle 123\rangle \langle 246\rangle}{\langle 124\rangle \langle 236\rangle}, \frac{\langle 12[34]56\rangle}{\langle 125\rangle \langle 346\rangle}, \frac{\langle 125\rangle \langle 134\rangle \langle 356\rangle}{\langle 135\rangle \langle 12[34]56\rangle}, \frac{\langle 124\rangle \langle 256\rangle \langle 346\rangle}{\langle 246\rangle \langle 12[34]56\rangle} \right\}, \tag{5.3.7}$$

in agreement with the restriction of the E_6 u-coordinates described in Chapter 3 to D_4 and also in agreement with the u-coordinates given in [150]. We observe that the $\mathcal{A}$-coordinates appear in the denominators of the corresponding u-coordinates.

Labelling the 16 u-coordinates generated by the cyclic classes of (5.3.7) as $\{u_1, \ldots, u_6\}$,

$\{u_7, \ldots, u_{12}\}$, $\{u_{13}, u_{14}\}$ and $\{u_{15}, u_{16}\}$, we find that they satisfy the identities

$$\begin{aligned} 1 &= u_1 + u_2u_6u_8u_{11}u_{13}u_{16} \\ &= u_7 + u_3u_6u_8u_{12}u_{14}u_{16} \\ &= u_{13} + u_1u_3u_5u_8u_{10}u_{12}u_{14}^2u_{15}u_{16} \\ &= u_{15} + u_2u_4u_6u_8u_{10}u_{12}u_{13}u_{14}u_{16}^2\,, \end{aligned} \tag{5.3.8}$$

which respect the boundary structure of the cluster polytope.

5.3.2 Gr(3, 7)

The Gr(3, 7) cluster fan posesses 42 rays, divided into 6 cyclic classes, each of size 7. Written in terms of Mandelstam variables introduced in (5.2.18) the classes are generated by

$$\begin{aligned} &s_{123}, \\ &t_{1234} + s_{q_{55}} + s_{q_{66}} + s_{q_{57}}, \\ &t_{1234567} + s_{q_{53}} + s_{q_{64}} + s_{q_{55}} + s_{q_{66}} + s_{q_{57}}, \\ &t_{1234567} + s_{134} + s_{234} + s_{q_{53}} + s_{q_{64}} + s_{q_{55}} + s_{q_{66}} + s_{q_{57}}, \\ &t_{1234567} + s_{167} + s_{267} + s_{q_{53}} + s_{q_{64}} + s_{q_{55}} + s_{q_{66}} + s_{q_{57}}, \\ &t_{1234} + t_{1267} + s_{125} + s_{q_{53}} + s_{q_{64}} + 2s_{q_{55}} + s_{q_{66}} + s_{q_{57}}\,, \end{aligned} \tag{5.3.9}$$

where $t_{1234567} = s_{123} + s_{124} + s_{125} + s_{126} + s_{127}$. Setting the $s_{q_{5i}}$ and $s_{q_{6i}}$ to zero in the above we recover the form of the rays given in Chapter 4 and [7]. The corresponding $\mathcal{A}$-coordinates are

$$\{\langle 124\rangle\,, \langle 125\rangle\,, \langle 134\rangle\,, \langle 135\rangle\,, \langle 12[34]67\rangle\,, \langle 12[35]67\rangle\}. \tag{5.3.10}$$

The equality of the two forms of the potential (5.3.2) and (5.3.3) becomes

$$\begin{aligned} &\sum_{i<j<k} s_{ijk} \log\langle ijk\rangle + \left[(s_{q_{51}} \log\langle 23[45]67\rangle + s_{q_{61}} \log\langle 56[72]34\rangle) + \text{cyc.}\right] \\ &= \sum_a v_a \log u_a\,. \end{aligned} \tag{5.3.11}$$

Due to the generalised momentum conservation relation (5.2.19) both sides are homogeneous and we obtain a linear system for the $\log u_a$. They are found to be

$$\begin{aligned} \Bigg\{ &\frac{\langle 123\rangle\langle 247\rangle}{\langle 124\rangle\langle 237\rangle}, \frac{\langle 12[34]57\rangle}{\langle 125\rangle\langle 347\rangle}, \frac{\langle 12[34]67\rangle}{\langle 134\rangle\langle 267\rangle}, \frac{\langle 134\rangle\langle 12[35]67\rangle}{\langle 135\rangle\langle 12[34]67\rangle}, \\ &\frac{\langle 267\rangle\langle 12[34]57\rangle}{\langle 257\rangle\langle 12[34]67\rangle}, \frac{\langle 125\rangle\langle 357\rangle\langle 12[34]67\rangle}{\langle 12[35]67\rangle\langle 12[34]57\rangle} \Bigg\}, \end{aligned} \tag{5.3.12}$$

in agreement with the u-coordinates found in Chapter 3. As in the Gr(3, 6) case, the $\mathcal{A}$-coordinates appear in the denominators of the corresponding u-coordinates.

The 42 u-coordinates of (5.3.12) obey the cluster connectivity and satisfy the identities

$$\begin{aligned}
1 &= u_1 + u_2u_7u_9u_{13}u_{17}u_{21}u_{22}u_{24}u_{27}u_{30}u_{32}u_{35}u_{36}u_{37}u_{39}u_{41} \\
&= u_8 + u_3u_7u_9u_{10}u_{13}u_{14}u_{18}u_{21}u_{23}u_{25}u_{27}u_{28}u_{30}u_{32}u_{33}u_{35}u_{37}^2u_{39}u_{40}u_{41}u_{42} \\
&= u_{15} + u_2u_6u_9u_{12}u_{16}u_{21}u_{23}u_{26}u_{28}u_{30}u_{32}u_{35}u_{37}u_{39}u_{40}u_{42} \\
&= u_{22} + u_1u_3u_6u_9u_{10}u_{12}u_{14}u_{16}u_{18}u_{21}u_{23}^2u_{25}u_{26}u_{28}^2u_{29}u_{30}u_{31}u_{32}u_{33}u_{35}u_{37}^2u_{38}u_{39}u_{40}^2u_{42}^2 \\
&= u_{29} + u_2u_5u_7u_9u_{11}u_{12}u_{14}u_{16}u_{19}u_{21}u_{22}u_{23}u_{25}u_{26}u_{27}u_{28}u_{30}^2u_{32}u_{33}u_{35}^2u_{37}^2u_{39}^2u_{40}u_{41}u_{42}^2 \\
&= u_{36} + u_1u_3u_5u_7u_9u_{10}u_{11}u_{12}u_{14}^2u_{16}u_{18}u_{19}u_{21}u_{23}^2u_{25}^2u_{26}u_{27}u_{28}^2u_{30}^2u_{31}u_{32}u_{33}^2u_{35}^2u_{37}^3u_{38} \\
&\qquad \times u_{39}^2u_{40}^2u_{41}u_{42}^3.
\end{aligned} \tag{5.3.13}$$

Powers of 3 appear for the first time.

5.3.3 Gr(3, 8)

The Gr(3, 8) cluster fan consists of 128 rays divided into 16 cyclic classes of size 8. Explicitly, in terms of the $\tilde{x}$ variables, the 128 rays (or g-vectors) are

$$\begin{aligned}
g_1 &= (1,0,0,0,0,0,0,0), & g_9 &= (0,0,1,0,0,0,0,0), \\
g_{17} &= (0,0,0,0,1,0,0,0), & g_{25} &= (0,1,0,0,0,0,0,0), \\
g_{33} &= (-1,0,0,1,0,0,0,0), & g_{41} &= (0,0,-1,0,0,1,0,0), \\
g_{49} &= (0,1,1,-1,0,0,0,0), & g_{57} &= (0,1,1,0,0,-1,0,0), \\
g_{65} &= (0,1,1,0,0,0,0,-1), & g_{73} &= (0,1,0,0,1,-1,0,0), \\
g_{81} &= (0,1,0,0,1,0,0,-1), & g_{89} &= (-1,0,0,1,1,-1,0,0), \\
g_{97} &= (-1,0,0,1,1,0,0,-1), & g_{105} &= (0,1,0,1,1,-1,0,-1), \\
g_{113} &= (-1,0,0,2,1,-1,0,-1), & g_{121} &= (-1,1,0,1,1,-1,0,-1)
\end{aligned} \tag{5.3.14}$$

and their cyclic rotations in the Mandelstam space. We recall that it is straightforward to map any g-vector to the Mandelstam space by evaluating all the $\mathcal{A}$-coordinates as tropical polynomials. The list of all 128 vertices in the Mandelstam space corresponding to the Speyer-Williams fan was given in Chapter 4. In fact, if we only include the s_{ijk} Mandelstam variables, eight of the vectors are redundant in that they are not true vertices of the fan. By extending the kinematics to include also 80 generalised Mandelstam variables corresponding to the 56 quadratic and 24 cubic $\mathcal{A}$-coordinates, we obtain the 128 rays of the cluster fan with no redundancies. The expressions are cumbersome so we omit them here.

The $\mathcal{A}$-coordinates are generated by cyclic rotations of the following,

$$\begin{aligned}
&\{\langle 124\rangle, \langle 125\rangle, \langle 126\rangle, \langle 134\rangle, \langle 135\rangle, \langle 136\rangle, \\
&\quad \langle 12[34]56\rangle, \langle 12[34]57\rangle, \langle 12[34]58\rangle, \langle 12[34]67\rangle, \langle 12[34]68\rangle, \langle 12[35]67\rangle, \langle 12[35]68\rangle, \\
&\quad \langle 12[34]8[67]45\rangle, \langle 12[35]8[67]45\rangle, \langle 12[34]8[67]35\rangle\},
\end{aligned} \tag{5.3.15}$$

where in the final line we have defined the cubic coordinates via

$$\begin{aligned}
\langle 12[34]5[67]89\rangle &\equiv \langle 124\rangle\langle 35[67]89\rangle - \langle 123\rangle\langle 45[67]89\rangle \\
&= \langle 12[34]57\rangle\langle 689\rangle - \langle 12[34]56\rangle\langle 789\rangle = -\langle 67[89]5[12]34\rangle.
\end{aligned} \tag{5.3.16}$$

In each of the 24 cubic $\mathcal{A}$-coordinates 7 indices appear once and 1 index appears twice. Denoting the quadratic $\mathcal{A}$-coordinates by q and the cubic ones by c, the generalised momentum conservation reads schematically

$$\sum_{j<k} s_{ijk} + \sum_{q|i\in q} s_q + \sum_{c|i\in c} s_c + 2\sum_{c|i^2\in c} s_c = 0\,, \qquad i = 1,\ldots,8\,, \tag{5.3.17}$$

where the factor of two in the final term accounts for the double appearance of i in the associated cubic coordinate.

As above we determine the u-coordinates from the equality of the two forms of the potential,

$$\sum_{i<j<k} s_{ijk}\log\langle ijk\rangle + \sum_q s_q\,\log q + \sum_c s_c\,\log c = \sum_a v_a \log u_a\,. \tag{5.3.18}$$

The u-coordinates are found to be

$$\left\{\begin{array}{l}
\frac{\langle 123\rangle\langle 248\rangle}{\langle 124\rangle\langle 238\rangle}, \frac{\langle 12[34]58\rangle}{\langle 125\rangle\langle 348\rangle}, \frac{\langle 12[45]68\rangle}{\langle 126\rangle\langle 458\rangle}, \frac{\langle 12[34]78\rangle}{\langle 134\rangle\langle 278\rangle}, \frac{\langle 134\rangle\langle 12[35]78\rangle}{\langle 135\rangle\langle 12[34]78\rangle}, \frac{\langle 13[45]6[78]12\rangle}{\langle 136\rangle\langle 12[45]78\rangle},\\
\frac{\langle 124\rangle\langle 34[56]28\rangle}{\langle 248\rangle\langle 12[56]34\rangle}, \frac{\langle 12[56]34\rangle\langle 34[57]28\rangle}{\langle 12[57]34\rangle\langle 34[56]28\rangle}, \frac{\langle 348\rangle\langle 12[34]5[67]82\rangle}{\langle 12[58]34\rangle\langle 34[67]28\rangle}, \frac{\langle 12[34]5[67]82\rangle}{\langle 258\rangle\langle 12[34]67\rangle},\\
\frac{\langle 268\rangle\langle 12[34]8[67]45\rangle}{\langle 12[68]34\rangle\langle 45[67]28\rangle}, \frac{\langle 125\rangle\langle 12[34]8[35]67\rangle}{\langle 12[34]58\rangle\langle 12[67]35\rangle}, \frac{\langle 12[68]34\rangle\langle 12[35]8[67]45\rangle}{\langle 12[68]35\rangle\langle 12[34]8[67]45\rangle},\\
\frac{\langle 45[67]28\rangle\langle 12[34]8[67]35\rangle}{\langle 35[67]28\rangle\langle 12[34]8[67]45\rangle}, \frac{\langle 358\rangle\langle 12[35]67\rangle\langle 12[34]8[67]45\rangle}{\langle 12[34]8[67]35\rangle\langle 12[35]8[67]45\rangle},\\
\frac{\langle 12[34]67\rangle\langle 35[67]82\rangle\langle 12[34]58\rangle}{\langle 12[34]5[67]82\rangle\langle 12[34]8[67]35\rangle}
\end{array}\right\} \tag{5.3.19}$$

and satisfy identities reflecting the cluster connectivity. The highest power appearing in the identities is 6.

In the generalised ϕ^3 amplitude corresponding to the Speyer-Williams fan, the last 8 g-vectors in (5.3.14) correspond to spurious poles. The facets containing them always combine together into bigger facets without them. When we introduce the generalised Mandelstam variables for each $\mathcal{A}$-coordinate (not just the minors) then this is no longer the case. The fan is simplicial and every vertex contributes on an equal footing. In the interpretation where the volume of each facet is thought of as a generalised Feynman diagram, each diagram now has the same number of poles.

It is possible to define u-coordinates for the polytope dual to the Speyer-Williams fan formed from only the first 120 g-vectors. Only 16 of the u-coordinates are affected. These are $u^{(120)}_{57} = u^{(128)}_{57}u^{(128)}_{121}$ and $u^{(120)}_{65} = u^{(128)}_{65}u^{(128)}_{125}$ and their cyclic rotations. Then the corresponding u-identities obey the connectivity of the resulting polytope after the removal of the last 8 g-vectors.

5.4 Tropically adjacent polylogarithms

The notion of cluster adjacency gives rise to an interesting class of polylogarithmic functions, associated to a given cluster algebra. Here we would like to generalise this notion to different possible choices of fan $F(\mathcal{S})$. The cluster adjacent polylogs in the sense

of [8] will correspond to the cluster fans. Those corresponding to less refined fans will obey additional constraints beyond the fact that adjacent pairs of letters must appear together in a cluster.

In Section 5.1 we discussed different tropical fans related to $\mathrm{Gr}(3,7) \cong \mathrm{Gr}(4,7)$, generated by different sets of tropical $\mathcal{A}$-coordinates. Here we will discuss this further and the implications these different fans have for cluster adjacency and scattering amplitudes in SYM.

Edges

If two rays are connected by an edge in the cluster fan this means their corresponding $\mathcal{A}$-coordinates appear together in a cluster in the cluster algebra and hence are cluster adjacent. The $\{a_1, \ldots, a_6\}$ fan in Table 5.2 is the most refined fan one could construct and is dual to the $\mathrm{Gr}(4,7)$ cluster polytope. This fan consists of 399 edges which correspond to all of the cluster adjacent pairs of different $\mathcal{A}$-coordinates. The $\{a_1, \ldots, a_5\}$ fan also contains all 399 edges and so offers no alteration to cluster adjacency at the level of edges. However, we will see that this fan does differ from the cluster fan at the level of triangles. The $\{a_1, \ldots, a_4\}$ fan also called the Speyer-Williams (SW) fan was the original tropical fan for $\mathrm{Gr}(3,7)$ discussed in [83]. This fan has 392 edges and is the first instance where we have a differing number of edges from that of the cluster fan as this fan has 392 edges. The $\{a_1, \ldots, a_3\}$ fan has 385 edges, 14 fewer than the cluster fan. These 14 edges correspond to the pairs

$$\{a_{21}, a_{64}\} \quad + \quad \text{dihedral} \tag{5.4.1}$$

which are the pairs observed to be missing from certain integrals and MHV amplitudes in Chapter 2. We note that the missing pairs are neighbours of 'disconnected' type in the language of Chapter 2. This can be seen in Table 2.1 in the row labelled by a_{21} and the fourth column in the a_{6i} block where the symbol $\bullet$ appears. That is, they appear together in the same cluster, but never connected by an arrow. As noted in Chapter 2, this has the consequence that, if the pair were to appear consecutively in a symbol, the integrability conditions would impose that they do so in a symmetric way. In other words, the corresponding weight-two function is simply a product of logarithms, $\log a_{21} \log a_{64}$. Therefore there is no distinction between the ordering shown in (5.4.1) and the reverse.

Triangles

Much like with edges mentioned above, if three rays are all connected to each other to form a triangle in the cluster fan then all three corresponding $\mathcal{A}$-coordinates can be found in a cluster together and hence are cluster adjacent. When considering the less refined fans, if we find that an edge is missing it follows that any triangles containing that edge are also missing. However, it is also possible for further triangles to be absent, even if all three edges of the triangle are still present. We have seen this phenomenon in the $\mathrm{Gr}(3,6)$ example discussed in Sect. 5.1. When any pair of connected tetrahedra in Fig. 5.3 becomes a bipyramid, the triangle at the interface is removed. The same phenomenon can happen in the $\mathrm{Gr}(3,7) \cong \mathrm{Gr}(4,7)$ case.

The cluster fan contains 1547 triangles but the $\{a_1, \ldots, a_5\}$ fan only has 1540 triangles,

7 fewer than the cluster fan. These missing triangles are

$$\{a_{11}, a_{41}, a_{51}\} \quad + \quad \text{cyclic.} \tag{5.4.2}$$

As mentioned above the $\{a_1, \ldots, a_3\}$ fan has 14 fewer edges than the cluster fan. These edges appear in $(8 \times 14) + 7 = 119$ triangles, corresponding to 8 triangles and their dihedral copies along with 7 triangles which contain 2 of the 14 missing edges. The other missing triangles are

$$\{a_{22}, a_{24}, a_{16}\} \quad + \quad \text{dihedral}\,, \tag{5.4.3}$$

$$\{a_{21}, a_{13}, a_{53}\} \quad + \quad \text{dihedral} \quad + \quad \text{parity}\,. \tag{5.4.4}$$

The triangles (5.4.2), (5.4.3) and (5.4.4) are fully disconnected in the sense that all three edges correspond to disconnected neighbours. For example, we see in Table 2.1 the symbol ● corresponding to the pairs $\{a_{11}, a_{41}\}$, $\{a_{11}, a_{51}\}$ and $\{a_{41}, a_{51}\}$. There are a total of 70 disconnected triangles in the cluster fan, 56 of which are missing from the $\{a_1, \ldots, a_3\}$ fan (the 49 in (5.4.2), (5.4.3) and (5.4.4) and the 7 which contain two missing edges of the form (5.4.1)). The remaining 14 disconnected triangles are of the form

$$\{a_{11}, a_{24}, a_{33}\} \quad + \quad \text{dihedral} \tag{5.4.5}$$

and these ones are *present* in the $\{a_1, \ldots, a_3\}$ fan.

Comparison to amplitudes

The variation in the number of edges and triangles in the above fans is interesting in the context of $\mathcal{N} = 4$ SYM loop amplitudes. At the level of edges all currently known MHV heptagon amplitudes are consistent with the edges from the $\{a_1, \ldots, a_3\}$ fan. The NMHV heptagon amplitude at four loops discussed above requires all 399 pairs (edges) [153] and so is consistent with either the $\{a_1, \ldots, a_5\}$ fan or the $\{a_1, \ldots, a_6\}$ fan.

We have also observed that the triangles missing from the $\{a_1, \ldots, a_3\}$ fan are also missing from all available MHV and NMHV amplitudes. Thus at the level of triangles there is no distinction between the currently known MHV and NMHV amplitudes, though, as we have stated above, there is at the level of edges. The disconnected triangles (5.4.5) which are present in the $\{a_1, \ldots, a_3\}$ fan *do* appear as consecutive triples of letters in known MHV and NMHV amplitudes.

The cluster adjacency conditions in heptagon functions seem to follow from the extended Steinmann conditions [70] and the physical initial entry condition (and integrability of the symbol), at least up to weight seven. It is interesting to note therefore that the conditions obtained by imposing the absence of the triples (5.4.2), (5.4.3) and (5.4.4) do not follow only from physical initial entry conditions and cluster adjacency, there being examples of functions in weight seven which do have the missing triangles in their symbols. Therefore, forbidding above the triangles is an extra condition that goes beyond cluster adjacency.

In summary, the known seven-point MHV amplitudes in planar $\mathcal{N} = 4$ SYM are consistent with the structure of the $\{a_1, \ldots, a_3\}$ tropical fan although there is limited data to verify this. One potential test would be to bootstrap the five-loop, MHV heptagon using

the restrictions following from the $\{a_1, \ldots, a_3\}$ and investigate whether a solution could be found. For NMHV seven-point amplitudes, the edge structure suggests that the minimal fan compatible with their singularities would be the $\{a_1, \ldots, a_5\}$ fan. This fan has all possible edges but seven missing triangles. It would be interesting to investigate whether such triangles indeed continue to be absent at higher orders.

Beyond seven points the $\mathrm{Gr}(4, n)$ cluster algebras become infinite. For $n = 8$ this infinity is of affine type and we will consider tropical fans in this case in the next chapter.

Chapter 6

Infinite to Finite and Algebraic Singularities

Although the original connection to cluster algebras was inspired by the all-multiplicity result for two-loop MHV amplitudes in [120], it has been clear for some time that additional ingredients are needed when going beyond seven points. In the first instance the cluster algebras are finite type only for $\mathrm{Gr}(4,6)$ and $\mathrm{Gr}(4,7)$. For $\mathrm{Gr}(4,8)$ and beyond there are infinitely many cluster $\mathcal{A}$-coordinates, so some truncation to a finite set needs to be specified, as happens for the two-loop MHV amplitudes. Moreover at eight points and beyond there is an additional problem which is present already at one loop for N^2MHV amplitudes. Four-mass box configurations appear which have letters which are not rational when expressed in terms of the Plücker coordinates for the Grassmannian spaces (i.e. in terms of momentum twistors [99]). Algebraic letters were also predicted for the two-loop NMHV amplitude [161, 162] by means of a Landau analysis (as initiated in this context in [163]) of the integrand provided by the amplituhedron [24, 164]. Letters containing square roots appear in the eight-point integrals considered in [132, 165]. Recently, a two-loop NMHV calculation [166] based on solving the $\overline{Q}$-equation of [121, 133] for the dual octagonal (super) Wilson loop [50–52, 97, 98] has revealed a specific set of 18 multiplicatively independent algebraic letters in addition to 180 rational ones. In this chapter we propose that an answer to both problems may be provided by tropical geometry.

6.1 Review of positive tropical $\mathrm{Gr}(4,8)$

Following the methods described by Speyer and Williams [83], in Chapter 4 we initiated a study of the fan describing the positive part of the tropical Grassmannian $\mathrm{Gr}(4,8)$. Here we will describe further features of the positive tropical Grassmannian $\mathrm{Gr}(4,8)$ which lead to the emergence of non-rational letters. Specifically, the $\mathrm{Gr}(4,8)$ cluster algebra is not finite, but of affine type $E_7^{(1,1)}$ [167]. This feature means that although the algebra is infinite, the infinity is controlled in a particular way and it makes $\mathrm{Gr}(4,8)$ a very natural example to consider in going beyond the finite cases. The affine nature of the cluster algebra leads us to natural infinite sequences of clusters which play a role in fully defining the Speyer-Williams fan (and related fans). Remarkably, the simplest infinite sequences

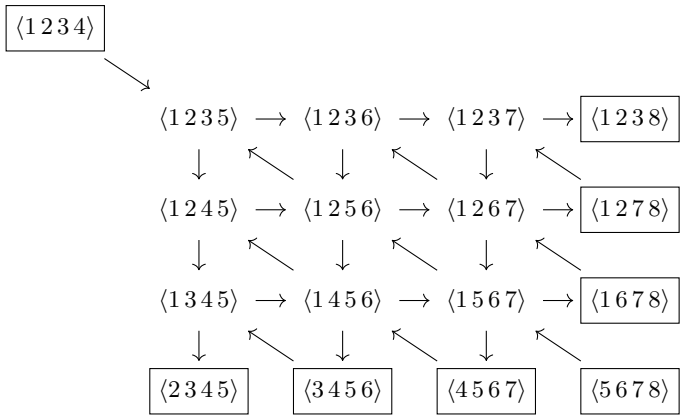

Figure 6.1: The initial cluster of the Grassmannian cluster algebra $\mathrm{Gr}(4,8)$.

lead to *exactly* the set of non-rational letters recently discovered in the two-loop eight-point NMHV amplitude [166].

A general introduction to cluster algebras is given in Chapter 2 but here we will describe the $\mathrm{Gr}(4,8)$ cluster algebra explicitly. The $\mathrm{Gr}(4,8)$ cluster algebra has an initial cluster of the form shown in Fig. 6.1 with $\mathcal{A}$-coordinates given by Plücker variables $\langle ijkl\rangle$. It has nine active nodes a_i (labelled $1,\ldots,9$ from the top left and descending column by column) and eight frozen nodes f_i indicated by boxes making 17 nodes in total,

$$\begin{aligned}\{a_1,...,a_9\} &= \{\langle 1235\rangle,\langle 1245\rangle,\langle 1345\rangle,\langle 1236\rangle,\langle 1256\rangle,\langle 1456\rangle,\langle 1237\rangle,\langle 1267\rangle,\langle 1567\rangle\},\\ \{f_1,...,f_8\} &= \{\langle 1234\rangle,\langle 2345\rangle,\langle 3456\rangle,\langle 4567\rangle,\langle 5678\rangle,\langle 1678\rangle,\langle 1278\rangle,\langle 1238\rangle\}\,. \end{aligned} \tag{6.1.1}$$

When we need to consider all 17 $\mathcal{A}$-coordinates together we order them as follows: $\{a_1,...,a_9,f_1,...,f_8\}$.

The arrows of the quiver diagram can be described by a square matrix b (the *exchange matrix*) with entries

$$b_{ij} = (\text{no. of arrows } i\to j) - (\text{no. of arrows } j\to i)\,. \tag{6.1.2}$$

Here the matrix b is skew-symmetric[14] with indices running over all nodes (active and frozen) and in the case of $\mathrm{Gr}(4,8)$ therefore has dimension (17×17). We do not need to record arrows between frozen nodes so the bottom right (8×8) submatrix of b is irrelevant in what follows.

In addition to the $\mathcal{A}$-coordinates and the b matrix we have more data associated to the initial cluster. We also have a *coefficient matrix*, taken to be the (9×9) identity matrix. Additionally, to each active node a_i we associate the $\mathbf{g}$-vector $\mathbf{e}_i$, the unit vector in the ith direction.

Given the data for the initial cluster we may obtain the data for every other cluster by repeated mutation on active nodes. If we follow the mutation rules given by (2.2.2, 2.2.3, 4.4.1, 4.4.3) one may obtain every cluster in the cluster algebra. In particular to each $\mathcal{A}$-coordinate generated there will be an associated $\mathbf{g}$-vector. For this reason we also

[14] More generally in the study of cluster algebras it need only be skew-symmetrisable.

use the notation $\mathbf{g}(a)$ for the $\mathbf{g}$-vector associated to the $\mathcal{A}$-coordinate a. As we described above the $\mathbf{g}$-vectors play a role in describing a tropical fan associated with the positive part of the tropical Grassmannian.

To describe the tropical fan of [83] we first introduce the cluster $\mathcal{X}$-coordinates. These may be obtained from the $\mathcal{A}$-coordinates of some cluster by writing for each active node j,

$$x_j = \prod_{i=1}^{17} a_i^{b_{ij}} \,, \tag{6.1.3}$$

where the product ranges over all $\mathcal{A}$ coordinates (active and frozen). From the initial cluster we obtain a set of cluster $\mathcal{X}$-coordinates,

$$\begin{aligned}
x_{11} &= \frac{\langle 1234\rangle\langle 1256\rangle}{\langle 1236\rangle\langle 1245\rangle} \quad x_{12} = \frac{\langle 1235\rangle\langle 1267\rangle}{\langle 1237\rangle\langle 1256\rangle} \quad x_{13} = \frac{\langle 1236\rangle\langle 1278\rangle}{\langle 1238\rangle\langle 1267\rangle} \\
x_{21} &= \frac{\langle 1235\rangle\langle 1456\rangle}{\langle 1256\rangle\langle 1345\rangle} \quad x_{22} = \frac{\langle 1236\rangle\langle 1245\rangle\langle 1567\rangle}{\langle 1235\rangle\langle 1456\rangle\langle 1267\rangle} \quad x_{23} = \frac{\langle 1237\rangle\langle 1256\rangle\langle 1678\rangle}{\langle 1236\rangle\langle 1567\rangle\langle 1278\rangle} \\
x_{31} &= \frac{\langle 1245\rangle\langle 3456\rangle}{\langle 1456\rangle\langle 2345\rangle} \quad x_{32} = \frac{\langle 1256\rangle\langle 1345\rangle\langle 4567\rangle}{\langle 1245\rangle\langle 3456\rangle\langle 1567\rangle} \quad x_{33} = \frac{\langle 1267\rangle\langle 1456\rangle\langle 5678\rangle}{\langle 1256\rangle\langle 4567\rangle\langle 1678\rangle} \,,
\end{aligned} \tag{6.1.4}$$

where we have chosen a labelling using a pair of indices for future convenience. This labelling is related to the usual labelling as follows

$$\{x_1, \ldots, x_9\} = \{x_{11}, x_{21}, x_{31}, x_{12}, x_{22}, x_{32}, x_{13}, x_{23}, x_{33}\} \,. \tag{6.1.5}$$

We may use the $\mathcal{X}$-coordinates (6.1.4) to parametrise a (4×8) matrix W (the web matrix) of the form

$$W = (\mathbb{1}_4 | M) \,, \tag{6.1.6}$$

where the (4×4) matrix M has entries

$$m_{ij} = (-1)^i \sum_{\underline{\lambda} \in Y_{ij}} \prod_{k=1}^{4-i} \prod_{l=1}^{\lambda_k} x_{kl} \,, \tag{6.1.7}$$

where Y_{ij} means the range $0 \leq \lambda_{4-i} \leq \ldots \leq \lambda_1 \leq j-1$. The above formula is equivalent to the sum over paths of the web diagram described in [83].

The minors $\langle ijkl\rangle$, formed from the columns i, j, k, l of the web matrix W evaluate to polynomials in the cluster $\mathcal{X}$-coordinates (6.1.4). They do so in such a way that the ratios of products of minors in (6.1.4) correctly evaluate to the $\mathcal{X}$-coordinates themselves. As examples of minors we find for instance

$$\begin{aligned}
\langle 1247\rangle &= 1 + x_{11} + x_{11}x_{12} \,, \\
\langle 2346\rangle &= 1 + x_{11} + x_{11}x_{21} + x_{11}x_{21}x_{31} \,.
\end{aligned} \tag{6.1.8}$$

To describe the positive tropical Grassmannian following [83] we evaluate these minors tropically. That is, we replace addition with minimum and multiplication with addition,

$$\begin{aligned}
\mathrm{Trop}\langle 1247\rangle &= \min(0, \tilde{x}_{11}, \tilde{x}_{11} + \tilde{x}_{12}) \,, \\
\mathrm{Trop}\langle 2346\rangle &= \min(0, \tilde{x}_{11}, \tilde{x}_{11} + \tilde{x}_{21}, \tilde{x}_{11} + \tilde{x}_{21} + \tilde{x}_{31}) \,,
\end{aligned} \tag{6.1.9}$$

where we remind the reader that these are tropical polynomials by using $\tilde{x}$ instead of x.

Each tropical minor defines a number of regions (each one a cone) of piecewise linearity in the $\tilde{x}$ space. Taking all tropical minors together we get many such regions whose overlap defines a fan. Each maximal cone of the fan is a region in which all tropical minors are linear functions. If we intersect the fan with the unit sphere in the (nine-dimensional) space of the $\tilde{x}$, each maximal cone becomes an eight-dimensional facet of a polyhedral complex.

The boundaries of the facets are locations where at least one minor is between two different regions of piecewise linearity. For example, the minor $\mathrm{Trop}\langle 1247\rangle$ in (6.1.9) has boundaries between regions of piecewise linearity if one of the following tropical hypersurface conditions holds,

$$\begin{aligned} & \tilde{x}_{11} = 0 \leq \tilde{x}_{11} + \tilde{x}_{12} \\ \text{or} \quad & \tilde{x}_{11} + \tilde{x}_{21} = 0 \leq \tilde{x}_{11} \\ \text{or} \quad & \tilde{x}_{11} = \tilde{x}_{11} + \tilde{x}_{22} \leq 0\,. \end{aligned} \tag{6.1.10}$$

Each eight-dimensional facet has seven-dimensional boundaries where one such condition is obeyed. The boundaries themselves have six-dimensional boundaries where two linearly independent equalities and the associated inequalities are obeyed. Proceeding in this way we arrive at zero-dimensional boundaries, called *rays*, where eight linearly independent tropical hypersurface conditions are obeyed.

In Chapter 5 we introduced tropical fans generated by different sets of cluster $\mathcal{A}$-coordinates, the most refined of these fans, generated by the set of *all* $\mathcal{A}$-coordinates, called the 'cluster' fan. In the case of the Grassmannian $\mathrm{Gr}(4,8)$ we cannot immediately do this since there are infinitely many $\mathcal{A}$-coordinates. We can nevertheless use the **g**-vectors of the cluster algebra as candidate rays of any fan $F(\mathcal{S})$ defined by tropical evaluation of a finite set $\mathcal{S}$ of cluster $\mathcal{A}$-coordinates. If we restrict ourselves to looking for rays, this approach is very effective. Systematically constructing the rays of the fan can be quite cumbersome for large fans but, given a candidate ray, it is trivial to check if it is truly a ray. As we already outlined in Chapter 4, if we consider the Speyer-Williams fan where we take $\mathcal{S}$ to be the set of all minors then we find that 356 **g**-vectors of the cluster algebra are also rays of the fan.

We can similarly determine that for $\mathcal{S} = \{\langle i\, i+1\, j\, j+1\rangle\,, \langle i-1\,, i\,, i+1\,, j\rangle\}$ (the maximal parity-invariant subset of minors) we find that 272 **g**-vectors are rays. For $\mathcal{S} = \{\langle ijkl\rangle\,, \langle\overline{ijkl}\rangle\}$ (the parity completion of all minors) we find that 544 **g**-vectors are rays. Passing from the cluster algebra to a choice of fan defined by a set $\mathcal{S}$ of $\mathcal{A}$-coordinates is therefore a natural way to obtain a finite truncation of the infinite set of cluster $\mathcal{A}$ coordinates.

Most interestingly, in none of the above cases do the **g**-vectors provide a complete set of rays. In fact we find additional rays which complete the above sets of **g**-vectors as shown in Table 6.1. As we will describe in the next section, the cluster algebra can also be used to find the extra rays which are not **g**-vectors. In fact they arise as limits of special infinite sequences of **g**-vectors so we refer to them as *limit rays*.

In Chapter 5 we also gave the f-vectors of the various fans considered and how their maximal cones split. Here we give some information on the structure of the various fans

$\mathcal{S}$	g-vector rays	limit rays
$\{\langle i\, i+1\, j\, j+1\rangle\,,\, \langle i-1\, i\, i+1\, j\rangle\}$	272	2
$\{\langle ijkl\rangle\}$	356	4
$\{\langle ijkl\rangle\,,\, \langle \overline{ijkl}\rangle\}$	544	4

Table 6.1: Number of rays of the fans $F(\mathcal{S})$ for different choices of $\mathcal{S}$.

in the infinite case $\mathrm{Gr}(4,8)$ studied in recent papers [11, 12, 153, 154]. We find for their f-vectors,

$$\begin{aligned}
f_{48,\mathrm{red}} &= (274, 5782, 46312, 189564, 447284, 635176, 536960, 249306, 49000),\\
f_{48,\mathrm{SW}} &= (360, 7984, 66740, 285948, 706042, 1047200, 922314, 444930, 90608),\\
f_{48,\mathrm{aug}} &= (548, 12748, 111104, 492548, 1251188, 1900152, 1706592, 836570, 172588).
\end{aligned}$$

The maximal cones of the three fans split as

$$\begin{aligned}
49000 &= 22636_9 + 7872_{10} + 4728_{11} + 4528_{12} + 2048_{13} + 2544_{14} + 960_{15} + 672_{16}\\
&\quad + 1488_{17} + 664_{18} + 232_{19} + 128_{20} + 128_{21} + 128_{22} + 32_{23} + 64_{24} + 48_{25}\\
&\quad + 64_{28} + 32_{34} + 4_{45},\\
90608 &= 50356_9 + 12320_{10} + 9116_{11} + 6064_{12} + 4448_{13} + 2332_{14} + 2176_{15} + 872_{16}\\
&\quad + 976_{17} + 676_{18} + 384_{19} + 336_{20} + 200_{21} + 48_{22} + 8_{23} + 80_{24} + 72_{25} + 24_{26}\\
&\quad + 48_{27} + 16_{29} + 20_{33} + 16_{34} + 16_{36} + 4_{49},\\
172588 &= 112708_9 + 21008_{10} + 13088_{11} + 10016_{12} + 4480_{13} + 3440_{14} + 2272_{15}\\
&\quad + 1184_{16} + 1888_{17} + 1168_{18} + 336_{19} + 160_{20} + 256_{21} + 192_{22} + 48_{23} + 128_{24}\\
&\quad + 80_{25} + 64_{28} + 32_{32} + 32_{34} + 8_{45}.
\end{aligned}$$

To each $\mathbf{g}$-vector is associated a cluster $\mathcal{A}$-coordinate. We will conclude this section by explicitly listing the $\mathcal{A}$-coordinates corresponding to the 272 $\mathbf{g}$-vector rays in the least refined fan described in Table 6.1. If we also include the eight frozen $\mathcal{A}$-coordinates then the resulting 280 $\mathcal{A}$ coordinates contain the 196 rational letters found in [162] as an alphabet predicted by Landau analysis for the two-loop NMHV amplitude. In fact the explicit result for the two-loop octagon found recently in [166] contains only 180 of these rational letters. In addition the two-loop NMHV octagon contains 18 multiplicatively independent algebraic letters involving square roots, only four of which (corresponding to the letters of the possible four-mass box integral topologies) are contained in the list in [162].

We begin the list of 280 letters (including 8 frozen) by recalling the 196 rational letters of [162],

- 68 four-brackets of the form $\langle a\, a+1\, b\, c\rangle$,
- 8 cyclic images of $\langle 12\bar{4}\cap\bar{7}\rangle$,
- 40 cyclic images of $\langle 1(23)(45)(78)\rangle$, $\langle 1(23)(56)(78)\rangle$, $\langle 1(28)(34)(56)\rangle$, $\langle 1(28)(34)(67)\rangle$, $\langle 1(28)(45)(67)\rangle$,
- 48 dihedral images of $\langle 1(23)(45)(67)\rangle$, $\langle 1(23)(45)(68)\rangle$, $\langle 1(28)(34)(57)\rangle$,

- 8 cyclic images of $\langle \bar{2} \cap (245) \cap \bar{8} \cap (856) \rangle$,
- 8 distinct images of $\langle \bar{2} \cap (245) \cap \bar{6} \cap (681) \rangle$,
- 16 dihedral images of $\langle\!\langle 12345678 \rangle\!\rangle$.

In addition, we have the following 84 rational letters,

- 2 letters, $\langle 1357 \rangle$ and $\langle 2468 \rangle$,
- 8 cyclic images of $\langle 1(23)(46)(78) \rangle$ (this set is closed under reflections),
- 16 dihedral images of $\langle 1(27)(34)(56) \rangle$,
- 2 cyclic images of $\langle \bar{2} \cap \bar{4} \cap \bar{6} \cap \bar{8} \rangle$ (this set returns to itself under two rotations and it is closed under reflections),
- 8 cyclic images of $\langle \bar{2} \cap (246) \cap \bar{6} \cap \bar{8} \rangle$ (this set is closed under reflections),
- 32 dihedral images of $\langle\!\langle 12435678 \rangle\!\rangle$, $\langle\!\langle 12436578 \rangle\!\rangle$,
- 16 dihedral images of $\langle 1234 \rangle \langle 1678 \rangle \langle 2456 \rangle - \langle 1267 \rangle \langle 1348 \rangle \langle 2456 \rangle + \langle 1248 \rangle \langle 1267 \rangle \langle 3456 \rangle$.

In the above we have defined $\langle\!\langle abcdefgh \rangle\!\rangle = \langle abcd \rangle \langle abef \rangle \langle degh \rangle - \langle abde \rangle \langle abef \rangle \langle cdgh \rangle + \langle abde \rangle \langle abgh \rangle \langle cdef \rangle$.

In an ancillary file we list the g-vectors and their corresponding letters for the first two cases of Table 1.

We now turn to describing the extra rays obtained by limits of infinite sequences and the resulting algebraic letters.

6.2 Infinite paths in $\mathrm{Gr}(4,8)$ and algebraic letters

As we have seen in the previous discussion, the relation between amplitude singularities and cluster algebra data requires some refinement when going beyond seven points. In the first instance, the two-loop NMHV octagon has algebraic letters which do not correspond to any cluster $\mathcal{A}$-coordinate. In addition, in truncating the infinite set of $\mathcal{A}$-coordinates by considering some tropical fan $F(\mathcal{S})$ as described above, the rays of $F(\mathcal{S})$ are not all described by **g**-vectors of the cluster algebra.

We may address both of the above difficulties by realising that the infinite number of clusters can usefully be organised into infinite sequences, each of which can be related to an infinite rank two cluster algebra with two nodes and a doubled arrow between them. Such algebras were considered in e.g. [168] and it was already noted there that under repeated mutation the **g**-vectors asymptote to a limiting vector. In fact, in the affine case which is relevant here, the same limiting vector can be obtained by repeated mutation with either choice of initial node (i.e. both directions asymptote to the same limit vector).

If we ignore the frozen nodes (and ignore the values of the $\mathcal{A}$-coordinates on the active nodes) there are 506 distinct quiver diagrams that arise in the $\mathrm{Gr}(4,8)$ cluster algebra. The fact that there are only finitely many is a feature of the affine cases of Grassmannian

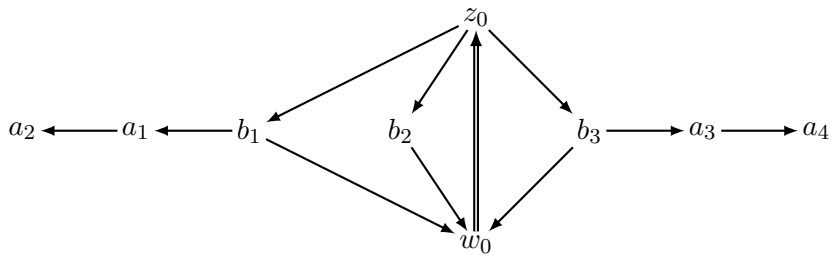

Figure 6.2: The $E_7^{(1,1)}$ shaped clusters with a doubled arrow between two cluster $\mathcal{A}$-coordinates, w_0 and z_0. By mutation on the a_i nodes we generate an $A_2 \times A_2$ subalgebra of clusters containing the same w_0, z_0 and b_i nodes. Frozen nodes are omitted here.

cluster algebras $\mathrm{Gr}(4,8)$ and $\mathrm{Gr}(3,9)$ and these algebras are referred to as *finite mutation type*. Out of the 506 quivers, 491 have only single arrows while 15 have a doubled arrow. These latter type have the shape of the $E_7^{(1,1)}$ quiver diagram shown in Fig. 6.2, or one related to it by mutation in the $A_2 \times A_2$ subalgebra generated by mutations on the a_i type nodes [167].

Each diagram of the form of Fig. 6.2 forms part of a doubly infinite rank-two affine sequence, generated by alternating mutations on the w_0 and z_0 nodes. In each such sequence we can find some cluster (actually an $A_2 \times A_2$ subalgebra of clusters) in which the frozen nodes are all outgoing from w_0 and incoming to z_0. We illustrate this by a simplified diagram which we refer to as an *origin cluster* where we ignore the a_i nodes, combine the three b_i nodes into a single node,

$$b = b_1 b_2 b_3 \,, \tag{6.2.1}$$

and combine all frozen nodes outgoing from w_0 into f_w and those incoming to z_0 into f_z,

$$f_w = \prod_{i=1}^{8} f_i^{m_i} \,, \qquad f_z = \prod_{i=1}^{8} f_i^{n_i} \,, \qquad m_i, n_i \in \mathbb{N}_0 \,. \tag{6.2.2}$$

Such a simplified diagram is illustrated at the top of Fig. 6.3.

The initial mutations to generate the infinite double sequence take the form

$$\begin{aligned} z_1 w_0 &= b + f_w z_0^2 \,, \\ w_1 z_0 &= b + f_z w_0^2 \,. \end{aligned} \tag{6.2.3}$$

Thereafter the mutations in the z-direction and w-direction take the uniform form for $n \geq 0$,

$$\begin{aligned} z_{n+2} z_n &= \mathcal{C}\mathcal{F}^n + z_{n+1}^2 \,, \\ w_{n+2} w_n &= \tilde{\mathcal{C}}\mathcal{F}^n + w_{n+1}^2 \,. \end{aligned} \tag{6.2.4}$$

The coefficients $\mathcal{C}$ and $\tilde{\mathcal{C}}$ are given by

$$\begin{aligned} \mathcal{C} &= b f_z \,, \\ \tilde{\mathcal{C}} &= b f_w \,, \end{aligned} \tag{6.2.5}$$

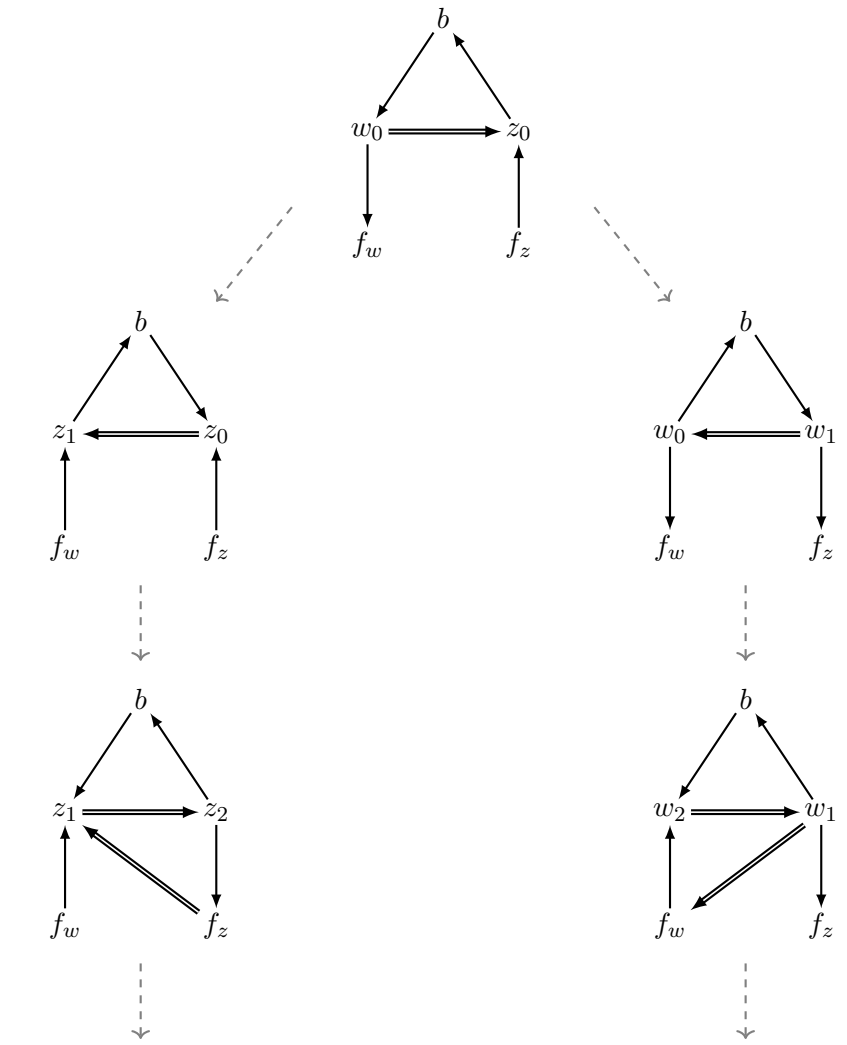

Figure 6.3: The doubly infinite sequence corresponding to the embeddings of the affine A_2 cluster algebra into the $\mathrm{Gr}(4,8)$ cluster algebra. After mutating one step from the origin cluster on either node, the repeated mutations give rise to a regular recurrence relation.

while the factor $\mathcal{F}$ is the product over the frozen nodes,

$$\mathcal{F} = f_w f_z \,. \tag{6.2.6}$$

The transformations of the $\mathbf{g}$-vectors while performing the doubly infinite sequence of mutations are very simple. After a few initial mutations the differences in consecutive $\mathbf{g}$-vectors stabilise and we arrive at the form

$$\mathbf{g}(z_{n+1}) - \mathbf{g}(z_n) = \mathbf{g}(w_0) - \mathbf{g}(z_0) = \mathbf{g}(w_{n+1}) - \mathbf{g}(w_n) \,. \tag{6.2.7}$$

This shows that in either direction the $\mathbf{g}$-vectors will asymptote to the limit ray

$$\mathbf{g}_\infty = \mathbf{g}(w_0) - \mathbf{g}(z_0) \,. \tag{6.2.8}$$

In fact we find many different origin clusters of the form shown at the top of Fig. 6.3, with different w_0 and z_0 (and hence different $\mathbf{g}(w_0)$ and $\mathbf{g}(z_0)$) but with the same limit ray $\mathbf{g}_\infty$.

We may recast the quadratic recurrence relations (6.2.4) in a matrix form,

$$\begin{pmatrix} z_{n+2} & z_{n+1} \\ z_{n+1} & z_n \end{pmatrix} = \begin{pmatrix} z_{n+1} & z_n \\ z_n & z_{n-1} \end{pmatrix} \begin{pmatrix} \mathcal{P} & 1 \\ -\mathcal{F} & 0 \end{pmatrix} = \begin{pmatrix} z_2 & z_1 \\ z_1 & z_0 \end{pmatrix} \begin{pmatrix} \mathcal{P} & 1 \\ -\mathcal{F} & 0 \end{pmatrix}^n \,, \tag{6.2.9}$$

and similarly for $z \to w$. Taking the determinant of the matrix relations (6.2.9) yields the original quadratic relations (6.2.4) since

$$z_2 z_0 = \mathcal{C} + z_1^2 \,. \tag{6.2.10}$$

We may verify that the matrix recursion (6.2.9) consistently generates the same sequence z_n as the quadratic recursion (6.2.4) provided that $\mathcal{P}$ obeys

$$z_2 = z_1 \mathcal{P} - z_0 \mathcal{F} \,. \tag{6.2.11}$$

Hence we require that $\mathcal{P}$ is related to $\mathcal{C}$ via

$$\mathcal{C} + z_1^2 + z_0^2 \mathcal{F} = z_0 z_1 \mathcal{P} \,. \tag{6.2.12}$$

Remarkably, $\mathcal{P}$ can be shown to be a polynomial, that is we can find a factor of $z_0 z_1$ within the combination on the LHS of (6.2.12). If we write $\mathcal{C}$ and $\mathcal{F}$ in terms of the cluster $\mathcal{A}$-coordinates of the origin cluster we find

$$\begin{aligned} \mathcal{C} + z_1^2 + z_0^2 \mathcal{F} &= b f_z + z_1^2 + z_0^2 f_w f_z \,, \\ &= z_1 (f_z w_0 + z_1) \,, \end{aligned} \tag{6.2.13}$$

where the second step is achieved by using the first relation in (6.2.3) to eliminate b. We have made the factor of z_1 manifest and it remains to show that there is also a factor of z_0 in the remaining combination $(f_z w_0 + z_1)$. To show this we consider instead the square of this combination,

$$\begin{aligned} (f_z w_0 + z_1)^2 &= f_z^2 w_0^2 + 2 f_z w_0 z_1 + z_1^2 \,, \\ &= f_z (w_1 z_0 - b) + 2 f_z (b + f_w z_0^2) + (z_2 z_0 - b f_z) \,, \\ &= z_0 (f_z w_1 + 2 f_z f_w z_0 + z_2) \,. \end{aligned} \tag{6.2.14}$$

In the second step we have used the relations (6.2.3) and the quadratic recurrence formula (6.2.4) for z in the case $n = 2$. We have succeeded in finding a factor of z_0 in the square factor, but since all quantities involved are *polynomials* in Plücker coordinates, it must be that the original factor without the square also has a factor of z_0. Hence we conclude that

$$\mathcal{P} = \frac{f_z w_0 + z_1}{z_0} \tag{6.2.15}$$

is a polynomial even if this property is not manifest from the above equation. By considering the w_n sequence instead we arrive at an equivalent formula for $\mathcal{P}$,

$$\mathcal{P} = \frac{f_w z_0 + w_1}{w_0}\,. \tag{6.2.16}$$

Note that both $\mathcal{P}$ and $\mathcal{F}$ are invariant under swapping the z sequence and the w sequence (along with swapping f_z with f_w). Note also that $\mathcal{P}$ is manifestly positive in the region where all $\mathcal{A}$-coordinates are positive.

Returning to the matrix recursion we see that it is equivalent to a linear recursion formula

$$z_{n+2} = z_{n+1}\mathcal{P} - z_n\mathcal{F}\,, \tag{6.2.17}$$

of which (6.2.11) is just the first case. Of course we also have the same recursion formula for the w_n. Once a polynomial form for $\mathcal{P}$ is obtained, this linear recursion formula provides a manifestly polynomial form for all the z_n cluster coordinates (and similarly the w_n). Note that the linear recursion would just be the Fibonacci recursion relation if we had $\mathcal{P} = -\mathcal{F} = 1$. The linear recursion formula is neatly solved by the following generating function

$$G_z(x) = \frac{z_1 - z_0\mathcal{F}x}{1 - \mathcal{P}x + \mathcal{F}x^2} = \sum_{n=0}^{\infty} z_{n+1}x^n\,, \tag{6.2.18}$$

and similarly for $w \leftrightarrow z$. It follows immediately that the asymptotic limit of the ratios of the z_n is controlled by the roots of the quadratic in the denominator,

$$\lim_{n\to\infty}\frac{z_n}{z_{n-1}} = \mathcal{P} + \sqrt{\Delta}\,, \qquad \Delta = \mathcal{P}^2 - 4\mathcal{F}\,. \tag{6.2.19}$$

Using this fact we can write an explicit form for the z_n,

$$z_n = \frac{1}{2^{n+1}}\left[(z_0 + B_z\sqrt{\Delta})(\mathcal{P} + \sqrt{\Delta})^n + (z_0 - B_z\sqrt{\Delta})(\mathcal{P} - \sqrt{\Delta})^n\right] \tag{6.2.20}$$

with B_z defined by

$$B_z = \frac{2z_1 - z_0\mathcal{P}}{\Delta}\,. \tag{6.2.21}$$

We have a similar formula for the w_n sequence obtained by swapping $z \leftrightarrow w$ everywhere. For a sequence of mutations generating $\mathbf{g}$-vectors which asymptote to a given limit ray $\mathbf{g}_\infty$, we find that $\mathcal{P}$ and $\mathcal{F}$ (and hence the limit of the ratio (6.2.19)) depend only on the limit ray. The actual path towards the limit (and therefore the z_n or w_n) is distinguished by the values of z_0 and z_1 (or w_0 and w_1).

In the limit of large n, the term with $(\mathcal{P} + \sqrt{\Delta})^n$ dominates over the term $(\mathcal{P} - \sqrt{\Delta})^n$. Its coefficient $(z_0 + B_z\sqrt{\Delta})$ depends on the path of approach to the limit. Since the product

$(z_0 + B_z\sqrt{\Delta})(z_0 - B_z\sqrt{\Delta})$ is rational[15] we identify the ratio

$$\phi_z = \frac{z_0 + B_z\sqrt{\Delta}}{z_0 - B_z\sqrt{\Delta}} = \frac{z_0\mathcal{P} - 2f_z w_0 + z_0\sqrt{\Delta}}{z_0\mathcal{P} - 2f_z w_0 - z_0\sqrt{\Delta}} \tag{6.2.22}$$

with a new algebraic letter associated to the path. We also have a letter obtained from the limit of the w sequence whose formula is the same except for swapping $z \leftrightarrow w$ everywhere,

$$\phi_w = \frac{w_0 + B_w\sqrt{\Delta}}{w_0 - B_w\sqrt{\Delta}} = \frac{w_0\mathcal{P} - 2f_w z_0 + w_0\sqrt{\Delta}}{w_0\mathcal{P} - 2f_w z_0 - w_0\sqrt{\Delta}}\,. \tag{6.2.23}$$

Note that we have many origin clusters, each of which provides two paths (the z branch and the w branch) towards the same limit ray $\mathbf{g}_\infty$. The square root $\sqrt{\Delta}$ which appears will be common for all algebraic letters coming from a given limit. Only the rational coefficients (determined by the data of the origin cluster) will depend on the actual path.

Let us recall that the smallest fan from those listed in Table 6.1 has two limit rays in addition to the 272 **g**-vector rays. For the case of a path that asymptotes to the first limit ray we find

$$\begin{aligned} \mathbf{g}_\infty^{(1)} &= (1,-1,0,-1,0,1,0,1,-1)\,, \\ \mathcal{P} &= \langle 1256\rangle\langle 3478\rangle - \langle 1278\rangle\langle 3456\rangle - \langle 1234\rangle\langle 5678\rangle\,, \\ \mathcal{F} &= \langle 1234\rangle\langle 3456\rangle\langle 5678\rangle\langle 1278\rangle\,. \end{aligned} \tag{6.2.24}$$

while the second limit ray

$$\mathbf{g}_\infty^{(2)} = (0,1,0,1,0,-1,0,-1,0)\,, \tag{6.2.25}$$

has $\mathcal{P}$ and $\mathcal{F}$ related to those in (6.2.24) by a cyclic rotation by one unit. The precise values of z_0 and z_1 (or w_0 and w_1) depend on the path of approach.

We find 64 origin clusters whose associated limit rays are either $\mathbf{g}_\infty^{(1)}$ or $\mathbf{g}_\infty^{(2)}$ described above. Among them are four clusters with the nodes w_0 and z_0 connected by the doubled arrow given by

$$\langle j(12)(ik)(78)\rangle \implies \langle 12ij\rangle \tag{6.2.26}$$

where $i \in \{3,4\}$ and (j,k) is a permutation of $(5,6)$. Each origin cluster with the rank two affine subalgebras of the form (6.2.26) has the limit ray $\mathbf{g}_\infty^{(1)}$ and frozen nodes given by

$$f_z = f_1 = \langle 1234\rangle, \quad f_w = f_3 f_5 f_7 = \langle 3456\rangle\langle 5678\rangle\langle 1278\rangle\,, \tag{6.2.27}$$

in agreement with eq. (6.2.24). The four origin clusters are listed in Table 6.2 along with the data from the original cluster diagram that they come from, including the b nodes and the $A_2 \times A_2$ subalgebra generated by the a_i type nodes of Fig. 6.2. The full set of 64 origin clusters whose limit rays are $\mathbf{g}_\infty^{(1)}$ or $\mathbf{g}_\infty^{(2)}$ are then obtained from the four described in (6.2.26) by dihedral transformations.

Each origin cluster produces two algebraic letters ϕ_z and ϕ_w defined by eqs. (6.2.22) and (6.2.23). Thus we have a set of 128 algebraic letters associated to the two limit rays $\mathbf{g}_\infty^{(1)}$ and $\mathbf{g}_\infty^{(2)}$. Each limit ray is therefore associated with significantly more data than

[15] For the cases we consider shortly, it is always a multiplicative combination of the 280 rational letters given in at the end of Sect. 6.1.

Sub affine A_2: $w_0 \Longrightarrow z_0$	$b = b_1 b_2 b_3$	Residual $A_2 \times A_2$
$\langle 5(12)(36)(87)\rangle \Longrightarrow \langle 1235\rangle$	$\langle 1256\rangle$ $\times\langle 3(12)(56)(78)\rangle$ $\times\langle 5(12)(34)(78)\rangle$	$\langle 1345\rangle \longrightarrow \langle 1346\rangle$ $\langle 1237\rangle \longrightarrow \langle 1247\rangle$
$\langle 6(12)(35)(78)\rangle \Longrightarrow \langle 1236\rangle$	$\langle 1256\rangle$ $\times\langle 3(12)(56)(78)\rangle$ $\times\langle 6(12)(34)(78)\rangle$	$\langle 1345\rangle \longrightarrow \langle 1346\rangle$ $\langle 1237\rangle \longrightarrow \langle 3567\rangle$
$\langle 5(12)(46)(87)\rangle \Longrightarrow \langle 1245\rangle$	$\langle 1256\rangle$ $\times\langle 4(12)(56)(78)\rangle$ $\times\langle 5(12)(34)(78)\rangle$	$\langle 1237\rangle \longrightarrow \langle 1247\rangle$ $\langle 1237\rangle \longrightarrow \langle 1247\rangle$
$\langle 6(12)(45)(78)\rangle \Longrightarrow \langle 1246\rangle$	$\langle 1256\rangle$ $\times\langle 4(12)(56)(78)\rangle$ $\times\langle 6(12)(34)(78)\rangle$	$\langle 1237\rangle \longrightarrow \langle 3567\rangle$ $\langle 1237\rangle \longrightarrow \langle 3567\rangle$

Table 6.2: Four types of clusters that act as origins of doubly-infinite sequences.

any **g**-vector ray, each of which is associated to a single rational letter. The 128 letters associated to $\mathbf{g}^{(1)}_\infty$ and $\mathbf{g}^{(2)}_\infty$ are not all multiplicatively independent and remarkably they generate the same space as the 18 multiplicatively independent algebraic letters found in [166]! The two-loop NHMV eight-point amplitude is therefore consistent with the data obtained from the smallest fan in Table 6.1 in that the associated alphabet is covered by the rays of the fan.

The set of 128 algebraic letters described above is closed under parity, as the doubly infinite sequences themselves map to each other under parity. The origin clusters themselves do not necessarily map to origin clusters but sometimes map to an adjacent cluster in the infinite sequence. In an ancillary file we explicitly list the 128 algebraic letters.

The other fans in Table 6.1 have four limit rays. These are similarly associated to their own set of origin clusters, again 64 such clusters, each generating two algebraic letters according to (6.2.22) and (6.2.23). In this case the $\mathcal{P}$ and $\mathcal{F}$ associated to $\mathbf{g}^{(3)}_\infty$ are as follows,

$$\begin{aligned}
\mathbf{g}^{(3)}_\infty = &\quad (-1,0,1,0,2,-1,1,-1,-1)\,,\\
\mathcal{P} = &\quad \langle 1237\rangle\langle 1458\rangle\langle 2468\rangle\langle 3567\rangle - \langle 1238\rangle\langle 1567\rangle\langle 2468\rangle\langle 3457\rangle\\
&-\langle 1238\rangle\langle 1678\rangle\langle 2345\rangle\langle 4567\rangle - \langle 1237\rangle\langle 1358\rangle\langle 2468\rangle\langle 4567\rangle\\
&-\langle 1234\rangle\langle 1278\rangle\langle 3456\rangle\langle 5678\rangle\,,\\
\mathcal{F} = &\quad \langle 1234\rangle\langle 2345\rangle\langle 3456\rangle\langle 4567\rangle\langle 5678\rangle\langle 1678\rangle\langle 1278\rangle\langle 1238\rangle\,.
\end{aligned} \tag{6.2.28}$$

The $\mathcal{P}$ associated to the other limit ray

$$\mathbf{g}^{(4)}_\infty = (1,1,-1,1,-2,0,-1,0,1)\,, \tag{6.2.29}$$

is related to that in (6.2.28) by a cyclic rotation by one unit while the $\mathcal{F}$ is the same

(note that $\mathcal{F}$ in (6.2.28) is the product of all frozen $\mathcal{A}$-coordinates and therefore is cyclic invariant). The algebraic letters associated to the limit rays $\mathbf{g}_\infty^{(3)}$ and $\mathbf{g}_\infty^{(4)}$ are therefore of a different nature with different square roots. So far we do not have any example of an amplitude where they appear. They might appear at higher loop orders in eight-point amplitudes than are currently known explicitly.

We should also stress that there are more origin clusters (infinitely many) each of which has its own limit vector associated to it and its own type of square roots. However the limit vectors obtained are not rays of any of the fans listed in Table 6.1. One could imagine making yet more refined fans $F(\mathcal{S})$ by taking yet larger sets $\mathcal{S}$ of $\mathcal{A}$-coordinates to define them. It is possible that the other limit vectors beyond the four described above become rays of such fans.

Chapter 7

Conclusions

This thesis consists of two main parts. In the first part, we introduced the notion of cluster adjacency, demonstrating how cluster algebras not only provide the list of singularities of alphabets for scattering amplitudes in $\mathcal{N} = 4$ SYM, but also how the geometry of the cluster polytope dictates which consecutive discontinuities or residues of an amplitude one is allowed to take. We then demonstrated cluster adjacency's power to reduce the free parameters of a bootstrap calculation, thus allowing us to calculate a previously unknown result - the seven-point, four-loop NMHV amplitude.

The second part of this thesis was focussed on the recently discovered connection between tropical geometry and the generalised biadjoint ϕ^3 theory, as well as a more generalised and systematic formulation of cluster adjacency. We expanded on the relationship between volumes of the positive region of tropical Grassmannians and tree-level biadjoint ϕ^3 amplitudes, demonstrating how the cluster algebra provides a straightforward algorithm for calculating these volumes. We then explored different classes of finite tropical fans being generated by different sets of cluster $\mathcal{A}$-coordinates, how these different fans give rise to a more generalised form of cluster adjacency, and the functions built on these fans. We also proposed a generalised form of the scattering equations. Finally tropical geometry allowed us to begin exploring an infinite cluster algebra $\mathrm{Gr}(4, 8)$, using our tropical geometry tools to truncate the infinite set of cluster $\mathcal{A}$-coordinates, again providing different finite fans, and conjecturing an alphabet for eight-point scattering in SYM. We also used our understanding of $\mathbf{g}$-vectors and their mutation properties to generate algebraic letters known to appear in eight-point scattering, but previously not extractable from the cluster algebra.

In this final chapter, we will present a short summary of our findings, concluding remarks, and an outlook of possible future research.

In Chapter 2 we first reviewed cluster algebras and their link to the singularities of scattering amplitudes in $\mathcal{N} = 4$ SYM. We discussed how the cluster $\mathcal{A}$-coordinates of the $\mathrm{Gr}(4, 6)$ and $\mathrm{Gr}(4, 7)$ cluster algebras provide the alphabets for six and seven particle scattering respectively.

We then introduced cluster adjacency as the rule by which only cluster $\mathcal{A}$-coordinates which appear in a cluster together can appear in adjacent slots of the symbol. We also used the bootstrap program, with cluster adjacency built in, to calculate the symbols of

certain seven-point, three-loop integrals demonstrating that our conjecture held not only for existing results but could also be used to simplify calculations. Confirmation of the cluster adjacency of existing one and two-loop amplitudes in SYM was provided in [169] through use of the Sklyanin bracket.

Lastly, we analysed the consequences of the adjacency rules, producing dimensions of cluster adjacent functions spaces for increasing weights and comparing these to Steinmann function spaces. We also introduced the notion of neighbour set functions and comparing the dimensions of these function spaces to that of the full function space. Cluster adjacency also has implications for integrability of general functions built on Grassmannians, even without any initial entry conditions. At weight two, cluster adjacency only imposes constraints on the symmetric words $[a \otimes b] + [b \otimes a]$, forcing the entries a and b to appear in a cluster together. At weight three, two interesting features arise. Either all three entries must appear together in a cluster or we have triplets of the form $[a \otimes b \otimes a']$, where a' is the result of mutating on a in some cluster and therefore b is the cluster $\mathcal{X}$-coordinate corresponding to that mutation.

In Chapter 3, we explored and extended the role of cluster algebras and their relation to the appearance of singularities in scattering amplitudes in SYM. The picture which emerges is very geometric in nature, the boundary structure of the cluster polytope controls the way in which both poles and branch cuts appear. Codimension-one faces of the cluster polytope correspond to unfrozen $\mathcal{A}$-coordinates which appear in the symbol alphabet. The branch cuts exhibit a non-abelian structure, with sequential cuts forbidden when corresponding to non-intersecting faces. Poles in BCFW terms for tree amplitudes (and more conjecturally Yangian invariants) exhibit an abelianised version of adjacency; they all correspond to $\mathcal{A}$-coordinates from the same cluster. The same adjacency structure also relates the poles of R-invariants and the final entries (i.e. derivatives) of the polylogarithms which appear in the NMHV amplitudes.

We also presented the computation of the symbol of the four-loop correction to the NMHV superamplitude of seven particles in SYM. This is the unique combination of weight-8 symbols whose letters are given by the $\mathrm{Gr}(4,7)$ cluster algebra, exhibit cluster adjacency in its iterated discontinuities, and has a well-behaved collinear limit. We then analysed the multi-Regge limit of our answer for the amplitude, confirming that it agrees with results derived for the latter up to next-to-leading logarithmic accuracy [76, 78] based on the BFKL approach, and also obtaining new predictions for an additional two logarithmic orders.

The a priori knowledge of cluster adjacency was key in our computation in two ways. Firstly, it allowed us to construct an ansatz for the polylogarithmic components of the amplitude with definite, monomial (final entry)$\otimes$(R-invariant) pairs. Secondly, it restricts the possible next-to-final entries for each of these pairs, drastically reducing the size of the original ansatz.

A peculiar feature of our ansatz for the heptagon amplitude is that it requires the inclusion of the entire set of 21 R-invariants to manifestly exhibit cluster adjacency. As a result, integrability of the symbol is verifiable only on the six identities that these invariants

satisfy. This creates a trade-off between two natural ways of presenting the symbol of the amplitude: one that manifestly corresponds to a function and one that reveals its cluster adjacent structure.

In this calculation, we only exploited the cluster adjacency of neighbouring symbol letters. However, as noted in Chapter 3, integrability of the symbols in a sense "propagates" the adjacency of adjacent letters to longer words. One particular example of this phenomenon is the triplets rule which predicts the combination of letters that come between a mutation pair separated by one site as the corresponding $\mathcal{X}$ coordinate. It would be interesting to investigate by how much the a priori implementation of this rule, and possible extensions thereof, facilitate the calculation of higher-loop amplitudes using the bootstrap approach.

Although we have conjectured finite alphabets for eight-point scattering, it would be very interesting to tackle more amplitudes beyond six and seven-points in SYM. For instance, the applicability of cluster adjacency, or extended Steinmann relations, to individual Feynman integrals [8, 170] strongly suggests that this is a general feature of local quantum field theories. Furthermore, cluster adjacency has an imprint on the amplitude also in special kinematics, such as the multi-Regge limit we studied, implying relations even between functions of different logarithmic order. Studying more amplitudes in the light of cluster adjacency may prove useful in developing a more general picture of their analytic structure.

The structures we have uncovered naturally lead to many further questions.

- Can we use adjacency to construct integrable words without having to apply the bootstrap techniques? This question is even of interest if we do not insist on the physical initial entry conditions, and indeed one can ask it for all finite cluster algebras, not just the cases of physical interest described here. A hint that this might be possible comes from the observation that mutation pairs $\{a, a'\}$ appearing in a triple always appear in the form $[a \otimes x(a, a') \otimes a']$ where $x(a, a')$ is the $\mathcal{X}$-coordinate associated to any mutation which takes a to a'.

- Can we extend our results to general N^{k}MHV BCFW terms or more generally Yangian invariants? Going beyond BCFW terms will lead to expressions which involve quantities more complicated that $\mathcal{A}$-coordinates. Perhaps we will learn something about how such singularities interact with the known ones and how they relate to adjacency. Recent work [171–174] has already shed some light on the cluster adjacency of Yangian invariants in SYM.

- In this thesis, we have only discussed cluster adjacency in the context on polylogarithmic functions. Despite their applicability to large classes of problems in high-energy physics, already at two-loops, polylogarithms are known not to exhaust the whole space of special functions required for the computation of Feynman integrals. A natural question is whether adjacency can be extended beyond the polylogarithmic case to include the elliptic functions appearing in e.g. the ten-point, two-loop N^{3}MHV amplitude.

- To what extent do adjacency constraints arise beyond planar $\mathcal{N} = 4$ amplitudes? For sufficiently many external legs there will always be Steinmann constraints on scattering amplitudes. A natural question is whether these extend to further constraints between pairs of singularities which are not both simple unitarity cuts of amplitudes. The geometrical picture of the relations between singularities described here suggests that it is important to understand the relevant geometry and its boundary structure in the more general setting. This geometry is necessarily more complicated in the general case of massless scattering where dual conformal symmetry is broken.

It will be fascinating to explore the above questions. Ultimately we might hope to be able to give a simple geometric or algebraic construction of physical scattering amplitudes.

In Chapter 4, we utilised cluster algebra technology to construct tree-level biadjoint amplitudes on $\mathrm{Gr}(3, n)$ for $n = 6, 7, 8$. These amplitudes arise from scattering equations on the corresponding Grassmannians [7, 143] and the relevance of cluster algebras for these amplitudes arises from the interpretation of these amplitudes as volumes of certain geometric objects. In the cases we studied in this thesis, these objects are polyhedra in $(k-1)(n-k-1)-1$ dimensions, where $k = 3$.

Cluster algebras provide a natural triangulation of the polyhedra whose volumes correspond to the scattering amplitudes. Therefore we were able to employ mutation rules to "bootstrap" the amplitude starting from a single term only. In particular, we provided a prescription for the volume of the simplex that corresponds to the initial cluster and obtained the volumes of the remaining simplexes through consecutive cluster mutations.

Each of the cases we considered has new features that provide important lessons. In $n = 6$ we saw that the clusters triangulate the bipyramids of $\mathrm{Tr}^+(3, 6)$ into two simplexes. In $n = 7$ we identified that positive rays that define cones of $\mathrm{Tr}^+(3, 7)$ are not rays of the $\mathrm{Tr}^+(3, 7)$ fan and are also not detected by the cluster algebra. When we studied the $n = 8$ case, we found that the cluster algebra generates redundant triangulations of the $\mathrm{Tr}^+(3, 8)$ fan.

In Chapter 5, expanded on the relationship between tropical geometry and scattering amplitudes by introducing different types of tropical fans which are generated by corresponding sets of cluster $\mathcal{A}$-coordinates. The first tropical Grassmannian where it is possible to have fans other than the cluster fan is $\mathrm{Tr}(3, 6)$ and we provide the geometric data associated to the three different fans one can construct. We also provide the geometric data for the four different fans one can generate for the tropical Grassmannian $\mathrm{Tr}(4, 7)$.

The link between the scattering equations and the tropical Grassmannian allowed for a generalisation of the scattering equations for $\mathrm{Gr}(2, n)$ [7]. We proposed a set of generalised scattering equations for each choice of tropical fan where the equations associated to the cluster fan are the most generalised form of the scattering equations. We then solve these generalised scattering equations numerically and check that the result for the amplitude obtained by summing over the solutions indeed matches the expected answer.

In Chapter 2, we introduced a method for calculating cluster face variables in terms of the cluster $\mathcal{X}$-coordinates of a cluster with the topology of the algebra's corresponding Dynkin diagram. In Chapter 5, we use the potential function defined in [7] to generalise the

original method to include any tree-shaped cluster. This allows us to define face variables for any cluster algebra which contains a tree-shaped cluster, but which may not have a Dynkin classification associated to it.

We also discussed polylogarithms built on different tropical fans and the singularity structure of these so-called tropically adjacent polylogarithms. We looked specifically at polylogarithms built on fans of $\mathrm{Gr}(4,7)$ and how the edges and triangles of particular fans are indicative of their relevance for different helicity configurations. In particular, the fans generated by the sets $\{a_1,\ldots,a_3\}$ and $\{a_1\ldots,a_6\}$ corresponding to MHV and NMHV amplitudes respectively. It remains to be seen if the fans we present do correspond to particular helicity amplitudes, and it would be interesting to see if one could compute the seven-point, five-loop MHV amplitude using the conjectured MHV tropically adjacent polylogarithms.

In Chapter 6, we continued our discussion of tropical geometry and its relationship with cluster adjacency. We utilised the **g**-vector mutation properties to conjecture finite sets of cluster $\mathcal{A}$-coordinates, which could possibly be alphabets for scattering amplitudes in SYM. These finite sets of $\mathcal{A}$-coordinates originate from different finite tropical fans. The fact that we find exactly the same letters appearing in [166] from tropical geometry and cluster algebras is very exciting. Ultimately, we must remember that the tropical problems we have been considering here arise purely from kinematics. Momentum twistors provide a natural, unconstrained set of coordinates for the kinematical space of colour-ordered amplitudes in the planar limit, and dual conformal symmetry [3] dictates that we should consider sl_4 invariant combinations of them. This leads directly to the association of the Grassmannian $\mathrm{Gr}(4,n)$, or more precisely $\mathrm{Conf}_n(\mathbb{P}^3) = \mathrm{Gr}(4,n)/(\mathbb{C}^*)^{n-1}$, to the kinematic space of massless scattering in planar SYM. The dual conformally invariant (or sl_4 invariant) quantities are the Plücker coordinates $\langle ijkl\rangle$ and they obey quadratic Plücker relations, for example the following,

$$\langle ijk[l\rangle\langle mnpq]\rangle = 0\,. \tag{7.0.1}$$

Tropicalising such polynomial relations gives the tropical Grassmannian as considered by Speyer and Sturmfels [145]. Considering its positive part leads to the tropical fans of Speyer and Williams [83]. As we have discussed, these have a direct connection to the Grassmannian cluster algebras. The **g**-vectors of the cluster algebras provide rays for the tropical fans, even in the case where the algebra is not finite, such as the case studied here $\mathrm{Gr}(4,8)$. To these rays are associated rational $\mathcal{A}$-coordinates which play the role of symbol letters characterising the singularities of the polylogarithmic functions describing the scattering amplitudes. Moreover, the additional rays of the fan arise as limits of natural infinite sequences of **g**-vectors. To these are associated sets of algebraic letters involving square roots.

Clarification is necessary in order to see which fans correspond to which amplitudes. We have seen that the letters of the two-loop NMHV octagon are included in the smallest fan we considered in Table 6.1. However, it could be that beyond two loops the MHV amplitude will also need recourse to the same set of algebraic letters. It could also be beyond two loops

the NMHV amplitude will require a bigger set of letters, say those arising in the largest fan considered in Table 6.1. Moreover, the N^2MHV amplitude requires algebraic letters (the four-mass box letters) at one loop already. These four algebraic letters are included in the set of 18 multiplicatively algebraic letters found in [166]. It would be very interesting to explore all of these amplitudes at higher loop orders than are currently known explicitly, to understand the general structure better.

It would also be enlightening to attempt bootstrapping eight-point integrals built on the alphabets we conjecture. Due to the lack of a BDS-like subtracted amplitude for $n = 0 \bmod 4$, eight-point amplitudes do not obey the Steinmann conditions and hence cluster adjacency. However, IR finite eight-point integrals should obey cluster adjacency. Therefore, once the rules for eight-point cluster adjacency can be determined, one could construct symbols of integrals and examine their properties. For example, an eight-point, two-loop massive double pentagon integral was presented in [132]. If this integral is assumed to be cluster adjacent, certain cluster adjacency rules could be deduced from its symbol. Moreover, in recent work, the cluster adjacency of all one-loop amplitudes has been checked up to nine-points [174], as well as that of the n-point one-loop NMHV ratio function [173].

We have only scratched the surface of the role tropical geometry plays in the analytic structure of amplitudes in SYM. We have reproduced the algebraic letters present in the two-loop NMHV octagon along with a second set of algebraic letters which do not appear in any known amplitudes. Do these letters appear in amplitudes at all, and if so at what loop order and helicity configuration? Can we understand the eight-point analytic structure in more detail from the tropical fan? These questions would be interesting to pursue in the future.

Appendix A

Spinor Conventions

In Chapter 1 we reviewed spinor-helicity variables, here we show the conventions used when manipulating those variables.

The vectors of the Pauli matrices take the form

$$(\sigma^\mu)_{\alpha\dot{\alpha}} = (\mathbb{1}, \vec{\sigma})_{\alpha\dot{\alpha}}, \quad (\bar{\sigma}^\mu)^{\dot{\alpha}\alpha} = (\mathbb{1}, -\vec{\sigma})^{\dot{\alpha}\alpha}, \tag{A.0.1}$$

where the Pauli matrices are

$$\sigma^0 = \begin{pmatrix} 1 & 0 \\ 0 & 1 \end{pmatrix}, \quad \sigma^1 = \begin{pmatrix} 0 & 1 \\ 1 & 0 \end{pmatrix}, \quad \sigma^2 = \begin{pmatrix} 0 & -i \\ i & 0 \end{pmatrix}, \quad \sigma^3 = \begin{pmatrix} 1 & 0 \\ 0 & -1 \end{pmatrix}. \tag{A.0.2}$$

In this notation the $SU(2)$ invariant tensors and their inverses are

$$\epsilon_{\alpha\beta} = \epsilon_{\dot{\alpha}\dot{\beta}} = i\sigma^2 = \begin{pmatrix} 0 & 1 \\ -1 & 0 \end{pmatrix}, \quad \epsilon^{\alpha\beta} = \epsilon^{\dot{\alpha}\dot{\beta}} = -i\sigma^2 = \begin{pmatrix} 0 & -1 \\ 1 & 0 \end{pmatrix} \tag{A.0.3}$$

hence

$$\epsilon_{\alpha\beta}\epsilon^{\beta\gamma} = \delta_\alpha^\gamma, \quad \epsilon_{\dot{\alpha}\dot{\beta}}\epsilon^{\dot{\beta}\dot{\gamma}} = \delta_{\dot{\alpha}}^{\dot{\gamma}}. \tag{A.0.4}$$

The indices of the spinors $\lambda_\alpha, \tilde{\lambda}_{\dot{\alpha}}$ are raised and lowered according to

$$\begin{aligned} \lambda_\alpha &= \epsilon_{\alpha\beta}\lambda^\beta, \qquad \lambda^\alpha = \epsilon^{\alpha\beta}\lambda_\beta, \\ \tilde{\lambda}_{\dot{\alpha}} &= \epsilon_{\dot{\alpha}\dot{\beta}}\tilde{\lambda}^{\dot{\beta}}, \qquad \tilde{\lambda}^{\dot{\alpha}} = \epsilon^{\dot{\alpha}\dot{\beta}}\tilde{\lambda}_{\dot{\beta}}, \end{aligned} \tag{A.0.5}$$

and the Pauli vectors $\sigma, \bar{\sigma}$ are related to each other by

$$(\sigma^\mu)_{\alpha\dot{\alpha}} = \epsilon^{\alpha\beta}\sigma^\mu_{\beta\dot{\beta}}\epsilon^{\dot{\alpha}\dot{\beta}}, \quad \sigma^\mu_{\alpha\beta} = \epsilon_{\dot{\alpha}\dot{\beta}}(\bar{\sigma}^\mu)^{\dot{\beta}\beta}\epsilon_{\alpha\beta}. \tag{A.0.6}$$

The spinor brackets are given by

$$\langle ij\rangle \coloneqq \langle \lambda_i \lambda_j\rangle = \epsilon_{\alpha\beta}\lambda_i^\alpha\lambda_j^\beta =: -\langle ji\rangle \tag{A.0.7}$$

$$[ij] \coloneqq [\tilde{\lambda}_i\tilde{\lambda}_j] = \epsilon^{\dot{\alpha}\dot{\beta}}\tilde{\lambda}_{i\dot{\alpha}}\tilde{\lambda}_{j\dot{\beta}} =: -[ji]. \tag{A.0.8}$$

where, in our conventions

$$\epsilon_{\alpha\beta}\lambda_i^\alpha\lambda_j^\beta = \lambda_i^\alpha\lambda_{j\alpha} = -\lambda_{i\alpha}\lambda_j^\alpha, \tag{A.0.9}$$

therefore

$$2(p_i \cdot p_j) = (\bar{p}_i)^{\dot{\alpha}\alpha}p_{j\alpha\dot{\alpha}} = \lambda_i^\alpha\tilde{\lambda}_i^{\dot{\alpha}}\lambda_{j\alpha}\tilde{\lambda}_{\dot{\alpha}j} = \langle ij\rangle[ji]. \tag{A.0.10}$$

Appendix B

Superconformal Algebra

As mentioned above, $\mathcal{N}=4$ SYM is a superconformal theory, the algebra of which we shall review here, following the conventions of [175]. The Poincaré algebra is generated by spacetime translations P_μ and Lorentz transformations (rotations and boosts) $M_{\mu\nu} = -M_{\nu\mu}, \mu,\nu = 0,1,2,3$. These satisfy the following commutation relations

$$\begin{aligned}[M_{\mu\nu}, P_\rho] &= -i\left(\eta_{\mu\rho}P_\nu - \eta_{\nu\rho}P_\mu\right), \\ [M_{\mu\nu}, M_{\rho\sigma}] &= -i\left(\eta_{\mu\sigma}M_{\nu\rho} + \eta_{\nu\rho}M_{\mu\sigma} - \eta_{\nu\sigma}M_{\mu\rho} - \eta_{\mu\rho}M_{\nu\sigma}\right),\end{aligned} \tag{B.0.1}$$

where $\eta_{\mu\nu} = \mathrm{diag}(1,-1,-1,-1)$ is the Minkowski metric. The Poincaré algebra can be extended to the conformal algebra by adding special conformal transformations K_μ and spacetime dilatations D. The additional commutation relations are

$$\begin{gathered}[D, P_\mu] = iP_\mu, \quad [D, M_{\mu\nu}] = 0, \quad [D, K_\mu] = -iK_\mu, \\ [M_{\mu\nu}, K_\rho] = -i\left(\eta_{\mu\nu}K_\nu - \eta_{\nu\rho}K_\mu\right), \\ [P_\mu, K_\nu] = 2i\left(M_{\mu\nu} + \eta_{\mu\nu}D\right).\end{gathered} \tag{B.0.2}$$

We have already introduced one extension of the Poincaré algebra, the supersymmetry algebra (1.3.2), the generators of which obey the following commutation relations

$$[M_\alpha{}^\beta, Q^A_\rho] = \delta_\rho{}^\beta Q^A_\alpha - \frac{1}{2}\delta_\alpha{}^\beta Q^A_\rho, \quad [\bar{M}^{\dot\alpha}{}_{\dot\beta}, \bar{Q}_{\dot\rho A}] = -\delta^{\dot\alpha}{}_{\dot\rho}\bar{Q}_{\dot\beta A} + \frac{1}{2}\delta^{\dot\alpha}{}_{\dot\beta}\bar{Q}_{\dot\rho A}. \tag{B.0.3}$$

where

$$M_\alpha{}^\beta = -\frac{i}{4}\sigma^\mu_{\alpha\dot\alpha}(\bar\sigma^\nu)^{\dot\alpha\beta}M_{\mu\nu}, \quad \bar{M}^{\dot\beta}{}_{\dot\alpha} = -\frac{i}{4}(\bar\sigma^\mu)^{\dot\beta\alpha}\sigma^\nu_{\alpha\dot\alpha}M_{\mu\nu}. \tag{B.0.4}$$

Demanding closure of the algebra requires the existence of a second set of supercharges - *superconformal* supercharges - $S^\alpha_A/\bar{S}^{\dot\alpha A}$ which can be obtained by the action of K_μ on the supercharges $Q/\bar{Q}$

$$[K^\mu, Q^A_\alpha] = -\sigma^\mu_{\alpha\dot\alpha}\bar{S}^{\dot\alpha A}, \quad [K^\mu, \bar{Q}_{\dot\alpha A}] = S^\alpha_A\sigma^\mu_{\alpha\dot\alpha}, \quad \{\bar{S}^{\dot\alpha A}, S^\alpha_B\} = 2\delta^A{}_B\bar{K}^{\dot\alpha\alpha} \tag{B.0.5}$$

as well as the $SU(4)\cong SO(6)$ R-symmetry generators $R_{AB}, A,B = 1,\ldots,4$. The commutation relations between the supercharges $Q,\bar{Q}/S,\bar{S}$ and the dilatation operator D are

$$[D, Q^A_\alpha] = \frac{i}{2}Q^A_\alpha, \quad [D, \bar{Q}_{\dot\alpha A}] = \frac{i}{2}\bar{Q}_{\dot\alpha A}, \quad [D, S^\alpha_A] = -\frac{i}{2}S^\alpha_A, \quad [D, \bar{S}^{\dot\alpha A}] = -\frac{i}{2}\bar{S}^{\dot\alpha A}. \tag{B.0.6}$$

Finally the commutation relations between the supercharges are

$$\begin{aligned}\{Q_\alpha^A, S_B^\beta\} &= 4[\delta^A{}_B(M_\alpha{}^\beta - \frac{i}{2}\delta_\alpha{}^\beta D) - \delta_\alpha{}^\beta R^A{}_B],\\ \{\bar{S}^{\dot\alpha A}, \bar{Q}_{\dot\beta B}\} &= 4[\delta^A{}_B(\bar{M}_{\dot\beta}^{\dot\alpha} + \frac{i}{2}\delta^{\dot\alpha}{}_{\dot\beta} D) - \delta^{\dot\alpha}{}_{\dot\beta} R^A{}_B].\end{aligned} \tag{B.0.7}$$

The superconformal group of $\mathcal{N}=4$ SYM is $PSU(2,2|4)$ which corresponds to the Lorentz group $SU(2)_L \times SU(2)_R$ times the R-symmetry group $SU(4)$.

Here we provide some of the multi-particle generators in the dual superspace $(x_i^{\alpha\dot\alpha}, \lambda_i^\alpha, \theta_i^{A\alpha})$ relevant for the discussions in this thesis. For a comprehensive list we direct the reader to [3]. The generators are

$$P_{\alpha\dot\alpha} = \sum_{i=1}^n \frac{\partial}{\partial x_i^{\alpha\dot\alpha}}, \tag{B.0.8}$$

$$Q_{A\alpha} = \sum_{i=1}^n \frac{\partial}{\partial \theta_i^{A\alpha}}, \tag{B.0.9}$$

$$\bar{Q}_{\dot\alpha}^A = \sum_{i=1}^n \theta_i^{A\alpha} \frac{\partial}{\partial x_i^{\alpha\dot\alpha}}, \tag{B.0.10}$$

$$S_\alpha^A = \sum_{i=1}^n \left[\theta_{i\alpha}^B \theta_i^{\beta A} \frac{\partial}{\partial \theta_i^{\beta B}} - x_{i\alpha}^{\dot\beta} \theta_i^{\beta A} \frac{\partial}{\partial x_i^{\beta\dot\beta}} - \lambda_{i\alpha} \theta_i^{\gamma A} \frac{\partial}{\partial \lambda_i^\gamma}\right], \tag{B.0.11}$$

$$\bar{S}_A^{\dot\alpha} = \sum_{i=1}^n x_i^{\alpha\dot\alpha} \frac{\partial}{\partial \theta_i^{A\alpha}}. \tag{B.0.12}$$

Bibliography

[1] Edward Witten. "Perturbative gauge theory as a string theory in twistor space". In: *Commun. Math. Phys.* 252 (2004), pp. 189–258. DOI: 10.1007/s00220-004-1187-3. arXiv: hep-th/0312171.

[2] Nima Arkani-Hamed et al. "A Duality For The S Matrix". In: *JHEP* 03 (2010), p. 020. DOI: 10.1007/JHEP03(2010)020. arXiv: 0907.5418 [hep-th].

[3] J.M. Drummond et al. "Dual superconformal symmetry of scattering amplitudes in $\mathcal{N} = 4$ super-Yang-Mills theory". In: *Nucl.Phys.* B828 (2010), pp. 317–374. DOI: 10.1016/j.nuclphysb.2009.11.022. arXiv: 0807.1095 [hep-th].

[4] Andreas Brandhuber, Paul Heslop, and Gabriele Travaglini. "A Note on dual superconformal symmetry of the N=4 super Yang-Mills S-matrix". In: *Phys. Rev. D* 78 (2008), p. 125005. DOI: 10.1103/PhysRevD.78.125005. arXiv: 0807.4097 [hep-th].

[5] L.J. Mason and David Skinner. "Dual Superconformal Invariance, Momentum Twistors and Grassmannians". In: *JHEP* 0911 (2009), p. 045. DOI: 10.1088/1126-6708/2009/11/045. arXiv: 0909.0250 [hep-th].

[6] John Golden et al. "Motivic Amplitudes and Cluster Coordinates". In: *JHEP* 1401 (2014), p. 091. DOI: 10.1007/JHEP01(2014)091. arXiv: 1305.1617 [hep-th].

[7] Freddy Cachazo et al. "Scattering Equations: From Projective Spaces to Tropical Grassmannians". In: (2019). arXiv: 1903.08904 [hep-th].

[8] James Drummond, Jack Foster, and Ömer Gürdoğan. "Cluster Adjacency Properties of Scattering Amplitudes in $N = 4$ Supersymmetric Yang-Mills Theory". In: *Phys. Rev. Lett.* 120.16 (2018), p. 161601. DOI: 10.1103/PhysRevLett.120.161601. arXiv: 1710.10953 [hep-th].

[9] James Drummond, Jack Foster, and Ömer Gürdoğan. "Cluster adjacency beyond MHV". In: *JHEP* 03 (2019), p. 086. DOI: 10.1007/JHEP03(2019)086. arXiv: 1810.08149 [hep-th].

[10] James Drummond et al. "Cluster adjacency and the four-loop NMHV heptagon". In: *JHEP* 03 (2019), p. 087. DOI: 10.1007/JHEP03(2019)087. arXiv: 1812.04640 [hep-th].

[11] James Drummond et al. "Tropical Grassmannians, cluster algebras and scattering amplitudes". In: *JHEP* 04 (2020), p. 146. DOI: 10.1007/JHEP04(2020)146. arXiv: 1907.01053 [hep-th].

[12] James Drummond et al. "Algebraic singularities of scattering amplitudes from tropical geometry". In: (2019). arXiv: 1912.08217 [hep-th].

[13] James Drummond et al. "Tropical fans, scattering equations and amplitudes". In: (2020). arXiv: 2002.04624 [hep-th].

[14] H. Lehmann, K. Symanzik, and W. Zimmermann. "Zur Formulierung quantisierter Feldtheorien". In: *Nuovo Cimento* 1 (1955), pp. 205–25.

[15] Stephen J. Parke and T. R. Taylor. "An Amplitude for n Gluon Scattering". In: *Phys. Rev. Lett.* 56 (1986), p. 2459. DOI: 10.1103/PhysRevLett.56.2459.

[16] Richard John Eden et al. *The analytic S-matrix*. Cambridge: Cambridge Univ. Press, 1966.

[17] Ruth Britto et al. "Direct proof of tree-level recursion relation in Yang-Mills theory". In: *Phys. Rev. Lett.* 94 (2005), p. 181602. DOI: 10.1103/PhysRevLett.94.181602. arXiv: hep-th/0501052 [hep-th].

[18] Zvi Bern et al. "One loop n point gauge theory amplitudes, unitarity and collinear limits". In: *Nucl.Phys.* B425 (1994), pp. 217–260. DOI: 10.1016/0550-3213(94)90179-1. arXiv: hep-ph/9403226 [hep-ph].

[19] Miguel F. Paulos et al. "The S-matrix Bootstrap III: Higher Dimensional Amplitudes". In: (2017). arXiv: 1708.06765 [hep-th].

[20] Andrea L. Guerrieri, Joao Penedones, and Pedro Vieira. "Bootstrapping QCD: the Lake, the Peninsula and the Kink". In: (2018). arXiv: 1810.12849 [hep-th].

[21] Riccardo Rattazzi et al. "Bounding scalar operator dimensions in 4D CFT". In: *JHEP* 12 (2008), p. 031. DOI: 10.1088/1126-6708/2008/12/031. arXiv: 0807.0004 [hep-th].

[22] Miguel F. Paulos et al. "The S-matrix bootstrap. Part I: QFT in AdS". In: *JHEP* 11 (2017), p. 133. DOI: 10.1007/JHEP11(2017)133. arXiv: 1607.06109 [hep-th].

[23] Nima Arkani-Hamed et al. "Scattering Amplitudes and the Positive Grassmannian". In: (2012). arXiv: 1212.5605 [hep-th].

[24] Nima Arkani-Hamed and Jaroslav Trnka. "The Amplituhedron". In: *JHEP* 1410 (2014), p. 30. DOI: 10.1007/JHEP10(2014)030. arXiv: 1312.2007 [hep-th].

[25] Kuo-Tsai Chen. "Iterated path integrals". In: *Bull. Am. Math. Soc.* 83 (1977), pp. 831–879. DOI: 10.1090/S0002-9904-1977-14320-6.

[26] E. Remiddi and J.A.M. Vermaseren. "Harmonic polylogarithms". In: *Int.J.Mod.Phys.* A15 (2000), pp. 725–754. DOI: 10.1142/S0217751X00000367. arXiv: hep-ph/9905237 [hep-ph].

[27] A. B. Goncharov. "Galois symmetries of fundamental groupoids and noncommutative geometry". In: *Duke Math. J.* 128 (2005), p. 209. DOI: 10.1215/S0012-7094-04-12822-2. arXiv: math/0208144 [math.AG].

[28] Francis C. S. Brown. "Multiple zeta values and periods of moduli spaces $M_{0,n}(\mathbb{R})$". In: *Annales Sci. Ecole Norm. Sup.* 42 (2009), p. 371. arXiv: math/0606419 [math.AG].

[29] Francis C. S. Brown and Andrey Levin. *Multiple Elliptic Polylogarithms*. 2011. arXiv: 1110.6917 [math.NT].

[30] Simon Caron-Huot and Kasper J. Larsen. "Uniqueness of two-loop master contours". In: *JHEP* 10 (2012), p. 026. DOI: 10.1007/JHEP10(2012)026. arXiv: 1205.0801 [hep-ph].

[31] Spencer Bloch and Pierre Vanhove. "The elliptic dilogarithm for the sunset graph". In: *J. Number Theor.* 148 (2015), pp. 328–364. DOI: 10.1016/j.jnt.2014.09.032. arXiv: 1309.5865 [hep-th].

[32] Jacob L. Bourjaily et al. "Elliptic Double-Box Integrals: Massless Scattering Amplitudes beyond Polylogarithms". In: *Phys. Rev. Lett.* 120.12 (2018), p. 121603. DOI: 10.1103/PhysRevLett.120.121603. arXiv: 1712.02785 [hep-th].

[33] Jacob L. Bourjaily et al. "Traintracks through Calabi-Yau Manifolds: Scattering Amplitudes beyond Elliptic Polylogarithms". In: *Phys. Rev. Lett.* 121.7 (2018), p. 071603. DOI: 10.1103/PhysRevLett.121.071603. arXiv: 1805.09326 [hep-th].

[34] Johannes Broedel et al. "Elliptic Feynman integrals and pure functions". In: (2018). arXiv: 1809.10698 [hep-th].

[35] Johannes M. Henn. "Multiloop integrals in dimensional regularization made simple". In: *Phys. Rev. Lett.* 110 (2013), p. 251601. DOI: 10.1103/PhysRevLett.110.251601. arXiv: 1304.1806 [hep-th].

[36] K. G. Chetyrkin and F. V. Tkachov. "Integration by Parts: The Algorithm to Calculate beta Functions in 4 Loops". In: *Nucl. Phys.* B192 (1981), pp. 159–204. DOI: 10.1016/0550-3213(81)90199-1.

[37] A. V. Kotikov. "Differential equations method: New technique for massive Feynman diagrams calculation". In: *Phys. Lett.* B254 (1991), pp. 158–164. DOI: 10.1016/0370-2693(91)90413-K.

[38] Zvi Bern, Lance J. Dixon, and David A. Kosower. "Dimensionally regulated pentagon integrals". In: *Nucl. Phys.* B412 (1994), pp. 751–816. DOI: 10.1016/0550-3213(94)90398-0. arXiv: hep-ph/9306240 [hep-ph].

[39] Ettore Remiddi. "Differential equations for Feynman graph amplitudes". In: *Nuovo Cim.* A110 (1997), pp. 1435–1452. arXiv: hep-th/9711188 [hep-th].

[40] Lance J. Dixon, James M. Drummond, and Johannes M. Henn. "Bootstrapping the three-loop hexagon". In: *JHEP* 1111 (2011), p. 023. DOI: 10.1007/JHEP11(2011)023. arXiv: 1108.4461 [hep-th].

[41] Lance J. Dixon, James M. Drummond, and Johannes M. Henn. "Analytic result for the two-loop six-point NMHV amplitude in $\mathcal{N} = 4$ super Yang-Mills theory". In: *JHEP* 1201 (2012), p. 024. DOI: 10.1007/JHEP01(2012)024. arXiv: 1111.1704 [hep-th].

[42] Lance J. Dixon et al. "Hexagon functions and the three-loop remainder function". In: *JHEP* 1312 (2013), p. 049. DOI: 10.1007/JHEP12(2013)049. arXiv: 1308.2276 [hep-th].

[43] Lance J. Dixon et al. "The four-loop remainder function and multi-Regge behavior at NNLLA in planar $\mathcal{N} = 4$ super-Yang-Mills theory". In: *JHEP* 1406 (2014), p. 116. DOI: 10.1007/JHEP06(2014)116. arXiv: 1402.3300 [hep-th].

[44] Lance J. Dixon and Matt von Hippel. "Bootstrapping an NMHV amplitude through three loops". In: *JHEP* 1410 (2014), p. 65. DOI: 10.1007/JHEP10(2014)065. arXiv: 1408.1505 [hep-th].

[45] James M. Drummond, Georgios Papathanasiou, and Marcus Spradlin. "A Symbol of Uniqueness: The Cluster Bootstrap for the 3-Loop MHV Heptagon". In: *JHEP* 03 (2015), p. 072. DOI: 10.1007/JHEP03(2015)072. arXiv: 1412.3763 [hep-th].

[46] Lance J. Dixon, Matt von Hippel, and Andrew J. McLeod. "The four-loop six-gluon NMHV ratio function". In: *JHEP* 01 (2016), p. 053. DOI: 10.1007/JHEP01(2016)053. arXiv: 1509.08127 [hep-th].

[47] Simon Caron-Huot et al. "Bootstrapping a Five-Loop Amplitude Using Steinmann Relations". In: *Phys. Rev. Lett.* 117.24 (2016), p. 241601. DOI: 10.1103/PhysRevLett.117.241601. arXiv: 1609.00669 [hep-th].

[48] Lance J. Dixon et al. "Heptagons from the Steinmann Cluster Bootstrap". In: *JHEP* 02 (2017), p. 137. DOI: 10.1007/JHEP02(2017)137. arXiv: 1612.08976 [hep-th].

[49] Simon Caron-Huot et al. "Six-Gluon amplitudes in planar $\mathcal{N} = 4$ super-Yang-Mills theory at six and seven loops". In: *JHEP* 08 (2019), p. 016. DOI: 10.1007/JHEP08(2019)016. arXiv: 1903.10890 [hep-th].

[50] Luis F. Alday and Juan Martin Maldacena. "Gluon scattering amplitudes at strong coupling". In: *JHEP* 0706 (2007), p. 064. DOI: 10.1088/1126-6708/2007/06/064. arXiv: 0705.0303 [hep-th].

[51] J.M. Drummond, G.P. Korchemsky, and E. Sokatchev. "Conformal properties of four-gluon planar amplitudes and Wilson loops". In: *Nucl.Phys.* B795 (2008), pp. 385–408. DOI: 10.1016/j.nuclphysb.2007.11.041. arXiv: 0707.0243 [hep-th].

[52] Andreas Brandhuber, Paul Heslop, and Gabriele Travaglini. "MHV amplitudes in $\mathcal{N} = 4$ super Yang-Mills and Wilson loops". In: *Nucl.Phys.* B794 (2008), pp. 231–243. DOI: 10.1016/j.nuclphysb.2007.11.002. arXiv: 0707.1153 [hep-th].

[53] J.M. Drummond et al. "On planar gluon amplitudes/Wilson loops duality". In: *Nucl.Phys.* B795 (2008), pp. 52–68. DOI: 10.1016/j.nuclphysb.2007.11.007. arXiv: 0709.2368 [hep-th].

[54] Z. Bern et al. "The Two-Loop Six-Gluon MHV Amplitude in Maximally Supersymmetric Yang-Mills Theory". In: *Phys.Rev.* D78 (2008), p. 045007. DOI: 10.1103/PhysRevD.78.045007. arXiv: 0803.1465 [hep-th].

[55] J.M. Drummond et al. "Hexagon Wilson loop = six-gluon MHV amplitude". In: *Nucl.Phys.* B815 (2009), pp. 142–173. DOI: 10.1016/j.nuclphysb.2009.02.015. arXiv: 0803.1466 [hep-th].

[56] Luis F. Alday et al. "An Operator Product Expansion for Polygonal null Wilson Loops". In: *JHEP* 1104 (2011), p. 088. DOI: 10.1007/JHEP04(2011)088. arXiv: 1006.2788 [hep-th].

[57] Benjamin Basso, Amit Sever, and Pedro Vieira. "Spacetime and Flux Tube S-Matrices at Finite Coupling for $\mathcal{N} = 4$ Supersymmetric Yang-Mills Theory". In: *Phys.Rev.Lett.* 111.9 (2013), p. 091602. DOI: 10.1103/PhysRevLett.111.091602. arXiv: 1303.1396 [hep-th].

[58] Benjamin Basso, Amit Sever, and Pedro Vieira. "Space-time S-matrix and Flux tube S-matrix II. Extracting and Matching Data". In: *JHEP* 1401 (2014), p. 008. DOI: 10.1007/JHEP01(2014)008. arXiv: 1306.2058 [hep-th].

[59] Benjamin Basso, Amit Sever, and Pedro Vieira. "Space-time S-matrix and Flux-tube S-matrix III. The two-particle contributions". In: *JHEP* 1408 (2014), p. 085. DOI: 10.1007/JHEP08(2014)085. arXiv: 1402.3307 [hep-th].

[60] Benjamin Basso, Amit Sever, and Pedro Vieira. "Space-time S-matrix and Flux-tube S-matrix IV. Gluons and Fusion". In: *JHEP* 1409 (2014), p. 149. DOI: 10.1007/JHEP09(2014)149. arXiv: 1407.1736 [hep-th].

[61] Juan Martin Maldacena. "The Large N limit of superconformal field theories and supergravity". In: *Int. J. Theor. Phys.* 38 (1999), pp. 1113–1133. DOI: 10.1023/A:1026654312961. arXiv: hep-th/9711200.

[62] John Golden et al. "Cluster Polylogarithms for Scattering Amplitudes". In: *J. Phys.* A47.47 (2014), p. 474005. DOI: 10.1088/1751-8113/47/47/474005. arXiv: 1401.6446 [hep-th].

[63] S Fomin and A Zelevinsky. "Cluster algebras I: Foundations". In: *J. Am. Math. Soc.* 15.2 (2002), pp. 497–529. DOI: 10.1090/S0894-0347-01-00385-X. arXiv: math/0104151 [math.RT].

[64] S Fomin and A Zelevinsky. "Cluster algebras II: Finite type classification". In: *Invent. Math.* 154.1 (2003), pp. 63–121. DOI: 10.1007/s00222-003-0302-y. arXiv: math/0208229 [math.RA].

[65] Sergey Fomin and Andrei Zelevinsky. "Cluster algebras IV: Coefficients". In: (2006). arXiv: math/0602259 [math.RA].

[66] Alexander B. Goncharov et al. "Classical Polylogarithms for Amplitudes and Wilson Loops". In: *Phys.Rev.Lett.* 105 (2010), p. 151605. DOI: 10.1103/PhysRevLett.105.151605. arXiv: 1006.5703 [hep-th].

[67] O Steinmann. "Über den Zusammenhang zwischen den Wightmanfunktionen und der retardierten Kommutatoren". In: *Helv. Physica Acta* 33 (1960), p. 257.

[68] O Steinmann. "Wightman-Funktionen und retardierten Kommutatoren. II". In: *Helv. Physica Acta* 33 (1960), p. 347.

[69] J. Bartels, L.N. Lipatov, and Agustin Sabio Vera. "BFKL Pomeron, Reggeized gluons and Bern-Dixon-Smirnov amplitudes". In: *Phys.Rev.* D80 (2009), p. 045002. DOI: 10.1103/PhysRevD.80.045002. arXiv: 0802.2065 [hep-th].

[70] Simon Caron-Huot et al. "The Cosmic Galois Group and Extended Steinmann Relations for Planar $\mathcal{N} = 4$ SYM Amplitudes". In: *JHEP* 09 (2019), p. 061. DOI: 10.1007/JHEP09(2019)061. arXiv: 1906.07116 [hep-th].

[71] Alan.R. White. "The Past and future of S matrix theory". In: (2000), pp. 1483–1504. arXiv: hep-ph/0002303 [hep-ph].

[72] E. A. Kuraev, L. N. Lipatov, and Victor S. Fadin. "Multi-Reggeon processes in the Yang-Mills theory". In: *Sov. Phys. JETP* 44 (1976), p. 443.

[73] E. A. Kuraev, L. N. Lipatov, and Victor S. Fadin. "The Pomeranchuk singularity in nonabelian gauge theories". In: *Sov. Phys. JETP* 45 (1977), p. 199.

[74] I. I. Balitsky and L. N. Lipatov. "The Pomeranchuk singularity in quantum chromodynamics". In: *Sov. J. Nucl. Phys.* 28 (1978), p. 822.

[75] Lance J. Dixon, Claude Duhr, and Jeffrey Pennington. "Single-valued harmonic polylogarithms and the multi-Regge limit". In: *JHEP* 1210 (2012), p. 074. DOI: 10.1007/JHEP10(2012)074. arXiv: 1207.0186 [hep-th].

[76] Vittorio Del Duca et al. "Multi-Regge kinematics and the moduli space of Riemann spheres with marked points". In: *JHEP* 08 (2016), p. 152. DOI: 10.1007/JHEP08(2016)152. arXiv: 1606.08807 [hep-th].

[77] Benjamin Basso, Simon Caron-Huot, and Amit Sever. "Adjoint BFKL at finite coupling: a short-cut from the collinear limit". In: *JHEP* 01 (2015), p. 027. DOI: 10.1007/JHEP01(2015)027. arXiv: 1407.3766 [hep-th].

[78] Vittorio Del Duca et al. "The seven-gluon amplitude in multi-Regge kinematics beyond leading logarithmic accuracy". In: *JHEP* 06 (2018), p. 116. DOI: 10.1007/JHEP06(2018)116. arXiv: 1801.10605 [hep-th].

[79] Freddy Cachazo, Song He, and Ellis Ye Yuan. "Scattering equations and Kawai-Lewellen-Tye orthogonality". In: *Phys. Rev.* D90.6 (2014), p. 065001. DOI: 10.1103/PhysRevD.90.065001. arXiv: 1306.6575 [hep-th].

[80] Freddy Cachazo, Song He, and Ellis Ye Yuan. "Scattering of Massless Particles in Arbitrary Dimensions". In: *Phys. Rev. Lett.* 113.17 (2014), p. 171601. DOI: 10.1103/PhysRevLett.113.171601. arXiv: 1307.2199 [hep-th].

[81] Freddy Cachazo, Song He, and Ellis Ye Yuan. "Scattering of Massless Particles: Scalars, Gluons and Gravitons". In: *JHEP* 07 (2014), p. 033. DOI: 10.1007/JHEP07(2014)033. arXiv: 1309.0885 [hep-th].

[82] Nima Arkani-Hamed et al. "Scattering Forms and the Positive Geometry of Kinematics, Color and the Worldsheet". In: *JHEP* 05 (2018), p. 096. DOI: 10.1007/JHEP05(2018)096. arXiv: 1711.09102 [hep-th].

[83] David Speyer and Lauren K. Williams. "The tropical totally positive Grassmannian". In: *arXiv Mathematics e-prints*, math/0312297 (2003), math/0312297. arXiv: math/0312297 [math.CO].

[84] Ruth Britto, Freddy Cachazo, and Bo Feng. "New recursion relations for tree amplitudes of gluons". In: *Nucl. Phys. B* 715 (2005), pp. 499–522. DOI: 10.1016/j.nuclphysb.2005.02.030. arXiv: hep-th/0412308.

[85] S.D. Badger et al. "Recursion relations for gauge theory amplitudes with massive particles". In: *JHEP* 07 (2005), p. 025. DOI: 10.1088/1126-6708/2005/07/025. arXiv: hep-th/0504159.

[86] Nima Arkani-Hamed et al. "The All-Loop Integrand For Scattering Amplitudes in Planar N=4 SYM". In: *JHEP* 1101 (2011), p. 041. DOI: 10.1007/JHEP01(2011)041. arXiv: 1008.2958 [hep-th].

[87] Rutger H. Boels. "On BCFW shifts of integrands and integrals". In: *JHEP* 11 (2010), p. 113. DOI: 10.1007/JHEP11(2010)113. arXiv: 1008.3101 [hep-th].

[88] Nima Arkani-Hamed, Freddy Cachazo, and Jared Kaplan. "What is the Simplest Quantum Field Theory?" In: *JHEP* 1009 (2010), p. 016. DOI: 10.1007/JHEP09(2010)016. arXiv: 0808.1446 [hep-th].

[89] Freddy Cachazo, Song He, and Ellis Ye Yuan. "Scattering Equations and Matrices: From Einstein To Yang-Mills, DBI and NLSM". In: *JHEP* 07 (2015), p. 149. DOI: 10.1007/JHEP07(2015)149. arXiv: 1412.3479 [hep-th].

[90] Louise Dolan and Peter Goddard. "Proof of the Formula of Cachazo, He and Yuan for Yang-Mills Tree Amplitudes in Arbitrary Dimension". In: *JHEP* 05 (2014), p. 010. DOI: 10.1007/JHEP05(2014)010. arXiv: 1311.5200 [hep-th].

[91] V. P. Nair. "A Current Algebra for Some Gauge Theory Amplitudes". In: *Phys. Lett.* B214 (1988), pp. 215–218. DOI: 10.1016/0370-2693(88)91471-2.

[92] J.M. Drummond and J.M. Henn. "All tree-level amplitudes in N=4 SYM". In: *JHEP* 04 (2009), p. 018. DOI: 10.1088/1126-6708/2009/04/018. arXiv: 0808.2475 [hep-th].

[93] J.M. Drummond et al. "The hexagon Wilson loop and the BDS ansatz for the six-gluon amplitude". In: *Phys.Lett.* B662 (2008), pp. 456–460. DOI: 10.1016/j.physletb.2008.03.032. arXiv: 0712.4138 [hep-th].

[94] Nathan Berkovits and Juan Maldacena. "Fermionic T-Duality, Dual Superconformal Symmetry, and the Amplitude/Wilson Loop Connection". In: *JHEP* 0809 (2008), p. 062. DOI: 10.1088/1126-6708/2008/09/062. arXiv: 0807.3196 [hep-th].

[95] Luis F. Alday and Juan Maldacena. "Null polygonal Wilson loops and minimal surfaces in Anti-de-Sitter space". In: *JHEP* 11 (2009), p. 082. DOI: 10.1088/1126-6708/2009/11/082. arXiv: 0904.0663 [hep-th].

[96] Luis F. Alday et al. "Y-system for Scattering Amplitudes". In: *J. Phys.* A43 (2010), p. 485401. DOI: 10.1088/1751-8113/43/48/485401. arXiv: 1002.2459 [hep-th].

[97] L.J. Mason and David Skinner. "The Complete Planar S-matrix of $\mathcal{N} = 4$ SYM as a Wilson Loop in Twistor Space". In: *JHEP* 1012 (2010), p. 018. DOI: 10.1007/JHEP12(2010)018. arXiv: 1009.2225 [hep-th].

[98] Simon Caron-Huot. "Notes on the scattering amplitude / Wilson loop duality". In: *JHEP* 1107 (2011), p. 058. DOI: 10.1007/JHEP07(2011)058. arXiv: 1010.1167 [hep-th].

[99] Andrew Hodges. "Eliminating spurious poles from gauge-theoretic amplitudes". In: *JHEP* 1305 (2013), p. 135. DOI: 10.1007/JHEP05(2013)135. arXiv: 0905.1473 [hep-th].

[100] James M. Drummond, Johannes M. Henn, and Jan Plefka. "Yangian symmetry of scattering amplitudes in $\mathcal{N} = 4$ super Yang-Mills theory". In: *JHEP* 0905 (2009), p. 046. DOI: 10.1088/1126-6708/2009/05/046. arXiv: 0902.2987 [hep-th].

[101] C. Anastasiou et al. "Planar amplitudes in maximally supersymmetric Yang-Mills theory". In: *Phys.Rev.Lett.* 91 (2003), p. 251602. DOI: 10.1103/PhysRevLett.91.251602. arXiv: hep-th/0309040 [hep-th].

[102] Lorenzo Magnea and George Sterman. "Analytic continuation of the Sudakov form factor in QCD". In: *Phys. Rev. D* 42 (12 1990), pp. 4222–4227. DOI: 10.1103/PhysRevD.42.4222. URL: https://link.aps.org/doi/10.1103/PhysRevD.42.4222.

[103] George Sterman and Maria E. Tejeda-Yeomans. "Multi-loop amplitudes and resummation". In: *Physics Letters B* 552.1-2 (2003), 48–56. ISSN: 0370-2693. DOI: 10.1016/s0370-2693(02)03100-3. URL: http://dx.doi.org/10.1016/S0370-2693(02)03100-3.

[104] J.M. Drummond et al. "Conformal Ward identities for Wilson loops and a test of the duality with gluon amplitudes". In: *Nucl.Phys.* B826 (2010), pp. 337–364. DOI: 10.1016/j.nuclphysb.2009.10.013. arXiv: 0712.1223 [hep-th].

[105] Zvi Bern, Lance J. Dixon, and Vladimir A. Smirnov. "Iteration of planar amplitudes in maximally supersymmetric Yang-Mills theory at three loops and beyond". In: *Phys. Rev.* D72 (2005), p. 085001. DOI: 10.1103/PhysRevD.72.085001. arXiv: hep-th/0505205 [hep-th].

[106] Johannes M. Henn et al. "Higgs-regularized three-loop four-gluon amplitude in N=4 SYM: exponentiation and Regge limits". In: *JHEP* 04 (2010), p. 038. DOI: 10.1007/JHEP04(2010)038. arXiv: 1001.1358 [hep-th].

[107] Z. Bern et al. "The Complete Four-Loop Four-Point Amplitude in N=4 Super-Yang-Mills Theory". In: *Phys. Rev. D* 82 (2010), p. 125040. DOI: 10.1103/PhysRevD.82.125040. arXiv: 1008.3327 [hep-th].

[108] Z. Bern et al. "The Five-Loop Four-Point Amplitude of N=4 super-Yang-Mills Theory". In: *Phys. Rev. Lett.* 109 (2012), p. 241602. DOI: 10.1103/PhysRevLett.109.241602. arXiv: 1207.6666 [hep-th].

[109] Z. Bern et al. "Two-loop iteration of five-point N=4 super-Yang-Mills amplitudes". In: *Phys. Rev. Lett.* 97 (2006), p. 181601. DOI: 10.1103/PhysRevLett.97.181601. arXiv: hep-th/0604074.

[110] Freddy Cachazo, Marcus Spradlin, and Anastasia Volovich. "Iterative structure within the five-particle two-loop amplitude". In: *Phys. Rev. D* 74 (2006), p. 045020. DOI: 10.1103/PhysRevD.74.045020. arXiv: hep-th/0602228.

[111] Stefano Catani. "The Singular behavior of QCD amplitudes at two loop order". In: *Phys. Lett.* B427 (1998), pp. 161–171. DOI: 10.1016/S0370-2693(98)00332-3. arXiv: hep-ph/9802439 [hep-ph].

[112] J.M. Drummond et al. "Magic identities for conformal four-point integrals". In: *JHEP* 0701 (2007), p. 064. DOI: 10.1088/1126-6708/2007/01/064. arXiv: hep-th/0607160 [hep-th].

[113] Zvi Bern et al. "The Four-Loop Planar Amplitude and Cusp Anomalous Dimension in Maximally Supersymmetric Yang-Mills Theory". In: *Phys.Rev.* D75 (2007), p. 085010. DOI: 10.1103/PhysRevD.75.085010. arXiv: hep-th/0610248 [hep-th].

[114] Z. Bern et al. "Maximally supersymmetric planar Yang-Mills amplitudes at five loops". In: *Phys.Rev.* D76 (2007), p. 125020. DOI: 10.1103/PhysRevD.76.125020. arXiv: 0705.1864 [hep-th].

[115] Luis F. Alday, Davide Gaiotto, and Juan Maldacena. "Thermodynamic Bubble Ansatz". In: *JHEP* 09 (2011), p. 032. DOI: 10.1007/JHEP09(2011)032. arXiv: 0911.4708 [hep-th].

[116] Vittorio Del Duca, Claude Duhr, and Vladimir A. Smirnov. "The Two-Loop Hexagon Wilson Loop in $\mathcal{N} = 4$ SYM". In: *JHEP* 1005 (2010), p. 084. DOI: 10.1007/JHEP05(2010)084. arXiv: 1003.1702 [hep-th].

[117] Claude Duhr. "Hopf algebras, coproducts and symbols: an application to Higgs boson amplitudes". In: *JHEP* 1208 (2012), p. 043. DOI: 10.1007/JHEP08(2012)043. arXiv: 1203.0454 [hep-ph].

[118] The SpaSM group. *SpaSM: a Sparse direct Solver Modulo p*. v1.2. http://github.com/cbouilla/spasm. 2017.

[119] Davide Gaiotto et al. "Pulling the straps of polygons". In: *JHEP* 1112 (2011), p. 011. DOI: 10.1007/JHEP12(2011)011. arXiv: 1102.0062 [hep-th].

[120] S. Caron-Huot. "Superconformal symmetry and two-loop amplitudes in planar $\mathcal{N} = 4$ super Yang-Mills". In: *JHEP* 1112 (2011), p. 066. DOI: 10.1007/JHEP12(2011)066. arXiv: 1105.5606 [hep-th].

[121] Simon Caron-Huot and Song He. "Jumpstarting the All-Loop S-Matrix of Planar $\mathcal{N} = 4$ Super Yang-Mills". In: *JHEP* 1207 (2012), p. 174. DOI: 10.1007/JHEP07(2012)174. arXiv: 1112.1060 [hep-th].

[122] Vittorio Del Duca. "Equivalence of the Parke-Taylor and the Fadin-Kuraev-Lipatov amplitudes in the high-energy limit". In: *Phys. Rev. D* 52 (1995), pp. 1527–1534. DOI: 10.1103/PhysRevD.52.1527. arXiv: hep-ph/9503340.

[123] L.N. Lipatov. "Reggeization of the Vector Meson and the Vacuum Singularity in Nonabelian Gauge Theories". In: *Sov. J. Nucl. Phys.* 23 (1976), pp. 338–345.

[124] L.N. Lipatov. "High-energy scattering in QCD and in quantum gravity and two-dimensional field theories". In: *Nucl. Phys. B* 365 (1991), pp. 614–632. DOI: 10.1016/0550-3213(91)90512-V.

[125] J. Bartels, V. Schomerus, and M. Sprenger. "Multi-Regge Limit of the n-Gluon Bubble Ansatz". In: *JHEP* 11 (2012), p. 145. DOI: 10.1007/JHEP11(2012)145. arXiv: 1207.4204 [hep-th].

[126] J. Bartels, V. Schomerus, and M. Sprenger. "The Bethe Roots of Regge Cuts in Strongly Coupled $\mathcal{N} = 4$ SYM Theory". In: (2014). arXiv: 1411.2594 [hep-th].

[127] Nima Arkani-Hamed. "Scattering amplitudes from combinatorial geometry at infinity". In: *talk at Amplitudes 2018* (2018).

[128] J. Bartels, L.N. Lipatov, and Agustin Sabio Vera. "$\mathcal{N} = 4$ supersymmetric Yang Mills scattering amplitudes at high energies: The Regge cut contribution". In: *Eur.Phys.J.* C65 (2010), pp. 587–605. DOI: 10.1140/epjc/s10052-009-1218-5. arXiv: 0807.0894 [hep-th].

[129] Georgios Papathanasiou. "The Steinmann Cluster Bootstrap for $\mathcal{N} = 4$ SYM Amplitudes". In: *talk at Amplitudes 2017* (2017).

[130] Nima Arkani-Hamed et al. "Local Integrals for Planar Scattering Amplitudes". In: *JHEP* 06 (2012), p. 125. DOI: 10.1007/JHEP06(2012)125. arXiv: 1012.6032 [hep-th].

[131] James M. Drummond, Johannes M. Henn, and Jaroslav Trnka. "New differential equations for on-shell loop integrals". In: *JHEP* 04 (2011), p. 083. DOI: 10.1007/JHEP04(2011)083. arXiv: 1010.3679 [hep-th].

[132] Jacob L. Bourjaily et al. "Rationalizing Loop Integration". In: *JHEP* 08 (2018), p. 184. DOI: 10.1007/JHEP08(2018)184. arXiv: 1805.10281 [hep-th].

[133] Mathew Bullimore and David Skinner. "Descent Equations for Superamplitudes". In: (2011). arXiv: 1112.1056 [hep-th].

[134] Jacob L. Bourjaily. "Efficient Tree-Amplitudes in N=4: Automatic BCFW Recursion in Mathematica". In: (2010). arXiv: 1011.2447 [hep-ph].

[135] G. P. Korchemsky and E. Sokatchev. "Symmetries and analytic properties of scattering amplitudes in N=4 SYM theory". In: *Nucl. Phys.* B832 (2010), pp. 1–51. DOI: 10.1016/j.nuclphysb.2010.01.022. arXiv: 0906.1737 [hep-th].

[136] J. Bartels et al. "BFKL approach and $2 \to 5$ maximally helicity violating amplitude in $\mathcal{N} = 4$ super-Yang-Mills theory". In: *Phys.Rev.* D86 (2012), p. 065026. DOI: 10.1103/PhysRevD.86.065026. arXiv: 1112.6366 [hep-th].

[137] Jochen Bartels, Andrey Kormilitzin, and Lev Lipatov. "Analytic structure of the $n = 7$ scattering amplitude in $\mathcal{N} = 4$ SYM theory at multi-Regge kinematics: Conformal Regge pole contribution". In: *Phys.Rev.* D89 (2014), p. 065002. DOI: 10.1103/PhysRevD.89.065002. arXiv: 1311.2061 [hep-th].

[138] Jochen Bartels, Andrey Kormilitzin, and Lev N. Lipatov. "Analytic structure of the $n = 7$ scattering amplitude in $\mathcal{N} = 4$ theory in multi-Regge kinematics: Conformal Regge cut contribution". In: *Phys. Rev.* D91.4 (2015), p. 045005. DOI: 10.1103/PhysRevD.91.045005. arXiv: 1411.2294 [hep-th].

[139] V.S. Fadin and L.N. Lipatov. "BFKL equation for the adjoint representation of the gauge group in the next-to-leading approximation at $\mathcal{N} = 4$ SUSY". In: *Phys.Lett.* B706 (2012), pp. 470–476. DOI: 10.1016/j.physletb.2011.11.048. arXiv: 1111.0782 [hep-th].

[140] Till Bargheer, Georgios Papathanasiou, and Volker Schomerus. "The Two-Loop Symbol of all Multi-Regge Regions". In: (2015). arXiv: 1512.07620 [hep-th].

[141] Francis C. S. Brown. "Single-valued hyperlogarithms and unipotent differential equations". In: (). URL: http://www.ihes.fr/~brown/RHpaper5.pdf.

[142] Francis C. S. Brown. "Notes on motivic periods". In: (2015). eprint: 1512.06410 (math.NT).

[143] Freddy Cachazo and Jairo M. Rojas. "Notes on Biadjoint Amplitudes, Trop $G(3, 7)$ and $X(3, 7)$ Scattering Equations". In: (2019). arXiv: 1906.05979 [hep-th].

[144] Sarah B. Brodsky, Cesar Ceballos, and Jean-Philippe Labbé. "Cluster Algebras of Type D_4, Tropical Planes, and the Positive Tropical Grassmannian". In: *arXiv e-prints*, arXiv:1511.02699 (2015), arXiv:1511.02699. arXiv: 1511.02699 [math.CO].

[145] David Speyer and Bernd Sturmfels. "The tropical Grassmannian". In: *Advances in geometry* 4.3 (2004), pp. 389–411. ISSN: 1615-715x. DOI: 10.1515/advg.2004.023.

[146] Sergey Fomin and Andrei Zelevinsky. "Cluster algebras IV: Coefficients". In: *arXiv Mathematics e-prints*, math/0602259 (2006), math/0602259. arXiv: math/0602259 [math.RA].

[147] Nathan Reading. "A fan for every cluster". Combinatorics and beyond: the many facets of Sergey Fomin's mathematics. 2018. URL: https://math.berkeley.edu/~williams/FominTalks/Reading.pdf.

[148] *Planes in six dimensional tropical projective space*. https://www.uni-math.gwdg.de/jensen/Research/G3_7/grassmann3_7.html. Accessed: 2019-06-23.

[149] Sven Herrmann, Michael Joswig, and David E Speyer. "Dressians, tropical Grassmannians, and their rays". In: *Forum Mathematicum* 26.6 (2012), pp. 1853–1881. ISSN: 1435-5337. DOI: 10.1515/forum-2012-0030.

[150] Nima Arkani-Hamed, Song He, and Thomas Lam. "Stringy Canonical Forms". In: (2019). arXiv: 1912.08707 [hep-th].

[151] Aidan Herderschee et al. "On Positive Geometry and Scattering Forms for Matter Particles". In: (2019). arXiv: 1912.08307 [hep-th].

[152] Nima Arkani-Hamed et al. "Binary Geometries, Generalized Particles and Strings, and Cluster Algebras". In: (2019). arXiv: 1912.11764 [hep-th].

[153] Niklas Henke and Georgios Papathanasiou. "How tropical are seven- and eight-particle amplitudes?" In: (2019). arXiv: 1912.08254 [hep-th].

[154] Nima Arkani-Hamed, Thomas Lam, and Marcus Spradlin. "Non-perturbative geometries for planar $\mathcal{N} = 4$ SYM amplitudes". In: (2019). arXiv: 1912.08222 [hep-th].

[155] Song He, Lecheng Ren, and Yong Zhang. "Notes on polytopes, amplitudes and boundary configurations for Grassmannian string integrals". In: (2020). arXiv: 2001.09603 [hep-th].

[156] Francisco Borges and Freddy Cachazo. "Generalized Planar Feynman Diagrams: Collections". In: (2019). arXiv: 1910.10674 [hep-th].

[157] Freddy Cachazo et al. "Planar Matrices and Arrays of Feynman Diagrams". In: (2019). arXiv: 1912.09422 [hep-th].

[158] Nick Early. "From weakly separated collections to matroid subdivisions". In: (2019). arXiv: 1910.11522 [math.CO].

[159] Nick Early. "Planar kinematic invariants, matroid subdivisions and generalized Feynman diagrams". In: (2019). arXiv: 1912.13513 [hep-th].

[160] Ewgenij Gawrilow and Michael Joswig. "polymake: a framework for analyzing convex polytopes". In: *Polytopes—combinatorics and computation (Oberwolfach, 1997)*. Vol. 29. DMV Sem. Birkhäuser, Basel, 2000, pp. 43–73.

[161] Igor Prlina et al. "All-Helicity Symbol Alphabets from Unwound Amplituhedra". In: *JHEP* 05 (2018), p. 159. DOI: 10.1007/JHEP05(2018)159. arXiv: 1711.11507 [hep-th].

[162] Igor Prlina et al. "Boundaries of Amplituhedra and NMHV Symbol Alphabets at Two Loops". In: *JHEP* 04 (2018), p. 049. DOI: 10.1007/JHEP04(2018)049. arXiv: 1712.08049 [hep-th].

[163] Tristan Dennen et al. "Landau Singularities from the Amplituhedron". In: *JHEP* 06 (2017), p. 152. DOI: 10.1007/JHEP06(2017)152. arXiv: 1612.02708 [hep-th].

[164] Nima Arkani-Hamed, Hugh Thomas, and Jaroslav Trnka. "Unwinding the Amplituhedron in Binary". In: *JHEP* 01 (2018), p. 016. DOI: 10.1007/JHEP01(2018)016. arXiv: 1704.05069 [hep-th].

[165] Jacob L. Bourjaily et al. "Rooting Out Letters: Octagonal Symbol Alphabets and Algebraic Number Theory". In: (2019). arXiv: 1910.14224 [hep-th].

[166] Chi Zhang, Zhenjie Li, and Song He. "Two-loop Octagons, Algebraic Letters and $\bar{Q}$ Equations". In: (2019). arXiv: 1911.01290 [hep-th].

[167] Anna Felikson, Michael Shapiro, and Pavel Tumarkin. "Skew-symmetric cluster algebras of finite mutation type". In: *Journal of the European Mathematical Society* (2012), 1135–1180. ISSN: 1435-9855. DOI: 10.4171/jems/329. URL: http://dx.doi.org/10.4171/jems/329.

[168] Nathan Reading. "A combinatorial approach to scattering diagrams". In: (2018). arXiv: 1806.05094 [math.CO].

[169] John Golden et al. "The Sklyanin Bracket and Cluster Adjacency at All Multiplicity". In: *JHEP* 03 (2019), p. 195. DOI: 10.1007/JHEP03(2019)195. arXiv: 1902.11286 [hep-th].

[170] Simon Caron-Huot et al. "The Double Pentaladder Integral to All Orders". In: *JHEP* 07 (2018), p. 170. DOI: 10.1007/JHEP07(2018)170. arXiv: 1806.01361 [hep-th].

[171] Jorge Mago et al. "Yangian invariants and cluster adjacency in $\mathcal{N} = 4$ Yang-Mills". In: *JHEP* 10 (2019), p. 099. DOI: 10.1007/JHEP10(2019)099. arXiv: 1906.10682 [hep-th].

[172] Tomasz ukowski et al. "Cluster Adjacency for $m = 2$ Yangian Invariants". In: *JHEP* 10 (2019), p. 158. DOI: 10.1007/JHEP10(2019)158. arXiv: 1908.07618 [hep-th].

[173] Jorge Mago et al. "A Note on One-loop Cluster Adjacency in N = 4 SYM". In: (May 2020). arXiv: 2005.07177 [hep-th].

[174] Ömer Gürdoğan and Matteo Parisi. "Cluster patterns in Landau and Leading Singularities via the Amplituhedron". In: (May 2020). arXiv: 2005.07154 [hep-th].

[175] F.A. Dolan and H. Osborn. "On short and semi-short representations for four-dimensional superconformal symmetry". In: *Annals Phys.* 307 (2003), pp. 41–89. DOI: 10.1016/S0003-4916(03)00074-5. arXiv: hep-th/0209056.